

LINEAR ACCELERATION AND HORIZONTAL
EYE MOVEMENTS IN MAN

by

MARK JOHN SHELHAMER

M.S./B.S. Electrical Engineering
Drexel University
(1982)

Submitted to the Department of Aeronautics and Astronautics and
Submitted to the Interdepartmental Program in Biomedical Engineering
in Partial Fulfillment of
the Requirements for the Degree of
Doctor of Science in Biomedical Engineering

at the

Massachusetts Institute of Technology

January 1990

© Massachusetts Institute of Technology 1990. All rights reserved.

Signature of Author _____
Interdepartmental Program in Biomedical Engineering
January 19, 1990

Certified by _____
Laurence R. Young
Professor, Department of Aeronautics and Astronautics
Thesis Supervisor

Certified by _____
Conrad Wall III
Associate Professor of Otolaryngology, Harvard Medical School

Certified by _____
James Lackner
Professor and Director, Ashton Graybiel Spatial Orientation Laboratory

Accepted by _____
Professor Alan J. Grodzinsky
Chairman, HST Committee on Biomedical Engineering and Physical Sciences

Accepted by _____
Harold Y. Wachman, Chairman, Department Graduate Committee
MASSACHUSETTS INSTITUTE OF TECHNOLOGY

FEB 26 1990

LIBRARIES

Aero

LINEAR ACCELERATION AND HORIZONTAL
EYE MOVEMENTS IN MAN

by

MARK JOHN SHELHAMER

Submitted to the
Department of Aeronautics and Astronautics and the
Interdepartmental Program in Biomedical Engineering
on January 19, 1989 in partial fulfillment of the requirements
for the Degree of Doctor of Science in Biomedical Engineering

ABSTRACT

Horizontal eye movements in humans were studied under several stimulus conditions: 1) Linear vestibulo-ocular reflex (LVOR) during lateral accelerations in the dark; 2) Tracking of a retinally-fixed after-image (AI) during identical accelerations; 3) Fixation suppression (FS) of LVOR by fixating on a subject-stationary target light during linear acceleration; 4) Smooth pursuit (SP) in response to a moving visual target; 5) Tracking a stationary target while undergoing linear accelerations, providing both visual and vestibular information (VV). The last condition determined the improvement in smooth pursuit due to additional vestibular sensory input. Subject and target motions were sinusoids of various frequencies and peak accelerations, acceleration steps, and pseudo-random sum-of-sinusoids. Frequency response functions were produced from gain and phase measurements of the eye motion with respect to the target/subject motion. Fast phases were removed from eye movement records via computer processing.

Results confirm that LVOR is highly variable, with a gain of about fifteen degrees per second of eye movement per g of acceleration, relatively constant across the frequency range 0.2 to 1.3 Hz. AI tracking improves the gain of the LVOR by a factor of two to ten. This provides support for a theory in which oculomotor efferent copy information is used to reconstruct an internal representation of target velocity, which is then tracked by the oculomotor system. Fixation suppression significantly reduces the LVOR gain.

Comparison of the VV and SP conditions shows that the additional linear motion information provided by accelerating the subject in the VV condition produces a small but significant improvement in oculomotor tracking. This improvement is manifest most consistently by a decrease in phase lag, and also by an increase in response gain (eye movement divided by target movement).

A Kalman filter-based model of the combination of visual and vestibular information for oculomotor tracking is developed. The model concentrates on predictable (sinusoidal) target motion, and contains a central pattern generator (CPG) which predicts the target motion and hence enhances the response. The CPG is a natural formulation of the Kalman filter when the input is known to be sinusoidal. The CPG requires an instantaneous estimate of the input frequency, provided by a frequency estimator subsystem derived from a linearized Kalman filter. The model performance is compared to the experimental data.

Thesis Supervisor: Dr. Laurence R. Young
Title: Professor of Aeronautics and Astronautics

TO MY PARENTS AND MY AUNT

Concern for man, himself,
and his fate must always form
the chief interest of all
technical endeavor...Never
forget this in the midst of your
diagrams and equations.
- Albert Einstein

Whatever you do, work at it
with all your heart, as
working for the Lord, not for
men...
- Colossians 3:23

ACKNOWLEDGEMENTS

I would like to extend my sincere thanks to the following:

The MVL and its staff: for my introduction to weightlessness, for many many sleepless nights, for a true sense of belonging and accomplishment, for the challenge, for trips and trips and trips - and the Spacelab Experience.

My thesis committee, Professors Lackner, Young, and Wall, whose combined scientific experience and insight is a genuine inspiration. It didn't hurt that they each have a sense of humor and were generally a joy to deal with.

Bob Renshaw, for continual good humor and sage advice, which I ignored a few times too many. And for a great summer cross-country trip.

Dan Merfeld, whose scientific incisiveness always cut through layers of obfuscation to the core of the matter, applying basic principles in profound and startling ways.

Bryan Sullivan, who always displayed good common sense, discipline, and an unpretentious attitude to some quite impressive accomplishments. Also the continual badger when necessary, which it was for most of my time here.

Tom Mullen, whose unfailing good cheer and even temper was and is a great example.

Barbara Glas, most recent in a long line of colorful characters who have graced the position of laboratory secretary. Alan Natapoff, always supportive and ready to remind me of the excitement of the scientific endeavor. Anthony Arrott, for my introduction to the MVL and his great guidance during those early years.

Thanks to Jennifer for being Jennifer, and to Sherry for being Sherry - two of the finest people I know; there is no higher honor I can pay them than to say that they are truly themselves.

The many students who have passed through the MVL during my stay; they have proved to be thoughtful, intelligent, delightful peers.

The creators of MATLAB, MACSYMA, and EXTEND, and those responsible for maintaining the computer systems they reside on and making these systems readily available.

The otoliths and eyes of my subjects, for data that fit the model, more or less. My prime subject especially, forever to be known only as "T", for willingly undergoing a multitude of preliminary experiments, and singing more and more joyfully as each one dragged on.

Finally and most importantly importantly, to my family for their never-ending support, and for knowing when to stop asking when I would finish.

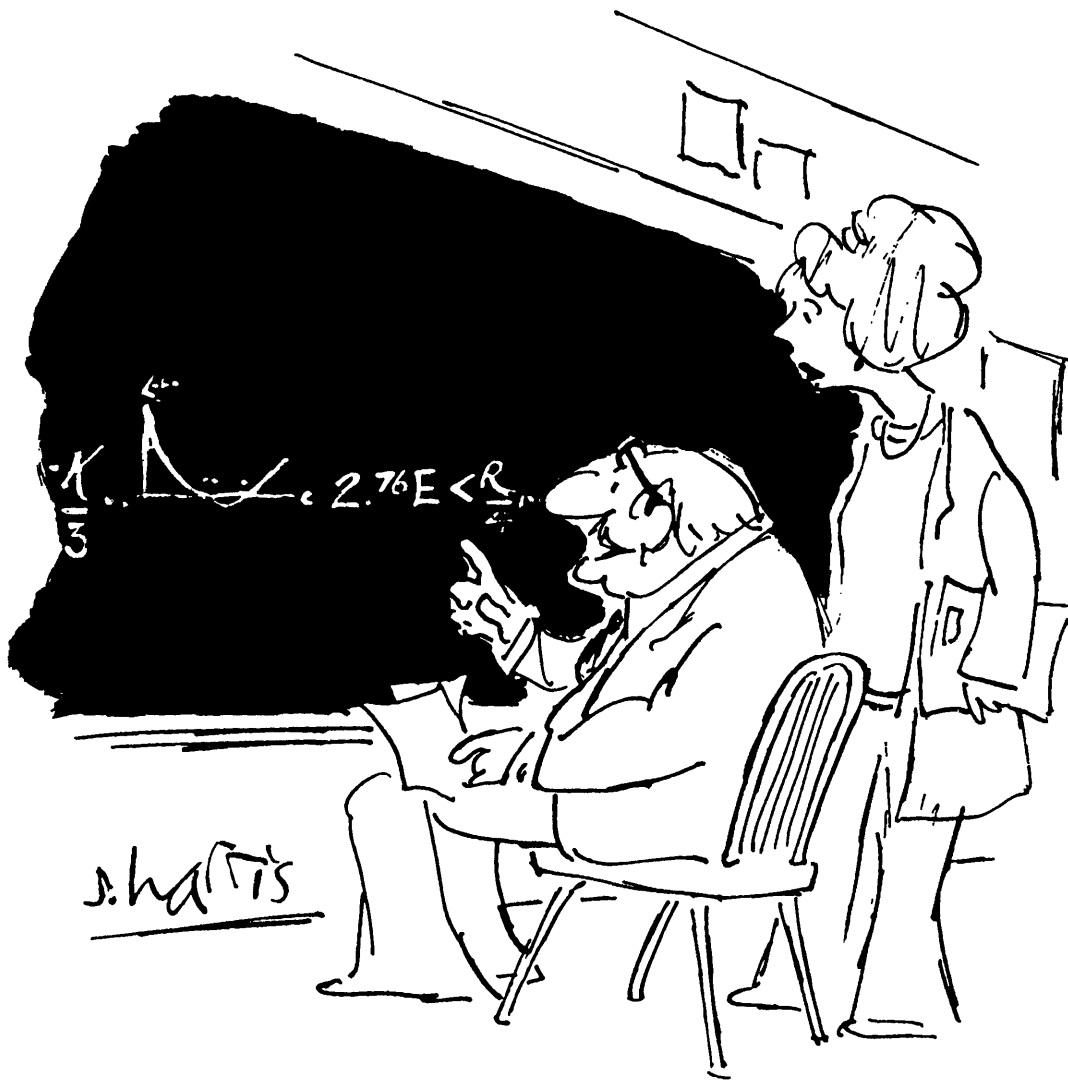
Supported by NASA contracts NAS9-15343, NASW-3651, NAS9-16523, grant NAG2-445, a Whitaker Health Sciences Fund Fellowship, and a National Science Foundation Fellowship.

Table of Contents

I Introduction	8
II Background	12
Multiple Sensory Inputs Contribute to Perception and Compensatory Reflexes...	12
Eye Movements in Response to Linear Acceleration.....	13
Otolith Afferent and Vestibular Nucleus Responses to Linear Accelerations.....	17
VOR: Effects of Instructions and Target Properties.....	18
Fixation Suppression of the VOR.....	19
Smooth Pursuit Eye Movements.....	20
Sensory Interactions and Eye Movements.....	23
Perceived Target Motion and Eye Tracking.....	26
Anti-Compensatory Eye Movements.....	26
Kalman Filter Approach to Physiological Modelling.....	27
III Methods	31
Equipment.....	31
Methods.....	32
1. Linear Vestibulo-Ocular Reflex (LVOR).....	32
2. After-Image Tracking (AI).....	33
3. Smooth Pursuit (SP).....	34
4. Visual+Vestibular Information (VV).....	34
5. Fixation Suppression.....	34
Stimuli.....	34
Data Analysis.....	36
Subjects.....	38
Flash Test.....	39
IV Results	42
Linear Vestibulo-Ocular Reflex (LVOR).....	42
Dark LVOR - Sinusoids.....	42
Dark LVOR - Steps.....	43
Dark LVOR - Luminous Line.....	44
After-Image Tracking.....	45
Smooth Pursuit and Visual+Vestibular (SP & VV).....	48
SP & VV - Sinusoids.....	48
SP & VV - Steps.....	49
Fixation Suppression.....	50
Anti-Compensatory Eye Movements.....	50
Summary and Comparison with Clinical Data.....	51
V Model	107
Phenomena to Be Modelled.....	107
Approach.....	107
Development.....	110
Frequency Estimator Subsystem.....	116
Model Fits/Parameter Values.....	116
Pursuit of Other Stimulus Patterns.....	118
Speculation on Noise Covariances.....	120
Interpretation of Parameters.....	121
Suggestions for Further Modelling Work.....	124
Model Predictions.....	125

VI Conclusions	152
Recommendations for Further Work.....	154
References	156
Appendix A Clinical Test Data	166
Summary of Clinical Testing of Experimental Subjects.....	166
Appendix B Models and Transfer Functions	180
PC-MATLAB Transfer Function Programs.....	193
EXTEND Models.....	199
Appendix C Frequency Estimator	202
Appendix D Parameters and Model Fitting	209
Appendix E Process and Measurement Noises	230

I Introduction



"THE BEAUTY OF THIS IS THAT IT IS ONLY OF THEORETICAL IMPORTANCE, AND THERE IS NO WAY IT CAN BE OF ANY PRACTICAL USE WHATSOEVER."

How is it that we are able to move about through our environment, orient ourselves properly with respect to our surroundings, and determine where we are? What are the processes that function in order to properly combine the various sensory inputs into a meaningful estimate of our orientation? Even more remarkable, how is it that this system can change itself to adapt to changes in our bodies through age or disease?

This thesis deals with one small piece of this area of human spatial orientation. Specifically, it deals with the generation of eye movements which compensate for linear motions of the body or of a visual target in the frontal plane (parallel to the front of the body).

An issue often taken for granted in this area of research is the importance of eye movements. As a motor reflex, eye movements can be considered as an attempt by the brain to correct for perceived body or environment motion. To the extent that reflexive eye movements correct for body motion, they can be viewed as the output of an internal orientation model. Indeed, they may be the most important output of any such system, for what better purpose would be served by an orientation model than to provide the basis for corrective actions to be taken to avoid harm, stabilize posture, and enhance vision. (This is in contrast to a point of view which stresses perception as the primary purpose of sensory and central nervous systems.) The fundamental approach taken here is to treat compensatory eye movements as the output of an internal system which combines sensory information to produce an estimate of head and body motion.

Many of the experiments described here have been done repeatedly for the case of rotation about a vertical axis. The present work extends these to the case of linear motions.

I will now briefly outline the experiments and analyses presented in this thesis. Smooth pursuit eye (SP) movements in response to sinusoidal and random point target motions are examined. The converse condition, in which the subject is moved while viewing a stationary point, is then examined to determine otolithic contributions to smooth tracking eye movements (visual+vestibular condition: VV). After-image tracking (AI) is examined, in which a retinally-fixed after-image is "tracked" by the subject during linear motions. This condition is compared to that in which all accelerations are done in complete darkness with no visual targets (this is the linear vestibulo-ocular reflex: LVOR). Finally, fixation suppression (FS) is tested, in which the subject attempts to attenuate reflexive eye movements (LVOR) by fixating on a point which moves with him or her on the sled. A Kalman filter model of the blending of the visual and vestibular information for the generation of compensatory eye movements is developed. Concepts from a previous model (Yasui, 1973) for tracking of perceived motion are incorporated to account for the after-image tracking data. Throughout, some additional issues of interest in the data are discussed.

The comparison of the LVOR and the AI conditions, and the comparison of the SP and VV conditions, for sinusoidal and sum-of-sines stimulation, are the major themes throughout the thesis. These data sets are the most thoroughly analyzed, and are used in the model development in chapter five. Several other themes are not as fully analyzed. The luminous line experiment described in the methods chapter did not work as anticipated, and its presentation in the results chapter consists mostly of possible explanations for its failure. Likewise, there were problems with the pseudo-random binary sequence (PRBS) experiments, and a brief section of the results chapter analyzes the most likely sources of the difficulty. Acceleration step stimuli were used in all of the conditions, but their analysis is limited to an example and short discussion for LVOR, and two graphs and a discussion for VV and SP. Finally, fixation suppression of LVOR is

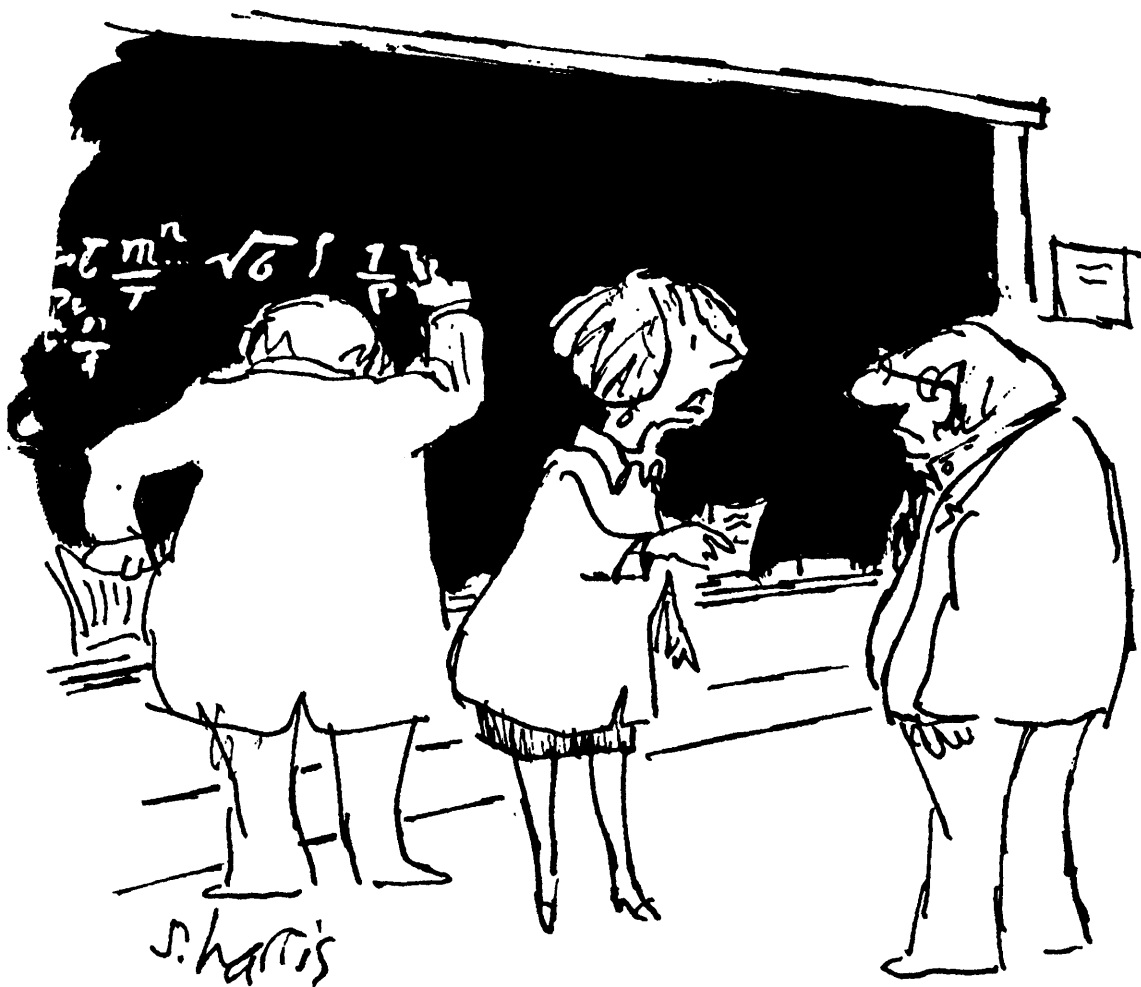
subject to only a brief analysis. The document will be easier to follow if these various threads are kept in mind.

The next chapter (Background) summarizes a large body of literature which pertains to the experiments in this work. The experimental methodology and equipment are then presented in chapter three, the results in chapter four, and the model development and parameter determination in chapter five. The major conclusions appear in chapter six. The appendices contain clinical test data on the subjects, derivation of model transfer functions, derivation and analysis of the frequency estimator subsystem used in the model, parameter values and transfer function plots for all subjects, and a preliminary analysis of Kalman filter process noise as it pertains to the model.

Three hypotheses guide the research presented here. First, that linear acceleration improves smooth pursuit. Second, that tracking of a retinal after-image yields larger responses than linear acceleration in the dark, verifying the perceptual feedback concept. Third, that the combination of visual and vestibular information can be adequately modelled with a Kalman filter based model.

The presentation here assumes that the reader is familiar with some of the appropriate background material. Specifically, the literature review in the next chapter presumes familiarity with the basics of vestibular and oculomotor function. Some knowledge of optimal estimation theory (especially Kalman filtering) will make the modelling chapter much easier to understand, although this knowledge is not necessary to grasp the basic idea of the model.

II Background



"WE COLLABORATE. I'M AN EXPERT, BUT NOT AN AUTHORITY, AND DR. GELPIS IS AN AUTHORITY, BUT NOT AN EXPERT."

MULTIPLE SENSORY INPUTS CONTRIBUTE TO PERCEPTION AND COMPENSATORY REFLEXES

The fact that several sensory systems work together to contribute to perception and reflexive responses has been known for a long time, and studied in detail in several systems. Most notably, the interaction between the semicircular canals and peripheral vision has been characterized and modeled in some detail (reviewed in Henn, Cohen & Young, 1982). During rotation in the light, the vestibular system's poor low frequency response is augmented by the visual system's accurate sensing of rotation, leading to an overall accurate perception of rotation, with corresponding compensatory eye movements (nystagmus).

Acoustic information has been shown to improve the performance of the linear vestibulo-ocular reflex (LVOR) (Buizza et al., 1979), even though acoustic information alone could not elicit smooth eye movements. Zambarbieri et al. (1981), on the other hand, could elicit smooth tracking with acoustic targets alone after considerable practice. Lackner (1977) also succeeded in producing nystagmus and an illusory perception of rotation in a stationary subject via a rotating acoustic stimulus.

A demonstration of the role of proprioceptive afferents comes from work with muscle vibration (Goodwin, McCloskey & Matthews, 1972). Vibration of the biceps muscle is thought to stimulate mainly muscle spindles, which register muscle length and velocity. Subjects thus stimulated perceived that their (unseen) arm was moving in a way which corresponded to stretching of the muscles being vibrated. Muscle spindle afferents were providing adequate information to influence perception of limb position. Lackner (1975) extended this work by asking subjects to track their unseen hand in the dark during muscle vibration. That they were able to produce smooth pursuit eye movements is evidence that muscle afferent information can be used centrally to construct an apparent

body posture model and contribute to oculomotor control. Levine and Lackner (1979) took advantage of this effect and placed a small target light on the subject's hand. Asked to describe their perceptions upon biceps muscle vibration in the dark, they reported that their forearms were being extended, even though the light did not move. Some also reported that the light did indeed move, and that they were tracking it with their eyes, even though eye fixation was steady. There is thus a very complex interrelation between the various sensory inputs which we use to produce perceptions of our limb and body positions. Lackner and Evanoff (1977) were also able to elicit smooth pursuit eye movements in subjects in the dark by moving a tactile stimulus along their forearm, as it was held horizontally in front of them. The pursuit thus produced has longer latency, more saccades, and less accurate localization than that in response to a visual stimulus. Mather and Lackner (1980) also demonstrated that multiple sensory cues, including proprioception, can aid the accuracy of smooth pursuit.

Proprioceptive limb-movement information has also been studied in regard to vection and nystagmus. Sitting inside a large drum in the dark, a subject following the drum rotation with his arm exhibited vection and weak nystagmus (Brandt et al., 1977). Subjects apparently walking around in a circle, while actually stationary with the floor counter-rotating under them, had similar effects of a greater magnitude (Bles, 1979). These latter proprioceptive contributions were shown to increase during compensation for vestibular dysfunction, indicating that other senses increase their relative contributions to perception and postural control to compensate for the loss (Bles et al., 1983).

EYE MOVEMENTS IN RESPONSE TO LINEAR ACCELERATION

Despite good positive evidence, there still seems to be some doubt as to whether or not the otoliths can drive smooth compensatory eye movements. Certainly, the functional nature of any such reflex has been called into question (Hain, 1986; Berthoz et al., 1987),

due to its low gain and highly variable phase. However, it is obvious that the LVOR (linear vestibulo-ocular reflex) gain must depend on target distance, if it is to be compensatory. "If the usual requirement in normal life is to stabilize a visual surround several meters from the subject, only very small eye rotations are needed to compensate even large lateral displacements. Thus, the contribution of the LVOR to visual stabilization can be functionally significant despite the small eye movement that can be produced by otolith stimulation" (Buizza, Schmid & Droulez, 1981, pp 519-520). Although it might not be strictly accurate to term the LVOR a functional reflex due to its inconsistency, the otolithic contribution to visual stabilization would make it valuable, and this is one of the points addressed in this thesis. There may be some controversy due to the fact that the rotational VOR, which certainly contributes to visual stabilization, has a rather high gain and consistent phase in the dark. Comparing the two basic reflexes in the dark, the LVOR looks quite poor, but it may be more appropriate to judge it in terms of its contribution to oculomotor control in the light for visual stabilization.

Such eye movements have been qualitatively described in several studies in rabbits (Sjoberg, 1931) and humans (Jongkees, 1961; Bles & Kapteyn, 1973). In cat and chinchilla, rhythmic vertical oscillation (about 1.0 g peak-to-peak) produced a regular nystagmus (McCabe, 1964). In cats, labyrinthectomy abolished the response, although destroying the canalicular neuroepithelium did not. Acoustic overstimulation of the chinchilla, presumably sufficient to damage the otoliths, also altered the response. The conclusion was drawn that the nystagmus was otolithic in origin. Similarly, a patient was described (Graybiel, Stockwell & Guedry, 1972) who had almost complete loss of canal function but retained otolith function, and exhibited a clear nystagmus during earth-horizontal axis rotation.

In an oft-cited study (Niven, Hixson & Correia, 1966), humans were oscillated laterally at 0.58g acceleration and 0.2, 0.4, and 0.8 Hz in darkness. Consistent horizontal nystagmus was measured, with an average gain of 16.2 deg/s per g (degrees per second eye velocity with respect to stimulus acceleration in units of one earth gravity, g). There was also a consistent phase lead of about 60 deg [note that phase values are expressed in this thesis such that zero degrees corresponds to perfect compensation]. A similar study by Kitchen (1983) found a gain of 9.8 deg/s per g between 0.2 and 0.9 g at 0.4 Hz. Gains increased by a factor of two to three over the 0.28-0.8 Hz range. Phase leads decreased over this same range. No response could be elicited below 0.2 g acceleration. Studies under different conditions revealed a very strong sensitivity to any ambient lighting, with complete darkness producing the best responses.

In squirrel monkey, gains of 15 deg/s per g at 0.5 Hz, and 30 deg/s per g at 5.0 Hz, were found at 0.36 g for both horizontal and vertical motions (Tomko & Paige, 1988). Phases in this range were relatively constant at zero (fully compensatory).

Baarsma and Collewijn (1975) studied vertical and torsional eye movements in response to sinusoidal and step accelerations in the rabbit. They found gains, defined as eye rotation divided by gravito-inertial force vector rotation, of 0.3 at 0.068 Hz, dropping to less than 0.01 above 1.0 Hz. Phase lags went from about zero to 180 degrees over the same frequency range, again measured in relation to vector rotations. Responses to steps of 0.02 to 0.11 g took several seconds to develop fully, with an approximately linearly increasing eye deviation over the duration of the acceleration, the slope depending on the acceleration magnitude. The conclusion was drawn that the otolith-ocular system is a slow system, responding to accelerations averaged over several seconds. Although not mentioned in the text of the paper, their graphical data show a small eye deviation in the

anti-compensatory direction at the onset of the stimulus. This issue will be discussed subsequently.

A clever approach to enhancing the LVOR was taken by Buizza et al. (1980). They were able to modulate the slow phase velocity (SPV) of optokinetic nystagmus (OKN) by using lateral linear accelerations. Using modulation of SPV as the measure of otolith-ocular response, gains of up to 60 deg/sec per g were found. The response was also elicited at a much lower acceleration (0.01 g) than found in other LVOR studies. Experiments in rabbits by Veenhof (1965) and in humans by Tokunaga (1977) similarly showed OKN enhancement by linear acceleration.

During rotation about a non-vertical axis in darkness (off-vertical axis rotation: OVAR), subjects exhibit a nystagmus which is maintained for the duration of the rotation (reviewed by Raphan & Cohen, 1985). The magnitude of this sustained nystagmus component varies with the cosine of the angle between the axis of rotation and the gravity vector. In addition, it depends on the velocity of rotation and the species of the subject. Gain (eye velocity over rotation velocity) in monkeys is close to one for stimulus velocities up to about 60 deg/sec. Several lines of evidence indicate that this continuous nystagmus is due to otolith stimulation by the rotating gravity vector. The response is not abolished by plugging or destroying the function of the semicircular canals (Correia & Money, 1970; Graybiel, Stockwell & Guedry, 1972). Canal afferent firing rate is not correlated with eye velocity during OVAR (Goldberg & Fernandez, 1982). The response is abolished if the utricular nerve is sectioned (Janeke et al., 1970).

The sustained OVAR response consists of a bias component upon which is overlaid a modulation component. The modulation component is a sinusoidal variation in the SPV, correlated with body position with respect to gravity. Correia and Guedry (1966)

measured modulation components (amplitude of sinusoidal component of SPV) of 9 deg/s at 0.2 Hz and 15 deg/s at 0.5 Hz. Benson and Bodin (1966) found values of 1.5 to 10 deg/s at 0.03 to 0.17 Hz. The bias component indicates that the continually-varying otolith stimulation is transformed to a velocity signal.

OTOLITH AFFERENT AND VESTIBULAR NUCLEUS RESPONSES TO LINEAR ACCELERATIONS

First-order otolith afferent neurons of the "regular" type (Fernandez & Goldberg, 1976) had directional polarizations and DC gains of 8.2 to 47.8 spikes/s per g. Gains were relatively constant from DC to 2.0 Hz, with usually no more than a two times increase. Phases decreased from a small lead to a small lag (10-20 deg each) over the same frequency range. Irregular units had much larger gain increases with frequency, and overall larger phase leads. Sinusoidal stimulus amplitude had no effect on regular unit gains and phases, and a small gain increase with decreasing amplitude for irregular units. Accelerations were sinusoidal with amplitudes of 0.4 g below 0.5 Hz, 0.2 g at 1.0 Hz, and 0.1 g at 2.0 Hz, superimposed on a bias of 0.46 g, produced by eccentric rotation.

Recordings from otolith-dependent units in cat vestibular nuclei (Melvill Jones & Milsum, 1969) similarly found units with directional polarizations. Gains varied widely, from 19 to 1100 spikes/sec per g, with a mean of 247. Minimum detectable modulation occurred at 0.005 g, which is close to human subjective threshold values for detection of linear acceleration (Guedry, 1974). Phase was likewise variable, and lags exceeded 180 deg at 2.0 Hz. In the squirrel monkey (Perachio, 1981), gains varied from about 160 to 60 spikes/s per g over 0.2 to 1.2 Hz. Phases were relatively constant at 60 to 80 deg lag with respect to acceleration (100 to 120 deg lead with respect to position), approximating a velocity-dependent response. A stage of temporal integration seems to occur between the afferents and the nucleus, at least as indicated by this particular result.

VOR: EFFECTS OF INSTRUCTIONS AND TARGET PROPERTIES

The task given to subjects during rotational VOR testing has been shown to greatly effect the resulting gain (Barr et al., 1976). Using mental arithmetic to preclude any specific task, gain ranged from 0.65 to 0.83 (over 0.3 to 0.8 Hz). Fixating a stationary target brought gains up to 1.0, while fixating an imaginary stationary target reduced gains only slightly below one. Fixation on a moving target (fixation suppression) reduced gains to about 0.1, and fixation on an imaginary moving target gave 0.4. Another study (Goldberg & Icaza, 1985) found that fixation of imaginary targets at 10 cm could produce gains greater than 1.0, as would be required for true compensation with actual targets at that distance (Virre et al., 1986). The distorted sinusoid form of the responses was also mentioned. The Barr study suggested the existence of a "spatial location" subsystem in the VOR, which adjusts the gain depending on (real or imaginary) target distance. It is apparent that vergence level would be a straightforward means of estimating target distance for this purpose, but this was not explicitly tested or discussed.

Tests with squirrel monkeys similar to those previously described, but with lights illuminating the walls of the animal container 0.20 m away (Paige & Tomko, 1988), revealed full visual suppression of the LVOR at 0.5 Hz / 0.36 g; but the gain at 5.0 Hz was actually double what it was in the dark. This was attributed to the fact that smooth pursuit (believed to account for fixation suppression) is ineffective at 5.0 Hz, and the container walls were then only providing an input to control vergence. Since looking at a near point requires a larger gain in order for eye movements to be compensatory than does looking at a far point, this near vergence "biased the LVOR for fixation on the container wall." Tests in the dark presumably allowed vergence to relax to a farther point. There is evidence that such changes in gain are necessary and actually do occur for rotational VOR (Post & Leibowitz, 1982; Virre et al., 1986). An experiment which may have some

bearing on the Paige and Tomko interpretation is described by Hydén et al. (1982). Rotational VOR gains above 3 Hz in the light were greater than one, as are such gains in the dark, whereas for active movements gains are held at one. Since smooth pursuit is relatively ineffective above 3 Hz, it was concluded that the "pure" vestibular gain, which would be greater than one at 3 Hz and above, is kept at one by "central motor programs" which can decrease the gain appropriately when active head movements are made.

In humans, eye tracking has been measured in response to lateral linear accelerations with an imaginary target (Berthoz et al., 1987). An actual target was presented at 63 cm, then turned off, and subjects were asked to track the remembered target position during linear oscillations at 0.22 Hz, 0.05-0.15 g. Composite tracking (smooth tracking plus saccades) slightly overestimated the linear displacements. Smooth components contributed very little to the response, with saccades making up most of the tracking. The cumulative smooth position was generally compensatory in direction, but phase was "inconsistent". Peak-to-peak amplitude never exceeded 12 degrees, although subject displacement ranged from 18 to 132 degrees peak-to-peak. Amplitude was not correlated to stimulus amplitude. Saccades were largely responsible for bringing the overall gain close to 1.0; saccade frequency and size increased with stimulus amplitude. Responses generally increased in size over the course of several cycles, consistent with psychophysical results (Guedry & Harris, 1963; cited by Berthoz et al., 1987), indicating that otolith information on head displacement drives a central mechanism which then drives saccadic eye movements (but not necessarily slow eye movements).

FIXATION SUPPRESSION OF THE VOR

Cancellation of the VOR takes place when the head turns to track a target rather than the eye. This phenomenon can be studied by providing a fixation point to subjects which

remains stationary with respect to them, and asking them to maintain gaze on the light while rotating in the dark. Such suppression of the VOR is very effective up to about 1.0 Hz (Barnes, Benson & Prior, 1978). Since this is the range at which smooth pursuit begins to break down (see section on smooth pursuit), it is generally accepted that smooth pursuit is used to suppress the VOR, although there is some debate on this issue (Robinson, 1982).

SMOOTH PURSUIT EYE MOVEMENTS

No attempt will be made here to present an exhaustive review of the literature on smooth pursuit (SP). Instead, a few of the key studies which describe results and concepts pertinent to the present research effort will be reviewed.

The basic characteristics are reviewed by Robinson (1981) (typical values presented here are for humans unless otherwise stated). Latency to large velocity changes is about 130 msec. Velocity saturation has been reported to occur at anywhere from 30 to 150 deg/sec (Meyer et al., 1985; Lisberger et al., 1981). Steady state velocity gain is about 0.80 to 0.90. The lack of a refractory period indicates that the system is continuous in nature. Above about 1.0 Hz, tracking of unpredictable stimuli degenerates rapidly. Retinal error velocity (difference between target and eye velocities) is the main input to the SP system. An actual visual target is generally necessary to stimulate smooth following eye movements, but studies have shown that perceived motions and limb motions can also drive smooth movements. Some of these topics will be elaborated upon. First, however, corresponding properties of the rotational VOR are presented for comparison. The VOR has about a 10 msec latency, a bandwidth up to about 5 Hz, and saturation velocities reported from 240 to over 400 deg/sec (Pulaski, Zee & Robinson, 1981; Raphan, Matsuo & Cohen, 1979 (monkeys); Robinson, 1975).

von Noorden and Mackensen (1962) found good quality smooth pursuit of single sines up to 0.4 Hz, with few saccades. The sinusoidal nature disintegrated at 0.5-0.8 Hz, and broke down into almost complete saccadic tracking at 1.0-1.3 Hz. A moving stimulus presented to a paralyzed eye induced smooth eye movements in the other (non-stimulated and motile) eye, indicating that retinal image motion is a sufficient stimulus.

Much higher maximum SP velocities were reached in another study (Lisberger et al., 1981), up to 150 deg/sec. SP gain was a consistent function of maximum target acceleration. Similarly, eye acceleration was a consistent function of retinal error velocity. The same basic relations held true for unpredictable stimuli, but with lower gains and eye accelerations. Stimuli were in the 0.3-2.1 Hz and 5-30 deg/sec range.

Collewijn and Tamminga (1984) found smooth component gains always less than 0.95, with saccades used to make up the difference. Unpredictable target tracking gains were lower than for single sines. The higher frequency components in a pseudo-random stimulus were pursued with higher gains than were the lower frequency components. Single sines yielded smaller tracking phase lags than pseudo-random stimuli, but the low frequency components in the random case produced a phase lead. Gains decreased as target velocity increased.

Velocity gain is typically 0.80-0.90. However, subjects can be trained to track targets moving at 0.57-11.45 deg/sec with lower (but not higher) gain (Steinman, Skavenski & Sansbury, 1969). After sufficient practice, a slow enough target (2.4 deg/sec constant velocity) could be tracked with a perfect gain of 1.0, but one slightly faster (although still well below the accepted velocity saturation level of about 30 deg/sec), 5.4 deg/sec, was only tracked with a gain of 0.95 (Kowler, Murphy & Steinman, 1978). Gains of 0.9 were also found by Buizza and Schmid (1986), for both predictable and unpredictable

target motions. However, they found no "hard" saturation for predictable motions up to 75 deg/sec, just a slight reduction in gain.

Significant differences between ocular pursuit of predictable and unpredictable target motions are well known. Whereas tracking of single frequency sinusoids (predictable) remains almost fully compensatory (gain = 1, phase lag = 0) up to at least 1 Hz, tracking of random-appearing sum-of-sines stimuli (unpredictable) may show significant gain decrease and phase lag at as low as the 0.2 Hz component (Stark, Vossius & Young, 1962). A predictor mechanism was thus postulated which overcomes the inherent lag of the oculomotor pursuit system when presented with predictable target motions. Using control theory to determine the open loop transfer functions for predictable sinusoid and unpredictable Gaussian random stimuli, Dallos and Jones (1963) determined the transfer function of this predictor element, which is presumed to operate in the forward loop when predictable stimuli are detected. Another model for the very low latency predictable tracking (Bahill & McDonald, 1983a) used the idea of a "target selective adaptive controller". This controller contains a menu of several common predictable waveforms, and a means of estimating target velocity (to set stimulus parameters) via computing derivatives and predicting future velocity. Data in support of this model include human zero-latency tracking of velocity triangles, with an eye velocity waveform which resembles the triangular stimulus waveform, indicating that the oculomotor system is internally generating an appropriate oculomotor signal (Bahill & McDonald, 1983b). Michael & Melvill Jones (1966) used filtered Gaussian noise, with filter bandwidths from 0.0 (pure sine) to 1.0 Hz, to demonstrate a significant increase in phase lag as stimulus predictability decreased.

Yasui and Young (1984) confirmed this and other reports that phase lag increased as pseudo-random stimulus bandwidth increased. They also showed that the purely smooth

pursuit component of tracking exhibits substantial phase lead at frequencies below about 0.3 Hz even during pseudo-random tracking. A predictor was hypothesized which operated even during unpredictable stimuli, optimized to minimize the average phase shift at some mean frequency in the stimulus bandwidth, and which uses perceptual feedback to make its predictions (see subsequent discussion on after-image tracking).

It should be noted that a completely different approach to the predictable-target issue has been developed (St-Cyr & Fender, 1969). Completely dismissing linear-system models of smooth pursuit, the authors show that the phase lags due to predictable and random stimuli can be modeled by simple time delays in the oculomotor system, and that these time delays depend on the information content in the stimulus. Random stimuli produce larger delays by this method. (See also previous note in regard to Yasui and Young paper). The model has a discrete-time nature, in that the delay time (which varies with stimulus type) is a period over which retinal displacement is measured and used to adjust eye motion. Theoretical delays of 114 to 524 msec are presented, which would seem to argue that smooth pursuit has a characteristic latency to target velocity changes. This has been shown not to be the case (Eckmiller & Mackeben, 1978).

SENSORY INTERACTIONS AND EYE MOVEMENTS

An attempt has been made to determine the interaction of LVOR and smooth pursuit (Buizza, Schmid & Droulez, 1981). While accelerating linearly at 0.2 Hz / 0.15 g, subjects tracked a target light which moved at a constant linear velocity with respect to them. Target and subject motions were not correlated. The target maximum velocity, when directly in front of the subject, was 65 deg/sec. Smooth pursuit of the target showed three phases: an acceleration during which eye velocity increased to match target velocity, a locked phase in which velocities matched, and a deceleration phase in which target and eye velocities decreased (although not in precise phase). There were two main

results. One was that, during linear accelerations, the initial eye acceleration during the acceleration phase of pursuit was much higher, leading to a more rapid matching of eye and target velocities. In addition, eye velocity was 95% of target velocity during subject accelerations, and 90% when stationary. A model analysis determined that the linear acceleration seemed to increase the open loop gain of SP from 10 to 20.

In the cat medial vestibular nucleus, the effect of vision on otolith responses was examined (Daunton et al., 1981). At 0.59 Hz and 0.15 g sinusoidal accelerations, 76% of 45 units were modified by both visual and acceleratory inputs. Some units showed an increase in gain when congruent visual information was provided during acceleration, while others had the opposite response. Visual suppression conditions (visual surround moving with the animal) did not seem to reduce the response gain. Phases in all cases were widely variable, but in general they tended to shift toward stimulus velocity when visual input was added.

Steinbach & Held (1968) showed that arm efferent information could be used to improve target tracking. Subjects could track self-moved targets more accurately than when their arms were moved passively along with the targets. A later study (Steinbach, 1969), however, showed that afferent information was also beneficial, by producing smooth tracking eye movements to an intermittent target which was passively moved along with the arm.

Further stretching the traditional view that a moving foveal target is necessary to trigger smooth pursuit, Steinbach (1976) demonstrated that subjects could track a portion of an object which was perceived to exist but was not actually visible. The commonly-cited example is the smooth pursuit of the center of a rolling wheel when two points on the rim of the wheel were the only visible stimuli.

Yasui and Young (1975a, 1975b) found that tracking of a retinal after-image during rotation significantly increased the gain of the VOR and decreased the number of nystagmus fast phases. Gain increased by an average of 1.55 times, and phase advanced an average of 21 deg, over .025 to 0.70 Hz. A "perceptual feedback hypothesis" was put forth to explain the results. As later expanded by Young (1977), the theory postulates that a variety of sensory and other information is integrated in a central "target velocity regenerator", which constructs an estimate of actual target velocity based on the information available. An efferent copy of the oculomotor signal is one of the inputs to this system, which explains the Yasui result: when the eye moves, the after-image remains centered on the fovea, giving the perception that the target also moved, leading to a continuing eye movement to track the "moving" after-image.

These experiments serve the notion that the brain constructs a perceptual target using a variety of visual and non-visual information, and then tracks that target. But other studies (Mack, Fendrich & Pleune, 1979; Mack, Fendrich & Wong, 1982) indicate that smooth pursuit can track targets which are perceived to be stationary, and sometimes will not track targets which are perceived to be moving but are actually stationary (generated by moving the background in the opposite direction). The authors conclude that perceived motion can drive pursuit only if the target has no "retinal image counterpart." Any true retinal image will override perception in generating pursuit. It may be that a shortcoming in the interpretation of some of these varied results lies in equating perceived target motion with the presumed centrally reconstructed target motion. It is not necessarily true that the consciously perceived target velocity is necessarily an accurate reflection of the centrally constructed target velocity. This is especially relevant in Yasui's original analysis (Yasui, 1973), as he uses the results of some perceptual studies to determine model gains. I will have more to say about this shortly.

PERCEIVED TARGET MOTION AND EYE TRACKING

Several experiments deal with perception of target motion and its relation to eye tracking movements. These reports are relevant for the development of the perceptual feedback model, in which an efferent copy of the eye movement command is added to retinal slip to produce perceived target motion. If subjects are asked to report the perceived velocity of a moving target, they consistently report velocities 1.6 to 1.8 times greater if their eyes are stationary than if they are actively tracking the target (Grüsser & Grüsser-Cornehls, 1973). In terms of the model, this would predict values for the efferent copy gain in the range of 0.4 to 0.2. Similarly, Sedgwick and Festinger (1976) produced perceptual illusions which they explained by postulating that the internal registration of eye movements underestimates the actual movement. This also corresponds to an efference copy gain of less than 1.0. Likewise, the fact that the retinal after-image in Yasui's experiments (Yasui, 1973) was perceived as moving leads to the conclusion that this gain must not be zero; otherwise, zero retinal slip would produce zero perceived velocity. Yasui also used the feedback model to explain the oculo-ocular illusion as being due to inaccurately-registered involuntary eye movements.

If the perceived velocity does indeed drive a "smooth pursuit subsystem", as in the model, the inherent gain of this subsystem (G) is not the gain of the overall SP response (S). We can show that the overall SP gain is in fact $S/(1 + K S - S)$; typical values of $K=0.2$ and $S=0.9$ give $G=4.7$, which is in the range of values usually given for the SP forward loop gain.

ANTI-COMPENSATORY EYE MOVEMENTS

During most ordinary head movements in the physiological range, the VOR typically provides for adequate visual stabilization. It has been found, however, that high-

acceleration head motion can induce an initial anti-compensatory saccadic eye movement (Melvill Jones, 1964). This saccade presumably functions to throw the eye ahead of the head and establish a target, allowing the compensatory VOR slow phase to track this target over a longer span. Relatively little has been reported on this effect. Figures in some reports, however, seem to show a small anti-compensatory component at the onset of acceleration steps (e.g. Baarsma & Collewijn, 1975, Figure 6). There is no discussion of these movements in the corresponding text. It is not clear whether they are saccades in all cases, or perhaps slow movements. Furthermore, I have only noticed it in reports of passive subject motion, so it may not be prevalent if active head and body movements are made.

KALMAN FILTER APPROACH TO PHYSIOLOGICAL MODELING

Borah, Young, and Curry (1988) developed a Kalman filter model which blends vestibular and peripheral visual sensory inputs to produce orientation estimates. Several well-known illusions can be reproduced with this model. The Kalman filter makes certain assumptions about the way the system is set up. For our purposes, this is described in terms of otolithic and foveal inputs. First, an internal model of the stimulus dynamics is embedded in the filter. This might take the form of a model of a system which reproduces the stimulus in close detail, for common or predictable stimuli. On the other hand, in general it might be more likely to reflect anticipated stimulus bandwidth and intensity. Internal knowledge, in some sense, of the noise characteristics of the various sensory systems is needed to determine the Kalman gain.

For predictable stimuli, two features sometimes found in physiological data are natural products of the Kalman filter. First, the response may continue after the stimulus ends. This has been found, for example, in rabbits (Collewijn, 1979; Collewijn & Grootendorst, 1979), where occasionally after a long period of peripheral visual

stimulation a spontaneous oscillation at the stimulus frequency occurred. "Such an after-effect, even though seen in only a small proportion of the rabbits, proves that the rabbit is able to store a movement pattern in its nervous system and to reproduce it." (Ibid, p. 101). Also, in humans, after two minutes of pursuing a repetitive unidirectional ramp stimulus, some subjects exhibited a continuing response of slow eye movement in the stimulus direction. Velocity decayed with a time constant of 5 to 15 seconds (Muratore & Zee, 1979). Other very interesting results were obtained in another study (von Noorden & Mackensen, 1962), which I will quote at some length:

If the target was made to disappear suddenly at any point in its course, the eye continued to carry out a smooth sine movement, as if still under stimulation by a moving visual object. The eye even came to a halt at a point where the target had previously reversed, and continued to move smoothly in the opposite direction for some distance. If the stimulus is interrupted by an electronic timing device it can be demonstrated that, with our experimentation, the critical time for stimulation interruption is approximately 100 sigma [apparently about one second, although not defined in the article]. Interruption of stimulation for longer than 100 sigma causes the smooth eye movement to disintegrate into saccades. . .

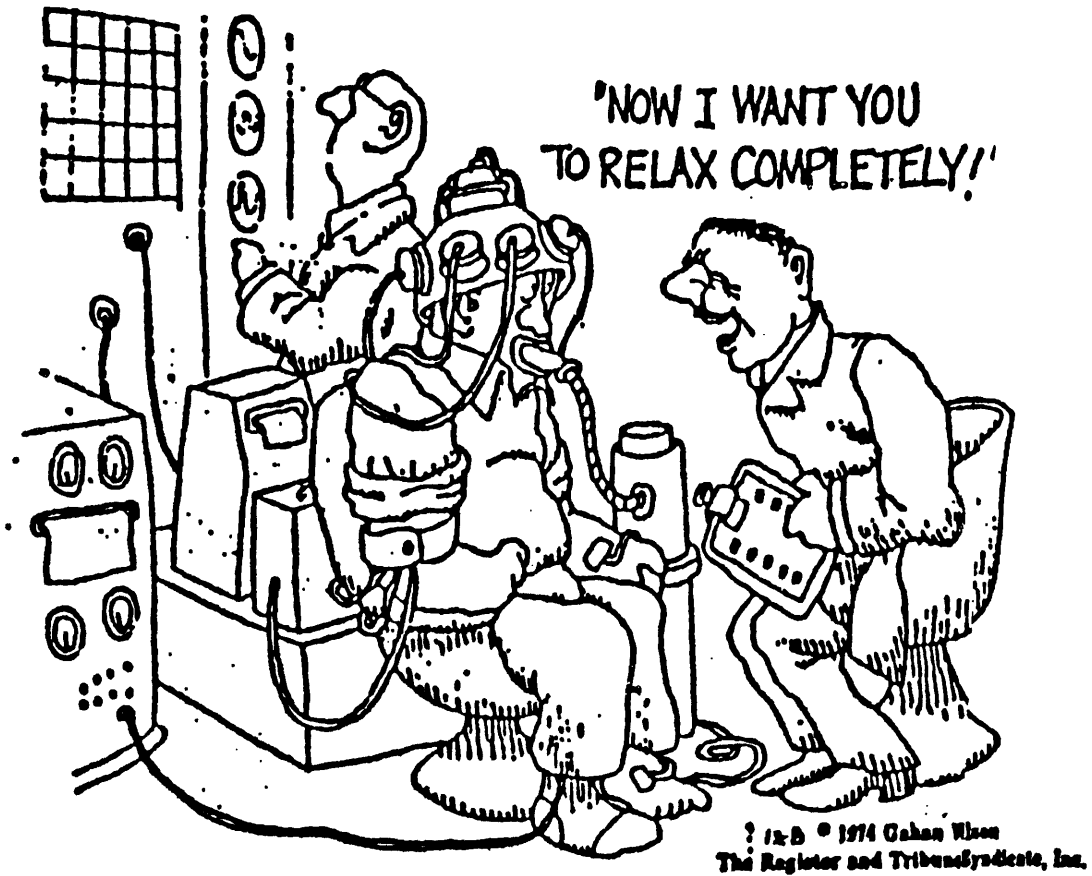
It must be assumed on the basis of these findings that pursuit movements are not only the result of constant motor adjustment to the changing position of the target by the fixation reflex, they are also regulated by a memory factor, which releases motor impulses according to the pattern stored, and enables the eye to continue a complicated movement with the same speed as under visual stimulation.

These results have been verified in humans (Whittaker & Eaholtz, 1982). Further work on this phenomenon in the monkey (Eckmiller & Mackeben, 1978) provided further verification, and demonstrated that oculomotor neurons exhibited changes in firing rate during stimulus disappearance commensurate with the eye movements. The separation of the required system into a predictor (or model) and an updating process was discussed.

Second, if the model is a sufficiently correct representation of the actual stimulus, zero-latency tracking can be accomplished, as is well-known for smooth pursuit eye movements (see previous section for review of smooth pursuit and predictable target motions). To take advantage of these properties, some means must be provided to adaptively update the internal model based on experience.

The internal model can be likened to the "neural store" of Reason (1978), or the "pattern center" of Groen (1960), by which repetitive stimuli are stored centrally and used to produce appropriate compensatory responses, cancel normal and expected sensory inputs from reaching conscious perception, and provide for a means of detecting and signalling the presence of unexpected stimuli. The internal pattern copy (von Holst & Mittelstaedt, 1950) can then lead to afterphenomena when the repetitive stimulus is suddenly removed (Groen, 1957).

III Methods



EQUIPMENT

All experiments used the MIT linear acceleration sled located in the Man-Vehicle Laboratory. The sled consists of a square aluminum cart which is supported on parallel rails by a set of four circulating bearings in pillow blocks. Mounted atop the cart is a chair assembly with a helmet and subject restraint system. The entire sled is driven by an electric motor which is controlled by a PDP-11 computer via an SCR controller. The system is capable of accelerations up to approximately 0.9 g and 2.0 Hz. The lower acceleration limit is determined by vibration, with accelerations in the neighborhood of 0.001 g being generally in the vibration noise level. Track length limits the lowest usable frequency, depending on acceleration.

The calibration and fixation light display consisted of five red light emitting diodes (LEDs), 0.5 cm in diameter, mounted 0.5 m from the eyes, at eye level. The luminous line was a 1.2 m length of 1.0 mm diameter clear plastic tubing, embedded in a groove which was milled in a piece of wood. The wood was coated with black ink to reduce reflections. For the LVOR and FS tests, the subject and cart were surrounded by a black cloth canopy, and the room lights were dimmed, to provide total darkness to the subject (except for the intended visual display).

Horizontal eye movements were recorded with surface EOG, one electrode on the outer canthus of each eye and one on the forehead. Amed type 600 pre-gelled disposable AG/AgCl electrodes were used, and the amplifier had a gain of 3000 and -3 dB bandwidth of 30 Hz. Subjects dark-adapted for at least twenty minutes prior to each experiment. When the subject was seated on the sled (for all tests except the SP series), wide band masking noise was presented through the communication system at close to the maximum tolerable level. Subject and operator were in constant contact through this communication system.

A potentiometer mounted on the sled drive motor shaft provided sled position information. A tachometer on the same shaft produced a sled velocity signal, and an accelerometer mounted on the sled chair, close to the subject's head, provided the acceleration signal. All of these signals were digitized and stored on computer disk along with the EOG signal. From the sled control/acquisition computer (a PDP-11/34 running the RT-11 operating system), data were transferred via a terminal line to an IBM PC. On the PC, a C program transformed the data files to a format compatible with the MATLAB software system, which was used for all of the subsequent analysis. Modeling and graphics were performed on Apple Macintosh computers.

METHODS

The methodology is straightforward. In order to determine the contribution of each sensory input (visual, vestibular) to the overall response, situations are created which test these systems individually, in conflict, and in harmony with one another. Five distinct cases were tested.

1. Linear vestibulo-ocular reflex (LVOR)

In order to determine the nature of the response to vestibular stimulation alone, the subject was exposed to accelerations along the frontal plane in the dark. In complete darkness, the traditional LVOR was tested. The subject was instructed to look straight ahead and not fixate on any point, real or imaginary, fixed or moving with the sled. Mental arithmetic was used as an alerting and diversionary task. Some subjects preferred other tasks to mental arithmetic, such as mentally recalling all team names in a certain football conference. Masking noise was presented to the subject through headphones in the helmet, set to a level judged by the subject to be as loud as possible without being

uncomfortable. This level was maintained relatively constant for a given subject through all tests performed on the sled.

1a. In order to control for any effects of accommodation and vergence, a subcondition was used. In this case, a luminous horizontal line was mounted 0.5 m in front of the subject. The line consisted of plastic tubing embedded in a grooved black wooden bar. A luminous chemical (removed from Cyalume® light sticks) was injected into the tubing, providing self-luminescence for approximately 0.5 to 1.0 hour. Since the line was oriented horizontally, horizontal eye movements could be made, and the line did not provide any visual cues that the eyes have moved. By maintaining accommodation on the line (so that it appeared as a single line, in focus), vergence was presumably controlled to some extent. Pilot trials verified that with sufficient coaching, a subject could change vergence by a noticeable amount (more than a few degrees) from a relaxed state.

2. After-image tracking (AI)

A small xenon flash tube, mounted on the sled 0.5 m in front of the subject, was used to induce a retinal after-image. For each such trial, the sled was positioned to the starting point, a small red fixation light came on, directly in front of and 0.5 m from the subject, the flash tube was triggered, the fixation light was extinguished, and the sled motion started a few seconds later. This small delay provided time for the after-image to fully develop and subside to a well-defined image. Since the flash tube surrounded the fixation light, the after-image was retinally centered. Occasionally there was a slight vertical misalignment, since the flash tube actually formed an inverted U around the light, and subjects tended to track the bend in the U, which was slightly above the light. This effect was small, and subjects tended to compensate for it by either looking slightly above the fixation light during the flash, or by tracking a different part of the after-image. The subject was instructed to track the after-image, that is, to follow it with his or her eyes.

3. Smooth Pursuit (SP)

The complementary condition to LVOR is visual stimulation alone, leading to smooth pursuit eye movements. The subject sat on the ground, stationary, 0.5 m in front of the sled. A small light was mounted on the sled at eye level. The sled executed the identical motions that were used to test LVOR and the other subject-moving conditions.

4. Visual+Vestibular Information (VV)

This is a condition in which visual and vestibular information were applied together, both presenting the same (correct) motion information to the subject. A small light source was mounted in front of the sled, fixed with respect to the room. With room lights off, the subject, seated on the sled, was accelerated along the frontal plane. The subject maintained gaze on the light as best as possible, with the aid of both the visual and vestibular inputs.

5. Fixation suppression (FS)

This is an example of conflicting visual and vestibular information. A point light source was mounted on the sled, and moved along with the sled and the subject seated in the sled. The subject attempted to fixate on the light, while being accelerated along the sled track in the dark. This tests the ability of vestibular stimulation to drive eye movements while the visual system attempts to suppress them and maintain stable fixation.

STIMULI

Several different sled motion stimuli were used. Sinusoidal profiles of different frequencies and accelerations were generated. Frequencies of 0.2, 0.3, 0.4, 0.5, 0.6, 0.7, 1.0, and 1.4 Hz were used, at accelerations of 0.1, 0.3, 0.5, 0.7, and 0.8 g. Not all combinations of frequency and acceleration were used. Profiles began at the zero-velocity

point, at one extreme of the sled position excursion. This caused profiles to begin at the maximum acceleration, which would cause a large transient response for the larger acceleration stimuli. Therefore, all 0.8 g profiles and some 0.5 g profiles began with a linear velocity ramp multiplied by the first two sinusoidal cycles. Profiles contained five complete cycles, and those with ramped beginnings contained five cycles after the ramp segment. Peak velocities of these profiles, for a target distance of 2.0 m, are in Table 3.1.

Steps of acceleration were also used. Magnitudes were 0.1, 0.2, 0.3, 0.4, 0.5, 0.6, 0.7, and 0.8 g. One series of steps started at the center of the track each time, and accelerated and decelerated at the same magnitude to reach the end of the track. Another series started alternately at either end of the track, and accelerated as long as possible before decelerating at 0.8g to reach the end of the track. Direction and magnitude were randomized, as was starting time of the step after the sled positioning phase was complete.

Pseudo-random sum-of-sines (SOS) profiles were also generated and used. Consisting of a number of non-harmonically related sinusoids at a given acceleration, these profiles allowed measurement of the response at several frequencies simultaneously. A technique and program developed by Hiltner (1983) was used to generate the profiles. Unfortunately, track length limited the acceleration and frequency content available. Two specific profiles were developed, each with 0.3 g components. One contained frequencies of 0.3, 0.5, and 0.7 Hz. The other contained 0.3, 0.5, 0.7, 1.1, and 1.3 Hz.

The last stimuli used were various pseudo-random binary sequences (PRBSs) (Davies, 1970). This is a wide band stimulus which appears random to the subject. It is generated by the software equivalent of a digital shift register with certain stages fed back through a modulo-2 adder to the first stage of the register. With a register of length n , sequences of

length $N=2^n-1$ are generated. If the fundamental time period of the register shifting is T seconds, the bandwidth of the generated sequence extends from $1/(NT)$ to $1/(3T)$ Hz (at -3 dB). The resulting sequence of zeros and ones is converted to a PRBS acceleration stimulus by setting the zero values to $-A$ and the ones to $+A$, where A is the acceleration level of the stimulus. This PRBS is integrated and scaled to give the required velocity command to drive the sled.

Data recording began two seconds before sled motion in all cases, and continued for two seconds afterward.

DATA ANALYSIS

Each signal (eye position, sled position, velocity, acceleration) was smoothed with a 9-point FIR filter, with -3 dB bandwidth of 7.8 Hz. The phase of the filter is a linear function of frequency, so no phase distortions were introduced. Further processing accounted for the slight filter time delay.

Sled position signals were converted from linear position in meters to visual angle via:

$$\text{angle} = \arctan\left(\frac{x}{d}\right)$$

where x =sled position, d =target distance (2.0 m).

Eye movement signals were processed as follows. First, the nine-point smoothing filter was used. Then, an algorithm developed and programmed by Merfeld (1990) was used to remove fast phases from the data. His report describes the process in detail; a preliminary version was used in this study. Briefly, eye acceleration is used to detect fast phases, based on a threshold which is determined from the variance of the data (noise level) surrounding each point. Examples of the performance of the algorithm are presented in Merfeld's dissertation (1990). Significant time delays are introduced by this processing,

which are compensated for by shifting the final eye position signal so as to remove the time delay; this is possible because two seconds of data are recorded before and after the stimulus is applied, giving "extra" points at the ends of the signal of interest.

Frequently, random large-amplitude "spikes" appear in the sampled data. There is a routine in the sled data acquisition program which reduces this occurrence by double-sampling at each sample time and always choosing that sample which is closest in value to the previously sampled value. If serious spikes remain, various manual and automatic methods are used to remove them as completely as possible. They are usually very easy to recognize, and so do not present a problem in terms of overall data validity.

Sinusoidal profiles were analyzed by correlation with a reference sinusoid of the same frequency as the stimulus. Amplitude and phase of the signal ($u(t)$) with respect to the reference are given by:

$$\begin{aligned} \text{amplitude} &= \sqrt{(CC^2 + SS^2)} & \text{phase} &= 57 \arctan\left(\frac{CC}{SS}\right) \\ s &= \sin(2\pi ft) & c &= \cos(2\pi ft) & SS &= 2us^T/N & CC &= 2uc^T/N \\ t &= 0 \dots (N-1)T_s & T_s &= \text{sample rate (0.01 s)} \end{aligned}$$

By correlating eye position and sled position or acceleration, and comparing the input and output amplitudes and phases, the response gain and phase can be calculated. To find gain in terms of eye velocity per sled acceleration (for LVOR and AI), the eye position per sled acceleration gain is found, and converted by the following:

$$\frac{2\pi f (\text{eye position [deg]})}{(\text{sled acceleration [m/s}^2\text{]) / 9.81}$$

SOS profiles were analyzed in the same way, correlating each frequency component separately. For all sinusoidal results, gains are expressed in one of two ways, depending

on the conditions: 1) degrees per second of eye movement per g unit of acceleration (for LVOR, AI, FS); 2) degrees of eye movement per degree of sled or target movement (for SP, VV). All phases are expressed such that zero degrees (not 180) represents perfect compensatory eye motion. Negative phase values represent oculomotor response lag with respect to stimulus, and positive values represent lead.

For the step responses, latency was determined by overlaying sled position and eye position on a grid and manually reading off times. This was found to be preferable to an automated technique, due to the variability of the eye movement patterns from trial to trial and the gradual onset which produced no obvious definite starting time. In all cases, an attempt was made to visually match the pattern of sled and eye movement and then extrapolate the eye position backwards to determine a starting time. Comparison to the sled position yielded latency when corrected for fast phase processing.

Maximum velocity was found by differentiating eye position and then smoothing. Peak velocity was readily determined, and checked to verify that it occurred within the time bounds of the stimulus.

SUBJECTS

Subjects were two students and one MIT employee. Subject T was a male, 22-24 years old over the course of the various experiments; subject J a 24 year old female; and subject S a 46 year old female. Subject T had extensive exposure to lateral accelerations on the sled, serving as subject for many pilot experiments. The others had occasionally been on the sled in the past. Subjects were tested for vestibular or oculomotor deficits in the Vestibular Laboratory of the Massachusetts Eye and Ear Infirmary. These tests consisted of smooth pursuit, random saccades, earth-horizontal axis VOR (including fixation suppression, optokinetic reflex, and visual-vestibular reflex), posturography, and Z-axis

recumbent ("BBQ spit") rotation. Responses are summarized in Appendix A. No gross abnormalities were noted. Individual differences are discussed in the results chapter.

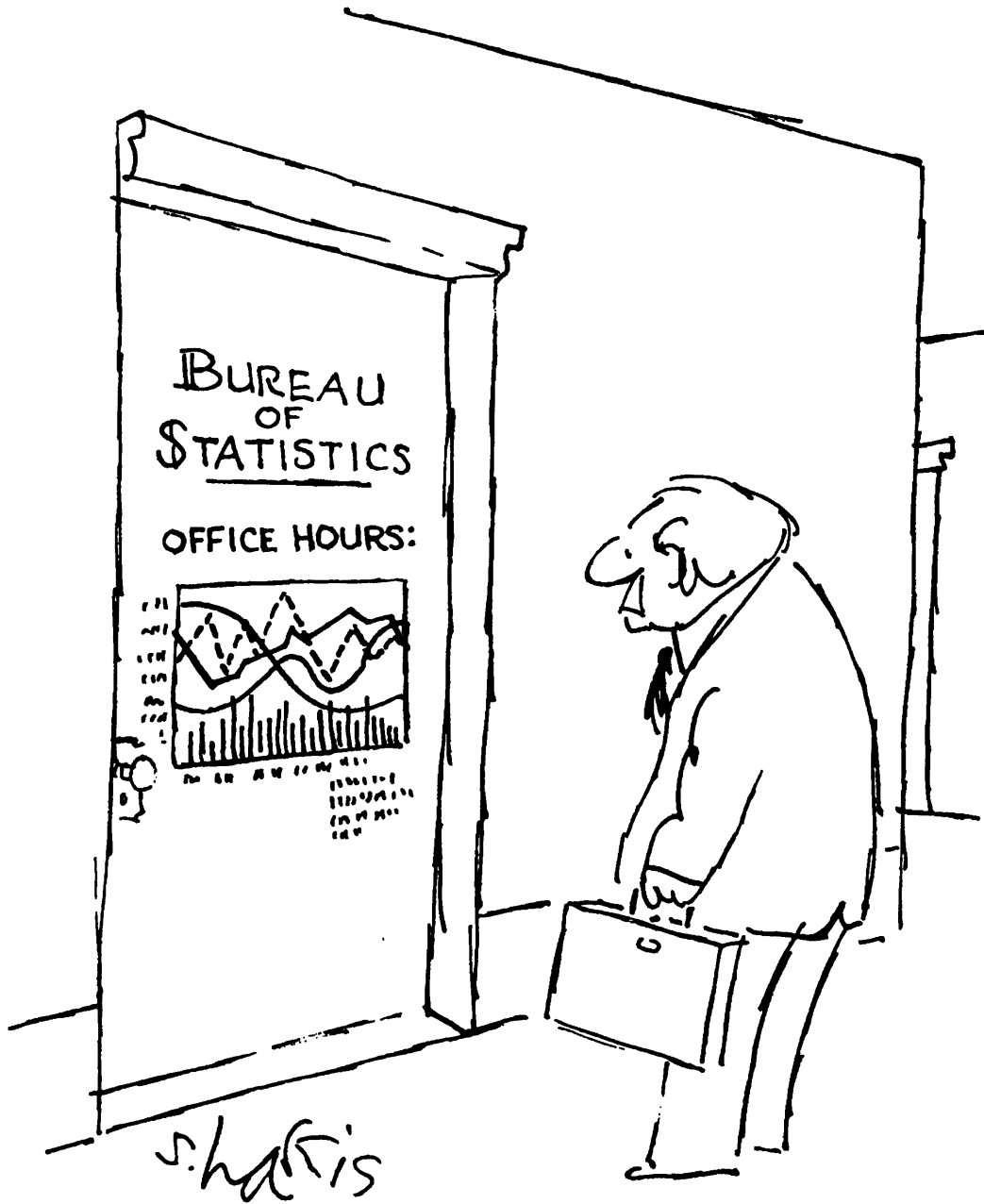
FLASH TEST

Before performing the after-image tracking experiments, a test was run on a separate subject to determine the effect of the light flash on EOG gain. After dark-adapting (as determined by a steady EOG gain, noted by frequent standard calibration maneuvers), the subject was exposed to the same flash, at the same distance, as would be used in the actual experiments. There was no significant lasting change in EOG gain due to the flash.

Frequency (Hz)	0.1 g	0.3 g	0.4 g	0.5 g
0.2	23			
0.3		45	75	120
0.4	11		56	
0.5		27	45	72
0.6	7.5		38	60
0.7		29	32	51
1.0	4.5		23	36

Table 3.1 Peak velocities of sinusoidal stimuli used in the experiments, for a target distance of 2.0 m.

IV Results



LINEAR VESTIBULO-OCULAR REFLEX (LVOR)

Dark LVOR - Sinusoids

Typical LVOR sinusoidal stimuli and responses are shown in Figures 4.1-4.3. For each subject, a trial of 0.2 Hz / 0.1 g and a trial of 0.5 Hz / 0.8 g are presented. The stimulus is in g-units, and the de-saccaded eye position is in degrees. All subjects produced smoother and slightly more periodic responses at the higher acceleration level.

Consistent periodic components in the eye movement responses to sinusoidal accelerations in the dark were found only at 0.3 g and above for subjects J and T, and only at 0.8 g for subject S. For subject J, the higher frequencies (0.6 and 1.0 Hz) at 0.1 g exhibited an occasional periodicity after a few stimulus cycles. The results for J and T are consistent with reported LVOR thresholds of 0.1 g (Kitchen, 1983; Buizza et al., 1979). Only those responses with significant periodic components at the stimulus frequency were analyzed further.

Figures 4.4 and 4.5 show the sinusoidal response gain and phase as a function of frequency. Although gain is in units of velocity per acceleration, phase is measured as velocity with respect to velocity (or position to position). Note that there are no data for 0.2 Hz, as the only trial at this frequency was at 0.1 g, which did not produce a periodic response, as discussed above. Both gain and phase are widely variable over the range of 0.3 to 1.0 Hz. Gains are grouped around 15 deg/s per g, with little increasing or decreasing trend with frequency. Figure 4.5 indicates a slight and fairly consistent phase lead up to 0.7 Hz, dropping off at 1.0 Hz. These values are consistent with past reports (Buizza et al., 1979).

Gain data of subject J are repeated in Figure 4.6 (without the means and standard deviations), with sum-of-sines (SOS) results included. SOS values are within the range

of those from single sine stimuli, except for one aberrant trial. Figure 4.7 presents the analogous phase information. For the narrower-bandwidth SOS (with frequencies of 0.3, 0.5, and 0.7 Hz only), values are close to the single-sine values, with an enhanced high-frequency lead. The wide-bandwidth SOS (0.3, 0.5, 0.7, 1.1, and 1.3 Hz), however, has significant phase variability, even at the low frequencies. The system appears to be relatively linear for frequencies below 1.0 Hz, with increasing nonlinear behavior when higher frequencies are added to the stimulus.

Another linearity analysis is shown in Figure 4.8, for single sinusoids only. Gain as a function of acceleration, although variable, is quite flat over the range presented (0.3 to 0.8 g). Another view of the LVOR gain is presented in Figure 4.9. The mean LVOR gain for each subject (for sinusoidal stimuli) is plotted at the bottom, while the theoretical gain necessary to completely compensate for lateral displacement while viewing a target at two meters distance is plotted at the top. The two meter target distance was used because it is the distance used in the SP and VV experiments. The graph demonstrates how poorly "unconstrained" (i.e. with no visual reference to set vergence or gain) LVOR would compensate for head displacements with close targets.

Dark LVOR - Steps

A typical step response (eye position with fast phases included) is shown in Figure 4.10 along with the acceleration stimulus, a 0.5 g step. Note that the response is not similar to a gaze deviation keyed to acceleration. That is, the eye position does not reverse direction when the acceleration polarity changes, as occurs with static deviations when the head is tilted. Rather, the eye position continues to change in the appropriate compensatory direction for the duration of the stimulus, perhaps indicating a transformation of the sensed acceleration to velocity somewhere in the system.

Step responses were in general much more variable than sinusoidal responses. It was quite rare to obtain anything resembling a step in eye position, and this only occurred for steps of 0.3 g and above. Table 4.1 presents data on the maximum slow phase eye velocity for those few trials which produced step-like responses. Although the data set is small, a trend of increasing velocity with stimulus acceleration is apparent.

These results resemble those of Baarsma and Collewijn (1975), although they were able to obtain reliable results in rabbits with much lower accelerations (0.02 to 0.11 g). They too found eye velocity positively correlated with step magnitude. A typical oculomotor response in their study also increased over the duration of the acceleration phase of the stimulus. However, when their animals were decelerated, the eyes immediately reversed direction, responding to the acceleration sense of the stimulus. The methodology in these experiments used lateral acceleration as the stimulus and vertical eye movements as the response. Since rabbits have eyes on the sides of their heads, this corresponds to a reflex which compensates for head tilt with respect to gravity, analogous to ocular counterrolling (OCR) in humans. Indeed, OCR in humans does have similar acceleration-dependent response properties (Lichtenberg, 1979). In addition, both rabbit vertical eye movements and human OCR exhibit phase lags over the 0.2 to 1.0 Hz range, whereas the human LVOR examined here exhibits phase lead over the same range. This again indicates the likelihood of a velocity-dependent response for human LVOR.

Dark LVOR - Luminous Line

Results with the luminous line were disappointing. No significant improvements were noted over the case of complete darkness. In some cases, the line seemed to produce poorer oculomotor responses. Several reasons for this can be suggested. First, the line might not have been sufficiently homogeneous. The luminous chemical liberates gas, which tended to form bubbles in the line after about half an hour of use. These bubbles,

and some slight variations in the machining of the mounting bar, may have provided sufficient fixation points to inhibit eye movements. Second, it is possible that the accommodative control of vergence was not powerful enough to have the desired effect. Subjectively, considerable effort was needed to maintain a sharp focus on the horizontal line, and to detect when the focus was not sharp. A vertical line would have served this purpose better, as loss of accommodation would cause the line to appear double; but of course this would not allow for unrestricted horizontal eye movements. Third, the line may have provided enough ambient illumination within the sled canopy to provide peripheral fixation cues.

AFTER-IMAGE TRACKING

Samples of after-image (AI) tracking and dark LVOR responses for each subject are in Figures 4.11-4.13. Each figure is a plot of the corresponding AI and LVOR de-saccaded eye position responses overlaid. The LVOR trials are the same as those in Figures 4.1b, 4.2b, and 4.3b in the LVOR section (0.5 Hz / 0.8 g sine stimuli). These results are typical, and demonstrate the dramatic improvement in response due to the after-image. Note that the dark LVOR is somewhat inconsistent and, although periodic, not very sinusoidal. The after-image tracking, on the other hand, is very consistent, sinusoidal, and of a much higher amplitude.

Additionally, the AI condition produced far fewer nystagmus fast phases. Subject J's AI and LVOR responses from Figure 4.11 (0.5 Hz / 0.8 g sine trial) are presented again in Figure 4.14 without fast phases removed. Comparison with Figure 4.11 shows that the LVOR response is highly nystagmic with many fast phases, while the AI response has few.

The AI data are summarized in Figures 4.15 and 4.16, which present AI gain and phase as a function of frequency for single-sinusoid stimuli. These graphs can be compared directly to Figures 4.4 and 4.5. There appears to be a significant downward trend of gain with frequency, but a relatively constant phase lead. The gains and phase leads are much larger than those for the LVOR dark condition. If the outlying values at 0.2 Hz are disregarded, the remaining trend approximately resembles a 2:1 gain reduction over 0.1 to 1.0 Hz.

The gain and phase responses can be normalized with respect to the corresponding LVOR responses, to better reveal the improvement due to AI tracking. This analysis is presented in Figures 4.17 and 4.18, for sinusoidal stimuli. The ratio of AI gain to LVOR gain, in Figure 4.17, reinforces the interpretation of response amplitude enhancement with an after-image. Likewise Figure 4.18 demonstrates the overall phase advance with AI tracking, by plotting the difference between AI phase and LVOR phase.

SOS responses for subject J are compared to this subject's sinusoidal responses in Figures 4.19 and 4.20. SOS gains are again within the same range as the sinusoidal gains, but phase values of the high-frequency components of the wide-bandwidth SOS drop considerably above 0.7 Hz.

Statistical test results of the AI/LVOR comparison are in Table 4.2. Paired t-tests, comparing corresponding frequency and acceleration trials, were made separately for each subject and for sinusoidal and random stimuli. AI gain is significantly higher than LVOR gain in all cases ($p < 0.005$). Phase results were less consistent. Subjects J and T had significant AI phase leads ($p = 0.05$, $p = 0.025$, $p < 0.005$). AI phase was not significantly different from LVOR phase for subject S.

Figure 4.21 shows the AI gain in a manner identical to that of Figure 4.9 for LVOR gain. The mean AI gain for each subject (for sinusoidal stimuli) is plotted at the bottom, and the theoretical gain needed to compensate for lateral displacement while viewing a target at two meters distance is plotted at the top. Comparing Figure 4.9, we see that tracking the after-image not only increases the response gain, but also seems to increase it in a way that would help to compensate for an actual fixed target. This effect lends support to the notion that the smooth pursuit system is involved in AI tracking.

Occasionally during AI trials, the subject will report (after the test) that the after-image had been "lost" temporarily, and that the subject had to bring his or her eyes back to the center to "find" it. An example of this is shown in Figure 4.22. After a few cycles of vigorous high-amplitude tracking, there is an obvious break in the pattern. At this point the eyes tend to come to the center, and eventually re-establish sinusoidal tracking. It appears that this "losing" of the after-image may occur when the eyes anticipate the remaining portion of a cycle and rush ahead, creating a significant phase lead from the actual sled position stimulus to the eye position. Careful investigation of the few occurrences of this phenomenon did not reveal a correlation with response phase, eye velocity, or stimulus magnitude. The perceptual issue involved is an interesting one, as apparently a discrepancy between anticipated sled motion (as indicated by the eye movement) and actual sled motion leads to some type of sensory conflict which is powerful enough to override the actual presence of the after-image. Complete fading of the after-image was not responsible for these effects, as can be seen by the fact that tracking continues again (with the same after-image) after the after-image has been "found". However, it is well known that after-images go through several positive and negative stages (Brown, 1965), and the image may indeed not be visible during these phase transitions. This periodic fading of the image may be the simplest explanation for the phenomenon.

Another interesting but sporadic occurrence is illustrated in Figures 4.23a and 4.23b. In about ten to twenty per cent of the AI trials, the response continued for a short time after the cessation of the stimulus (this will sometimes be called an “ongoing” response in further discussion). For subject T, this only occurred when the response phase lead was less than 30 degrees (0.8 g/0.7 Hz, 0.5 g/0.7 Hz, 0.5 g/1.0 Hz, 0.8 g/1.0 Hz). It was not correlated with response gain or response amplitude. For subject J, the effect was more prevalent but less obvious on average, and did not seem to be related to phase. Subject S had the fewest occurrences. Also in Figure 4.23b is an example of the same effect in a sample of dark LVOR data. Ongoing responses were very rare in this condition, but did occur occasionally. They were slightly less rare in smooth pursuit trials, where tracking continues after stimulus end, with a reversal of the eye direction even though the stimulus has stopped.

SMOOTH PURSUIT & VISUAL+VESTIBULAR (SP & VV)

SP & VV - Sinusoids

Overlaid graphs of corresponding SP and VV responses (and the stimulus waveform) are in Figures 4.24-4.26, for 0.3 Hz / 0.5 g sine stimuli, for each subject individually. All signals are position in degrees, and the eye movements have been de-saccaded. Close inspection reveals that the VV responses match the stimulus more closely than do the SP responses. For subject S especially the difference is very apparent. Note also the brief ongoing response (reversal in eye movement after stimulus end) in Figure 4.24.

Gain and phase plots comparing smooth pursuit (SP) tracking to visual plus vestibular (VV) tracking, for single sinusoid and sum-of-sines (SOS) stimuli, for each subject individually, are in Figures 4.27 to 4.38. The sinusoidal gain data show a small but consistent higher gain with the additional vestibular information (VV>SP). High variability at 1.0 Hz may be due to a lack of the ability of the sled to accurately reproduce

sines at this frequency, and also to some motion of the subject's head relative to the sled. SOS data indicate the same general trend, especially evident in Figure 4.37 (note that subject T was not tested with the wide-bandwidth SOS). Although it may appear strange at first that the SOS gain increases somewhat with frequency, this phenomenon is reported in the literature (Collewijn & Tamminga, 1984). It may be an attempt by the system to track the highest frequency accurately, sacrificing performance at the lower frequencies.

Phase plots do not yield a general trend. All phase lags tend to increase above 0.7 Hz. Gain ratios and phase differences, comparing corresponding VV and SP trials, are plotted in Figures 4.39 and 4.40. Table 4.3 contains results of paired t-tests performed on corresponding VV and SP trials, separately for each subject and for sinusoids and SOS. All VV gains are significantly higher than the corresponding SP gains; this is especially so for subject S. Phase differences are not as strong; only subject S had consistently lower phase lags in the VV condition.

SP & VV - Steps

Figure 4.41 plots SP and VV step response maximum velocity against the maximum velocity of the corresponding step stimulus. The SP data show a saturation at about 60 deg/sec. The VV data show no saturation effect. It appears that the vestibular stimulation allows the oculomotor tracking to overcome the SP saturation.

Similar data for SP and VV latencies are in Figure 4.42. The trend is not nearly so clear in this case, but most of the VV responses do have a shorter latency.

FIXATION SUPPRESSION

The complementary condition to VV is fixation suppression (FS), presented in Figures 4.43 and 4.44. As for the LVOR analysis, trials were reviewed manually to determine those with consistent periodic components at the stimulus frequency. Also as before, only stimuli greater than 0.1 g yielded consistent responses. All subjects have reduced oculomotor responses compared to LVOR in the dark, although suppression is not complete. The ratio of FS gain to LVOR gain was found for those nineteen pairs of trials which produced, with identical stimuli, identifiable periodic responses. This ratio varied from 0.11 to 0.47, and did not appear to follow a trend with frequency or acceleration.

ANTI-COMPENSATORY MOVEMENTS

An example of a VV step response is in Figure 4.45. Note that there is a very short-latency response in the "incorrect" direction, that is, in the anti-compensatory direction. Several trials exhibited this phenomenon. It was most prevalent during the VV condition, and for steps above 0.1 g. The magnitude of this component seemed to be loosely correlated with stimulus step magnitude. Close examination of the unfiltered eye movement records verified that this movement was not purely saccadic, although it has been suggested (L. R. Young, personal communication) that it may be a saccade superimposed on smooth pursuit that had already commenced.

The presence of this effect made PRBS-evoked responses very difficult to analyze, as the PRBS stimulus is basically a series of randomly-spaced acceleration steps. At each step, there is a certain probability that this anti-compensatory response component will occur, as shown for a sample PRBS trial in Figure 4.46. For this reason, PRBS data are not included in this report. Further research in this area might go towards recognizing and removing these responses when they occur, and then analyzing the remaining signal.

Resulting models might include a stochastic additive process which introduces the anti-compensatory components into the slow phase velocity.

SUMMARY AND COMPARISON WITH CLINICAL DATA

Appendix A presents a summary of the clinical tests performed on each of the subjects. On the smooth pursuit test, all subjects' gains were similar and in the normal range. Subject S's phase lag was slightly but consistently larger than that of subjects J and T. In the experiments performed in the present study, and discussed previously, subject S had a consistently larger phase lag than the other subjects. This subject also had a considerably lower gain than the others, which is not indicated by the clinical test. The tests in this study, however, went well beyond the clinical ones in terms of frequency (1.0 Hz pure sine versus 0.3 Hz) and peak velocity (120 versus 33.9 deg/s). Thus it is to be expected that subject S's performance be reduced, consistent with the phase lag in the clinical data and the literature on aging and smooth pursuit (Sharpe & Sylvester, 1978; Spooner, Sakala & Baloh, 1980). (Recall the ages of the subjects: J: 24, S:46, T:22-24.)

The clinical random saccade data are consistent with this analysis. Subjects J and T had mean saccadic latencies of 0.173 and 0.168 sec, respectively. Mean latency for subject S was 0.210 sec, about 24% greater. Increased delays in input and output processing (discussed in the modelling section) would provide an explanation for both the pursuit lag and saccade latency results.

VOR gains for subjects S and T were near the high end of the distribution for normal clinical subjects. Gains for subject J were generally on the low side of normal. All phases were consistently close to normal. Subject J's VVOR gain, however, was higher than normal, and higher than that of the other subjects.

In the ZAR results, subject S produced an abnormally low SCC time constant (TAU). This value is not consistent with this subject's VOR phase characteristic. (Note, however, that the VOR and ZAR tests were performed on different days for this subject.) The other interesting anomaly in this data is subject J's low modulation and bias components (MOD and BIAS).

A clear and concise picture of the relationship of the clinical tests to the data from the present study is not evident. Certainly for subject S, the increased oculomotor delays are consistent across the various tests. Part of subject J's reduced VOR and ZAR responses may be due to this subject's especially fatigued state on the day of the experiments. It is interesting to note that subject J had the lowest VOR gain, but the highest VVOR gain, indicating that either: 1) fatigue was present but greatly overcome in novel or lighted conditions; or 2) an especially high visual "weighting" compensates for an especially low vestibular "weighting" in this subject. The data from the present study do not support the second hypothesis, as LVOR and AI gain values for subject J are within or even above those for the others.

Note that subject S had the largest VV/SP ratio (Figure 4.39) (since the SP gain was so low). But this subject also had the lowest AI/LVOR ratio and did not have the highest LVOR gain. This leads to the conclusion that acceleration information modulates smooth pursuit so as to bring the gain close to one, as opposed to just adding to the SP response.

Acceleration (g)	Maximum Eye Velocity (°/sec)
0.3	11
0.3	13
0.5	19
0.5	25
0.8	44

Table 4.1 Maximum eye velocity reached during dark LVOR acceleration step responses.

Sum of Sines

Subject	Variable	Measurements	t Statistic	p
J	Gain	16	8.07	<0.005
J	Phase	16	2.01	0.05
S	Gain	14	5.15	<0.005
S	Phase	16	0.16	NS
T	Gain	0		
T	Phase	0		

Sinusoids

Subject	Variable	Measurements	t Statistic	p
J	Gain	15	9.17	<0.005
J	Phase	15	2.48	0.025
S	Gain	5	5.20	<0.005
S	Phase	5	-0.25	NS
T	Gain	12	5.91	<0.005
T	Phase	12	3.79	<0.005

Table 4.2 Results of paired t-tests comparing After-Image tracking to Linear VOR. Tests are one-sided, testing for (AI gain > LVOR gain) in the upper table, and (AI phase > LVOR phase) in the lower table. (NS=not significant).

Sum of Sines

Subject	Variable	Measurements	t Statistic	p
J	Gain	19	1.97	0.05
J	Phase	19	-0.30	NS
S	Gain	19	3.75	<0.005
S	Phase	19	2.00	0.05
T	Gain	19	1.93	0.05
T	Phase	19	-2.46	NS

Sinusoids

Subject	Variable	Measurements	t Statistic	p
J	Gain	16	1.66	0.10
J	Phase	16	2.26	0.025
S	Gain	16	7.27	<0.005
S	Phase	16	3.95	<0.005
T	Gain	6	4.49	<0.005
T	Phase	6	1.03	0.20

Table 4.3 Results of paired t-tests comparing Visual+Vestibular tracking to Smooth Pursuit. Tests are one-sided, testing for (VV gain > SP gain) in the upper table, and (VV phase < SP phase) in the lower table. (NS=not significant).

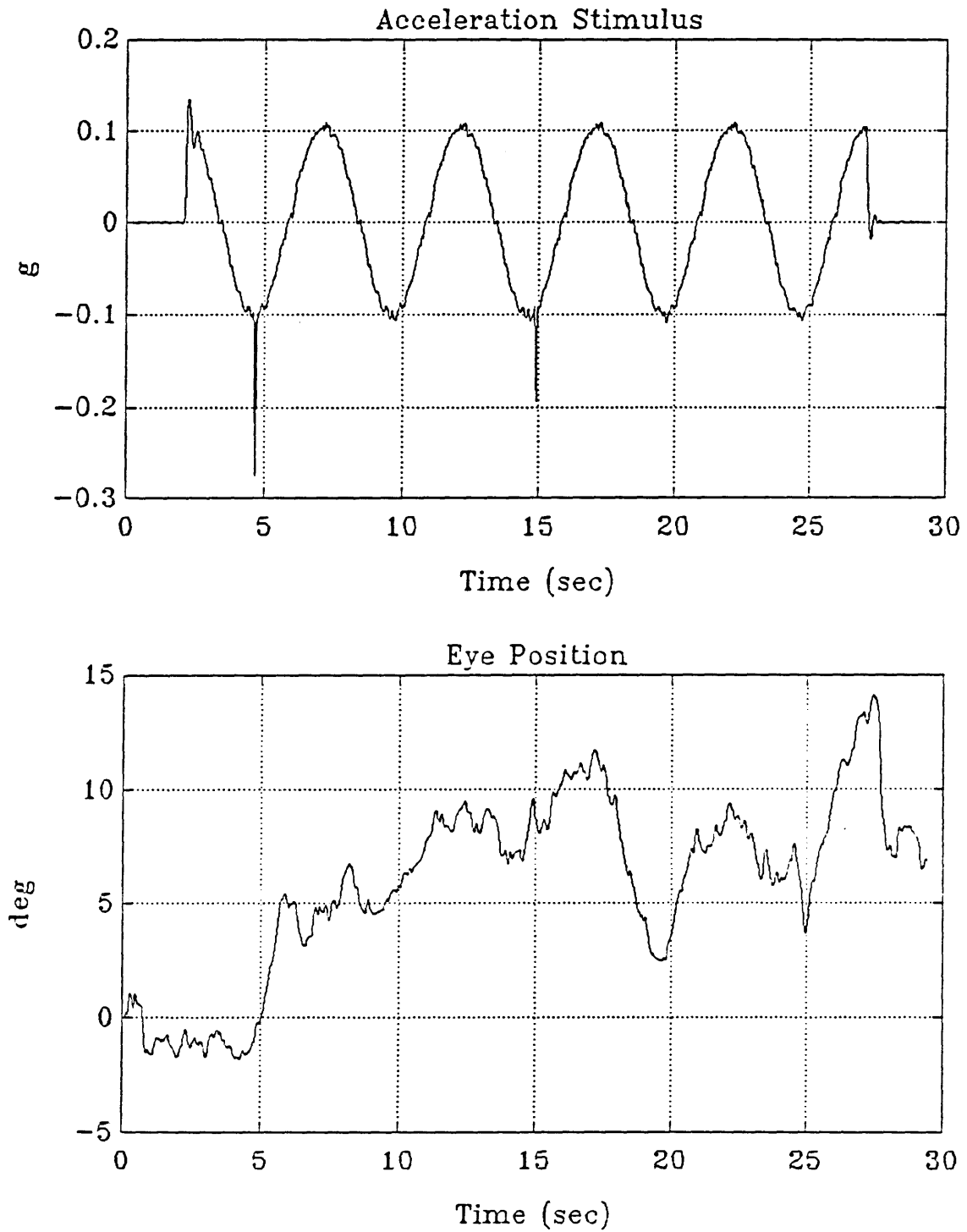


Figure 4.1a Example of dark LVOR acceleration stimulus (top) and eye position response (bottom). Subject J, 0.2 Hz, 0.1 g.

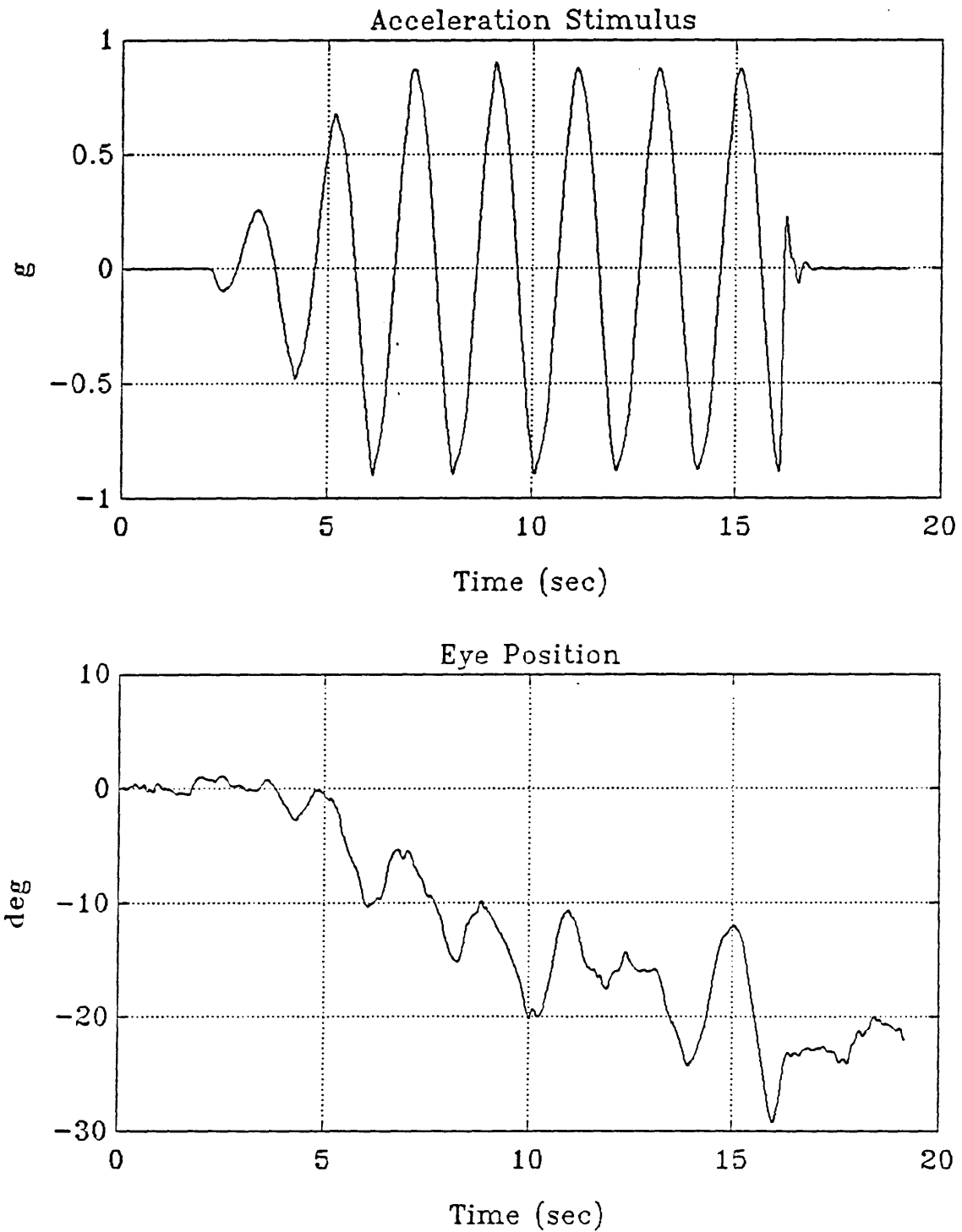


Figure 4.1b Example of dark LVOR acceleration stimulus (top) and eye position response (bottom). Subject J, 0.5 Hz, 0.8 g.

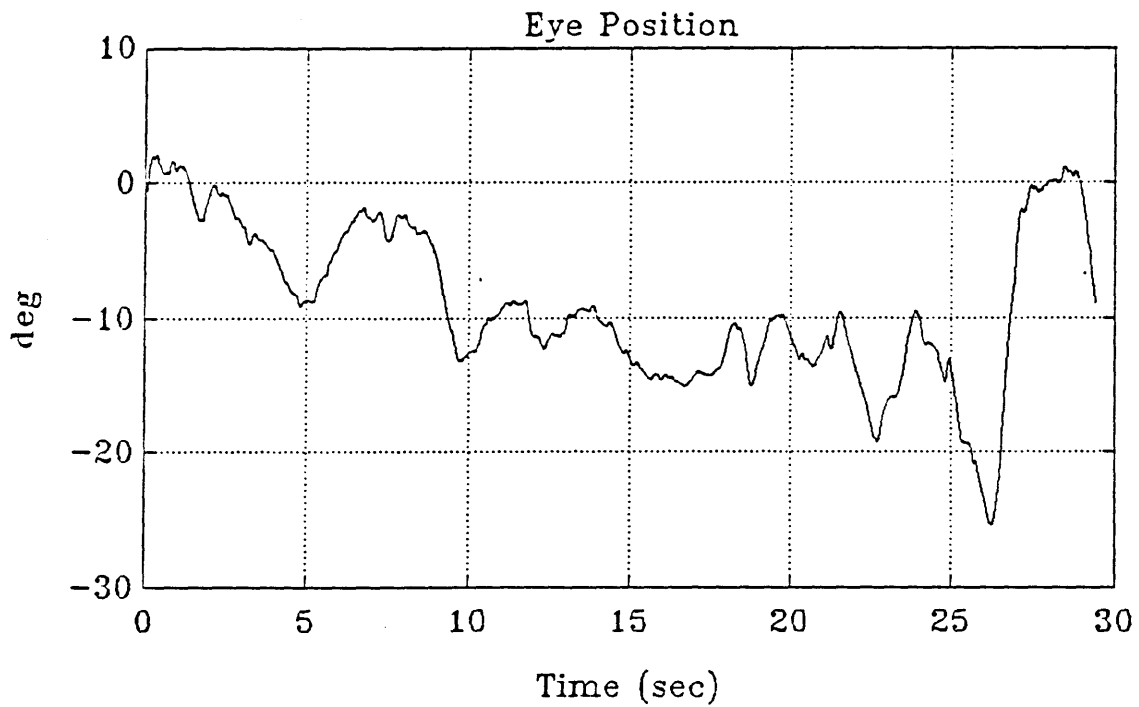
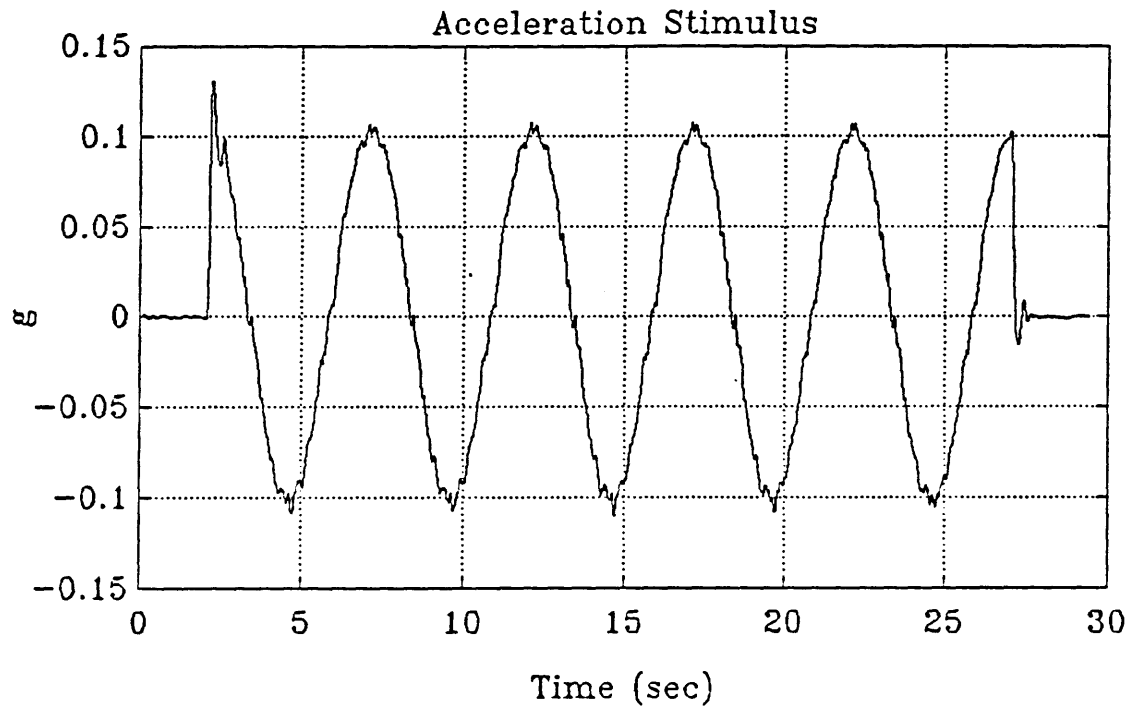


Figure 4.2a Example of dark LVOR acceleration stimulus (top) and eye position response (bottom). Subject S, 0.2 Hz, 0.1 g.

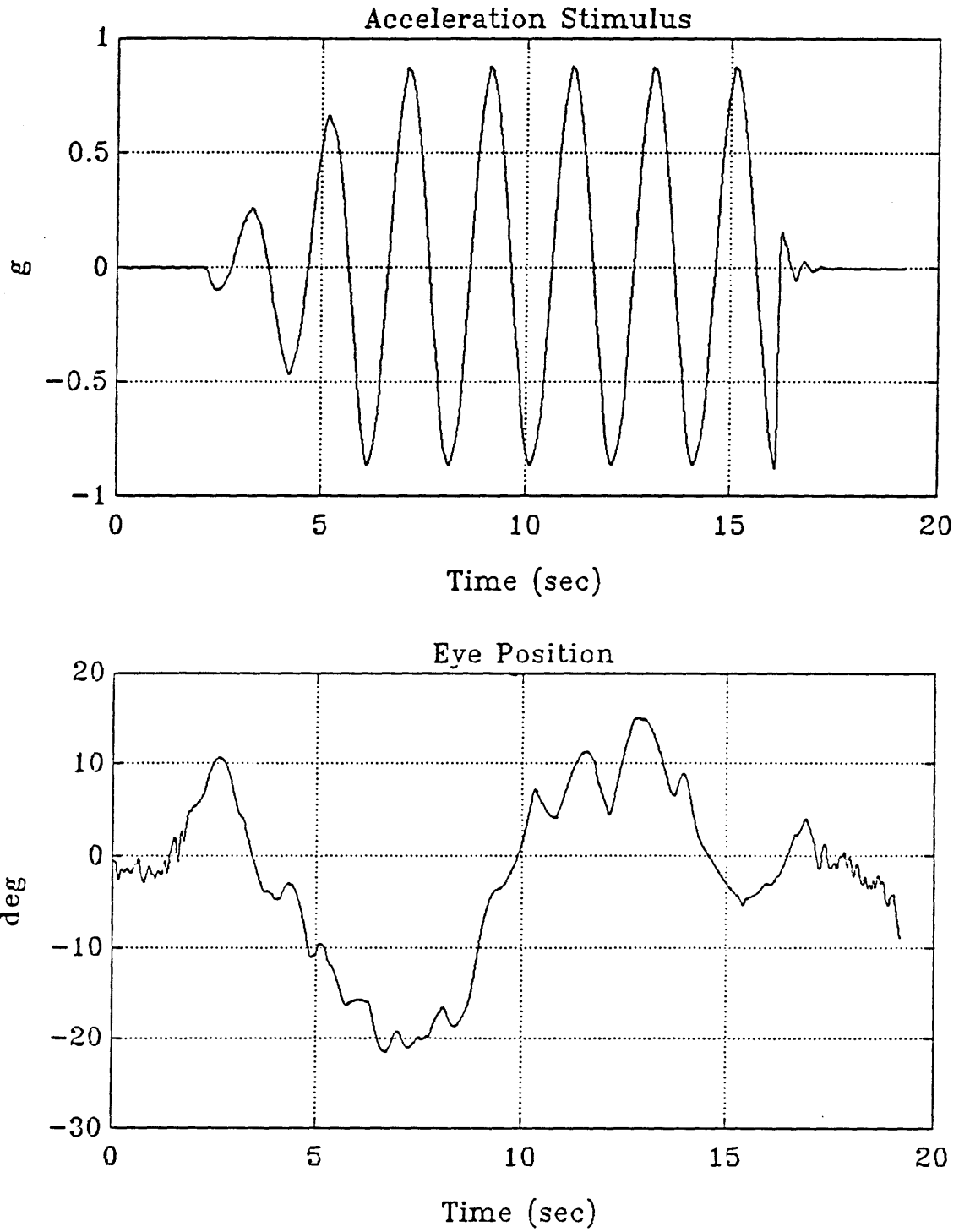


Figure 4.2b Example of dark LVOR acceleration stimulus (top) and eye position response (bottom). Subject S, 0.5 Hz, 0.8 g.

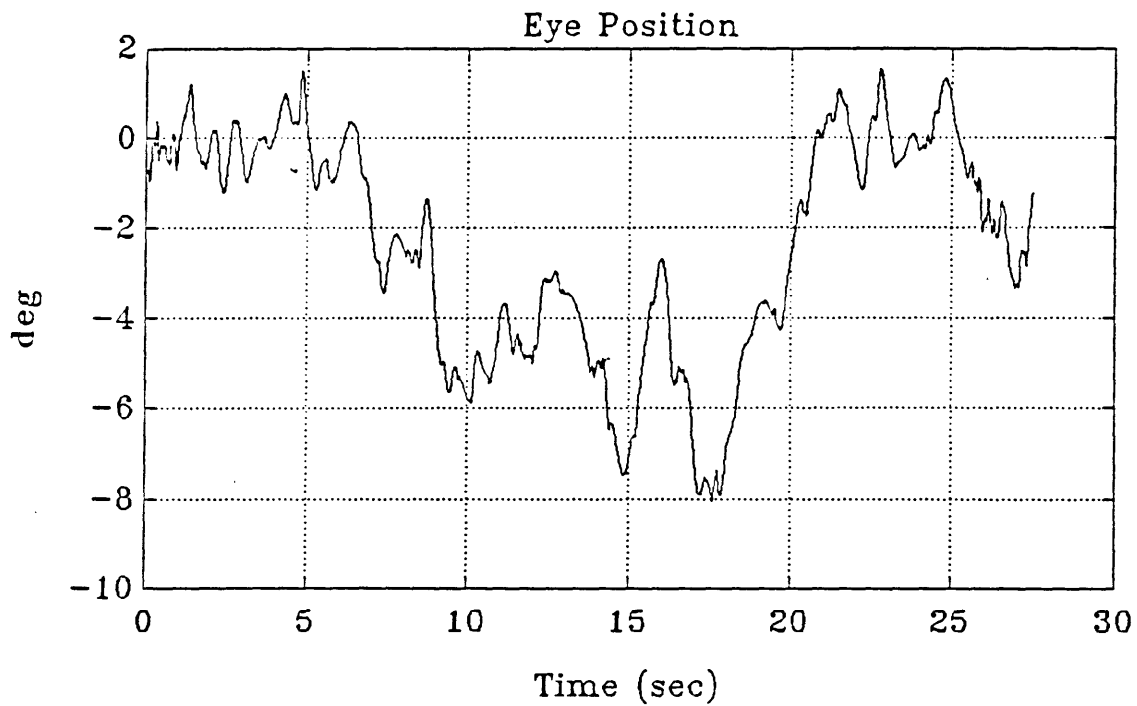
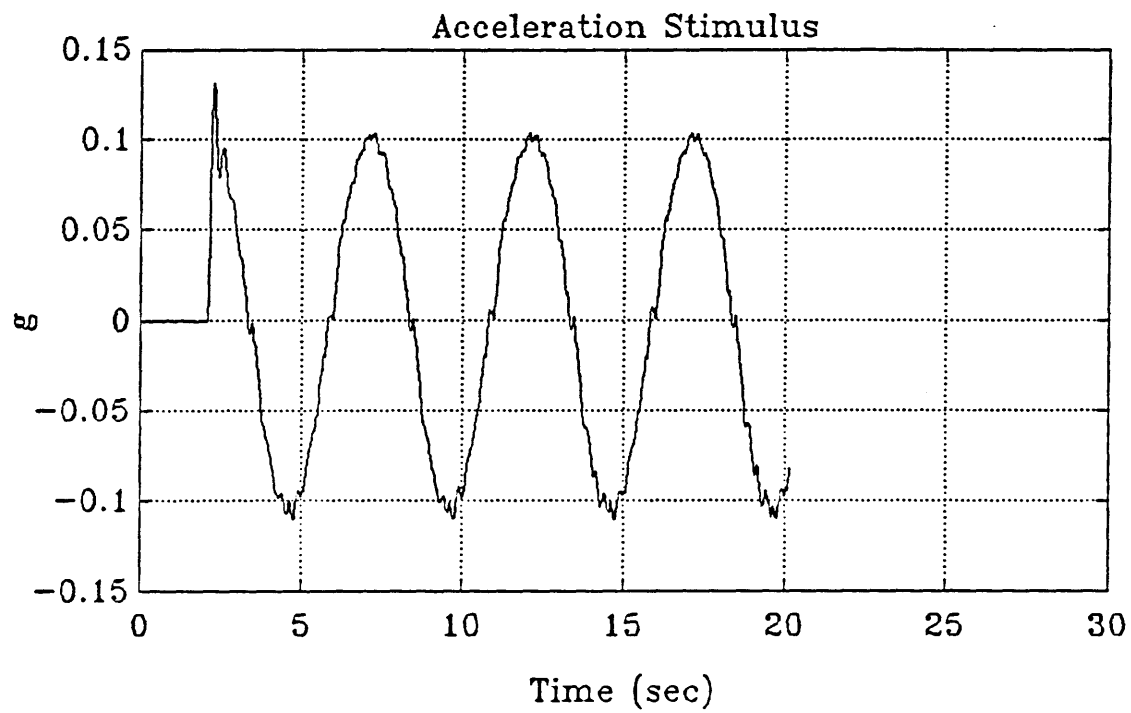


Figure 4.3a Example of dark LVOR acceleration stimulus (top) and eye position response (bottom). Subject T, 0.2 Hz, 0.1 g.

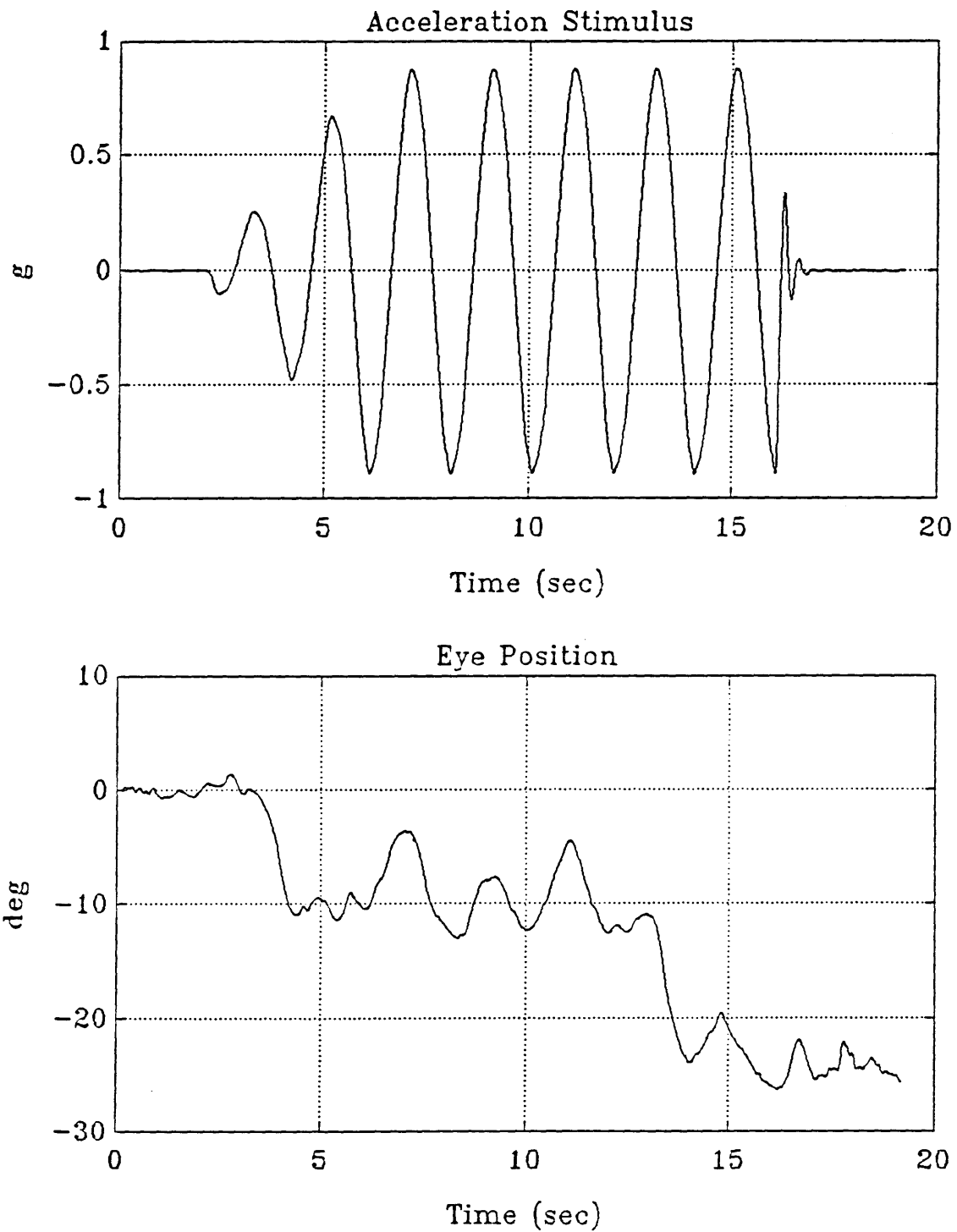


Figure 4.3b Example of dark LVOR acceleration stimulus (top) and eye position response (bottom). Subject T, 0.5 Hz, 0.8 g.

LVOR - Dark
Single Sinusoids

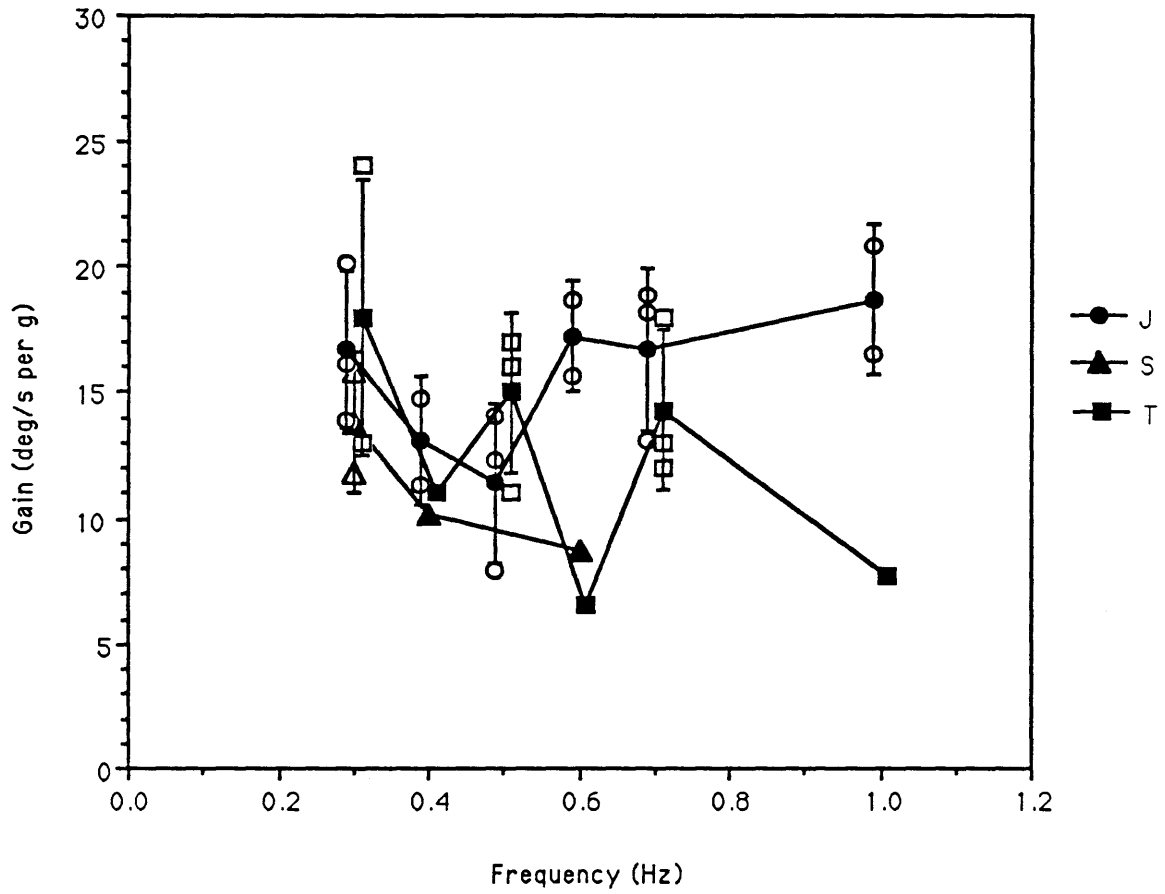


Figure 4.4 Linear vestibulo-ocular reflex in the dark with predictable sinusoids; gain for all three subjects. (Solid symbols are means for each subject at each frequency. Bars are ± 1 s.d.)

LVOR - Dark
Single Sinusoids

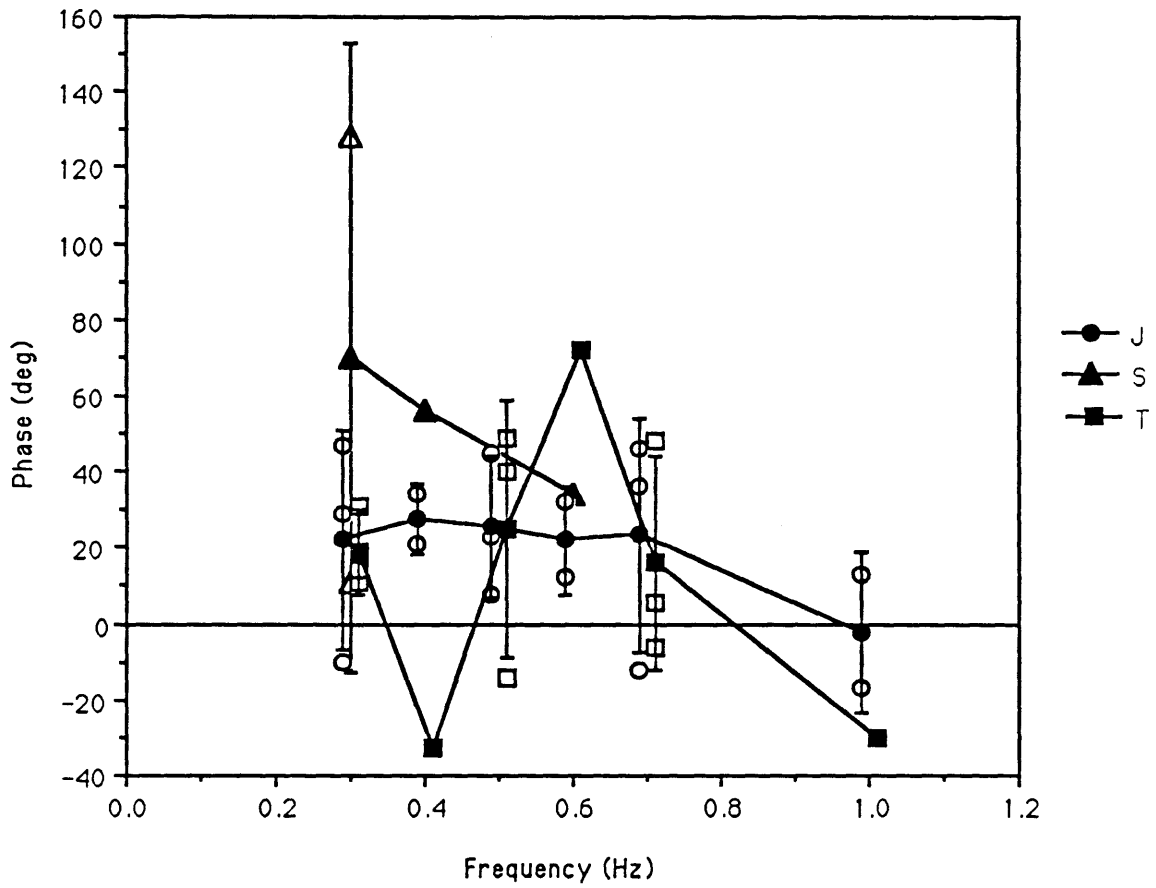


Figure 4.5 Linear vestibulo-ocular reflex in the dark with predictable sinusoids; phase for all three subjects. (Solid symbols are means for each subject at each frequency. Bars are ± 1 s.d.)

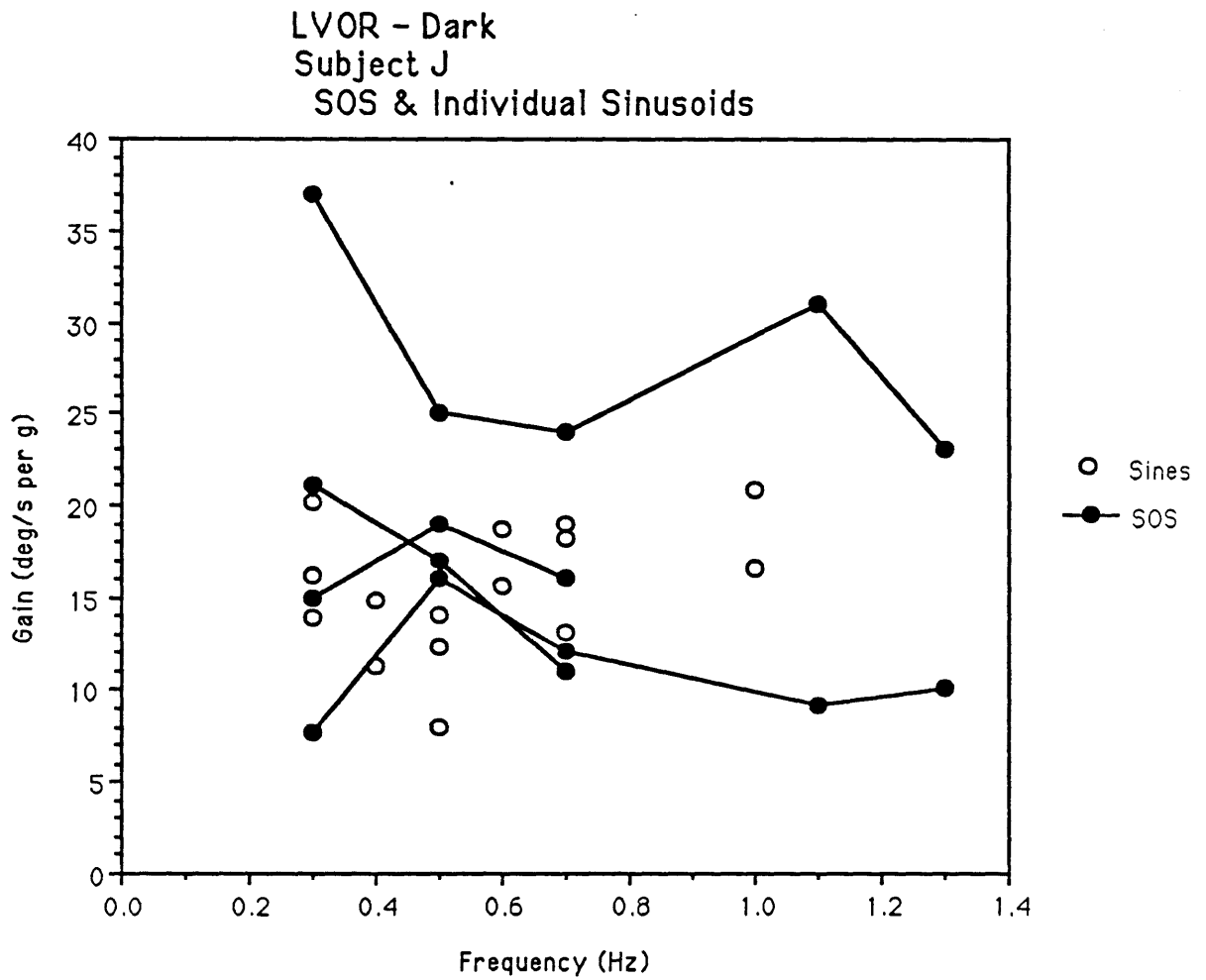


Figure 4.6 Gain of linear vestibulo-ocular reflex in the dark for subject J; predictable sinusoids and unpredictable sum-of-sinusoids. (Means of sine data are plotted.)

LVOR - Dark
Subject J
SOS & Individual Sinusoids

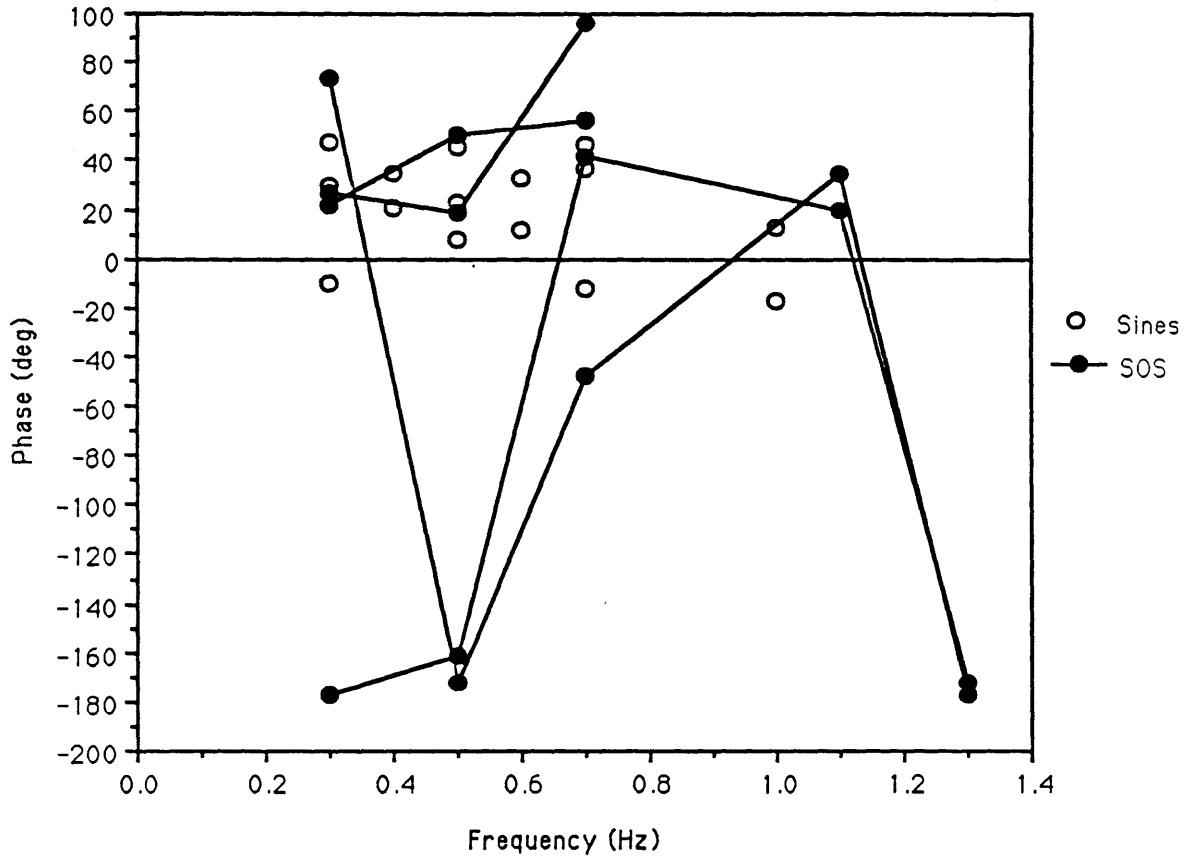


Figure 4.7 Phase of linear vestibulo-ocular reflex in the dark for subject J; predictable sinusoids and unpredictable sum-of-sinusoids. (Means of sine data are plotted.)

LVOR - Dark
Gain vs. Acceleration

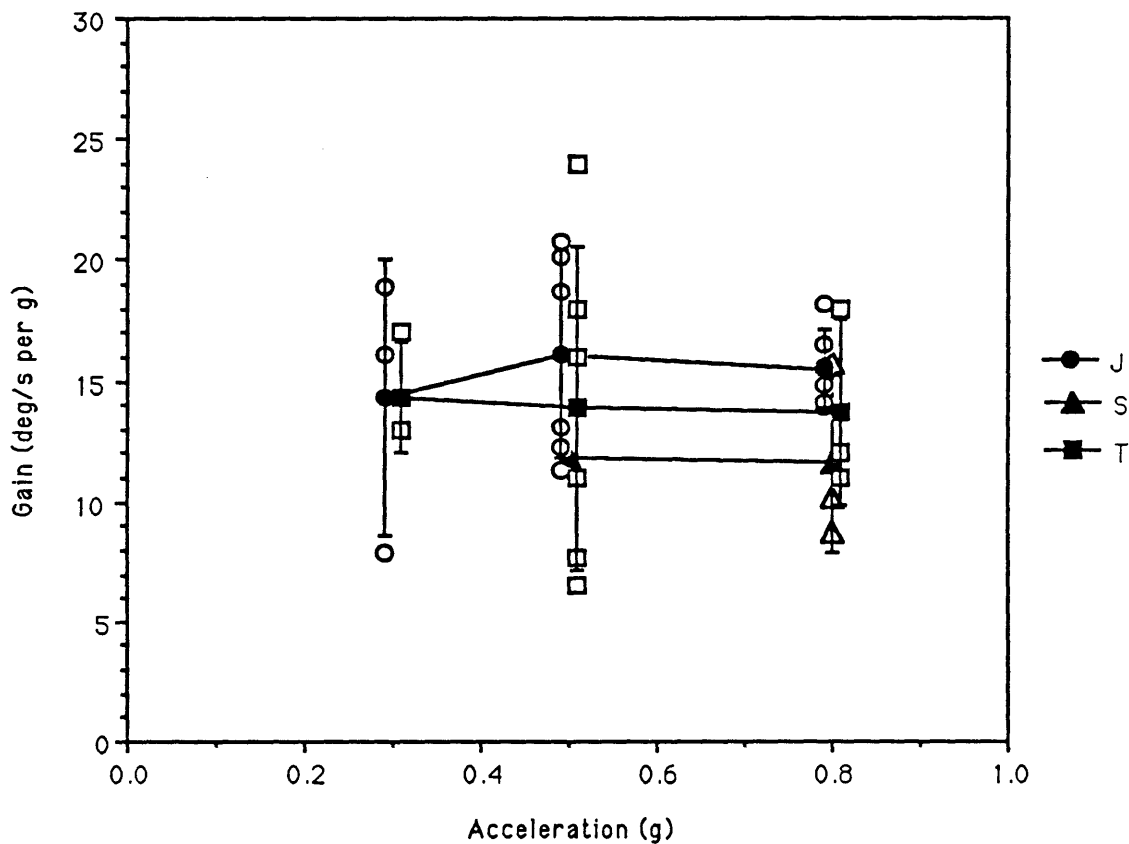


Figure 4.8 Gain of linear vestibulo-ocular reflex gain as a function of peak acceleration of sinusoidal stimulus. (Solid symbols are means for each subject at each frequency. Bars are ± 1 s.d.)

LVOR - Dark
with Theoretical Compensatory Gain

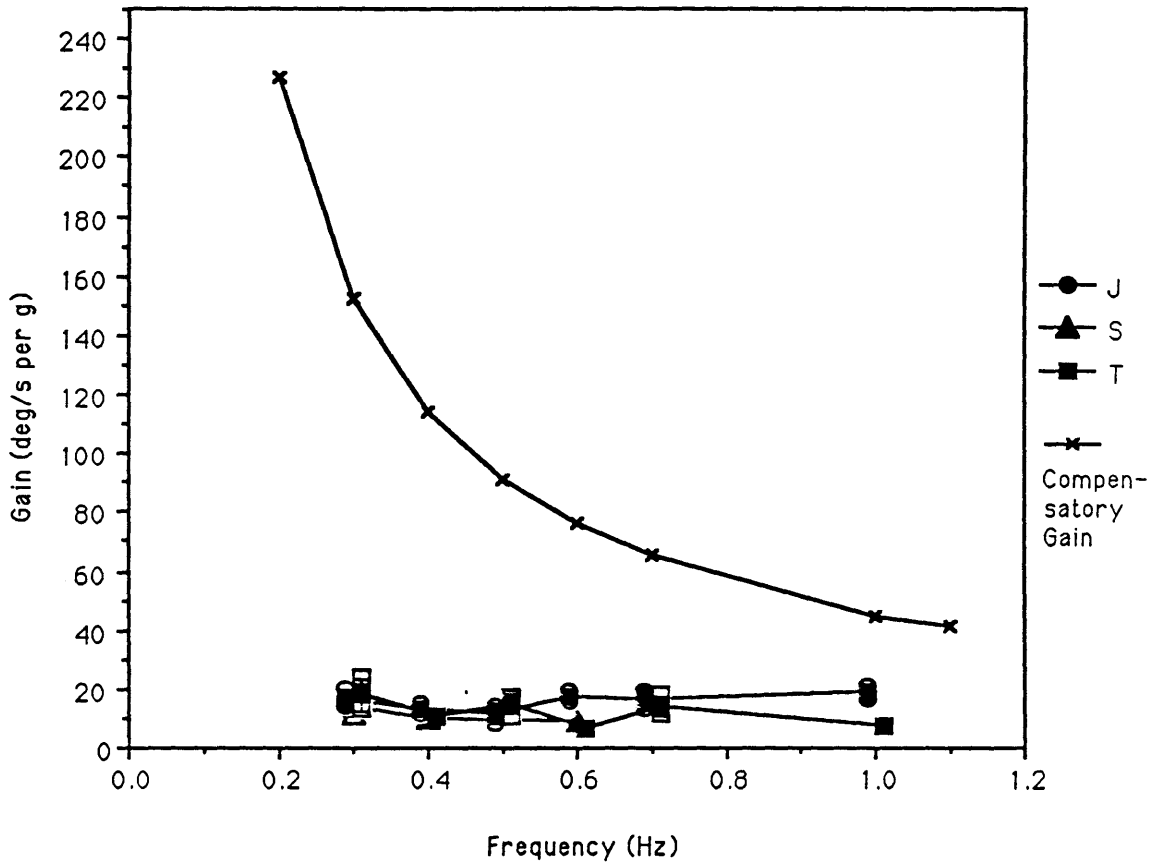


Figure 4.9 Linear vestibulo-ocular reflex with predictable sinusoids; gain for all three subjects. The calculated gain required to produce perfect compensatory eye movements for a target at two meters distance is also shown. (Solid symbols are means for each subject at each frequency. Bars are ± 1 s.d.)

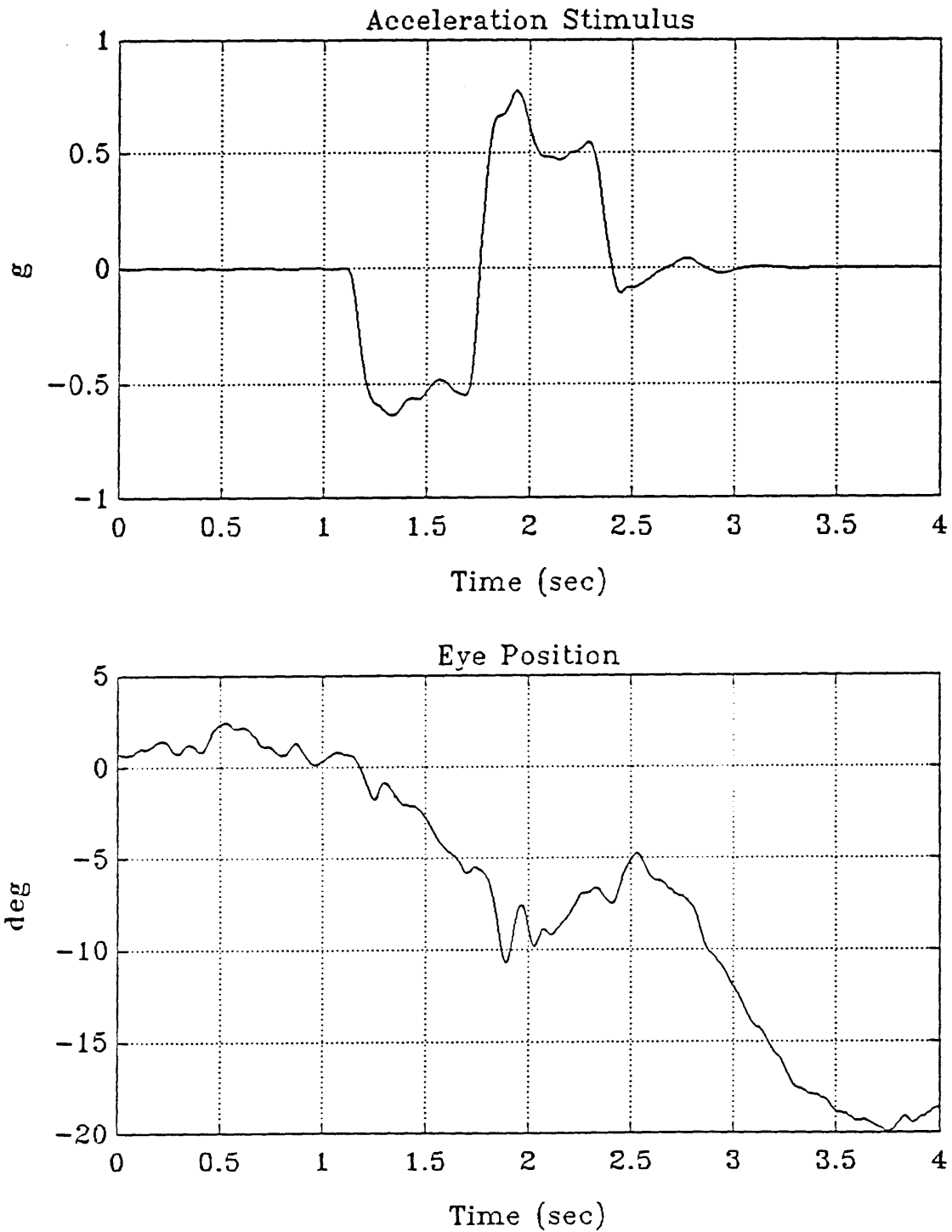


Figure 4.10 Dark LVOR step response; acceleration stimulus and eye position. Fast phases not removed. Subject S, 0.5 g step.

After-Image and Dark LVOR

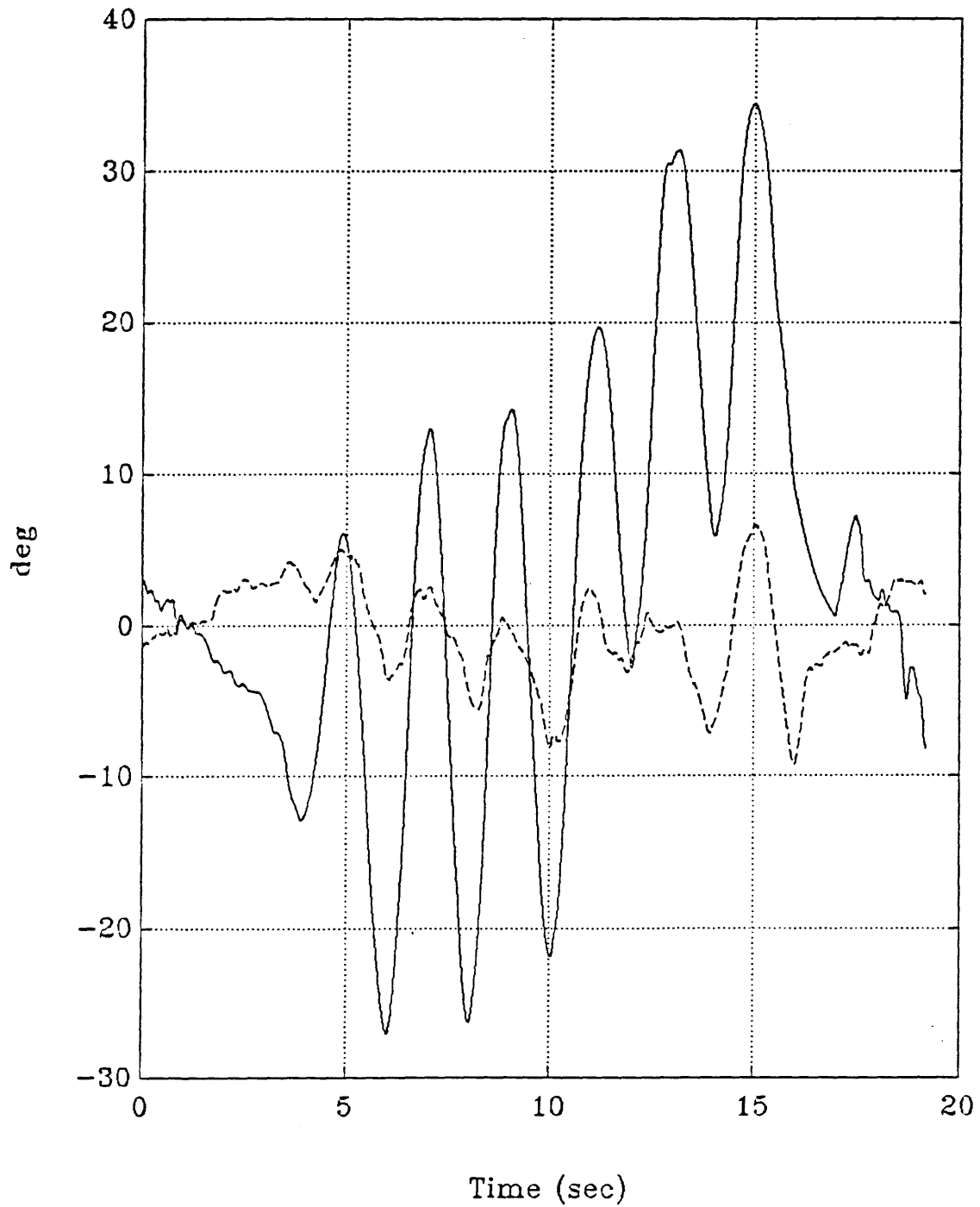


Figure 4.11 Example of dark LVOR (dashed line) and AI tracking (solid line) eye position responses. Subject J, 0.5 Hz, 0.8 g. LVOR response is that shown in Figure 4.1b.

After-Image and Dark LVOR

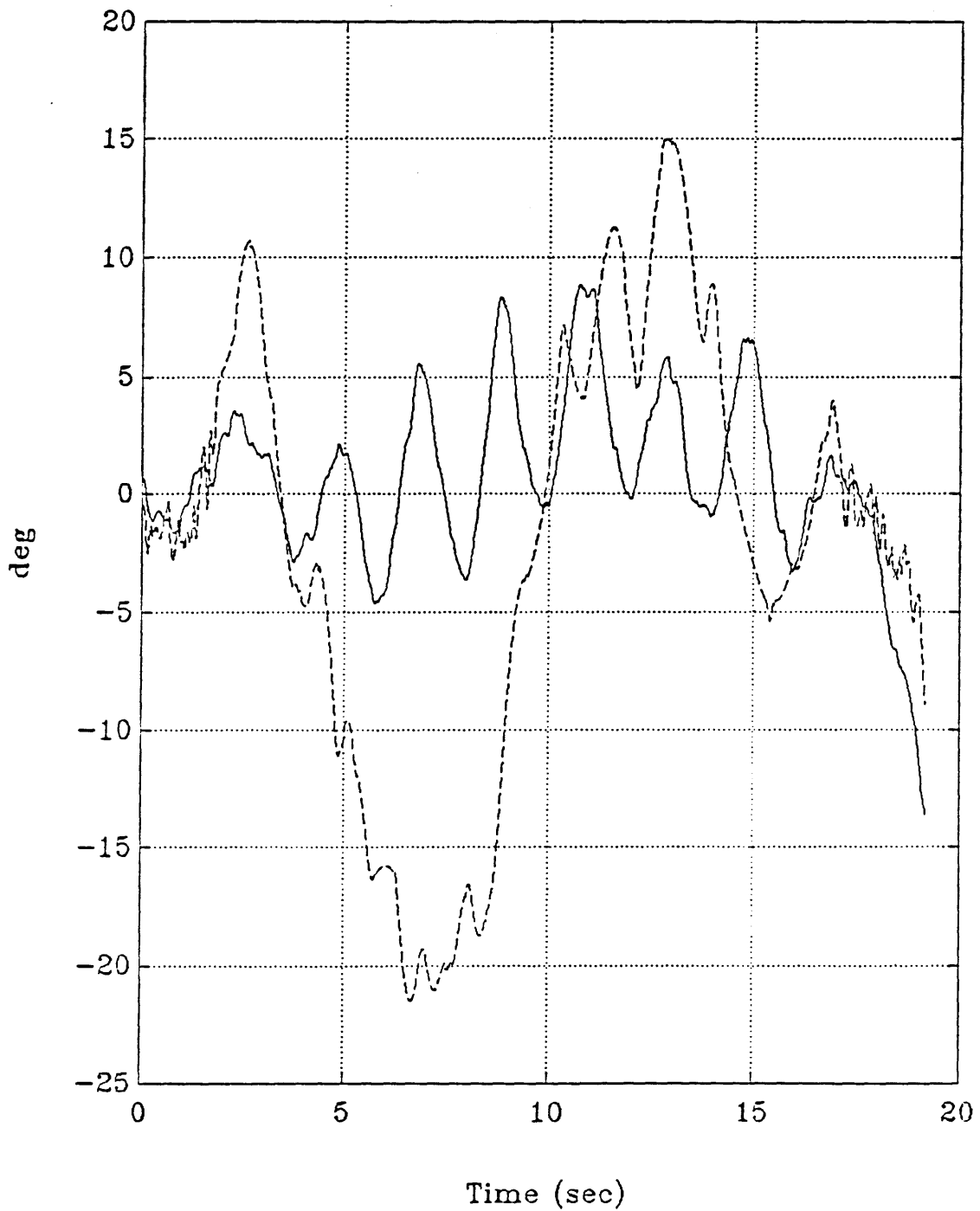


Figure 4.12 Example of dark LVOR (dashed line) and AI tracking (solid line) eye position responses. Subject S, 0.5 Hz, 0.8 g. LVOR response is that shown in Figure 4.2b.

After-Image and Dark LVOR

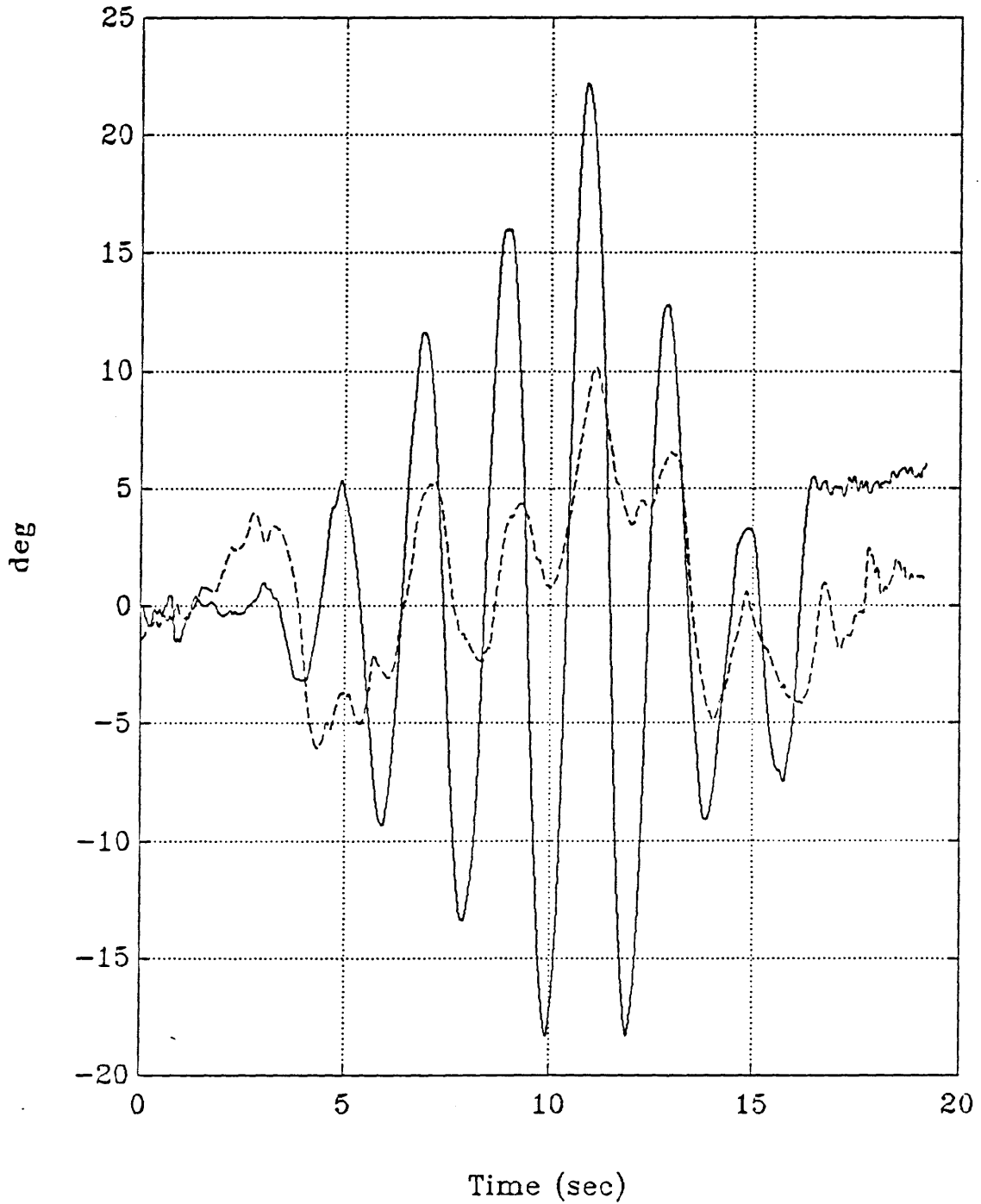


Figure 4.13 Example of dark LVOR (dashed line) and AI tracking (solid line) eye position responses. Subject T, 0.5 Hz, 0.8 g. LVOR response is that shown in Figure 4.3b.

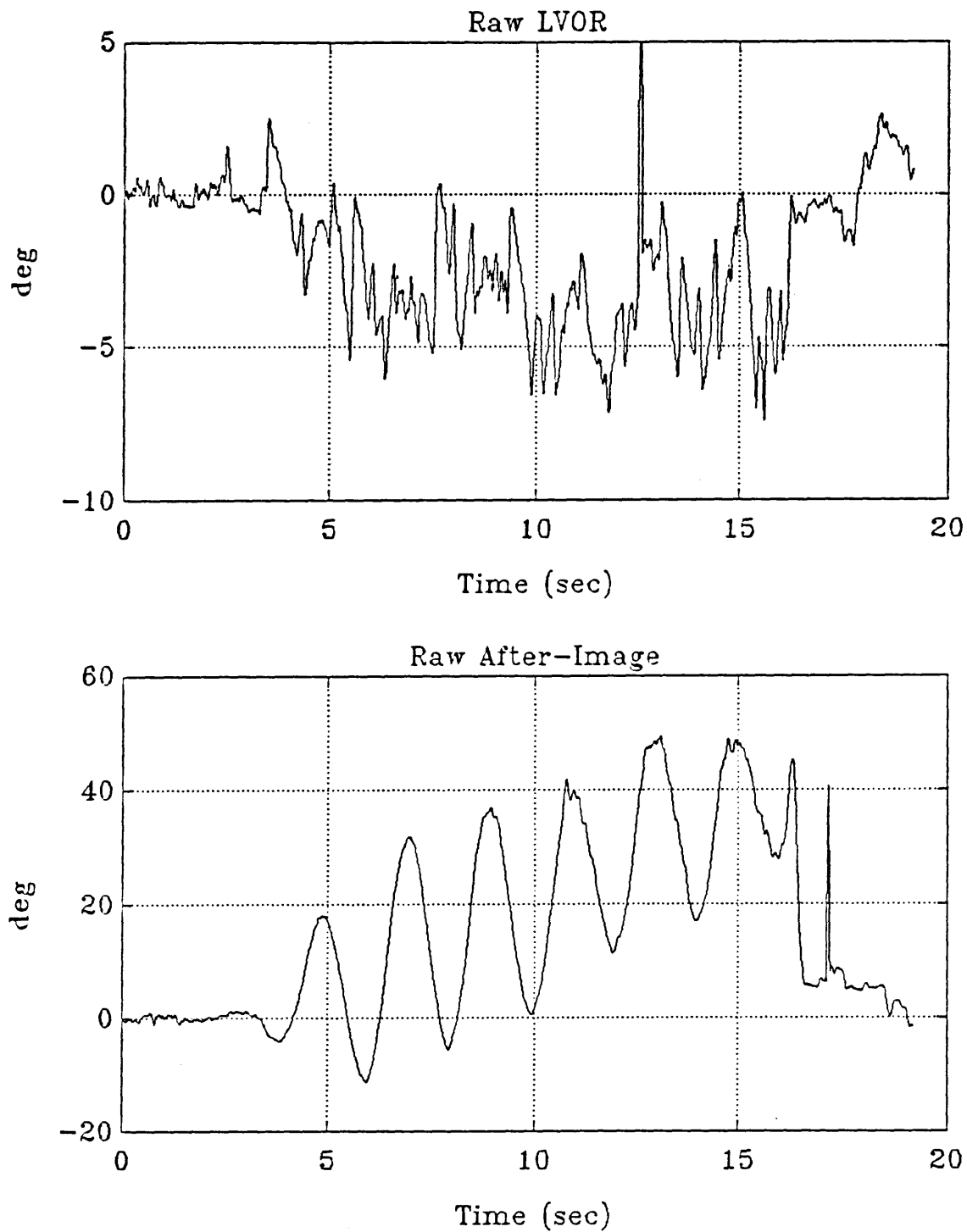


Figure 4.14 Example of dark LVOR (top) and AI tracking (bottom) eye position responses, with fast phases included. Subject J, 0.5 Hz, 0.8 g. Compare with identical responses from Figure 4.11, which have fast phases removed.

After-Image Tracking Single Sinusoids

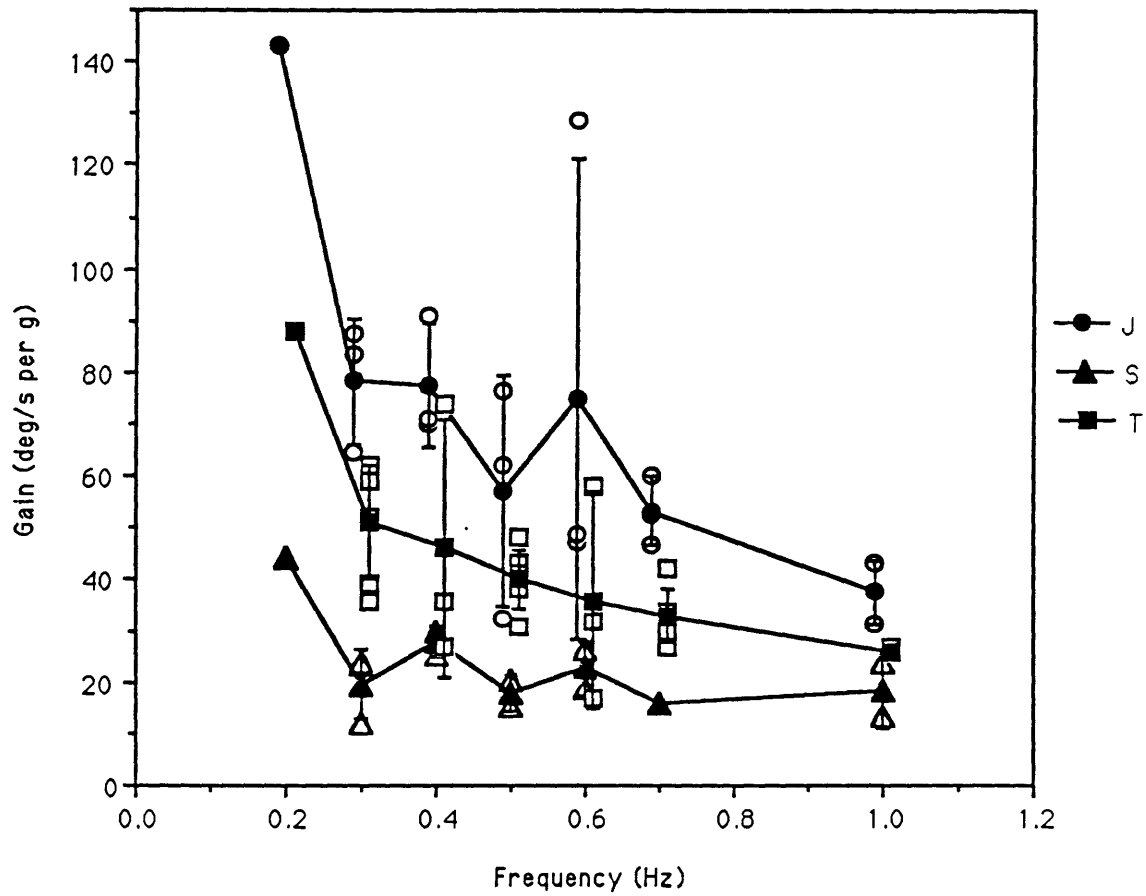


Figure 4.15 After-Image tracking of predictable sinusoids; gain for all three subjects. (Solid symbols are means for each subject at each frequency. Bars are ± 1 s.d.)

After-Image Tracking Single Sinusoids

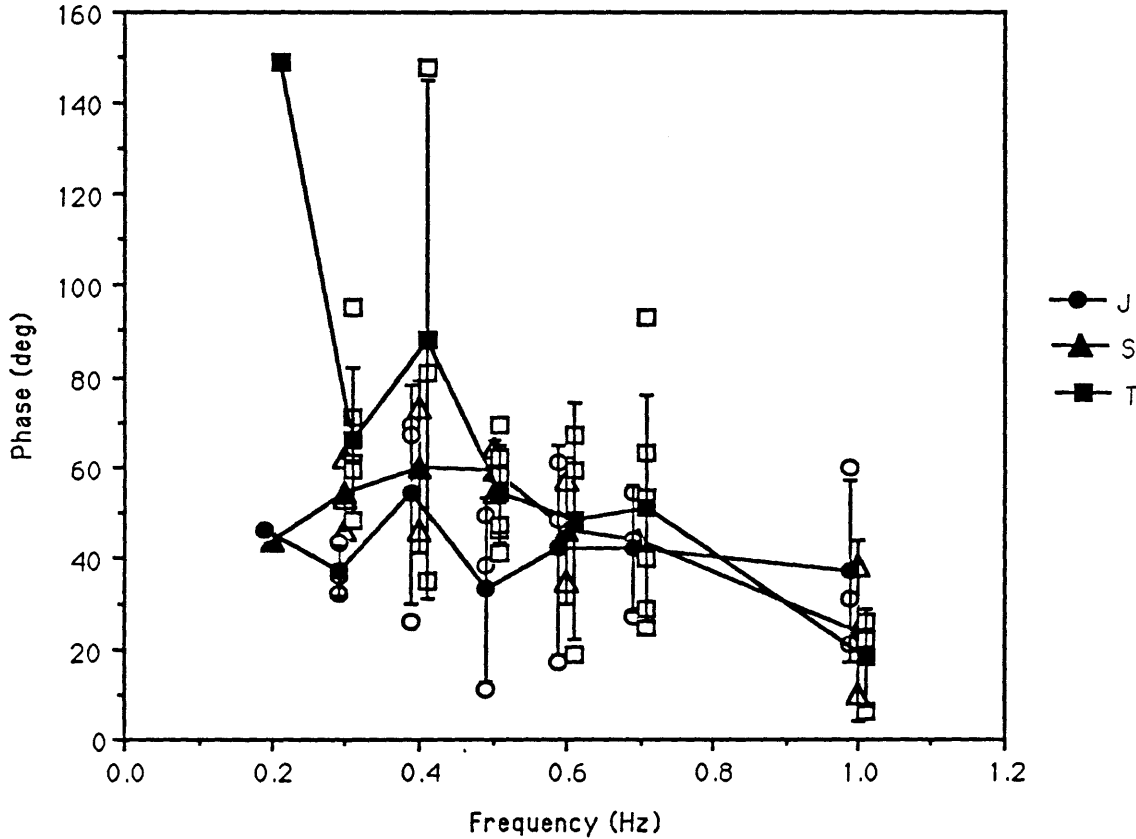


Figure 4.16 After-Image tracking of predictable sinusoids; phase for all three subjects. (Solid symbols are means for each subject at each frequency. Bars are ± 1 s.d.)

(After-Image) / (LVOR)
Single Sinusoids
Gain Ratio

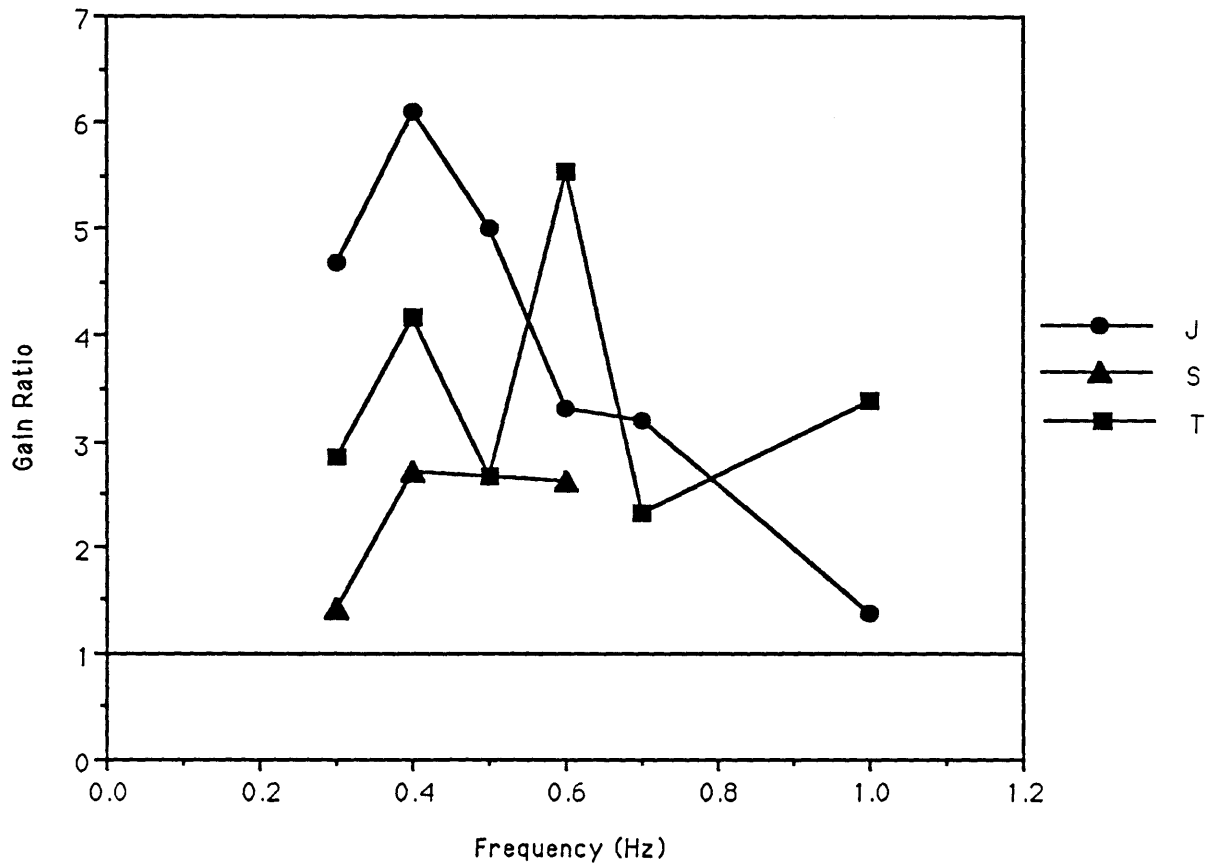


Figure 4.17 Ratio of after-image tracking gain to dark LVOR gain for predictable sinusoids. (Using mean value at each frequency for each subject.)

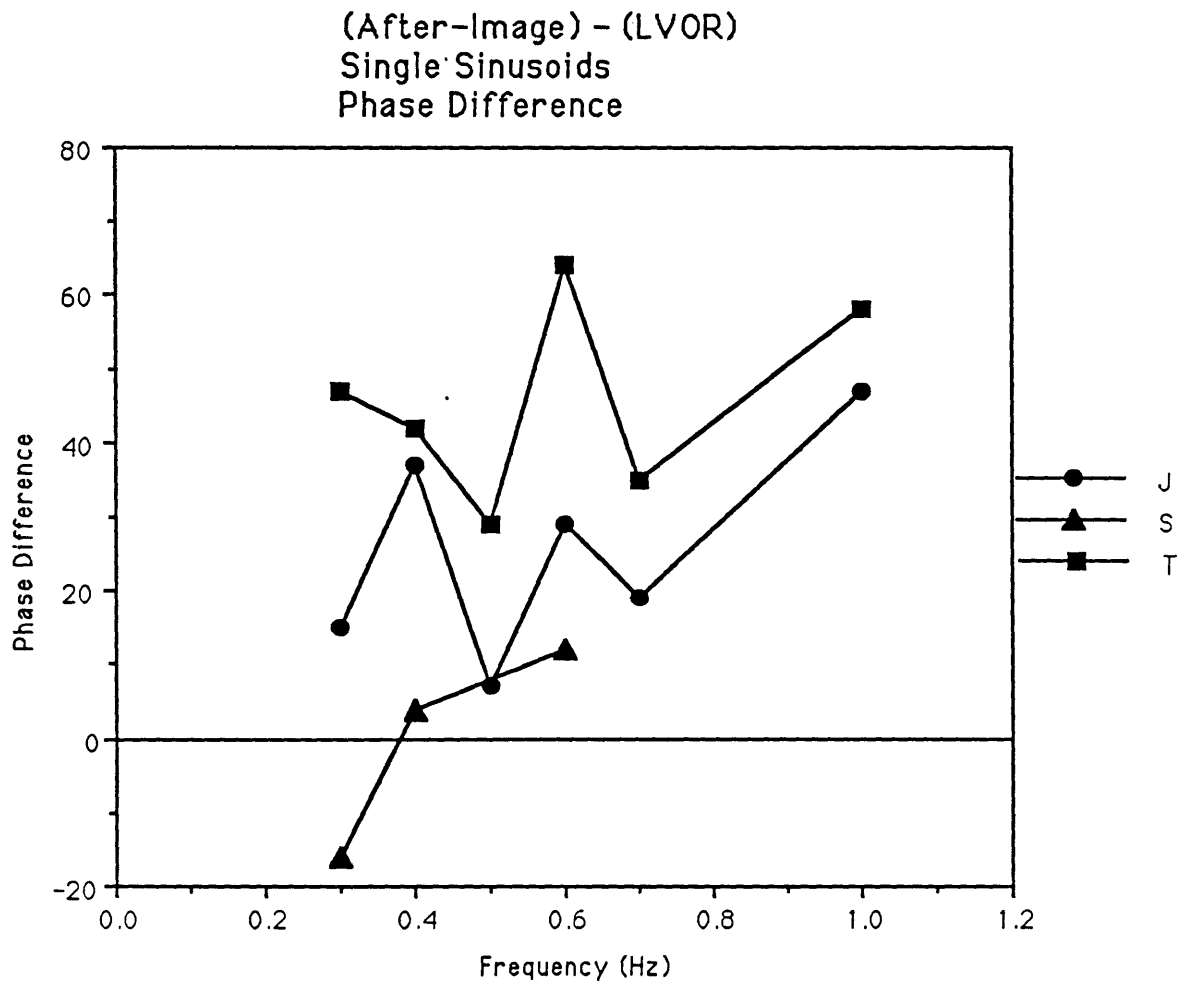


Figure 4.18 Difference between after-image tracking phase and dark LVOR phase for predictable sinusoids. (Using mean value at each frequency for each subject.)

After-Image Tracking
Subject J
SOS & Individual Sinusoids

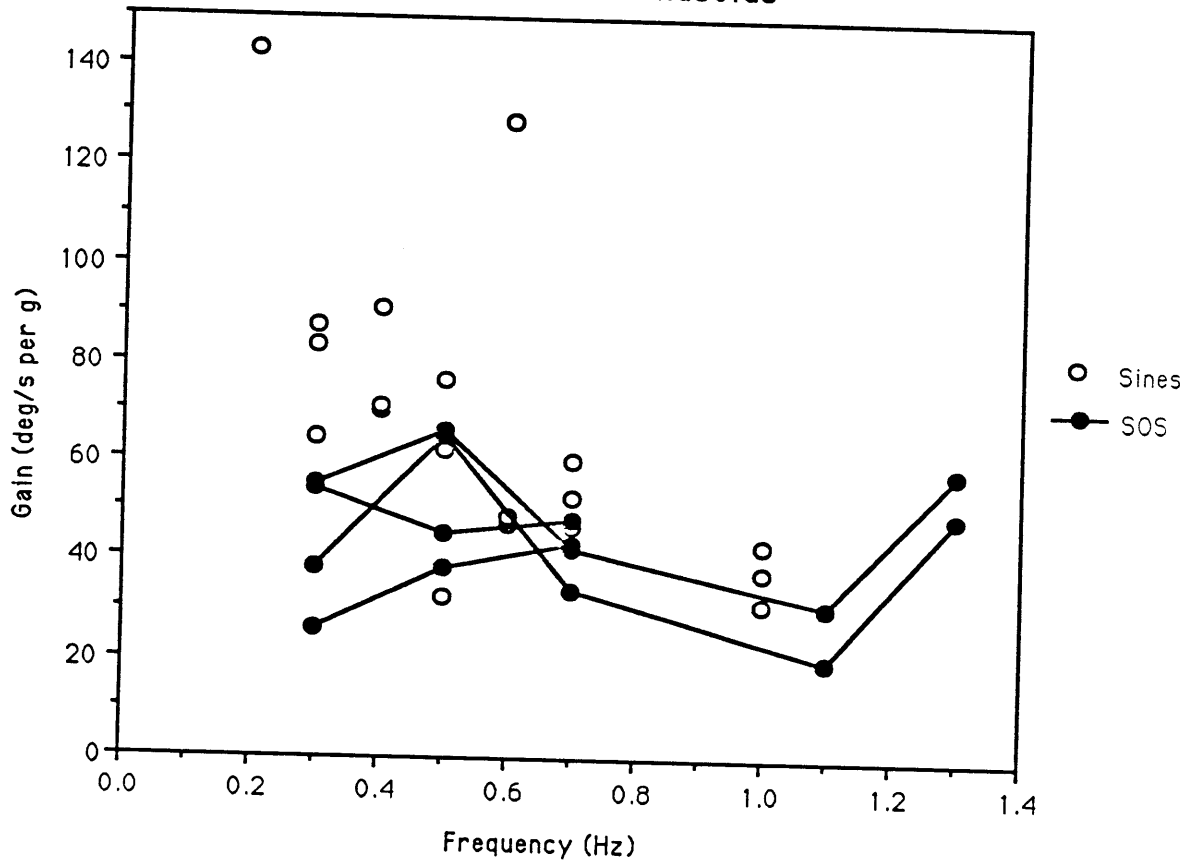


Figure 4.19 After-image tracking gain for subject J; predictable sinusoids and unpredictable sum-of-sines.

After-Image Tracking
Subject J
SOS & Individual Sinusoids

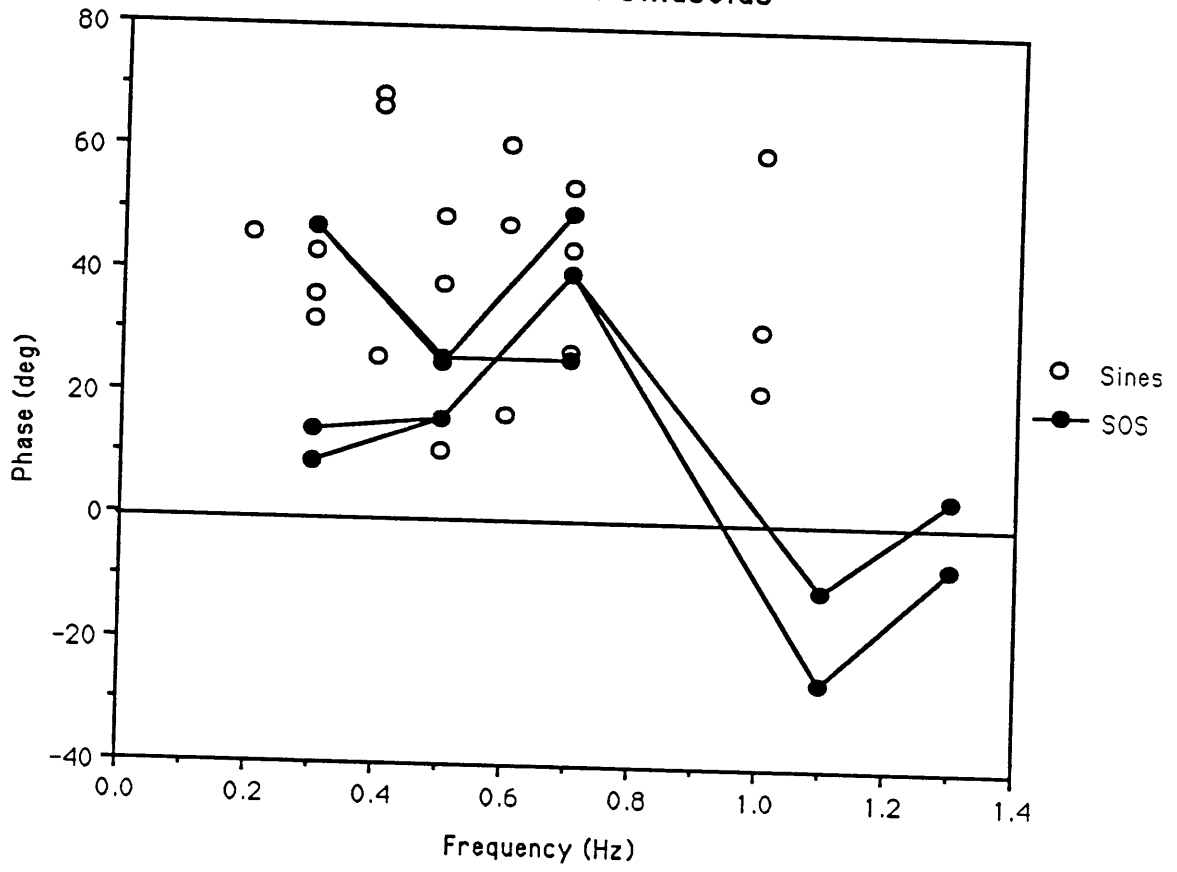


Figure 4.20 After-image tracking phase for subject J; predictable sinusoids and unpredictable sum-of-sines.

After-Image Tracking with Theoretical Compensatory Gain

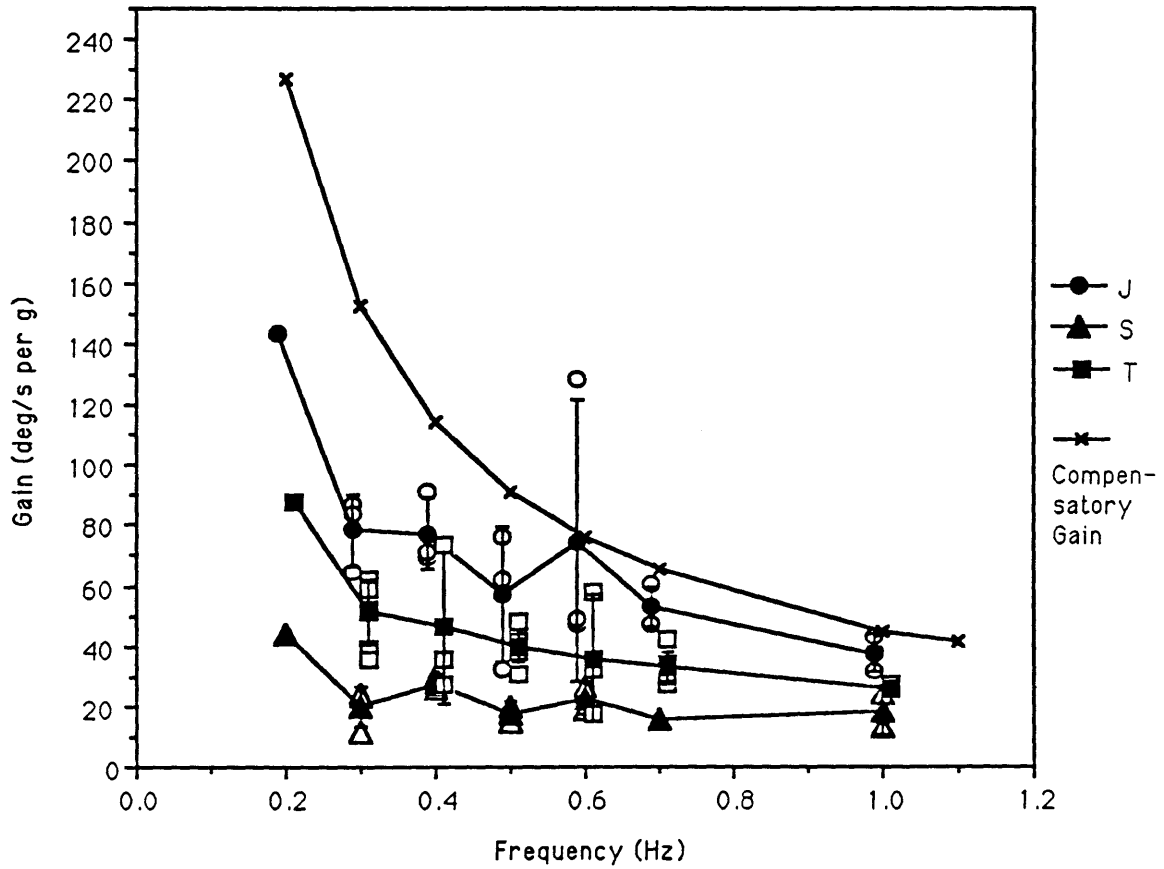


Figure 4.21 After-Image tracking of predictable sinusoids; gain for all three subjects. The calculated gain required to produce perfect compensatory eye movements for a target at two meters distance is also shown. (Solid symbols are means for each subject at each frequency. Bars are ± 1 s.d.)

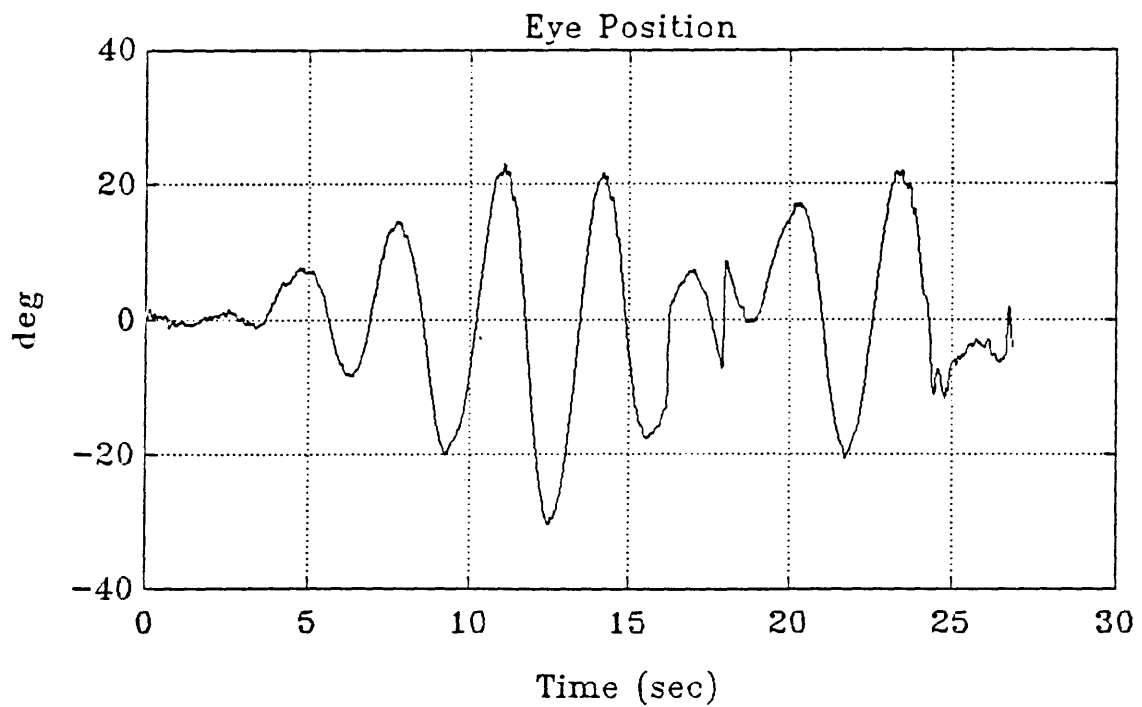
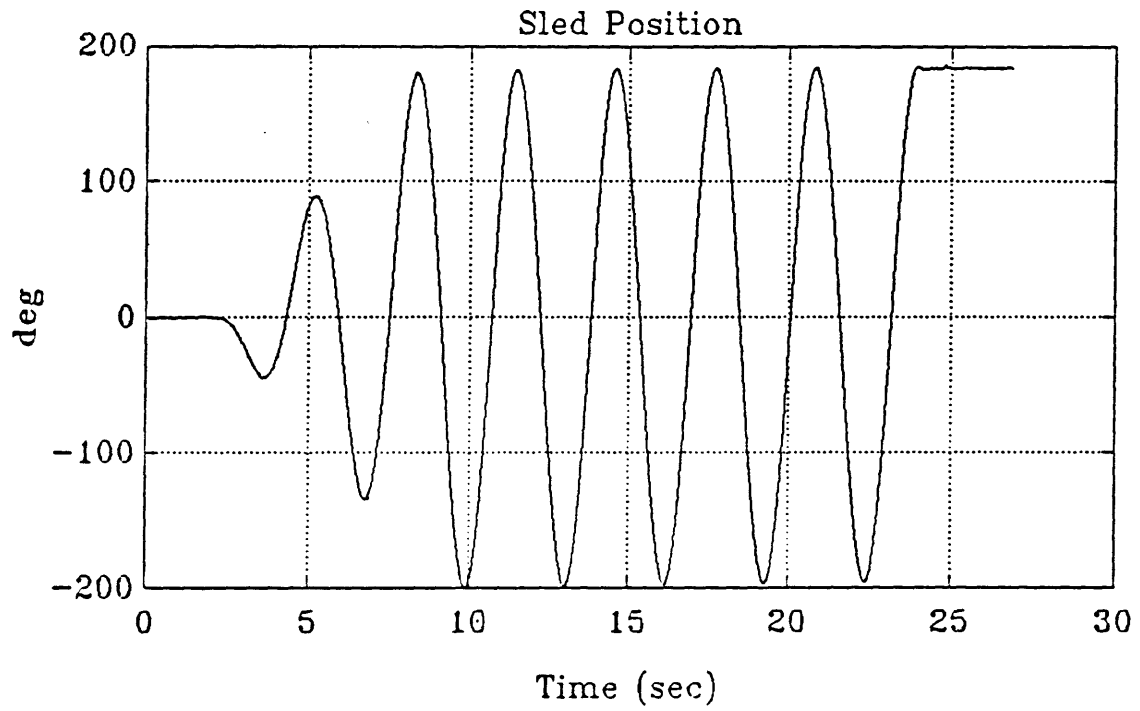


Figure 4.22 Example of "lost" after-image. Note break in eye tracking pattern at 17 seconds. Subject T, 0.32 Hz, 0.8 g.

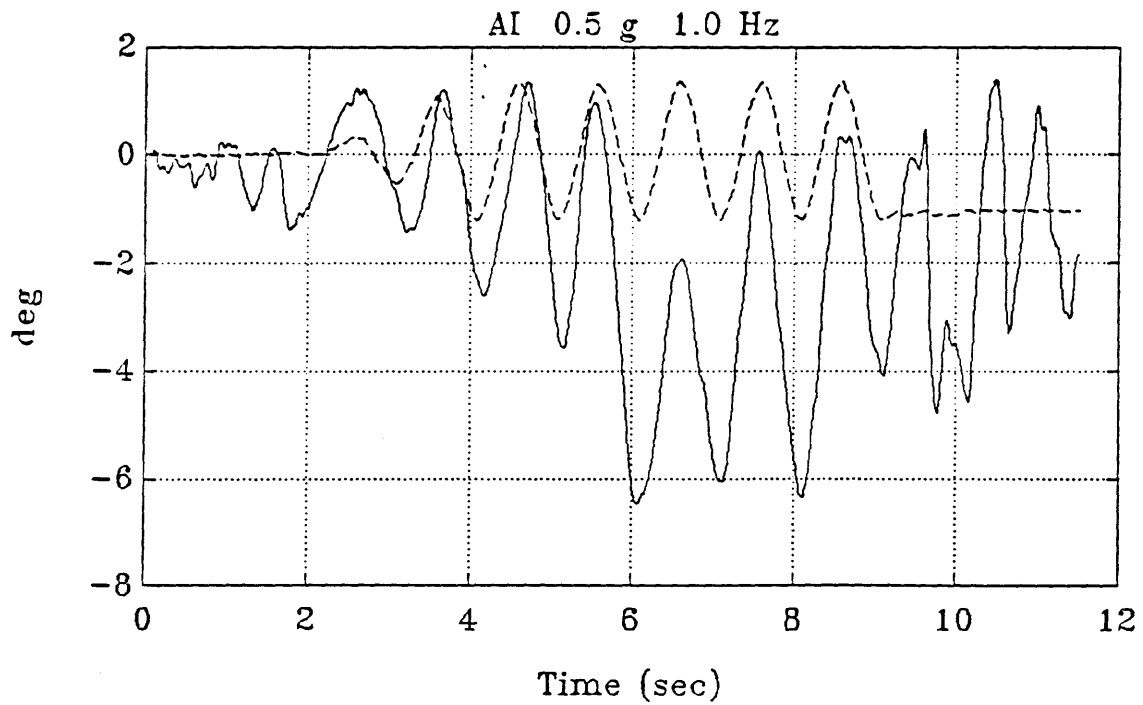
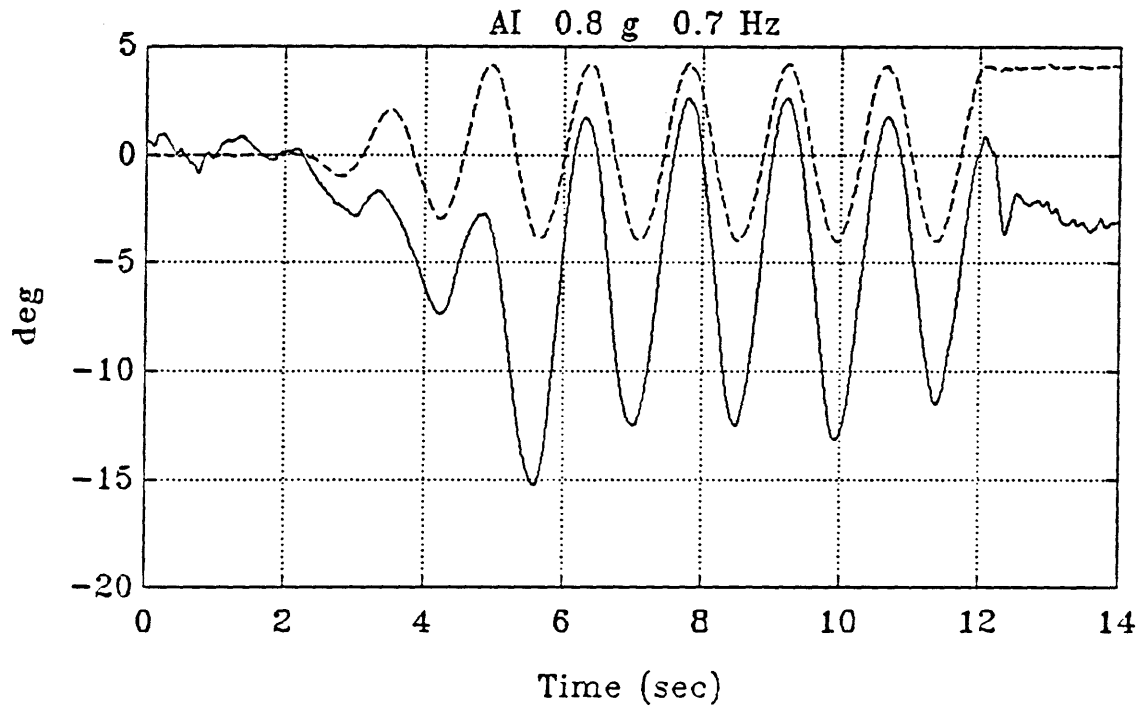


Figure 4.23a Example of "ongoing" AI responses which continue after stimulus cessation. Subject T. (Dashed line is arbitrarily-scaled sled position, solid line is eye position.)

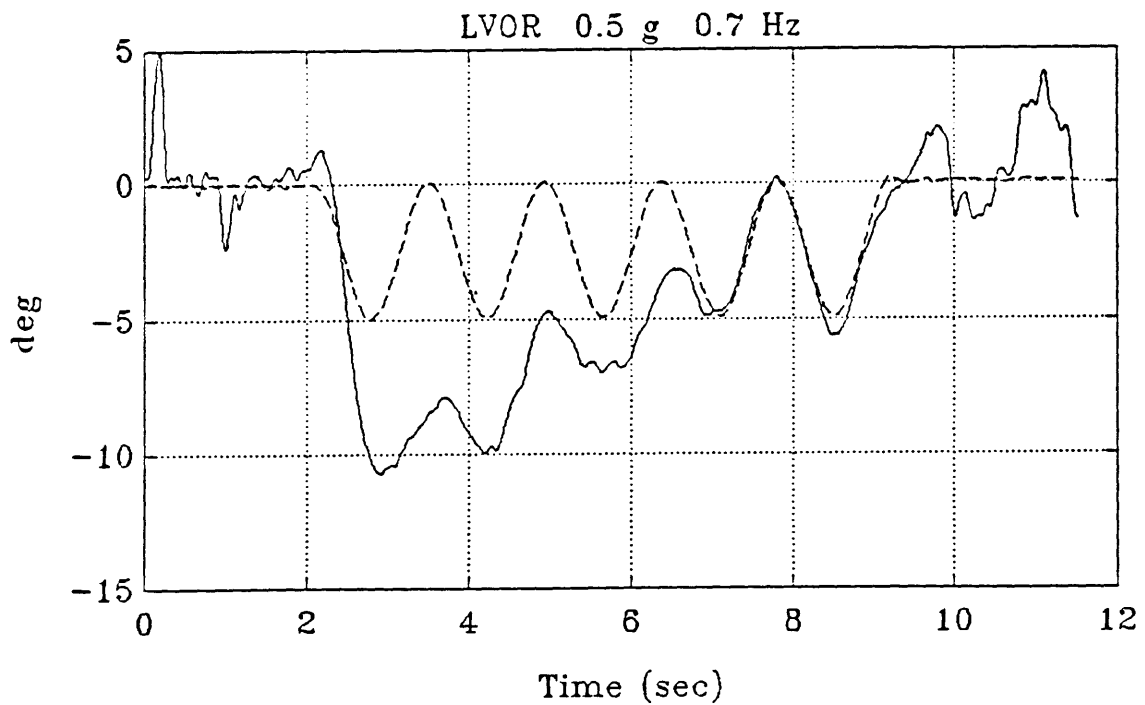
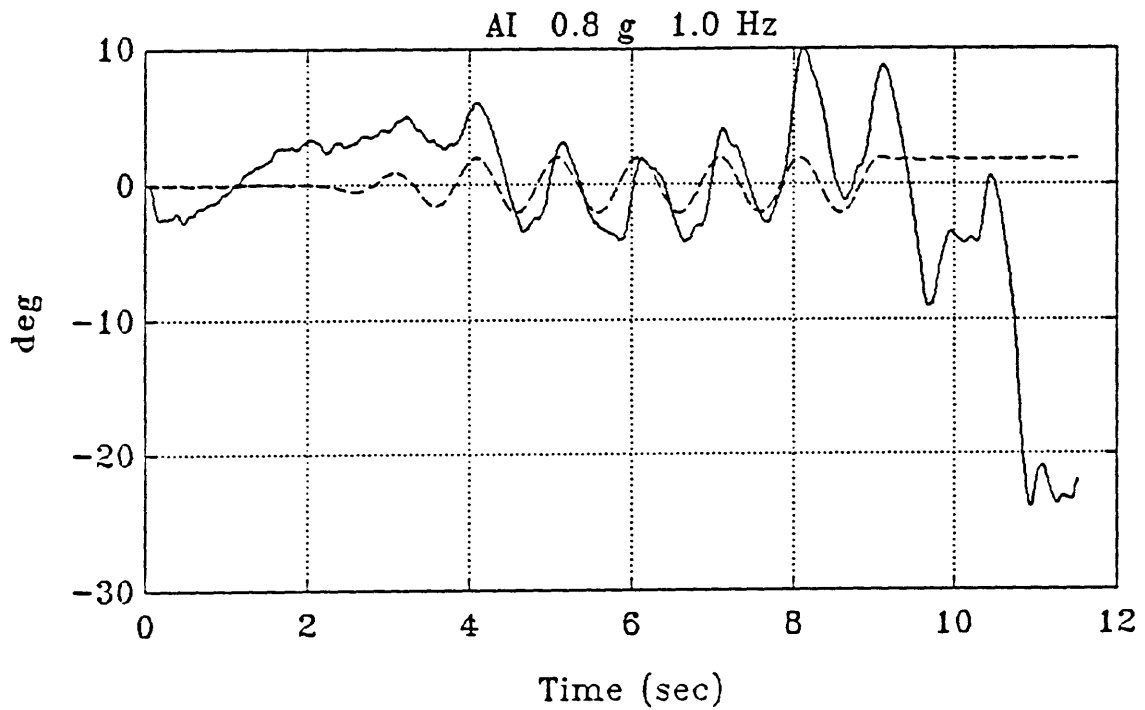


Figure 4.23b Example of "ongoing" AI (top) and LVOR (bottom) responses which continue after stimulus cessation. Subject T. (Dashed line is arbitrarily-scaled sled position, solid line is eye position.)

Smooth Pursuit and Visual+Vestibular

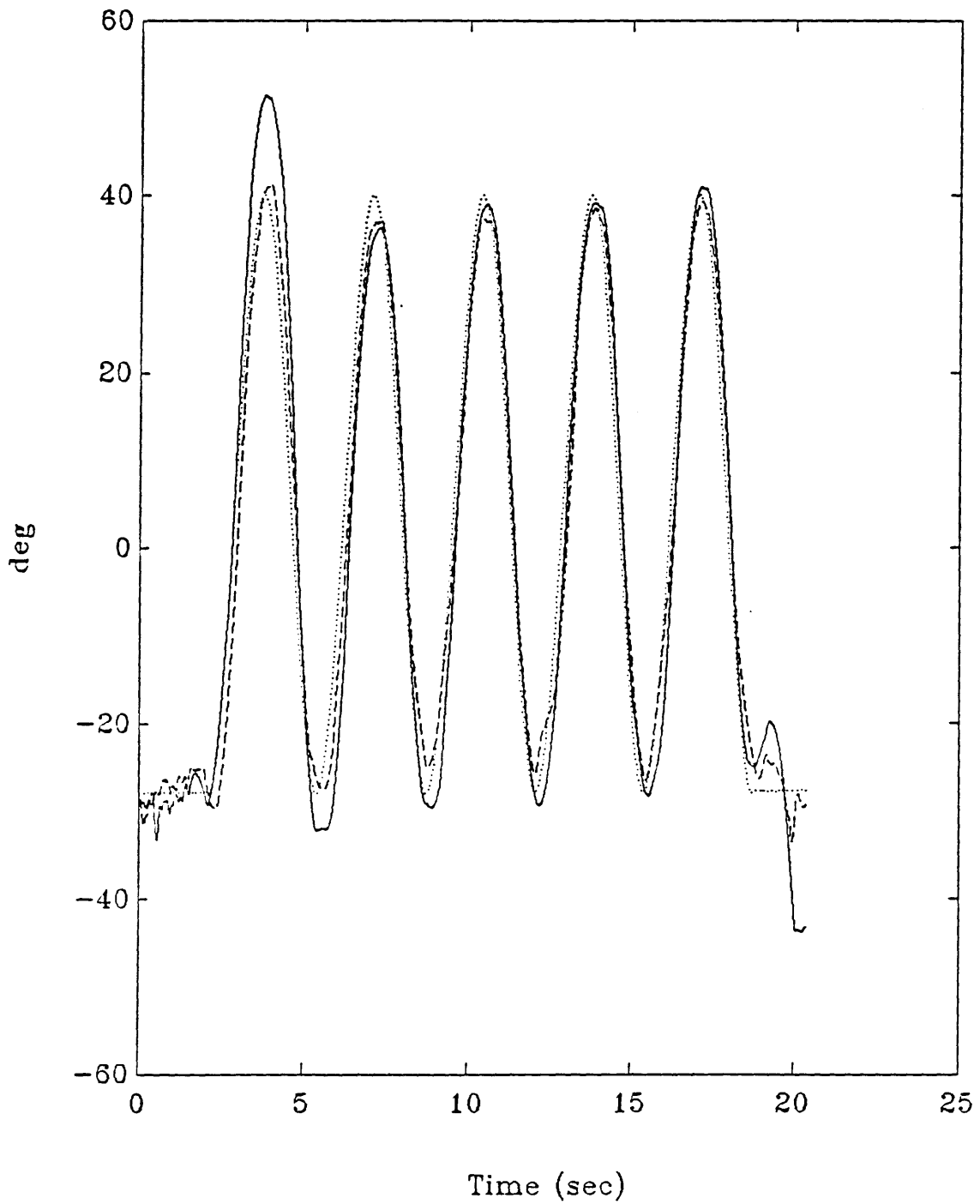


Figure 4.24 Overlaid stimulus (dotted line), smooth pursuit (dashed line), and visual+vestibular (solid line) responses. Subject J. 0.3 Hz, 0.5 g.

Smooth Pursuit and Visual+Vestibular

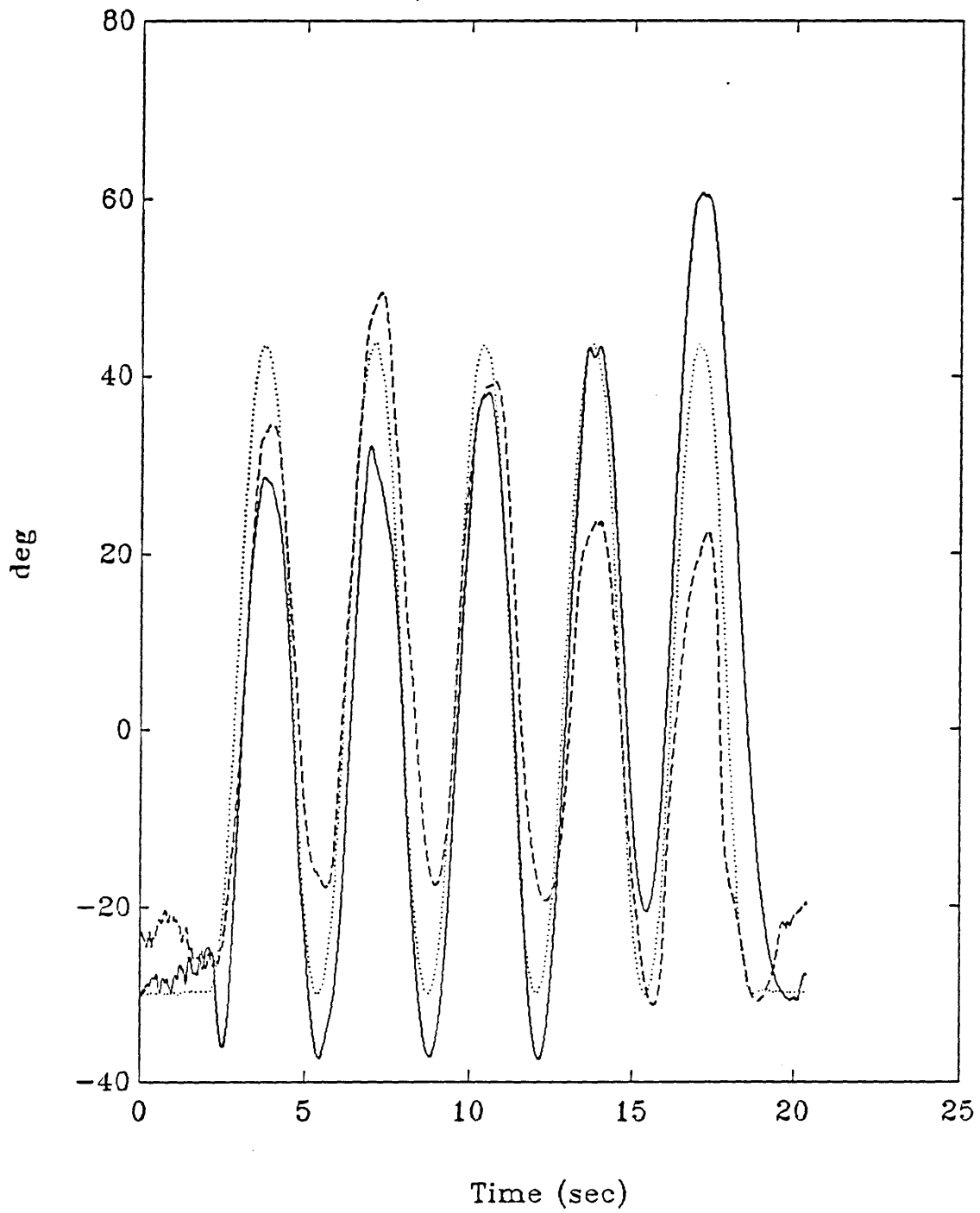


Figure 4.25 Overlaid stimulus (dotted line), smooth pursuit (dashed line), and visual+vestibular (solid line) responses. Subject S. 0.3 Hz, 0.5 g.

Smooth Pursuit and Visual+Vestibular

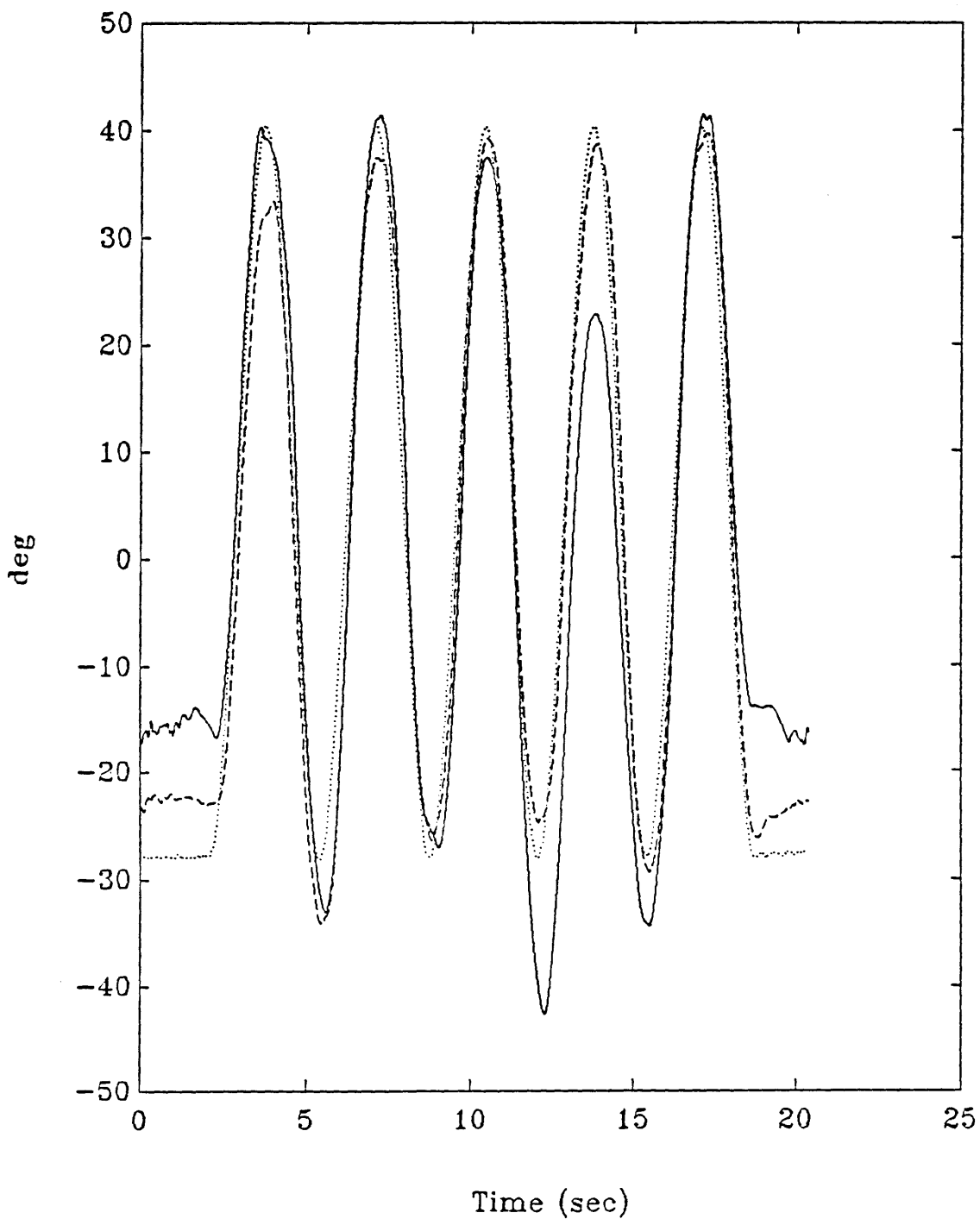


Figure 4.26 Overlaid stimulus (dotted line), smooth pursuit (dashed line), and visual+vestibular (solid line) responses. Subject T. 0.3 Hz, 0.5 g.

Smooth Pursuit & Visual+Vestibular
 Subject J
 Single Sinusoids

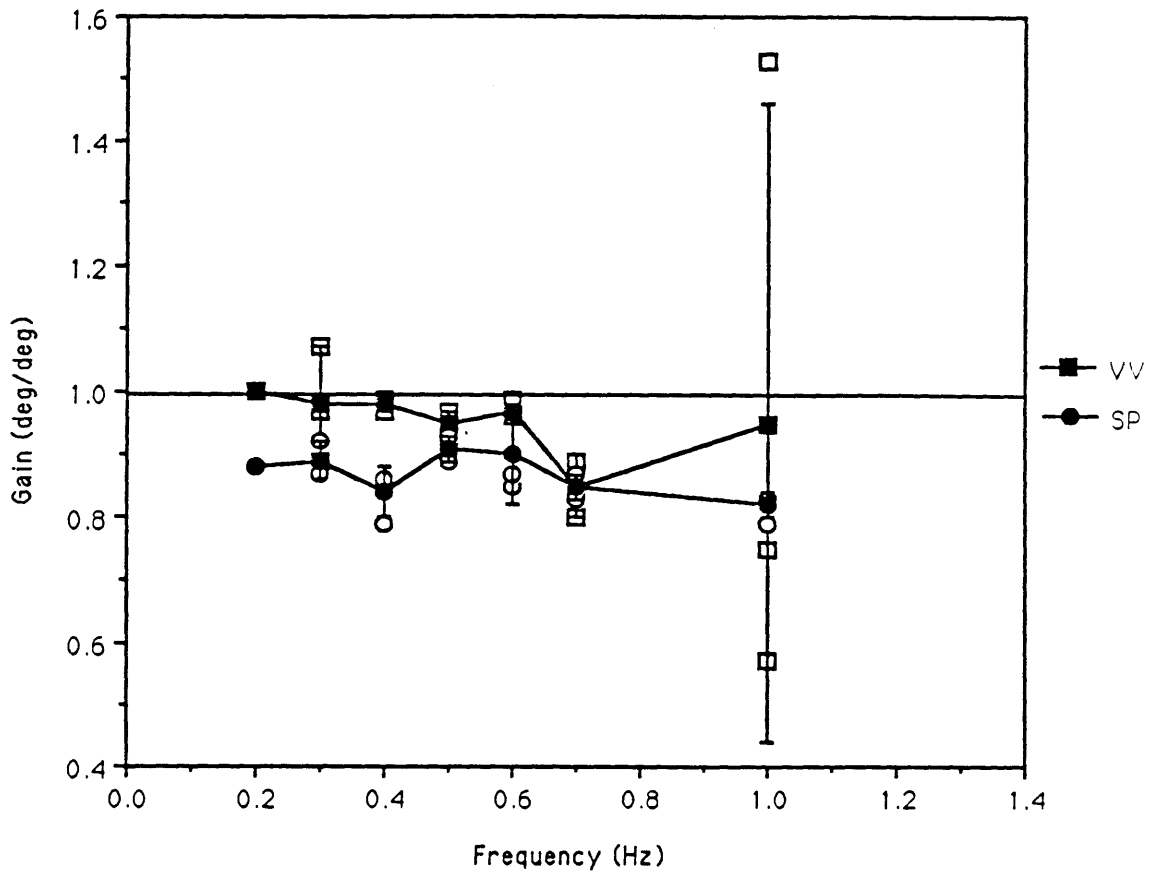


Figure 4.27 Smooth pursuit and visual+vestibular tracking of predictable sinusoids; gain for subject J. (Solid symbols are means at each frequency. Bars are ± 1 s.d.)

Smooth Pursuit & Visual+Vestibular
 Subject J
 Single Sinusoids

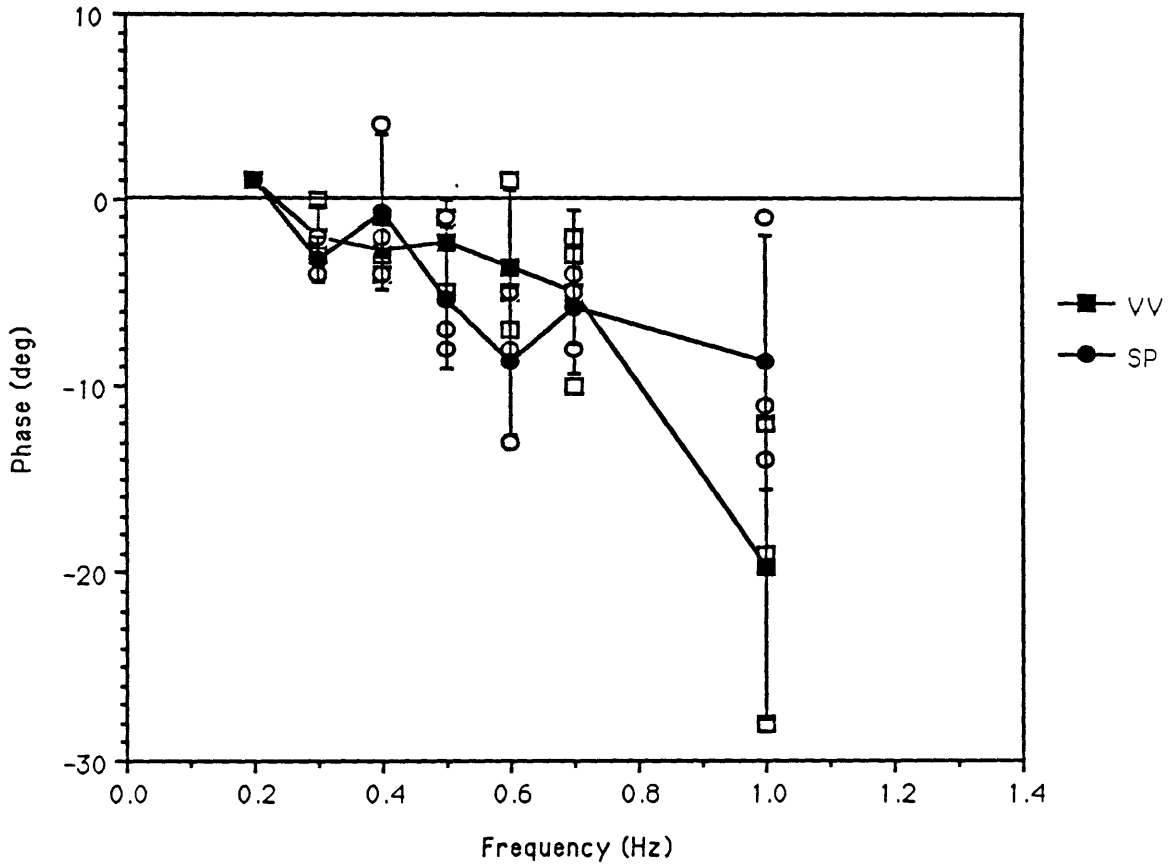


Figure 4.28 Smooth pursuit and visual+vestibular tracking of predictable sinusoids; phase for subject J. (Solid symbols are means at each frequency. Bars are ± 1 s.d.)

Smooth Pursuit & Visual+Vestibular
 Subject S
 Single Sinusoids

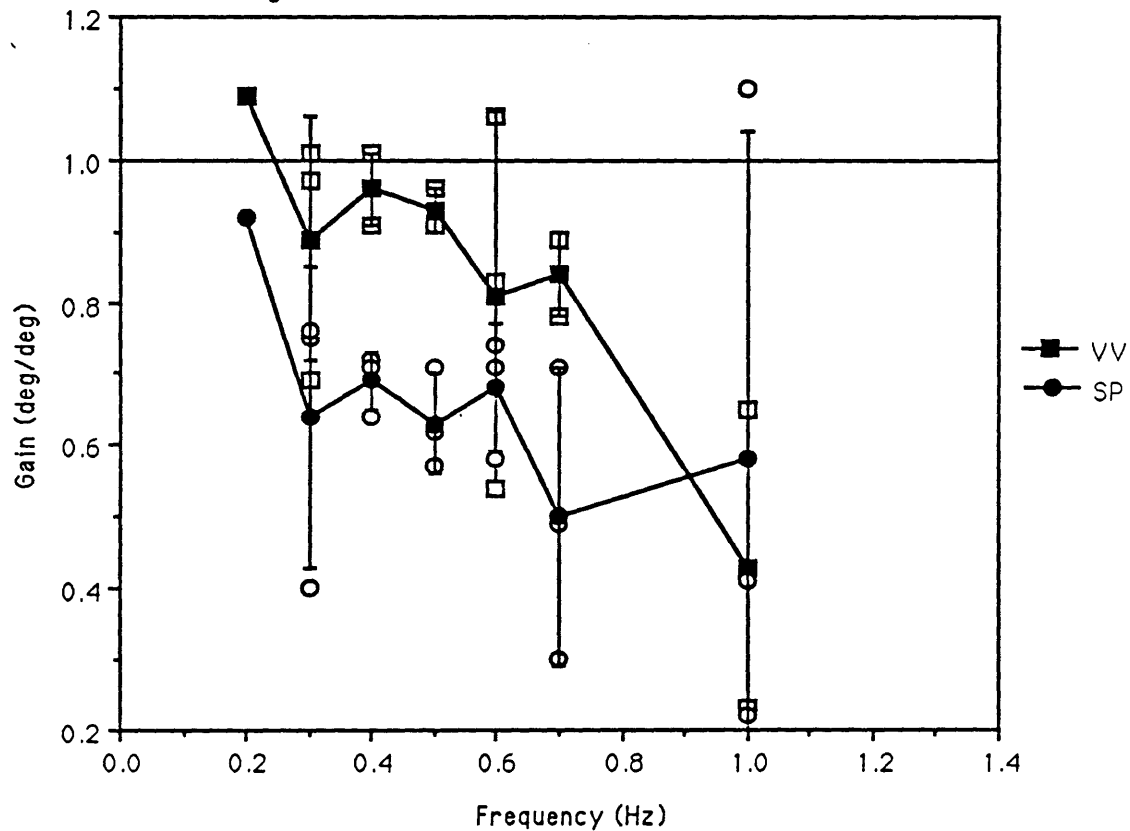


Figure 4.29 Smooth pursuit and visual+vestibular tracking of predictable sinusoids; gain for subject S. (Solid symbols are means at each frequency. Bars are ± 1 s.d.)

Smooth Pursuit & Visual+Vestibular
Subject S
Single Sinusoids

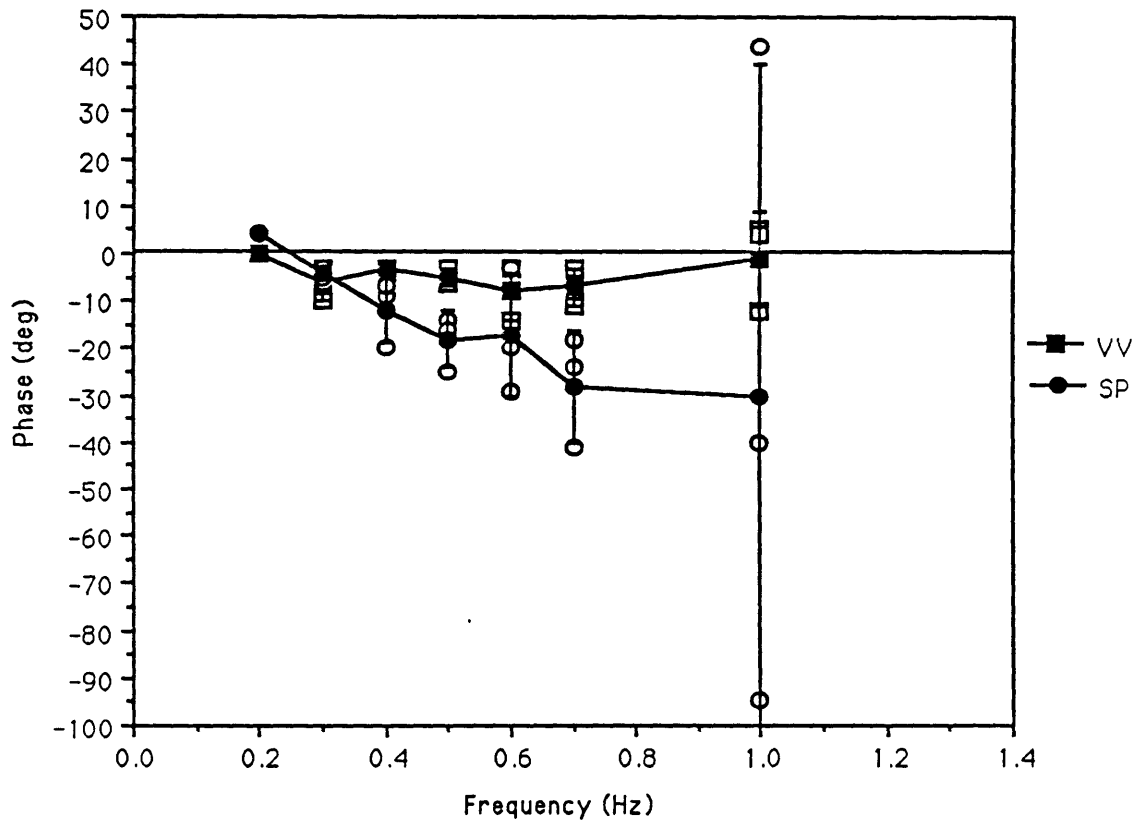


Figure 4.30 Smooth pursuit and visual+vestibular tracking of predictable sinusoids; phase for subject S. (Solid symbols are means at each frequency. Bars are ± 1 s.d.)

Smooth Pursuit & Visual+Vestibular
 Subject T
 Single Sinusoids

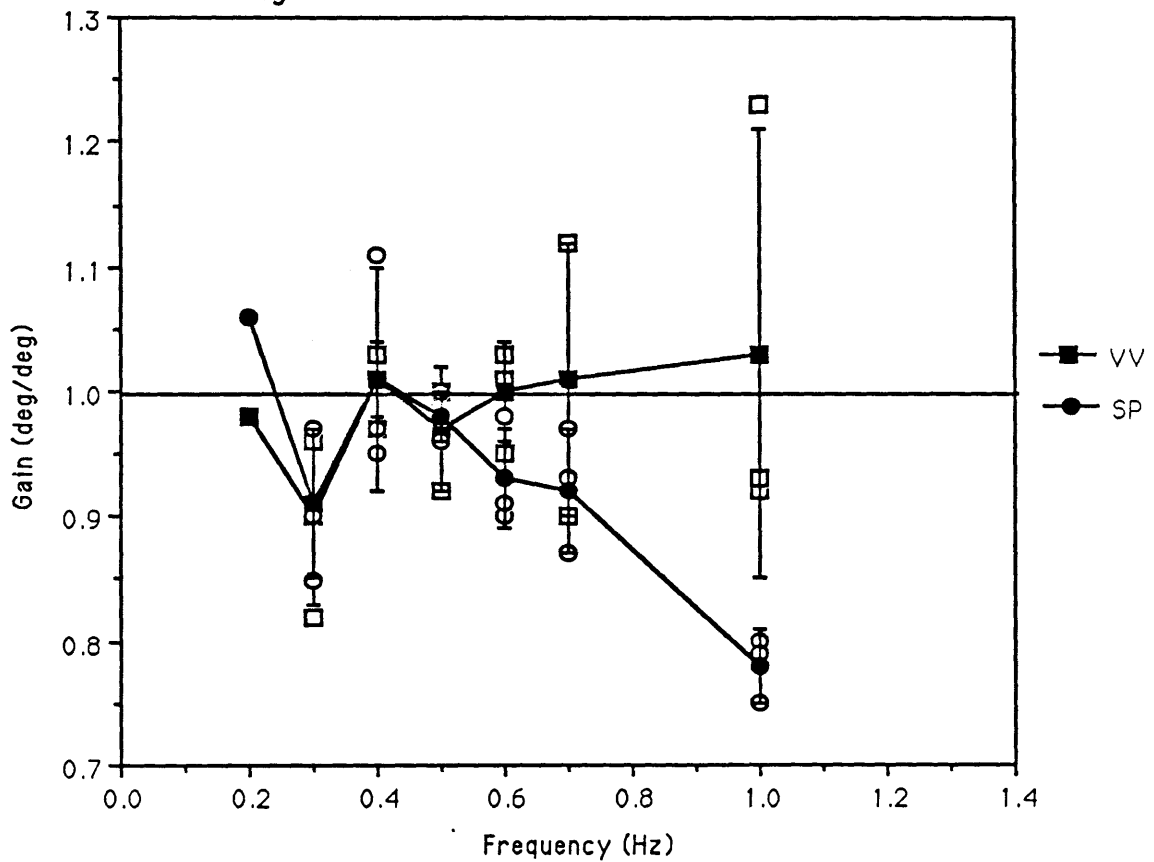


Figure 4.31 Smooth pursuit and visual+vestibular tracking of predictable sinusoids; gain for subject T. (Solid symbols are means at each frequency. Bars are ± 1 s.d.)

Smooth Pursuit & Visual+Vestibular
 Subject T
 Single Sinusoids

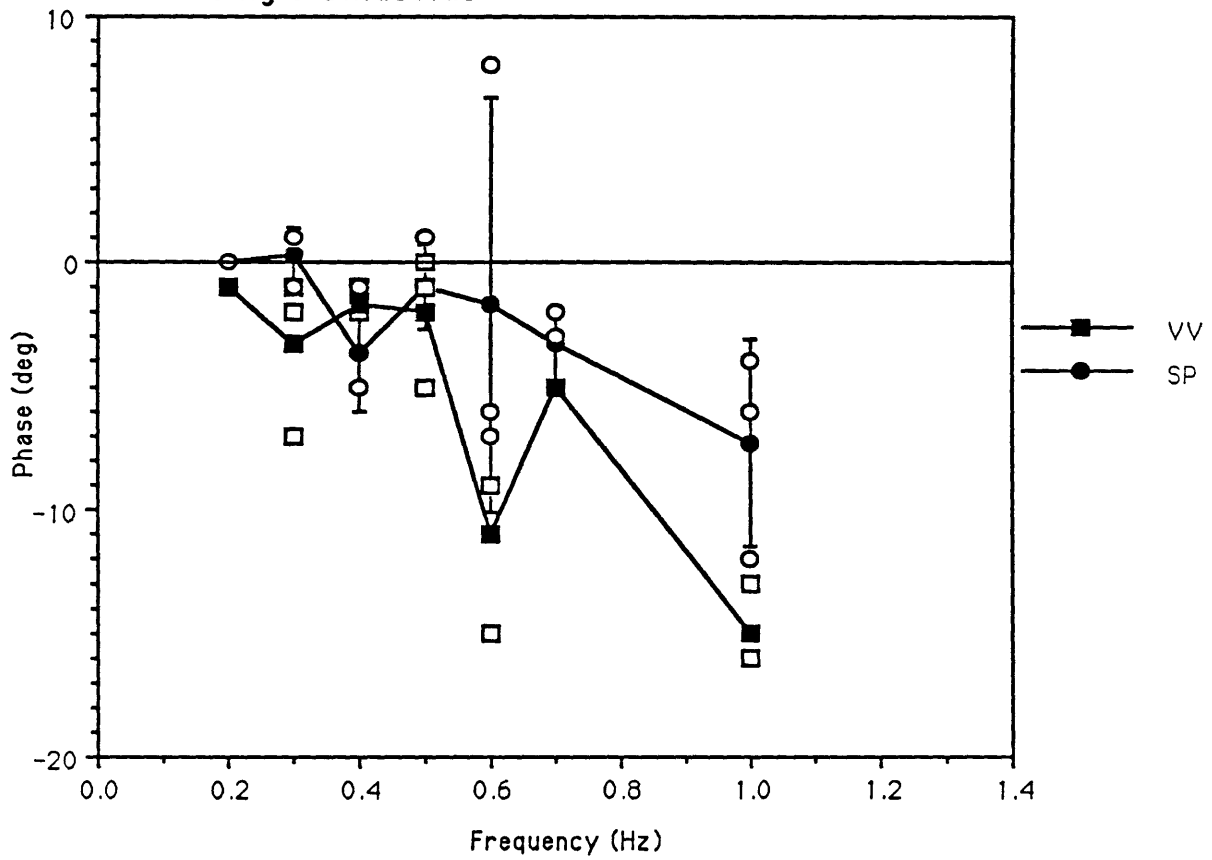


Figure 4.32 Smooth pursuit and visual+vestibular tracking of predictable sinusoids; phase for subject T. (Solid symbols are means at each frequency. Bars are ± 1 s.d.)

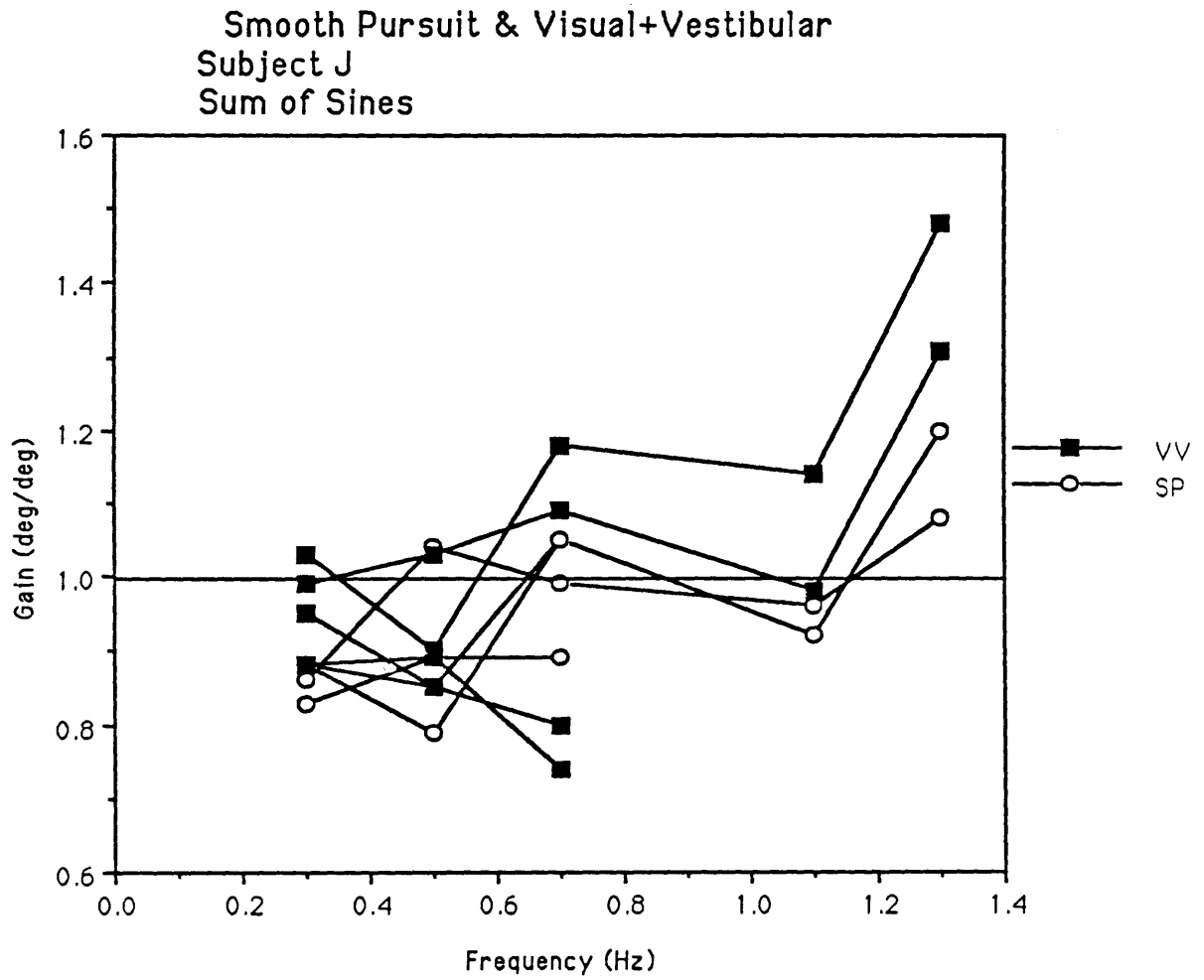


Figure 4.33 Smooth pursuit and visual+vestibular tracking of unpredictable sum-of-sinusoids; gain for subject J.

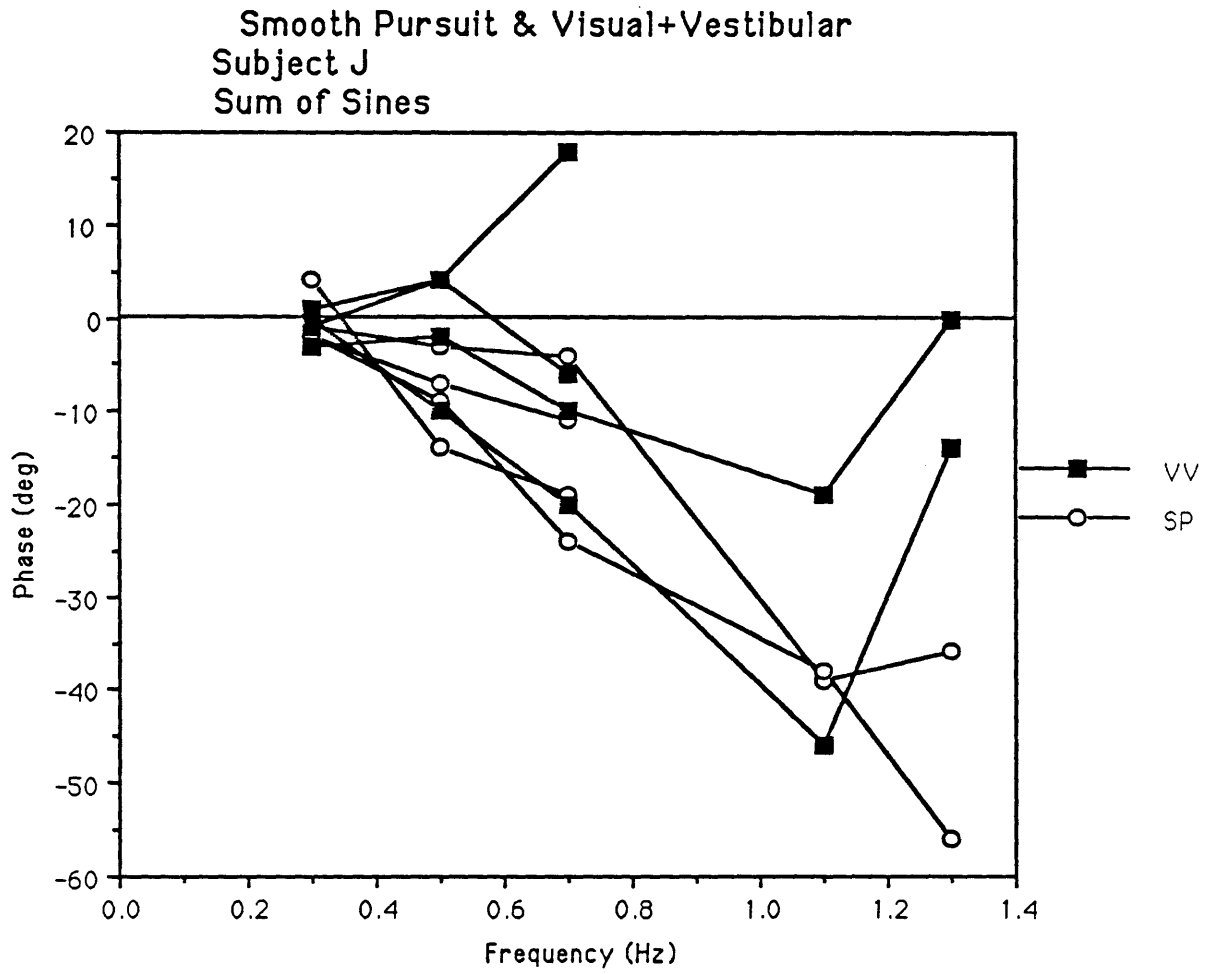


Figure 4.34 Smooth pursuit and visual+vestibular tracking of unpredictable sum-of-sinusoids; phase for subject J.

Smooth Pursuit & Visual+Vestibular
Subject S
Sum of Sines

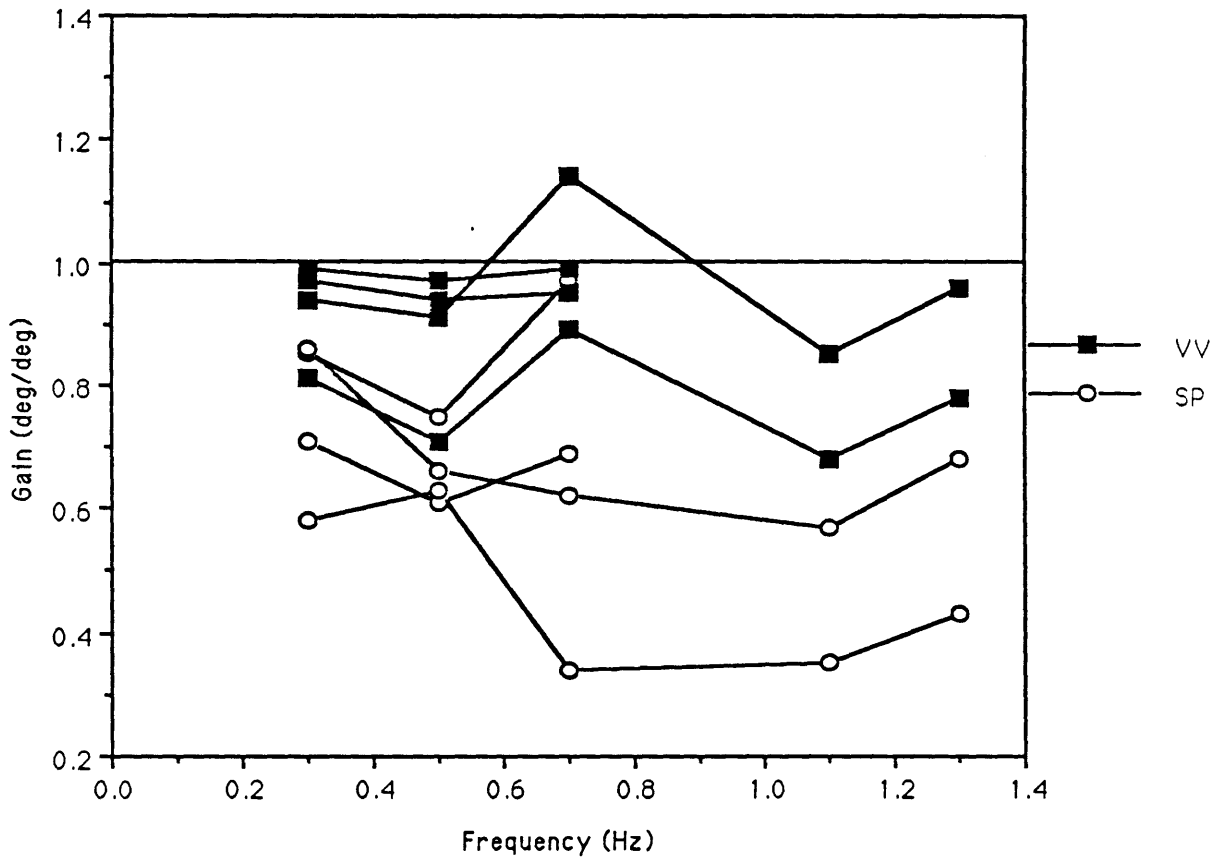


Figure 4.35 Smooth pursuit and visual+vestibular tracking of unpredictable sum-of-sinusoids; gain for subject S.

Smooth Pursuit & Visual+Vestibular
Subject S
Sum of Sines

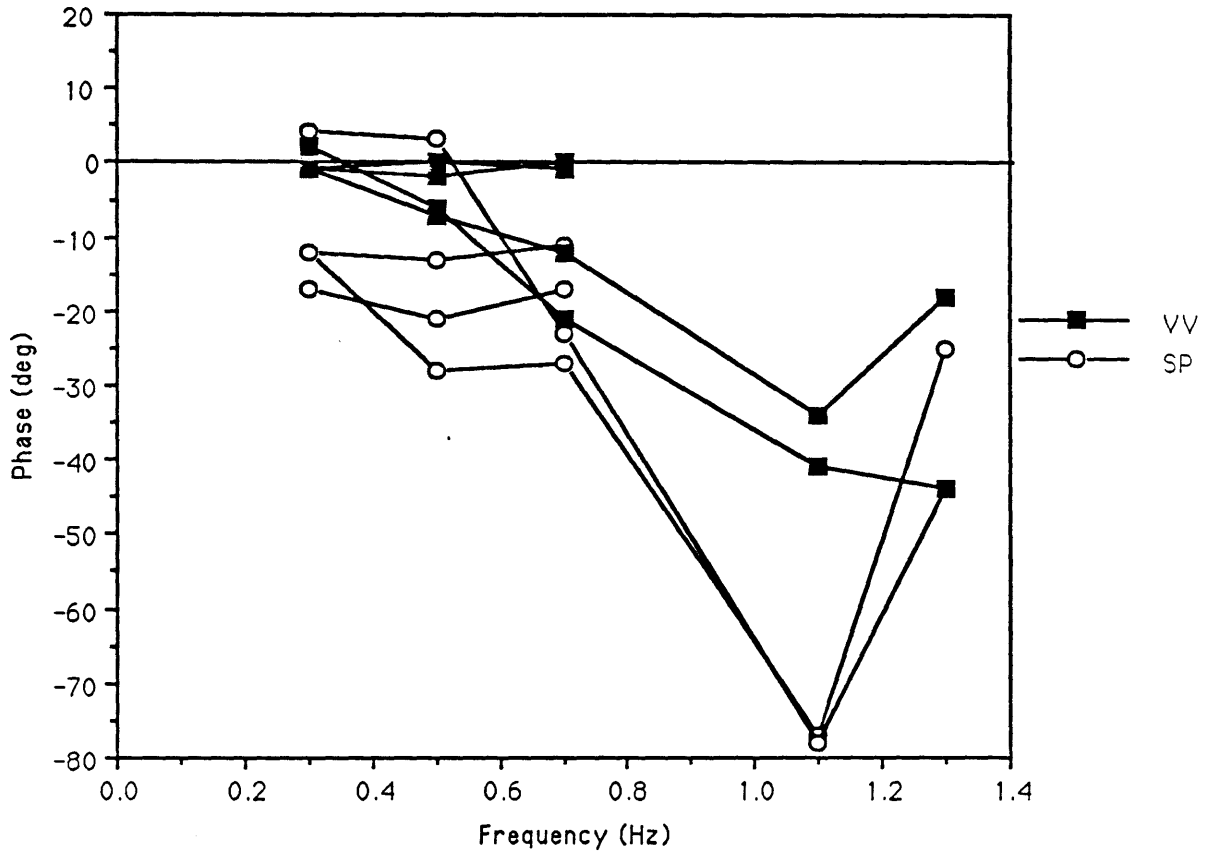


Figure 4.36 Smooth pursuit and visual+vestibular tracking of unpredictable sum-of-sinusoids; phase for subject S.

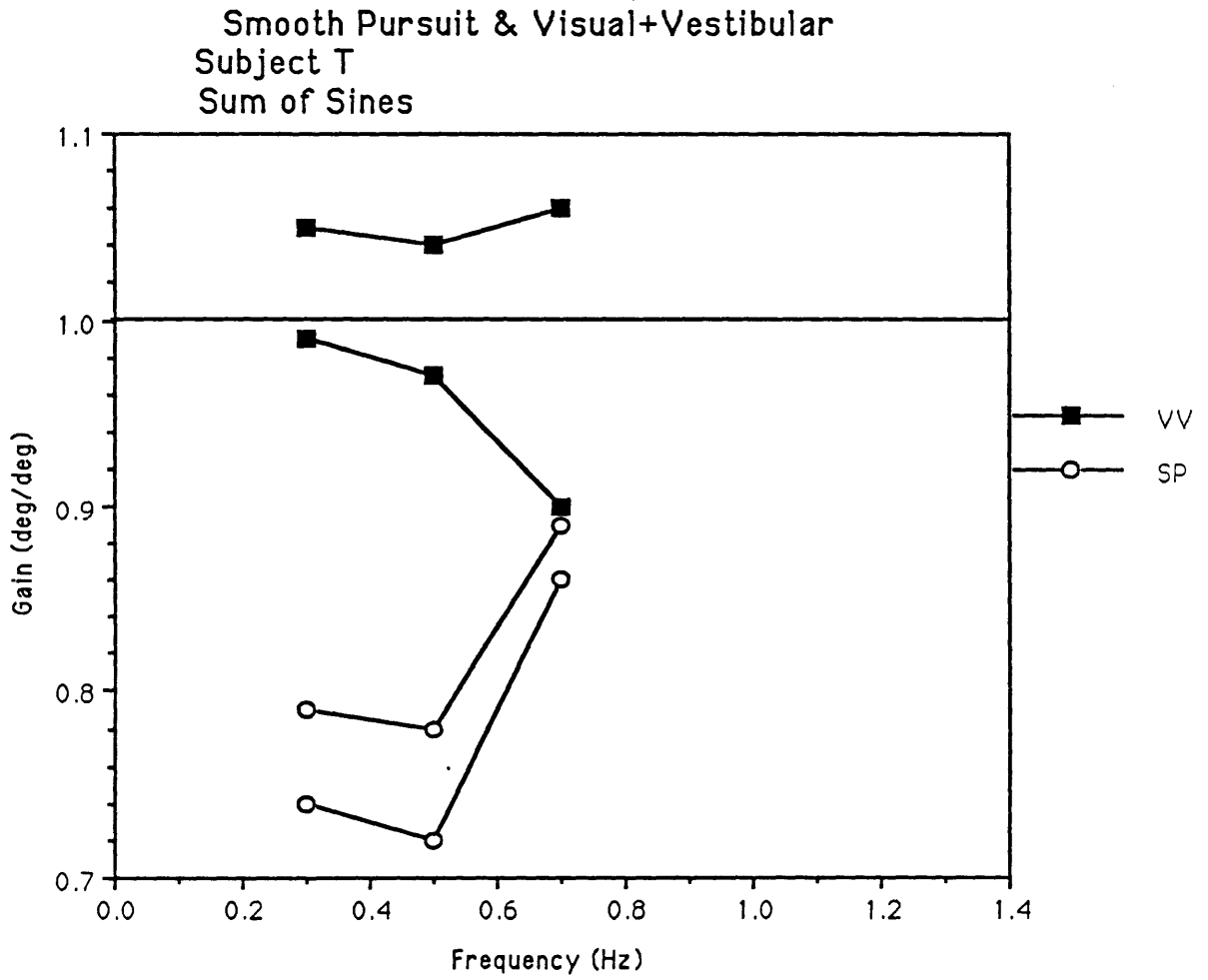


Figure 4.37 Smooth pursuit and visual+vestibular tracking of unpredictable sum-of-sinusoids; gain for subject T.

Smooth Pursuit & Visual+Vestibular
Subject T
Sum of Sines

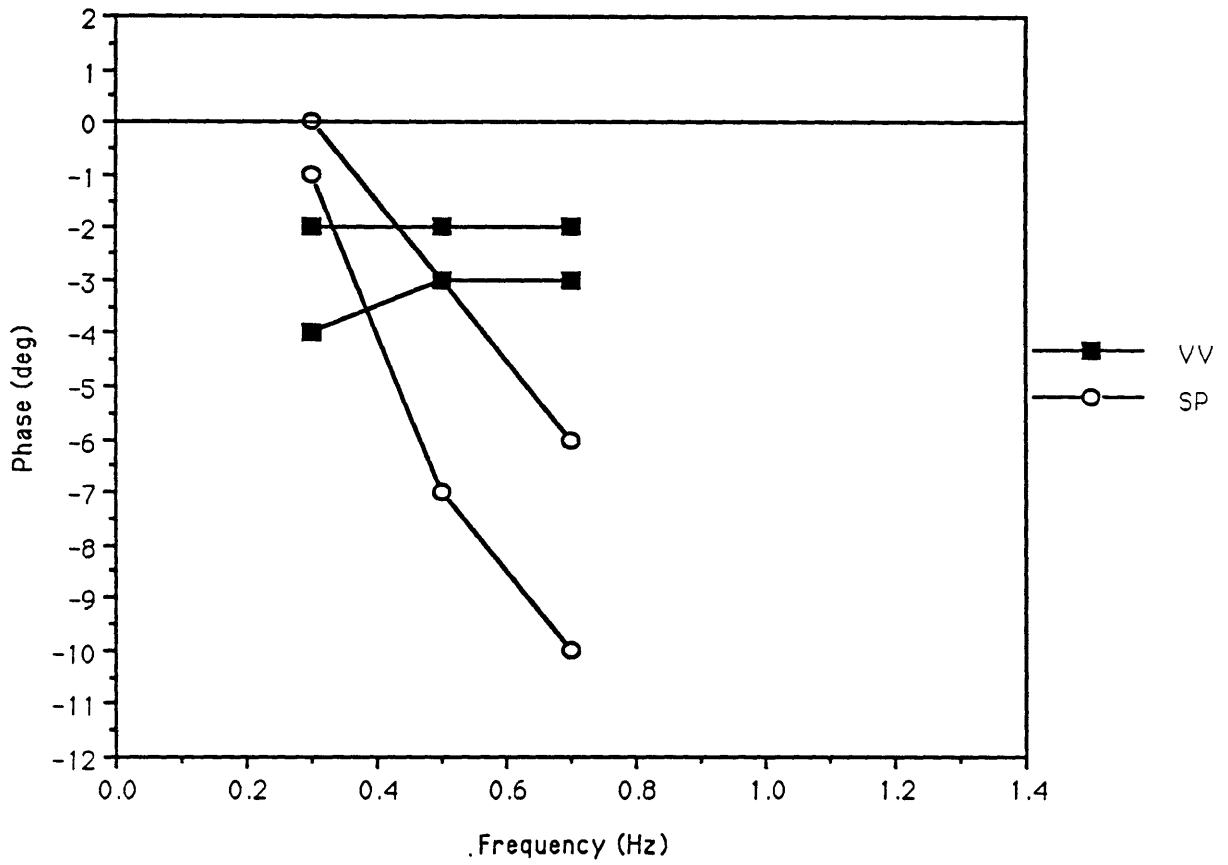


Figure 4.38 Smooth pursuit and visual+vestibular tracking of unpredictable sum-of-sinusoids; phase for subject T.

(Visual+Vestibular) / (Smooth Pursuit)
Single Sinusoids
Gain Ratio

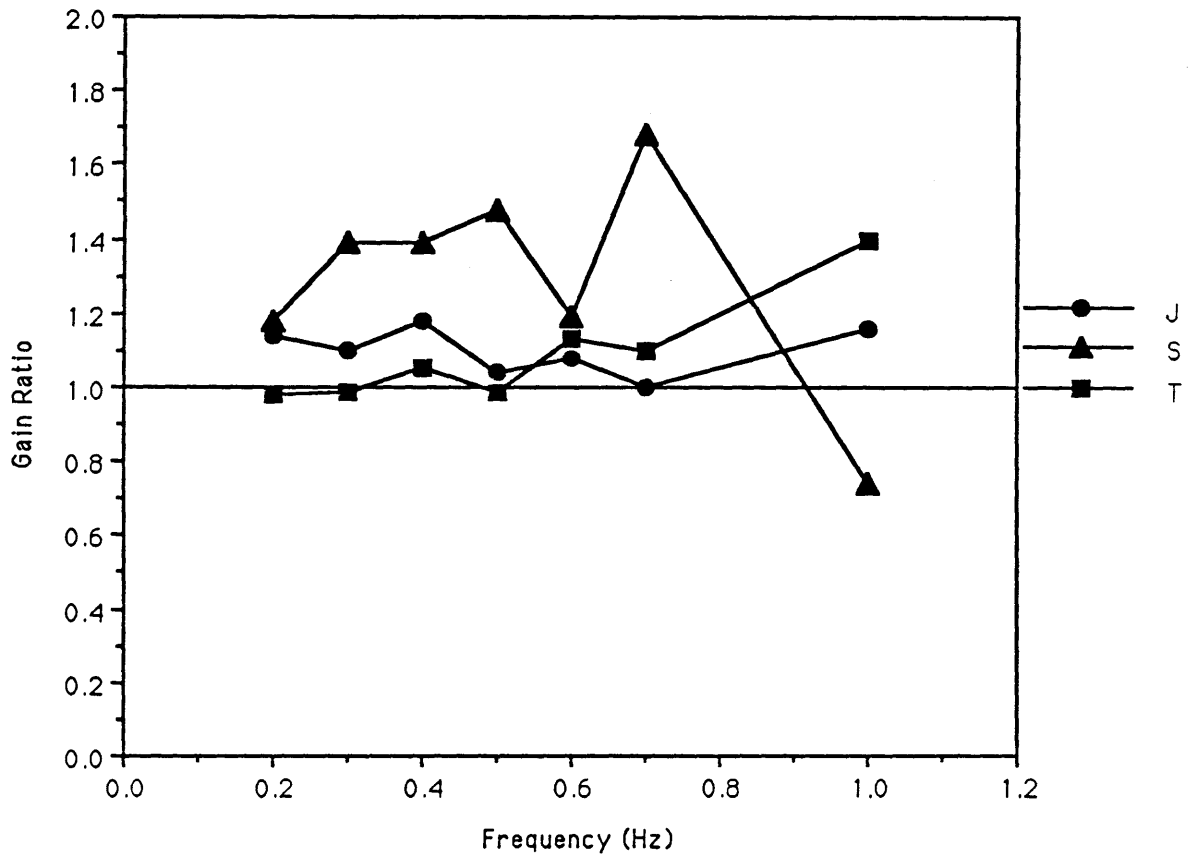


Figure 4.39 Ratio of visual+vestibular tracking gain to smooth pursuit gain for predictable sinusoids. (Using mean value at each frequency for each subject.)

(Visual+Vestibular) - (Smooth Pursuit)
Single Sinusoids
Phase Difference

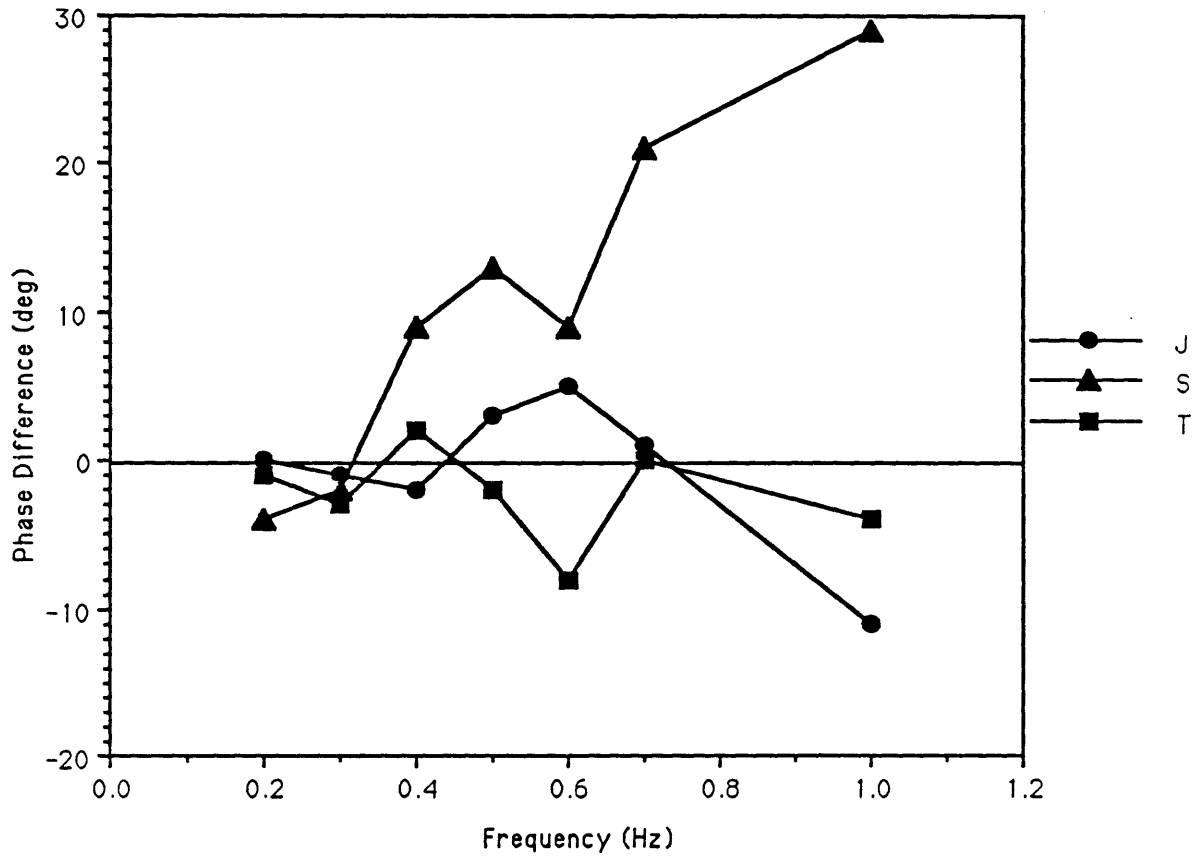


Figure 4.40 Difference between visual+vestibular tracking phase and smooth pursuit phase for predictable sinusoids. (Using mean value at each frequency for each subject.)

Smooth Pursuit & Visual+Vestibular Steps

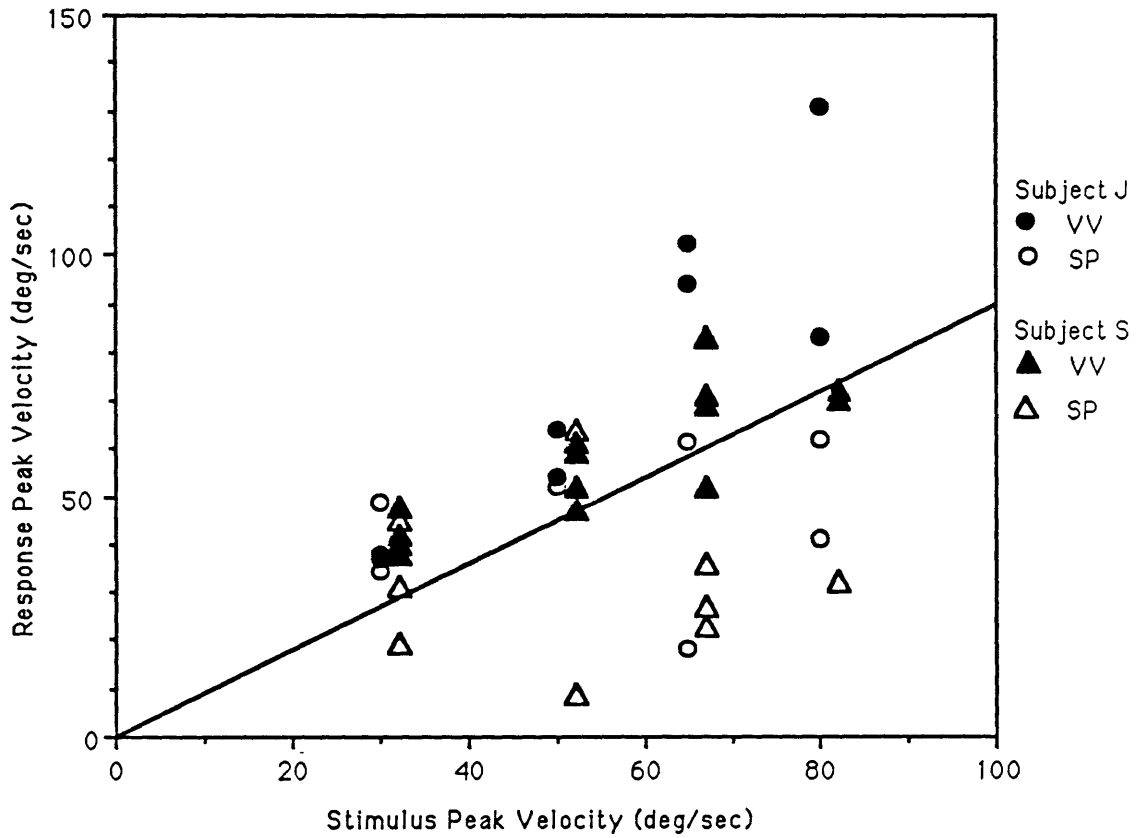


Figure 4.41 Peak velocity of eye movement response as a function of step response velocity, for visual+vestibular and smooth pursuit conditions; subjects J and S.

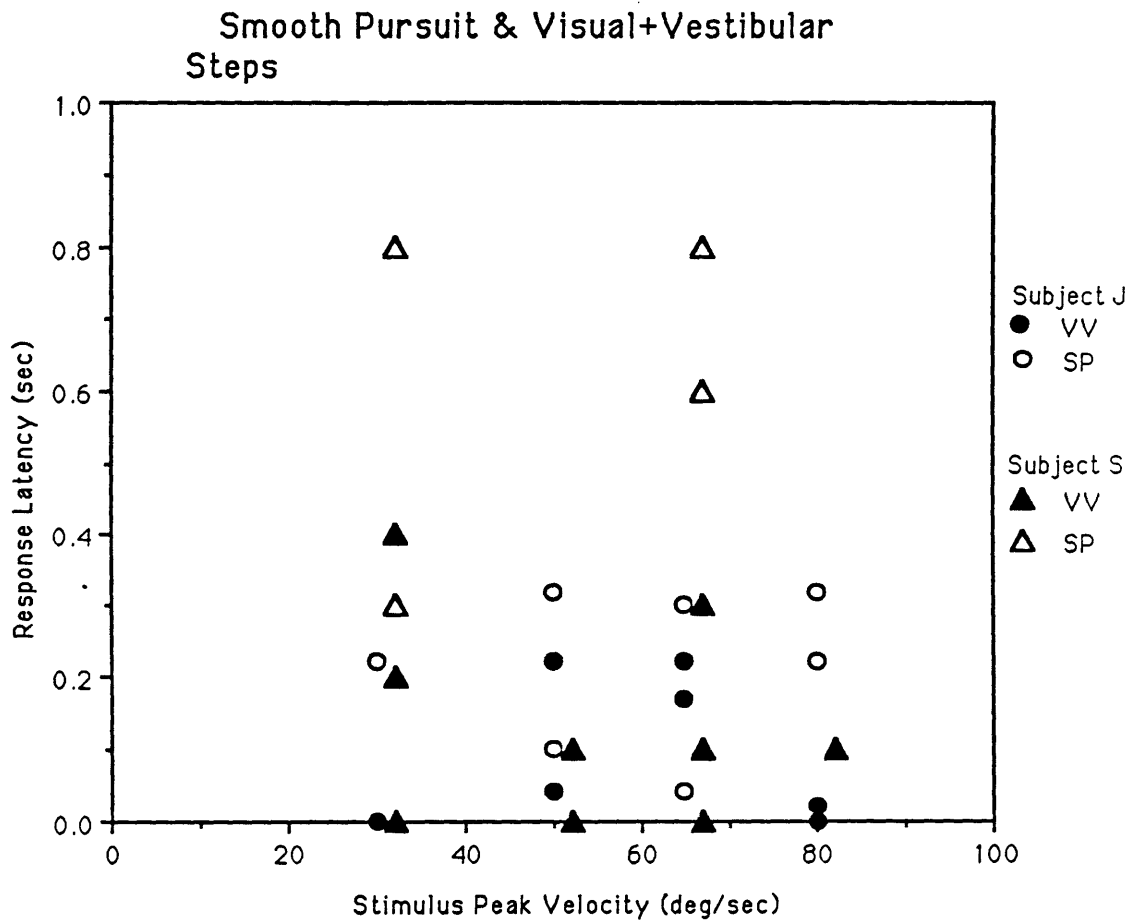


Figure 4.42 Latency of eye movement response as a function of step response velocity, for visual+vestibular and smooth pursuit conditions; subjects J and S.

Fixation Suppression Single Sinusoids

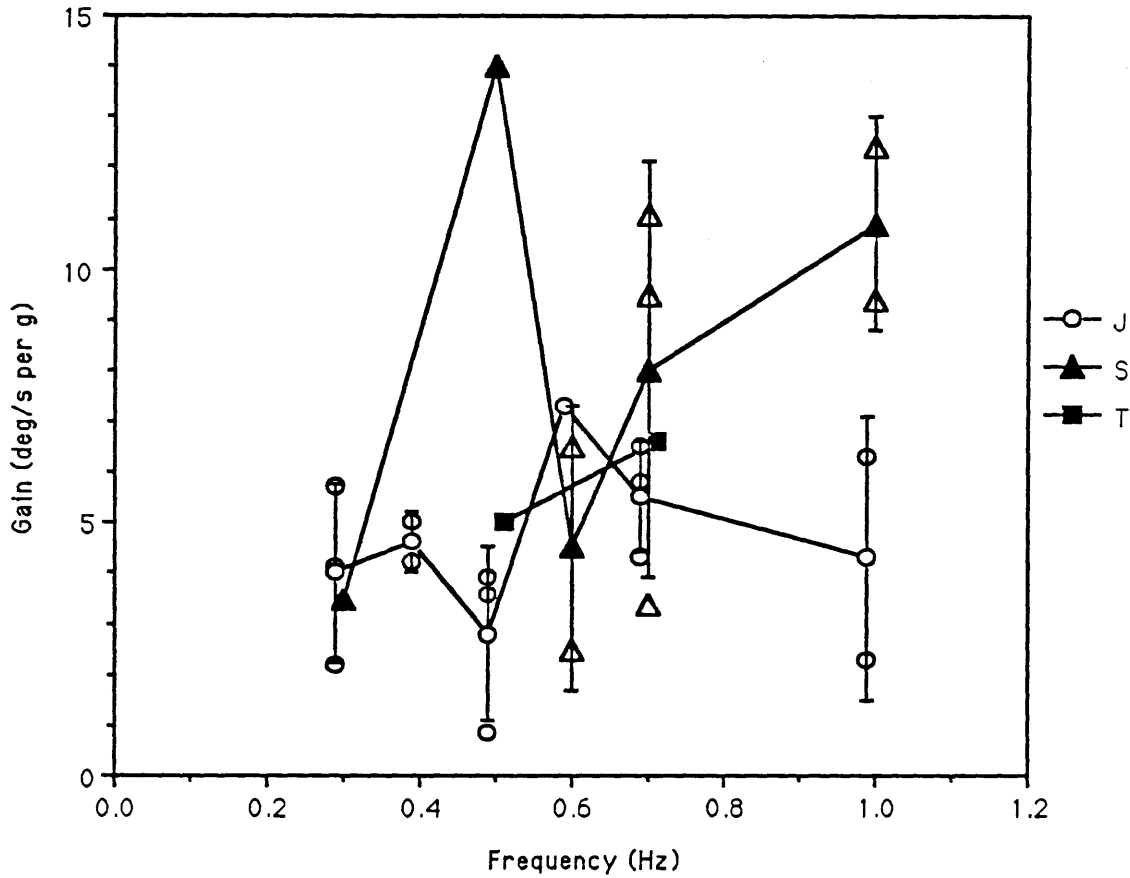


Figure 4.43 Fixation suppression of LVOR with predictable sinusoids; gain for all three subjects. (Solid symbols are means for each subject at each frequency. Bars are ± 1 s.d.)

Fixation Suppression
Subject J
SOS & Single Sinusoids

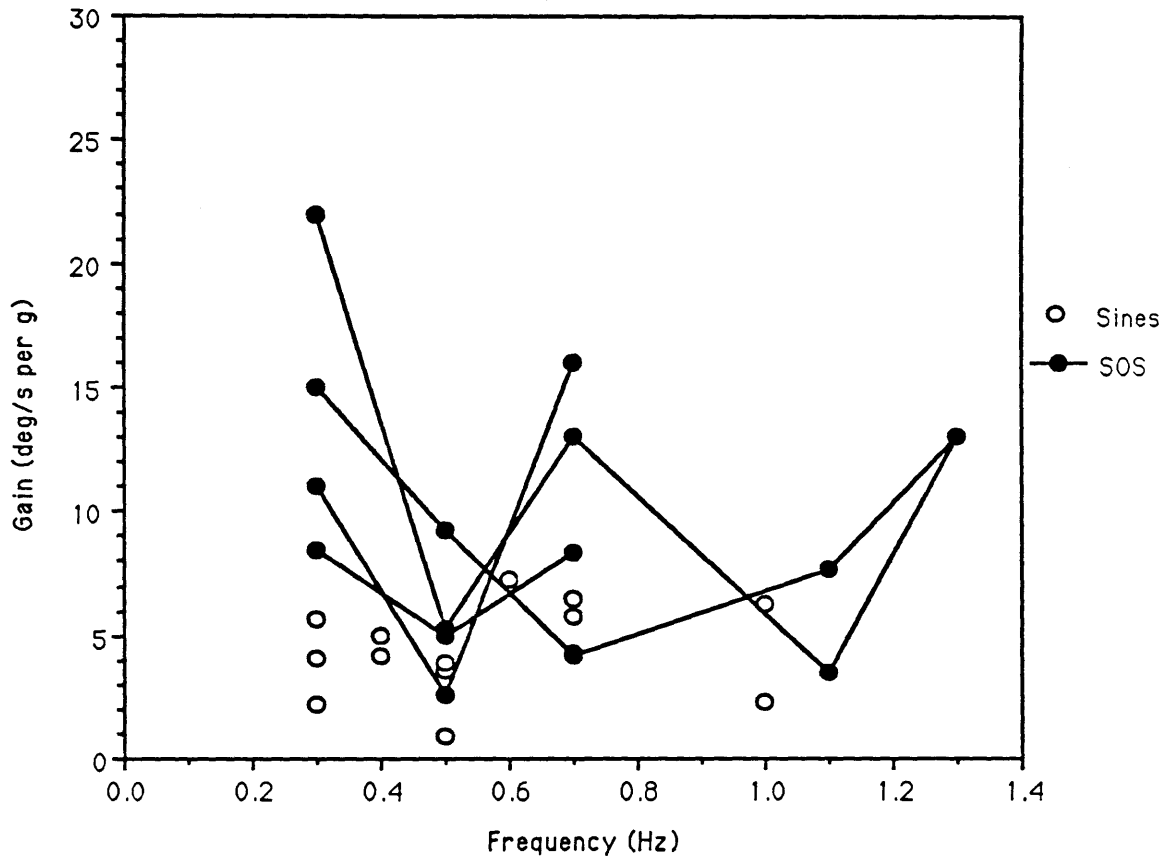


Figure 4.44 Fixation suppression of LVOR with predictable sinusoids and unpredictable sum-of-sinusoids; gain for all three subjects. (Solid symbols are means for each subject at each frequency. Bars are ± 1 s.d.)

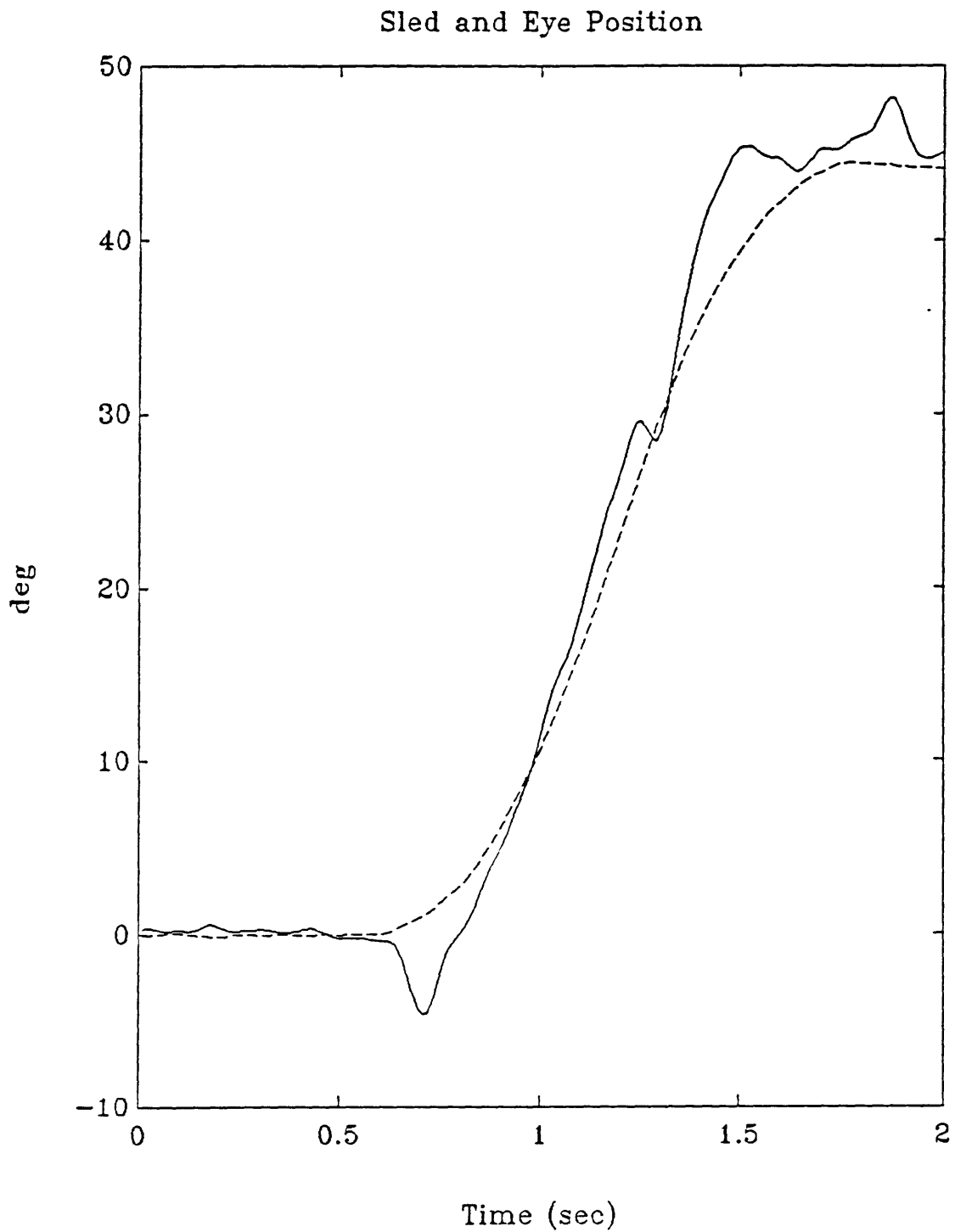


Figure 4.45 Example of anti-compensatory eye movement at step stimulus onset. Fast phases not removed. VV condition. Subject T. 0.5 g.

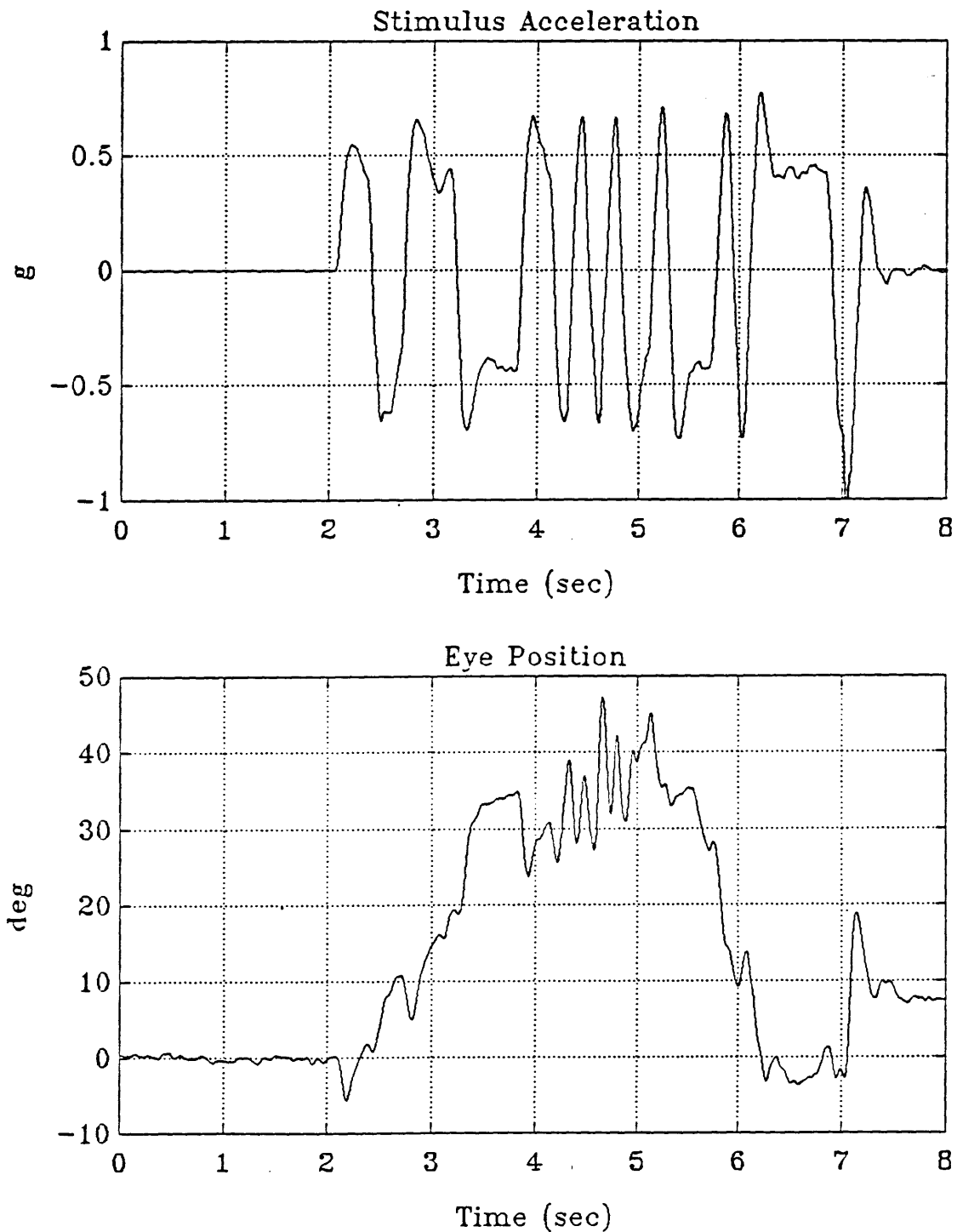
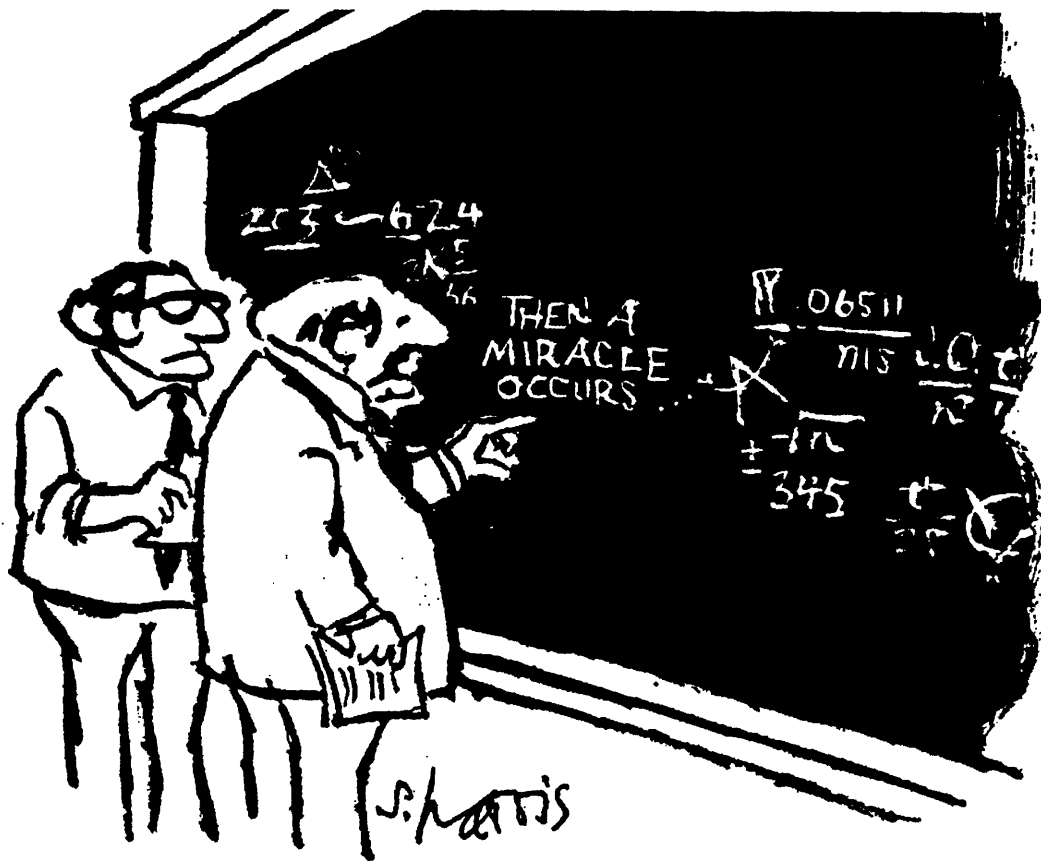


Figure 4.46 Example of PRBS acceleration stimulus (top) and eye position response (bottom), showing anti-compensatory movements at acceleration steps. Fast phases not removed. Subject T. 0.4 g, 0.2-2.0 Hz PRBS.

V Model



"I THINK YOU SHOULD BE MORE EXPLICIT
HERE IN STEP TWO."

PHENOMENA TO BE MODELLED

An analytical model is now developed, which will attempt to predict some key features of the results previously presented. The following important areas are addressed:

1. Gain and phase characteristics of smooth pursuit (SP), visual+vestibular tracking (VV), and after-image tracking (AI). Frequency dependence of these quantities will be considered, although stimulus constraints limited the acquisition of accurate data to a relatively small frequency range.
2. Improved SP and VV gain and phase responses with predictable stimuli.
3. Ongoing response which continues for a brief period after stimulus cessation. With AI, SP, and LVOR, with predictable sinusoidal stimuli, a reversal in the direction of eye movement occasionally occurs after the stimulus ends, with a corrective movement shortly thereafter. The reversal indicates that the oculomotor system is intending to continue to follow the stimulus. For random stimuli, the ongoing response consists of a short period in which the eyes continue in the same direction as they were going when the stimulus ended, indicating only a simple processing delay in this case.

APPROACH

Formalisms of Kalman filtering theory will be used in developing the model. Specifically, the system model will contain an internal representation of the stimulus generation, and implicit information about stimulus and sensor characteristics. As a brief review, one should recall that the Kalman filter is the optimal linear estimator for a given situation. For Gaussian process and measurement noises in the system model, it is the optimal estimator of any kind (i.e. a non-linear estimator will not perform better). Optimality is defined in

the least mean-square-error sense. Figure 5.1 shows a conceptual model of the Kalman filter structure and underlying input process generation (adapted from Gelb et al., 1974, page 123). The "system model" is a hypothetical model of input process generation; this corresponds to what the Kalman estimator "knows" about the process it is expected to estimate. Both stimulus generation and sensor dynamics are subsumed by this model. There is uncertainty about the exact nature of the estimator input signal, which is manifest by driving the system model with Gaussian white noise (GWN), $w(t)$. This noise process passes through an input matrix B (which can be embedded in the covariance structure $Q(t)$ of $w(t)$ if desired). The system matrix A specifies the system dynamics, producing the state variable vector $x(t)$, which is to be estimated by the Kalman filter proper. The Kalman filter accepts, as an input, linear combinations of this state vector via the measurement matrix C . These measurements are contaminated by another GWN process, the measurement noise $v(t)$ (with covariance matrix $R(t)$). The Kalman filter itself has, imbedded in its structure, knowledge of the system and measurement matrices A and C . The Kalman gain, K , is determined by solving the Riccati equation (see Gelb). This nonlinear differential equation specifies K in terms of the statistics of the noise processes and the matrices A , B , and C . Solving for K produces the least-mean-square error estimator for the given model and noise structure.

In the general case, all quantities in the Kalman filter are time-varying. However, it is assumed here that the input process is in the statistical steady state, that the various noise processes are statistically stationary, and that the filter has been in operation for a sufficiently long time to have reached its steady state. In practical terms, this means that the Riccati equation is solved for $\dot{P}=0$, and the quantities A , B , C , K , Q , and R are independent of t .

The Kalman filter structure will be used in developing a combined visual-vestibular model for tracking of predictive (sinusoidal) targets. This modelling approach should be considered a "proof of concept" effort. No attempt will be made to find the most precisely-fit parameters. Rather, typical parameter values to match the data from each subject will be found, more with respect to reproducing the general form of the response trends than with finding mathematically optimal values. The approach is somewhat akin to the philosophy of Hamming (1973): "The purpose of computing is insight, not numbers." The parameter values, their physical meaning, and their effect on the model response will be discussed. A major goal is to determine the validity of the Kalman filter formulation in this particular problem. Due to the embedded time delays necessary for adequate visual system representation, and the desire to constrain some of the parameters to realistic ranges, the fitting is done iteratively and interactively by varying parameters and assessing the resulting transfer functions. This method also allows one to get a better insight into the effects of the various parameters on the model response.

Emphasis in the modelling is on the responses to predictable sinusoidal stimuli and the presumed central pattern generator (CPG), or internal model of stimulus generation and sensor dynamics. Key elements of the SP subsystem which is developed for unpredictable stimuli (sum-of-sines, SOS) are maintained as inputs to the CPG model; these elements include an input processing delay and an output motor delay. For combined VV tracking, acceleration information as provided by the otolith organs is blended with the visual velocity information. A simple reconfiguration provides a model of AI tracking with the same structure. Two of the major characteristics to be expected from the model are, for predictable stimuli: 1) low phase lag tracking, despite input and output delays; 2) capability for ongoing responses after stimulus cessation. Both of these effects are direct consequences of the internal model (CPG) structure. Note that some

important features will not be manifest in the transfer functions, but only in time-domain simulations.

The philosophy of the modelling is to treat the control of eye movement as an estimation problem. Since the dynamics of the eyeball are negligible relative to the stimulus and response dynamics considered here (Robinson, 1981), the control system aspects of the problem are not considered. Rather, it is treated as if the central nervous system blends sensory inputs in some optimal way so as to create an internal estimate of head/body motion. The resulting estimate is used more or less directly to drive the eye movement in a compensatory manner. In this way we can treat the eye movement as the observable output of an optimal estimator for head/body motion.

DEVELOPMENT

The model development will be presented in several steps. First, a simple first-order model of smooth pursuit (SP) with unpredictable stimuli (SOS) is discussed. Then, additional otolith input information is added, creating a second-order Kalman filter model of visual+vestibular (VV) tracking. Finally, this model will be modified slightly for predictable (sinusoid) tracking, for both the SP and the VV conditions. The modification will yield a model which has information about stimulus predictability embedded in it in the form of a central pattern generator (CPG). This CPG will arise naturally from the Kalman filter formulation.

Figure 5.2 presents the basic SP/SOS model. It is in the general form of a first-order Kalman filter. The A matrix (actually a scalar in this case) is zero, however, so that there is no pole. This provides adequate unpredictable stimulus (SOS) modelling, with a straightforward addition easily made (the CPG) for predictable stimulus modelling. Sensory input processing and output motor processing delays are included; these values

are nominally 50 and 30 msec, respectively (based on data reviewed in Robinson, Gordon & Gordon, 1986). For the present purposes the values are not critical, but the delays serve an important purpose for evaluating the sinusoidal-tracking enhancements to be made to the model: for reduced-phase tracking the CPG must compensate for these delays. An efferent copy of the eye movement is added to the retinal slip velocity to create a central representation of target velocity. The efferent copy is a copy of the motor command sent to the extraocular muscles, and is used to maintain perceptual stability of the seen world during eye movements (MacKay, 1973). This efferent copy is scaled by a gain K_e and delayed appropriately so as to be in synchrony with the delayed retinal slip velocity input. The central velocity representation is processed by a Kalman filter with feedback gain C_{11} , Kalman gain K_{11} , and no pole. The filter output is sent through a motor delay (approximating the neural propagation time from premotor circuits to eye muscles and the oculomotor plant lag), to produce the slow phase velocity (SPV) eye movement output.

The model at this point resembles that of Robinson, Gordon, and Gordon (1986) on some major points. The input and output delays are identical. The efferent copy is likewise added to delayed retinal slip velocity to produce an internal representation of target velocity, and the efferent copy delay also matches the sum of the input and output delays. The efferent copy gain, however, is assumed to be 1.0 in their model, while here it is free to vary within a region around 1.0 as necessary.

The efferent copy gain K_e and feedback gain C_{11} warrant some explanation. They are in a sense redundant, and could be combined into one equivalent parameter. (In fact, the transfer function derivations in Appendix B use such an equivalent C_{11} .) There is, however, a distinction between the two which justifies their separation. The feedback gain C_{11} is inherent to the CPG/Kalman filter subsystem, and parallels a similar element (C_{22})

which will occur in the otolith processing branch. The efferent copy gain K_e , on the other hand, is independent of the central processing, is common to other models, and has a distinct purpose.

Note that the internal model may have delays associated with it, but it is assumed that these central processing delays are negligible in comparison with the input and output delays. This argument is perhaps strongest for the sinusoidal CPG model to be described later, for which it could be argued that the CPG "resonates" in such a way that its inherent delays are insignificant.

The transfer function of this model (note that all transfer function computations are reviewed in Appendix B) is:

$$\frac{SPV}{v} = \frac{K_{eye}K_{11}D_1D_2}{s+K_{11}(K_{eye}(D_1D_2-K_eD_e)+C_{11})} = \frac{\text{slow phase eye velocity}}{\text{stimulus velocity}}$$

Where:

- T_1 = input delay [$D_1=e^{-sT_1}$]
- T_2 = output delay [$D_2=e^{-sT_2}$]
- K_{eye} = input gain
- K_{11} = Kalman gain for visual input
- C_{11} = Kalman filter feedback gain
- K_e = efferent copy gain
- T_e = efferent copy delay (here equal to T_1+T_2) [$D_e=e^{-sT_e}$]

The addition of acceleration information as sensed via the otoliths (in the VV condition) leads to the model of Figure 5.3. The transfer function is derived and presented in Appendix B. The principle of the model is straightforward. It is a Kalman filter without

cross terms C_{12} , C_{21} , K_{12} , K_{21} . (These terms would create error signals based on comparing each state variable with the other state variable in addition to itself, and would feed these errors through separate gains to both integrators.) The terms were found to be unnecessary for adequate modelling, especially considering the resulting model simplicity and the difficulty in physically interpreting the cross-terms. The SP model of Figure 5.2 is repeated along the upper portion of the new model. Otolith (transduced acceleration) input is introduced at the bottom. The acceleration signal has its own Kalman filter integrator, feedback gain, and Kalman gain. So, K_{22} corresponds to K_{11} , C_{22} corresponds to C_{11} , and K_{oto} corresponds to K_{eye} .

The internal stimulus generation model in this case is simply a pair of cascaded integrators, since the input signals (velocity and acceleration) are related to each other through a mathematical integration. The upper state variable (at the output of the integrator) is a velocity signal, and becomes the slow phase eye velocity (SPV) output after an appropriate delay. The bottom state variable is an acceleration signal. Note that it follows from the Kalman filter formulation that the velocity error signal (reconstructed target velocity minus the scaled velocity state variable) contributes to the *change* in velocity (that is, the input to an integrator, the output of which is velocity). Likewise, the acceleration error signal contributes to a *change* in acceleration at the bottom. It is helpful to keep in mind the dimensions of these various signals when studying the model.

Recall from the earlier discussion that the Kalman filter internal model (A, C, and K) contains information about expected stimuli and also sensor dynamics. That is, it is a model of what the Kalman filter per se expects to receive as an input, which is the stimulus modified by the sensors. In the present case, sensor dynamics have been neglected. Over the frequency and acceleration ranges studied here, there is good evidence that the sensor dynamics are negligible. Certainly for visual information, there is no

reason to believe that stimuli with motions below 2.0 Hz are not transduced veridically (van de Grind, Grüsser & Lunkenheimer, 1973). As for acceleration information, it is presumably not used directly to drive LVOR SPV. This can be deduced from the fact that the dark LVOR phase is about 20 degrees leading, whereas a 90 degree lead would occur if an acceleration signal drove eye velocity output more or less directly. I will assume here that this characteristic is mainly due to later processing of the otolith signals, and that relatively pure acceleration information from the otoliths is available to the CPG. Certainly this is not a problem from the point of view of the otolith response, as primary afferent recordings indicate that this information is veridical over at least the stimulus range of this study (Fernandez & Goldberg, 1976). Note that dark LVOR is not modelled adequately by this arrangement. In particular, the otolith gain K_{oto} is not determined by the dark LVOR response (whereas K_{eye} is determined by the SP response data). There is no completely satisfactory explanation, coincident with the present model, for the transformation of linear acceleration to SPV. Buizza et al. (1980) resolve the LVOR gain modelling problem by stating that the otolith gain must change from the dark condition to the light condition, which is essentially the approach taken here.

The final, two-input (visual and vestibular), predictable stimulus motion, model is in Figure 5.4. (Again, see Appendix B for the transfer function.) The only change from the previous model is the addition of a cross-feed gain of $-\hat{\omega}^2$ from the upper to the lower integrator, where ω is the frequency of the sinusoidal input stimulus. This corresponds to the fact that, for a sinusoid:

$$\text{velocity} = \beta \sin(\omega t)$$

$$\text{acceleration} = \beta \omega \cos(\omega t)$$

$$\text{jerk} = -\beta \omega^2 \sin(\omega t) = (-\omega^2) \text{velocity}$$

The sine-wave generator formed by the cross-coupled integrators in this model is presented for clarity in Figure 5.5. Recall that the top state variable is velocity, and the bottom one is acceleration. The input to the second integrator is actually a jerk signal, since it is integrated to produce the acceleration state variable estimate. So, by multiplying the velocity variable by $-\hat{\omega}^2$ and sending it to the jerk signal, cross-coupled integrators are produced which are an internal model of a sine wave generator. The two input signals as transduced by the visual and vestibular systems correspond naturally to the dimensions of the two state variables.

This central pattern generator provides some unique characteristics, which are present in the data but not common to other visual-vestibular models. Some of these properties are reviewed at the end of the Background chapter. In particular, responses will continue after the cessation of the stimulus, to an extent determined by the parameter values. This phenomenon of the model is demonstrated in a later section.

A simple modification of the full VV/sine model of Figure 5.4 will produce a smooth pursuit/predictable stimulus (SP/sine) model, shown in Figure 5.6. Quite simply, the otolith input segment has been removed, along with its feedback gain path C_{22} and its Kalman gain K_{22} . What remains is the SP/SOS model of Figure 5.2 combined with the CPG of Figure 5.5.

Two other variations produce after-image tracking models. The VV/SOS model of Figure 5.3 is changed by removing the retinal slip feedback loop, since retinal slip is zero with a retinal after-image. The resulting model is in Figure 5.7. Note that the visual efferent copy is retained. Similarly for predictable sinusoidal stimuli, the VV/sine model of Figure 5.4 leads to the AI/sine model of Figure 5.8.

FREQUENCY ESTIMATOR SUBSYSTEM

The system matrix A in the Kalman filter (equivalently, the internal CPG structure) contains a parameter whose value is equal to the frequency of the input sinusoid. This is the $-\hat{\omega}^2$ term appearing in the sinusoidal tracking models. For predictable stimuli, this parameter must be determined. A separate subsystem is postulated which estimates this frequency. Full details are in Appendix C. Briefly, a Kalman filter is linearized to estimate the frequency of the reconstructed target velocity signal. The resulting, surprisingly simple, model works quite well for sinusoidal signals. The fact that the model itself determines the value of ω explains why this term is always presented in the models as $\hat{\omega}$, that is, as an estimate of the actual frequency. Further work on this subsystem might be useful in reproducing the behavior observed in some other SP experiments (see "Further Results" below).

The frequency estimator is presumed to connect to the rest of the model at such a place that accurate information on the target stimulus motion is available. One obvious choice is the "reconstructed target velocity" signal.

The particular estimator described in Appendix C has the property of producing an estimate of zero in most cases of non-sinusoidal signals. The SOS and sine tracking versions of the model differ only in that the $\hat{\omega}$ term is missing (that is, equal to zero) in the SOS version. Therefore, the same model, when used with the frequency estimator described here, will model both predictable and non-predictable tracking.

MODEL FITS/PARAMETER VALUES

Parameter values and the resulting transfer function curves for all subjects are in Appendix D. Those for subject J are presented here with a discussion of some significant points.

Typical parameter values determined for subject J's smooth pursuit with an unpredictable stimulus (SP/SOS) are shown in Figure 5.9, along with the resulting model gain and phase responses. The error bars (± 1 s.d) for subject J's actual SP/SOS data are overlaid on the graphs. The important point to note is the significant phase lag, due to the system's inability to compensate for the input and output delays. With predictable sinusoidal stimuli, the response improves by reducing the phase lag, as in Figure 5.10. The gain remains relatively unchanged. Note that the CPG model can effectively overcome the input and output delays and produce reduced-latency (smaller phase lag) tracking.

The addition of vestibular information with unpredictable stimuli leads to the VV/SOS model results in Figure 5.11. Note a slight gain increase from the SP/SOS response, and also a slight phase improvement. Similarly, Figure 5.12 adds the vestibular information to the predictable model, providing the best gain (closest to 1.0) and lowest phase lag responses of all the conditions and all the models.

After-image tracking model results are shown in Figures 5.13 (SOS) and 5.14 (sine). Parameters are those previously determined from the SP and VV responses, and so the model fit in the AI cases is not as good. Note especially the phase responses. The gain values, however, are surprisingly good, considering that the parameters were selected based on the previous sets of experimental conditions.

A computer simulation of these models using the EXTEND package on a Macintosh computer is presented in the next six figures. All simulation trials were performed with parameters determined for subject J (as previously discussed) and with an input sinusoidal signal of 1.0 Hz ($\omega=2\pi$). Figures 5.15-5.17 present the unpredictable stimulus (SOS) model results for SP, VV, and AI models respectively. (Note that although the

input is a predictable sinusoid in each case, the models are unpredictable stimulus (SOS) models). Corresponding simulations with the predictable sinusoid models are in Figures 5.18-5.20, for SP, VV, and AI respectively. Included in these plots is the running frequency estimate ($\hat{\omega}$). Note that the correct value for $\hat{\omega}$ in these cases is $2\pi \approx 6.28$, which is reached quite rapidly. Comparing these six figures validates the model transfer function results of Figures 5.9-5.14. Note that, as in a few actual experiment trials, the response tends to continue after cessation of the stimulus. This lends support to the concept of the CPG. The AI cases especially (Figures 5.17 and 5.20) have a smooth ongoing response, and also an initial cycle or so during which the response builds to its final level. Both of these aspects are exhibited in occasional AI data, as in Figures 4.11-4.14 and Figure 4.23 (especially the build up in Figure 4.13). The SP and VV responses, on the other hand, attain their steady-state levels almost immediately (see Figures 4.24-4.26). Unfortunately, the actual responses in these cases do not show quite the same ongoing behavior as do the simulations.

PURSUIT OF OTHER STIMULUS PATTERNS

Bahill and McDonald (1983b) performed human smooth pursuit experiments with several predictable stimuli in addition to sines. An attempt is made here to model the results which they obtained with velocity triangle trajectories (position parabolas): near zero-phase tracking with the eyes producing a triangular velocity pattern, indicating that the internal CPG can generate an appropriate triangular velocity command. Figures 5.21 through 5.23 show the modelling results using, respectively, the SP/SOS model, SP/sine model with frequency estimator, and SP/sine model with the frequency set to the correct value (1.0 Hz) a priori and not allowed to vary. Note immediately that all variants of the model produce essentially the same results: non-zero phase tracking, and a non-triangular response. Even with the CPG frequency set to the correct value manually (Figure 5.23), the tracking is poor. Note also that the frequency estimator does a poor job on the

triangular waveform, eventually settling on an estimate of zero, shown in Figure 5.24 (repeat of Figure 5.22 with $\hat{\omega}$ added).

In summary, the sinusoidal CPG used in this model does not perform adequately in tracking a triangular waveform. This is separate from the fact that the frequency estimator does not do an adequate job of estimating the frequency of a triangular signal, since the SP/sine model with $\hat{\omega}$ set a priori performs no better. It would appear that a separate CPG might be needed for each different class of predictable signals, unless suitable modifications can be made to the current model. This would be an interesting area for further work.

Along the same lines, Michael and Melvill Jones (1966) found that SP phase lag increased as the bandwidth of a random stimulus increased (from 0.0 to 1.0 Hz). Attempts to duplicate this result were not successful. Random stimuli of the same bandwidths as used in their study were created and introduced to the SP/sine model. Without exception, frequency estimates $\hat{\omega}$ converged to zero, even with the narrowest bandwidth (except for 0.0 Hz: a pure sine) of 0.05 Hz. This is not surprising in light of the discussion in Appendix C. The result was that the model became essentially the SP/SOS model. However, at 1.0 Hz center frequency, all model phase lags were 47 deg, regardless of bandwidth. Thus it seemed as if the model was tracking one certain frequency component of the input waveform in all cases. However, a 1.0 Hz pure sine only yields a phase lag of 26 deg in the SP/SOS model. Any frequency component that the model was tracking would then have to have been well beyond 1.5 Hz to produce a 47 deg lag. At any rate, a different type of frequency estimator subsystem will be needed to reproduce these types of experimental results. The Kalman filter-based estimator here has the disadvantage that the Kalman gain trajectory is predetermined by the noise process values, and after a few seconds the filter essentially stops responding to new input information. Some way to

force the filter to periodically increase K , perhaps based on some measure of increasing retinal error or recognition of a change in stimulus predictability, would be a good first step in modifying the model.

SPECULATION ON NOISE COVARIANCES

Appendix E contains theoretical calculations of the process and measurement noise covariance matrices Q and R for the VV condition for each subject. This is a highly speculative analysis. In the usual Kalman filter application, engineering insight is applied to choose values for these noise processes, and the Ricatti equation is solved for \hat{P} , thereby also providing the Kalman gain. In this study, the Kalman gains K_{11} and K_{22} were set manually so as to reproduce the experimental data. Likewise for the elements of the B matrix (K_{oto}) and the C matrix (C_{11} , C_{22} , K_e , and K_{eye}). Appendix E contains an argument for setting values of the measurement noise covariance R based on threshold values for motion detection by the visual and otolith systems. With these values, one can work backwards and deduce the underlying theoretical values of the process noise covariance Q . This analysis is very preliminary, as some questionable assumptions were made, such as neglecting the delays in the vision section and using the same threshold data (R values) for all subjects.

The resulting values for the cross terms (Q_{12} and P_{12}) vary with frequency for sinusoidal tracking. The other elements are the same for either the SOS or the sinusoidal tracking models. For the SOS structure, the values for each subject are:

For J and T:

$$Q = \begin{bmatrix} 1.0 & -10^{-5} \\ -10^{-5} & 10^{-6} \end{bmatrix}$$

For S:

$$Q = \begin{bmatrix} 25 & -4 \times 10^{-5} \\ -4 \times 10^{-5} & 1.6 \times 10^{-7} \end{bmatrix}$$

$$P = \begin{bmatrix} 0.036 & 0 \\ 0 & 0.01 \end{bmatrix}$$

$$P = \begin{bmatrix} 0.17 & 0 \\ 0 & 0.02 \end{bmatrix}$$

$$\text{units} \equiv \begin{bmatrix} \left(\frac{\text{deg}}{\text{sec}}\right)^2 & \left(\frac{\text{deg}}{\text{sec}}\right) \times \left(\frac{\text{m}}{\text{sec}^2}\right) \\ \left(\frac{\text{deg}}{\text{sec}}\right) \times \left(\frac{\text{m}}{\text{sec}^2}\right) & \left(\frac{\text{m}}{\text{sec}^2}\right)^2 \end{bmatrix}$$

The elements of the error covariance matrix P are the Kalman filter's own estimate of the error of its state variable estimates. Thus P_{11} is a measure of the error in the velocity state variable estimate, which is of primary interest as it leads directly to SPV output. Elements of the process noise covariance matrix Q are related to the range of input stimuli which the Kalman filter "expects" to see.

INTERPRETATION OF PARAMETERS

Note first that P is based directly on K, C, and R; since $K=PC^TR^{-1}$, the elements of K are proportional to the ratio of the state estimate error (P_{ii}) to the corresponding measurement error (R_{ii}). So, large K values generally indicate a greater confidence in the incoming measurements than in the current estimate. Analysis of P will thus provide some insight into K and C.

Keeping in mind that the P and Q values derived above relate to the VV condition, there is nonetheless some insight in examining the LVOR and SP conditions also. Comparing the entries in the P matrices above, we see that $P_{22}(S) > P_{22}(JT)$, where the term in parentheses refers to the subject. It appears from this perspective that subject S's confidence in the acceleration estimate is less than that for subjects J and T (i.e. the error variance is higher, so the confidence is lower). There is some experimental support for this; subject S had a higher LVOR threshold, and (with sinusoidal stimulation) produced

far fewer consistent and periodic dark LVOR responses (five, versus 17 for J and 12 for T), than did the other subjects. It is also the case that $P_{11}(S) > P_{11}(JT)$, implying that the velocity estimate error for S is likewise greater than that for J and T. Some experimental support for this position may be found in the lower portion of Table 5.1, which is a listing of the response standard deviations for each subject at each frequency (each trial produced one measurement). Clearly, in the majority of the cases (10 out of 12) subject S's deviations were greater than the other subjects'. The numerical values do not correspond well (one might expect that the covariance ratio $P_{11}(S)/P_{11}(JT)$ would be approximately equal to the square of the s.d. ratio at each frequency), but the trend is apparent nonetheless. This analysis is promising, because a derivation based on a theoretical choice of measurement noise R, and manually-determined parameters K and C selected to fit experimental frequency response data, produced a result which is consistent with the variability of the experimental data. This type of reasoning may be helpful in understanding and interpreting variability in normal physiological responses.

Looking at the values of K directly (Table D.1), $K_{11}(S)$ is five times the value of $K_{11}(JT)$, indicating that S places a high reliance on the visual velocity measurement relative to the current internal velocity state estimate, although $K_{11}(JT)$ is relatively large also. All subjects seem to have great faith in the visual velocity measurements, using a large K_{11} to give high weighting to incoming sensory information. The values of K_{22} are not as large. $K_{22}(JT)$ is one, indicating about equal confidence in otolith sensory input and the current internal acceleration state estimate. $K_{22}(S)$ is two, indicating somewhat greater reliance on sensory input. Overall, visual velocity information is much more heavily weighted than otolith acceleration information in this formulation.

Another effect which can be related to relative values of K is the ongoing response. A scalar Kalman filter will illustrate the concept. The transfer function and impulse response of such a filter are:

$$\frac{K}{s-a+KC} \quad K e^{(a-KC)t}$$

(Recall that $a < 0$.) A brief inspection shows that as K increases, the exponential decay time decreases. This makes sense also in terms of the Kalman filter formulation; large K means that incoming sensory information is heavily weighted, and when the stimulus goes to zero (stops) and the sensory information indicates this, a large K will cause the system output to go to zero more rapidly. A somewhat subjective analysis of the ongoing responses of the three subjects seems to indicate that subject S had the fewest ongoing responses. This subject also had the largest K values, which is what we would expect based on the previous argument. This analysis is based on the subjective nature of determining ongoing responses, but is another example of the insight which might be gained from the Kalman filter approach.

It is not very clear how to interpret the values of Q , especially since they were calculated based on some preliminary analyses. In general, the process noise is introduced into the Kalman filter to account for uncertainty in the model parameters (A , B , and C), unmodelled dynamics, and statistical knowledge of the process to be estimated. Referring to Table D.1, we see that $Q_{11}(S) > Q_{11}(JT)$, indicating that subject S has a greater uncertainty of what to expect in terms of visual information (uncertainty which may presumably arise from any of the factors just mentioned). On the other hand, $Q_{22}(S) < Q_{22}(JT)$, indicating that S has less uncertainty about the acceleration input. The former inequality may be reflected in the low SP gain of subject S, who is "not sure" of what to expect from the visual input and therefore does not "lock on" to the target as do the other subjects. The interpretation of the process noise is seldom clear even in more

common engineering applications, and we should exercise caution to not over-interpret its meaning here.

SUGGESTIONS FOR FURTHER MODELLING WORK

There are some other elements which could be incorporated into this type of model:

- Fixation suppression (FS) should be easily modelled with no changes to the structure.
- Better model performance in the AI case might be obtained by determining parameters for this condition first, and then fitting the other conditions. There is considerable freedom in the choice of parameter values which might make this possible. A better interpretation of the physiology behind the AI tracking might result from examining the parameters of such a model.
- Based on results which indicate that the smooth pursuit steady state response has a component derived from retinal error acceleration (Lisberger et al., 1981), retinal slip acceleration could be used as an additional input. SP velocity saturation is evident in the step responses in this study but not the sinusoidal responses, but it is overcome in the VV condition.
- It would be interesting to add a velocity saturation to the model and see the effect of the otolith input.
- Other frequency estimation schemes should be investigated. Although the one used here is simple and works well, it will not respond to even a discrete change in frequency, and this is decidedly unphysiological.
- The addition of appropriate dynamics to the efferent copy (now just a gain K_e) may improve the AI model phase prediction.
- An attempt could be made to quantify the nature of the ongoing responses, to see if they occur under certain conditions or randomly, or based on previous experience and anticipation.

- A more realistic decay of the ongoing responses might be incorporated, perhaps consisting of a fast decay element switched in a short amount of time after it is observed that the stimulus has ended. The delay time before this element takes effect could be related to past experience with similar predictable stimuli (an internal model of number of cycles expected, anticipated duration, etc.).
- By assuming no process noise in the stimulus ($Q=0$) and steady state conditions, the Riccati equation can be solved for the measurement noise R . This variation of the noise analysis used here might provide more insight into these noise processes.

MODEL PREDICTIONS

There are some predictions based on the model structure and concepts presented here which could be tested experimentally:

- The central pattern generator, in the sinusoidal cases analyzed here, produces a sinusoidal signal which is phase advanced relative to the oculomotor output. This is how the motor delays are effectively bypassed to produce low phase lag tracking. Careful neurophysiological measurements of the input and output neural delays and sinusoidally-modulated cells in the brain (possibly the cerebellum) could reveal if the CPG oscillates with the phase predicted by the model.
- The CPG as presented here has both sine and cosine components, which might be present in single-cell recordings during sinusoidal stimulation.

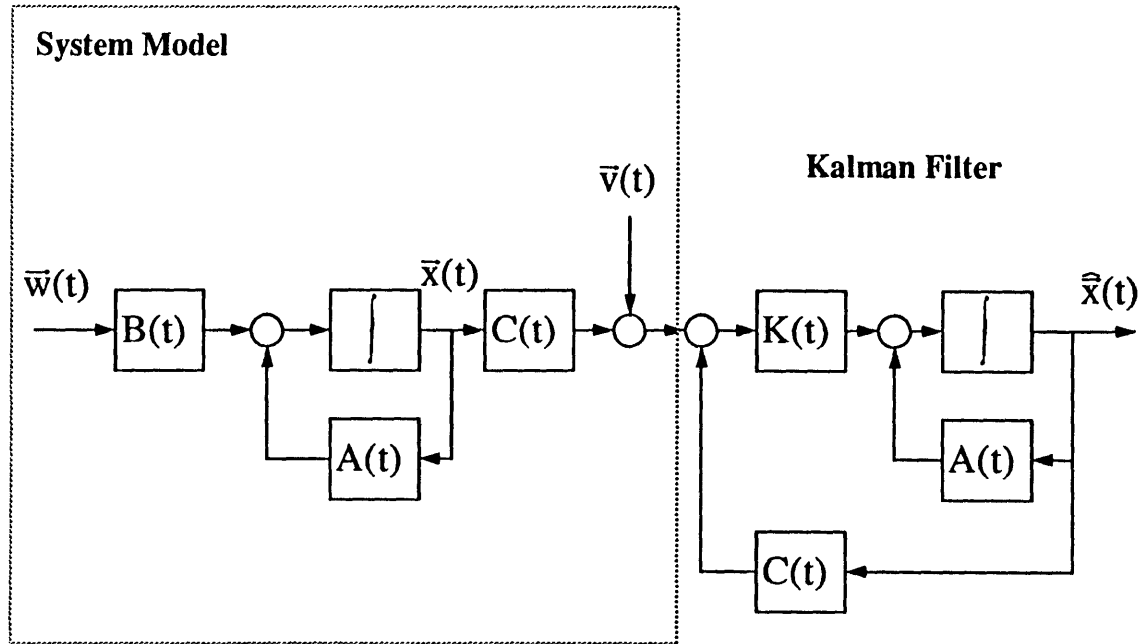
Visual+Vestibular / Predictable Sine Stimuli: Standard Deviations

Frequency (Hz)	Number of Measurements	Subject J	Subject S	Subject T
0.2	1			
0.3	3	0.09	0.17	0.07
0.4	3	0.01	0.65	0.03
0.5	3	0.02	0.03	0.05
0.6	3	0.02	0.26	0.04
0.7	3	0.05	0.06	0.11
1.0	3	0.51	0.21	0.14

Smooth Pursuit / Predictable Sine Stimuli: Standard Deviations

Frequency (Hz)	Number of Measurements	Subject J	Subject S	Subject T
0.2	1			
0.3	3	0.03	0.21	0.06
0.4	3	0.04	0.04	0.07
0.5	3	0.02	0.07	0.02
0.6	3	0.08	0.09	0.03
0.7	3	0.02	0.21	0.05
1.0	3	0.02	0.46	0.02

Table 5.1 Standard deviations of SP/sine and VV/sine data for all subjects.

**System**

$$\dot{\bar{x}}(t) = A\bar{x}(t) + B\bar{w}(t)$$

$$\bar{w}(t) \sim N(0, Q(t))$$

Measurement

$$\bar{y}(t) = C\bar{x}(t) + \bar{v}(t)$$

$$\bar{v}(t) \sim N(0, R(t))$$

$$\text{State Estimate } \hat{\bar{x}}(t) = A\hat{\bar{x}}(t) + K(t)[\bar{y}(t) - C\hat{\bar{x}}(t)]$$

$$\text{Error Covariance } \dot{P}(t) = AP(t) + P(t)A^T + BQ(t)B^T - P(t)C^TR^{-1}(t)C$$

$$\text{Kalman Gain } K(t) = P(t)C^TR^{-1}(t)$$

Figure 5.1 Conceptual model of Kalman filter (from Gelb, 1974).

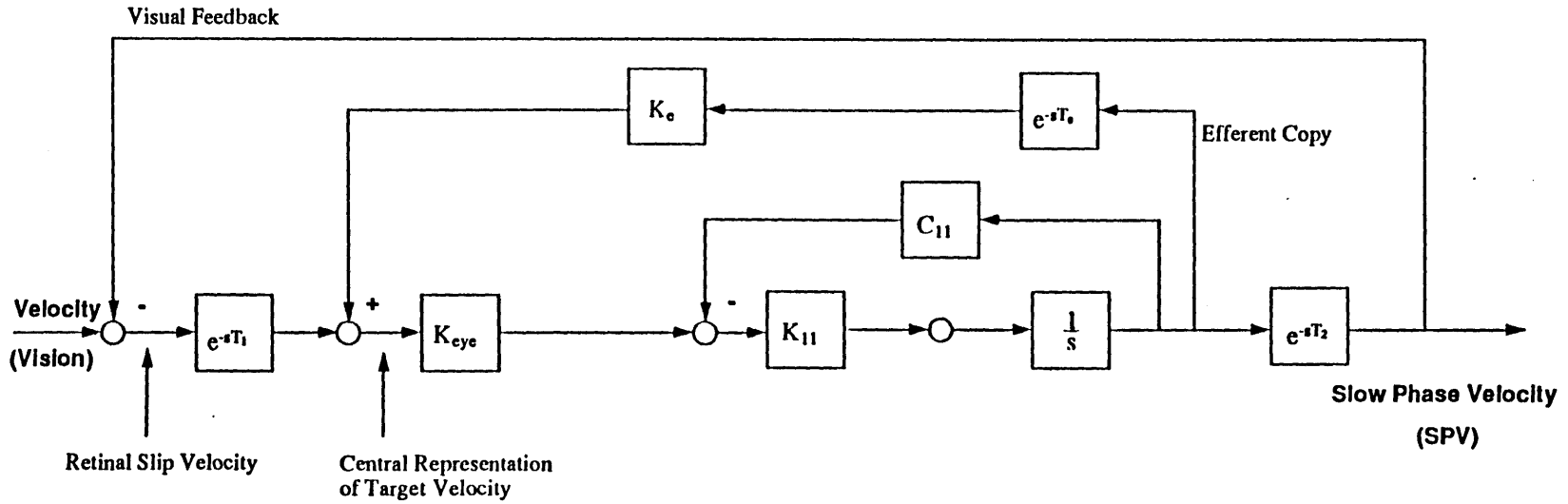


Figure 5.2 Smooth pursuit / unpredictable stimuli model (SP/SOS).

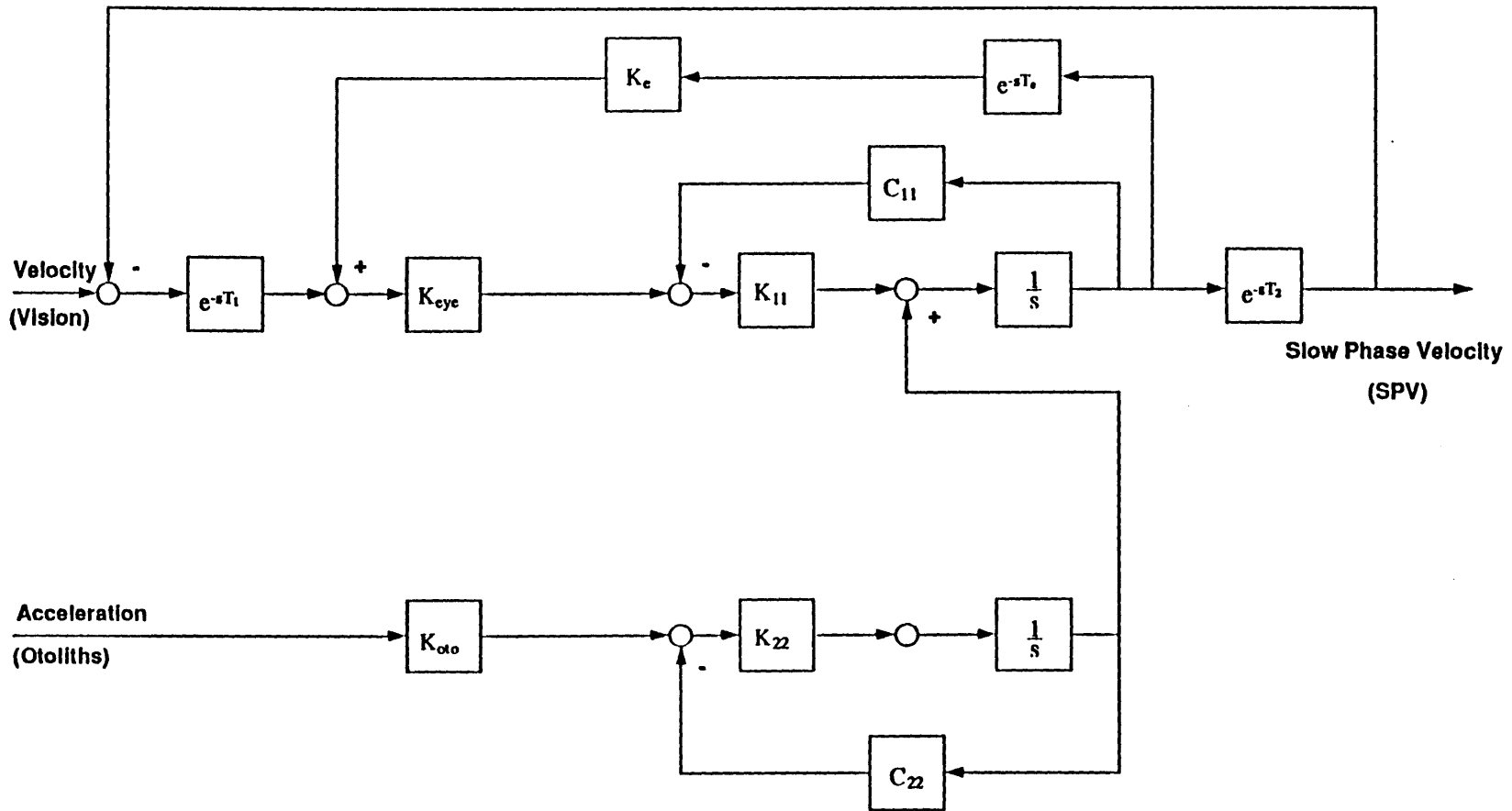


Figure 5.3 Visual+vestibular / unpredictable stimuli model (VV/SOS).

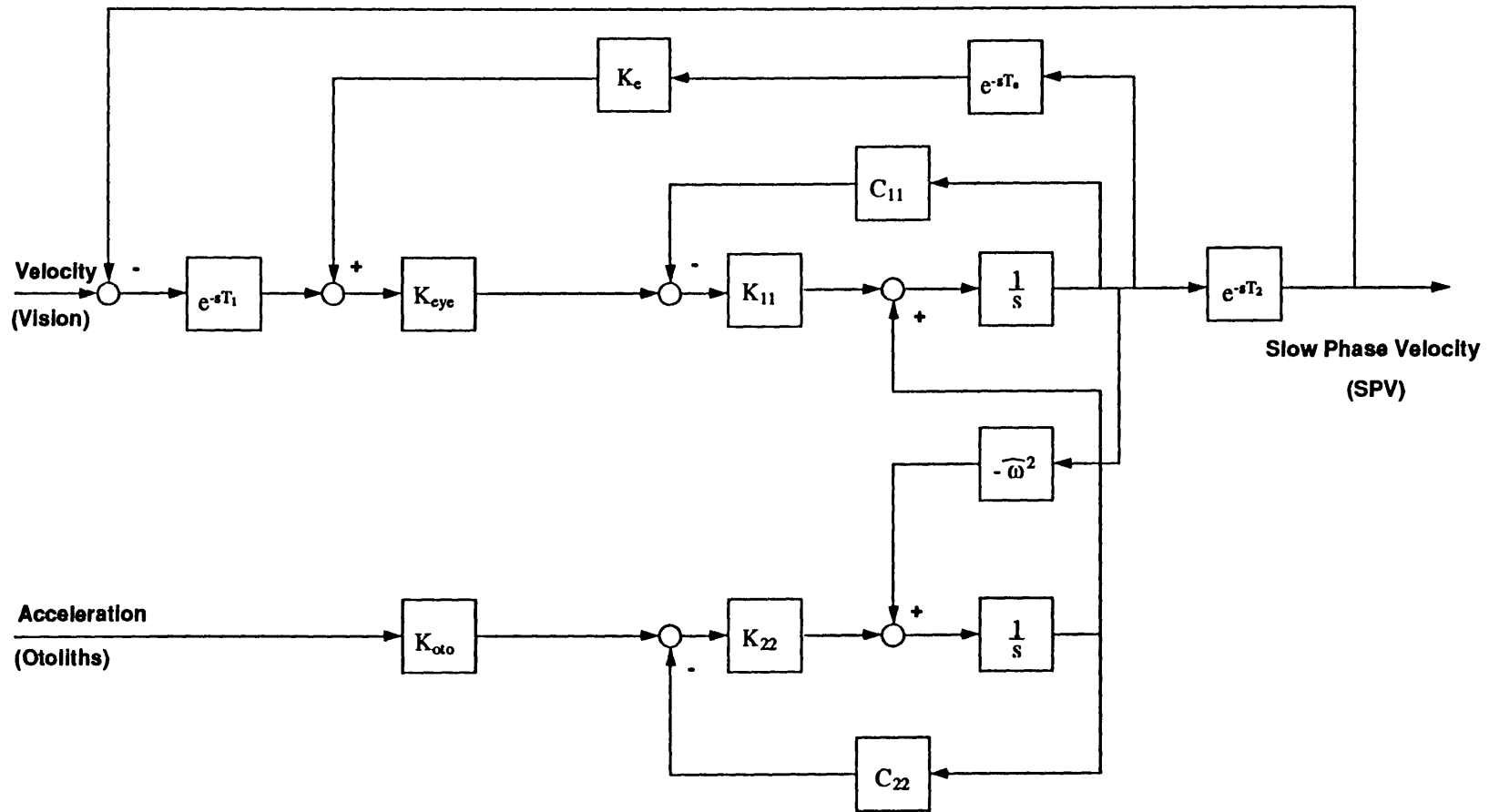


Figure 5.4 Final 2-input (visual+vestibular) / predictable (sinusoidal) stimuli model (VV/sine).

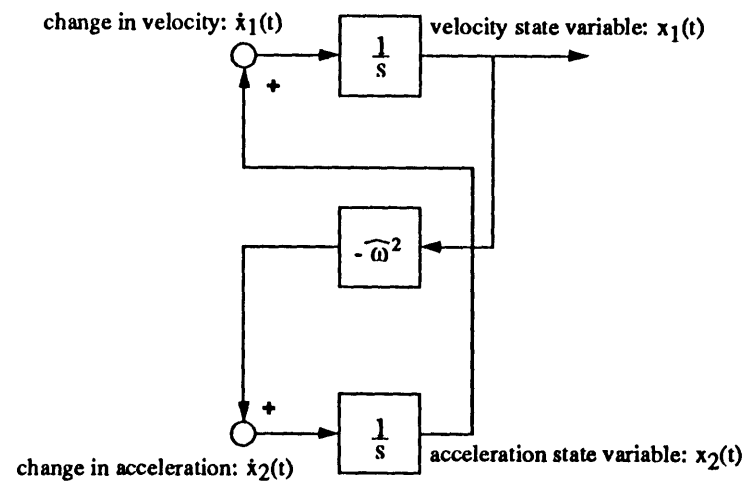


Figure 5.5 Sine-wave generator / central pattern generator (CPG) / stimulus generation subsystem from VV/sine model.

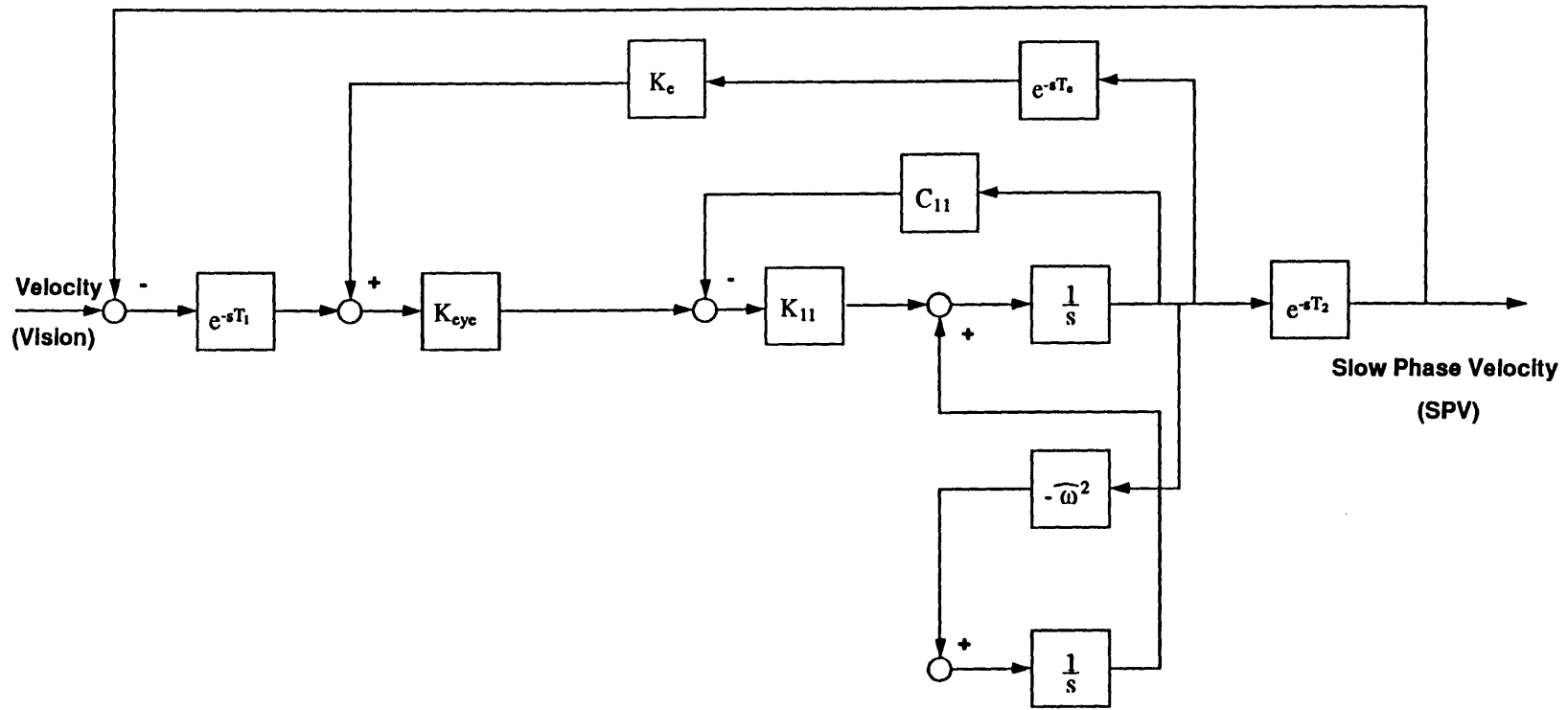


Figure 5.6 Smooth pursuit / predictable stimuli model (SP/sine), derived from VV/sine (Figure 5.4) by removing otolith input branch.

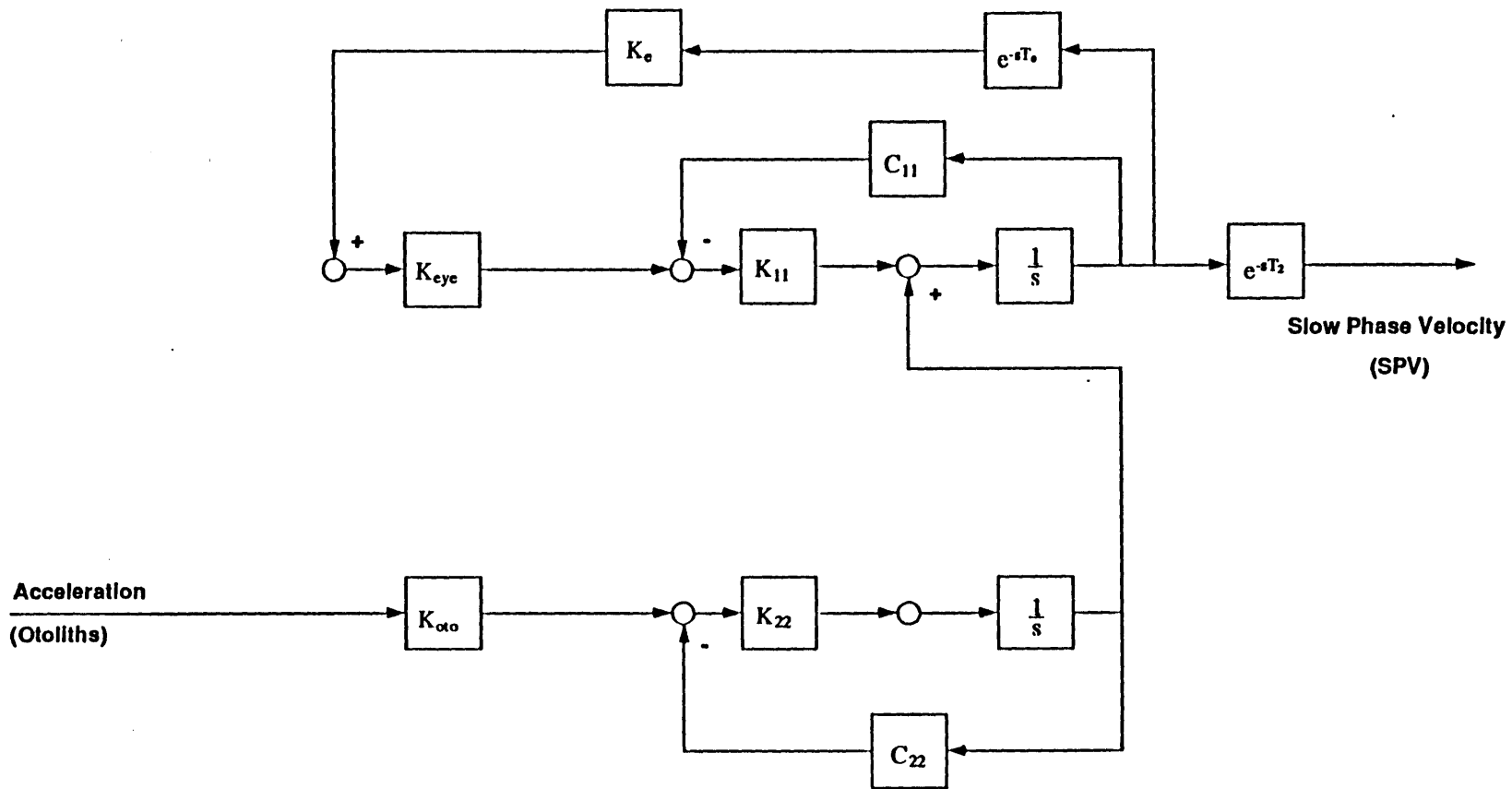


Figure 5.7 After-image / unpredictable stimuli model (AI/SOS), derived from VV/SOS (Figure 5.3) by setting retinal slip to zero.

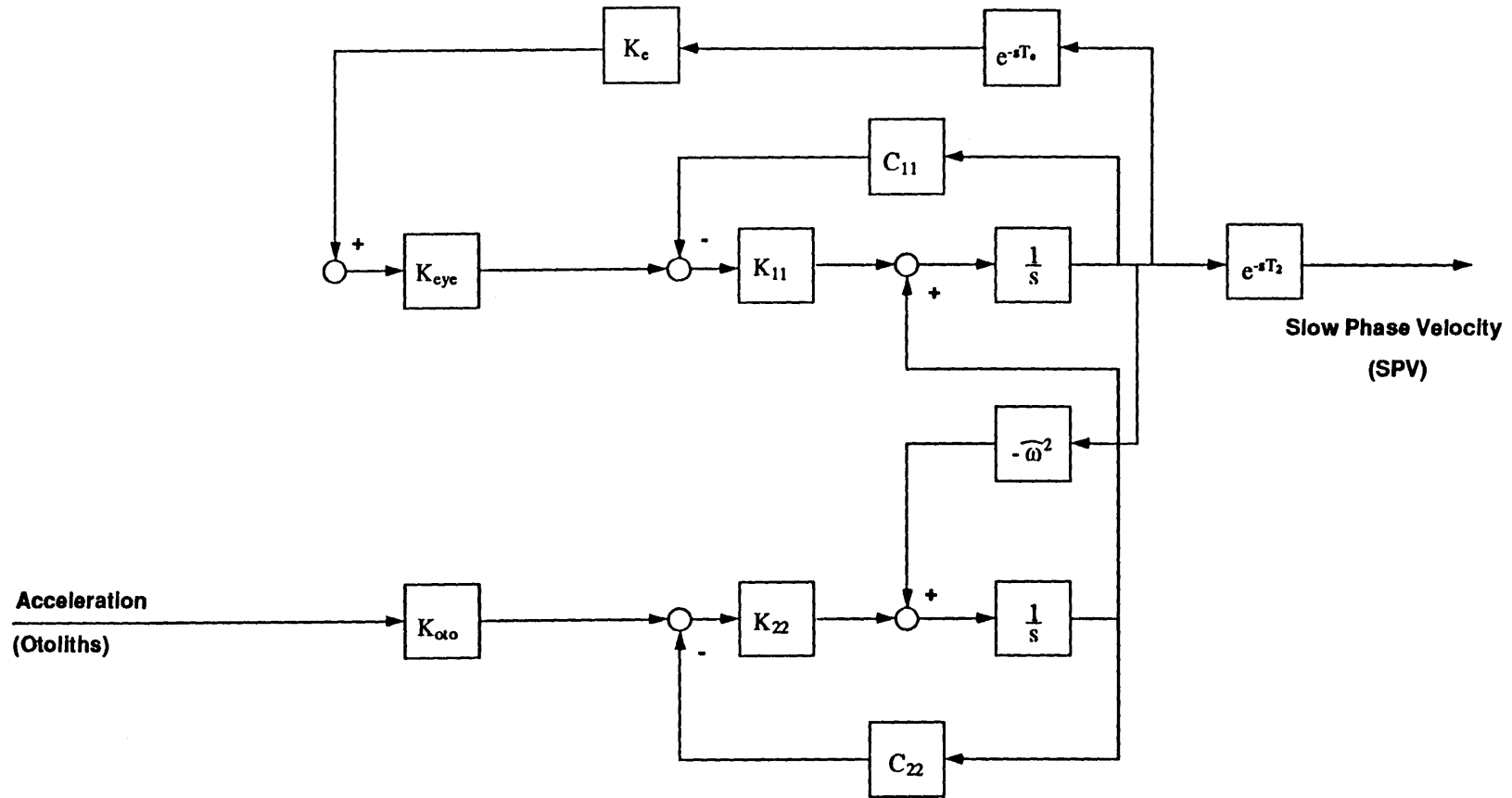


Figure 5.8 After-image / predictable stimuli model (AI/sine), adapted from VV/sine (Figure 5.4) by setting retinal slip to zero.

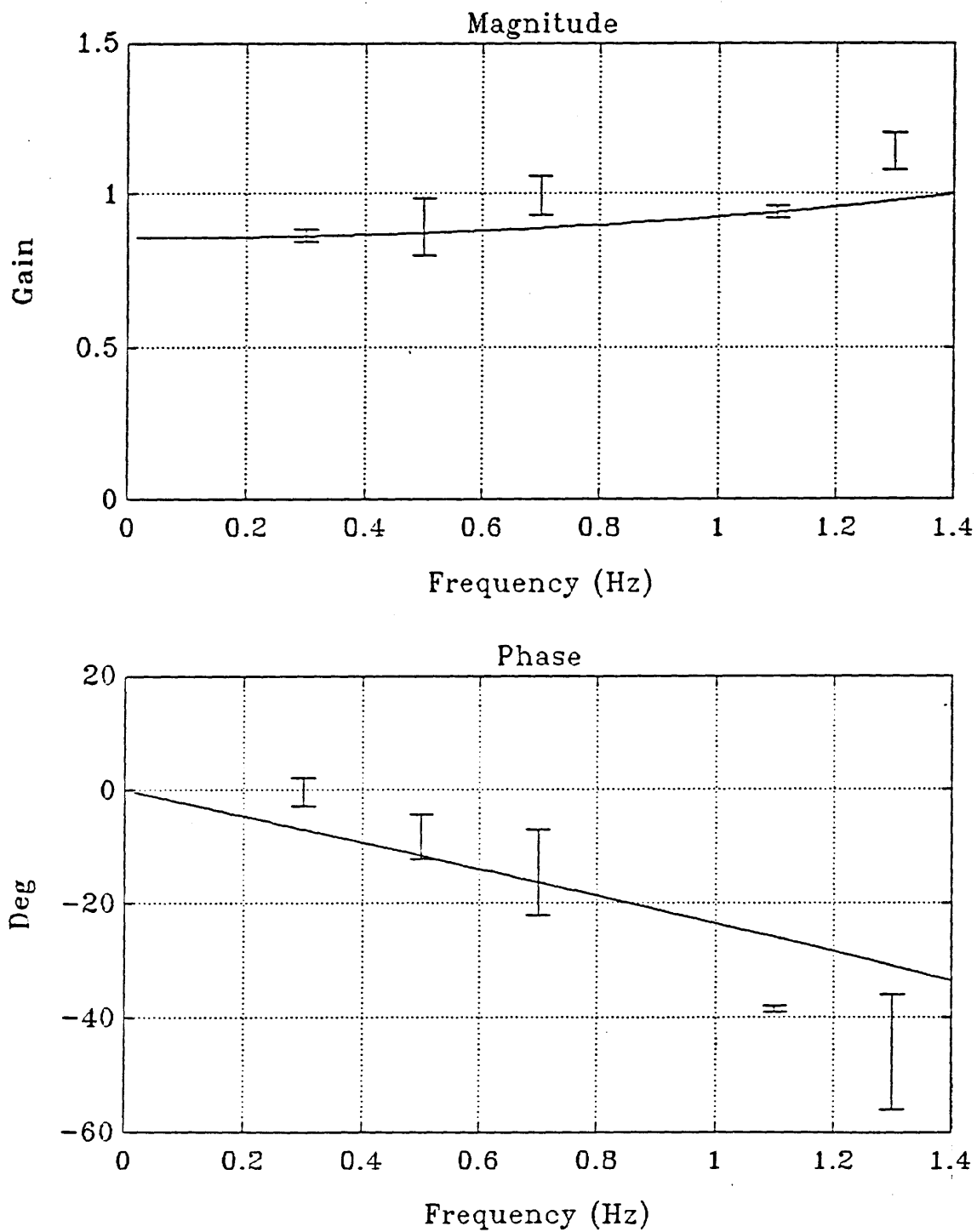


Figure 5.9 Model transfer function and experiment results for subject J SP/SOS. (Solid lines are model transfer function; bars are experiment data, ± 1 s.d. centered at mean.) [$K_e=0.25$, $K_{eye}=1.19$, $K_{11}=20$, $C_{11}=0.5$]

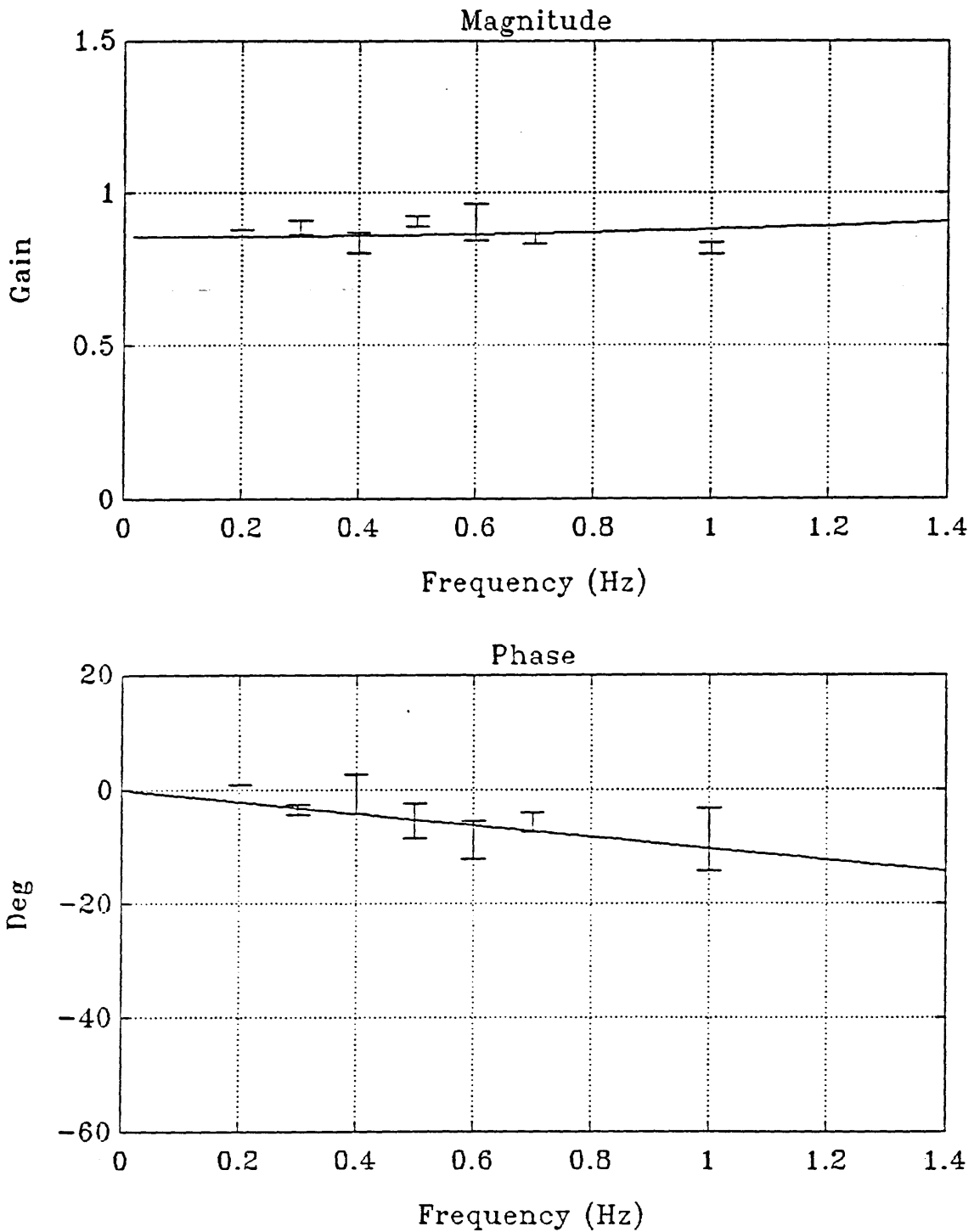


Figure 5.10 Model transfer function and experiment results for subject J SP/sine. (Solid lines are model transfer function; bars are experiment data, ± 1 s.d. centered at mean.)

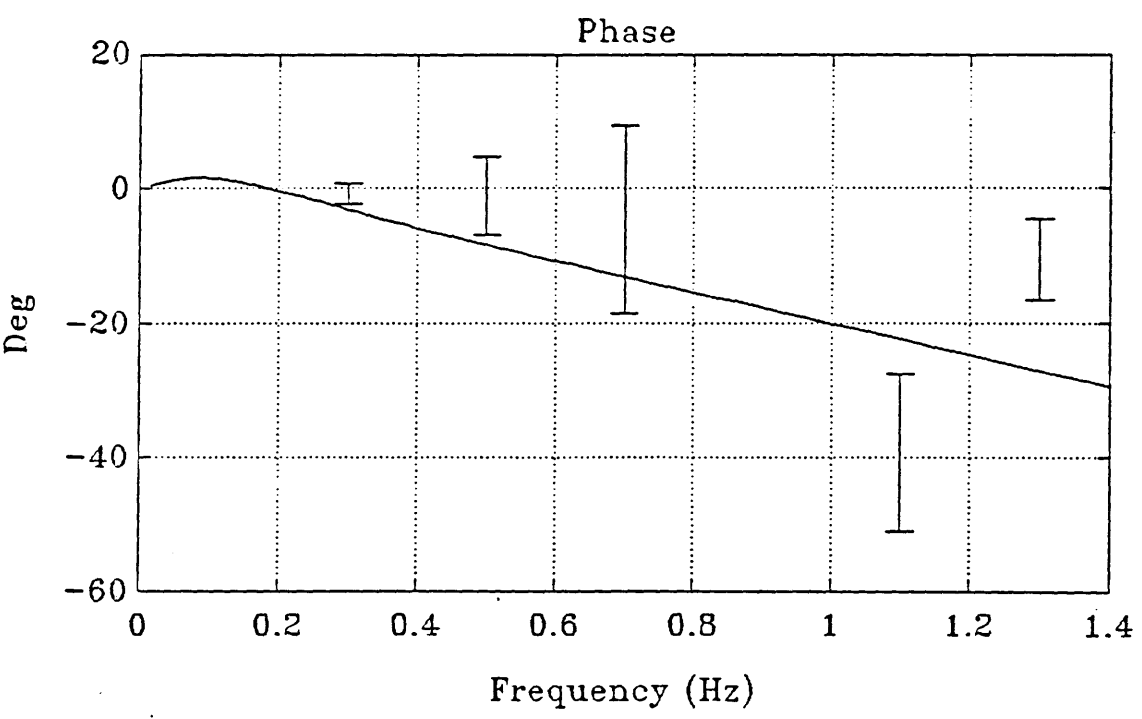
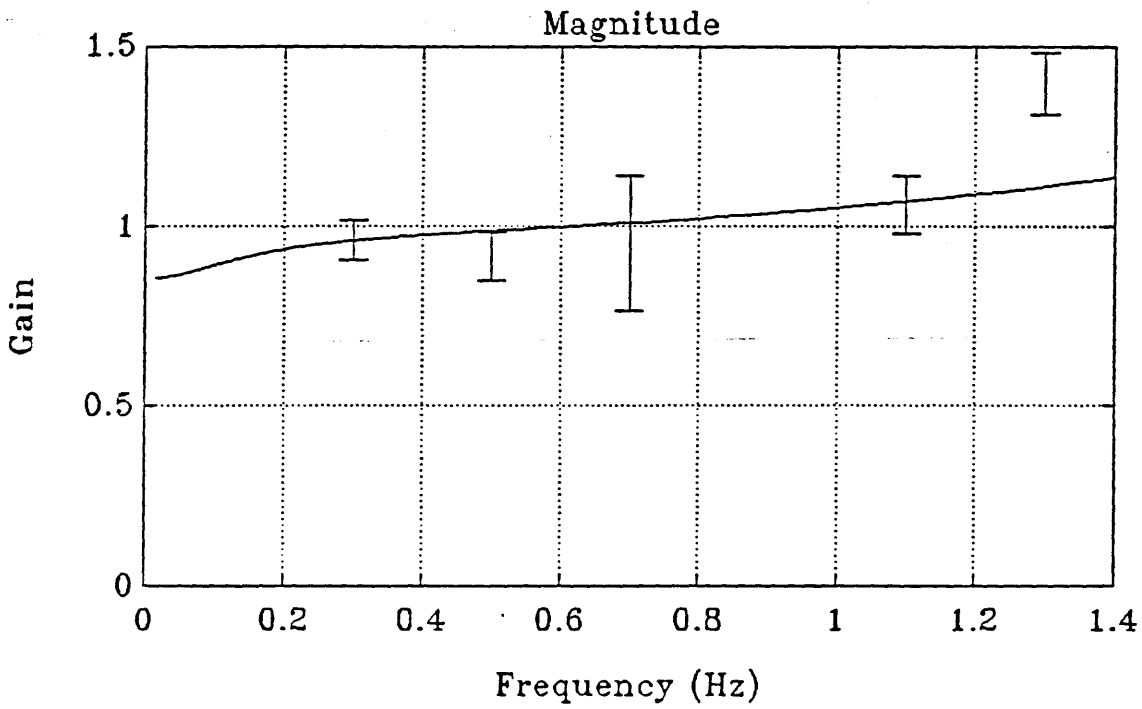


Figure 5.11 Model transfer function and experiment results for subject J VV/SOS. (Solid lines are model transfer function; bars are experiment data, ± 1 s.d. centered at mean.)

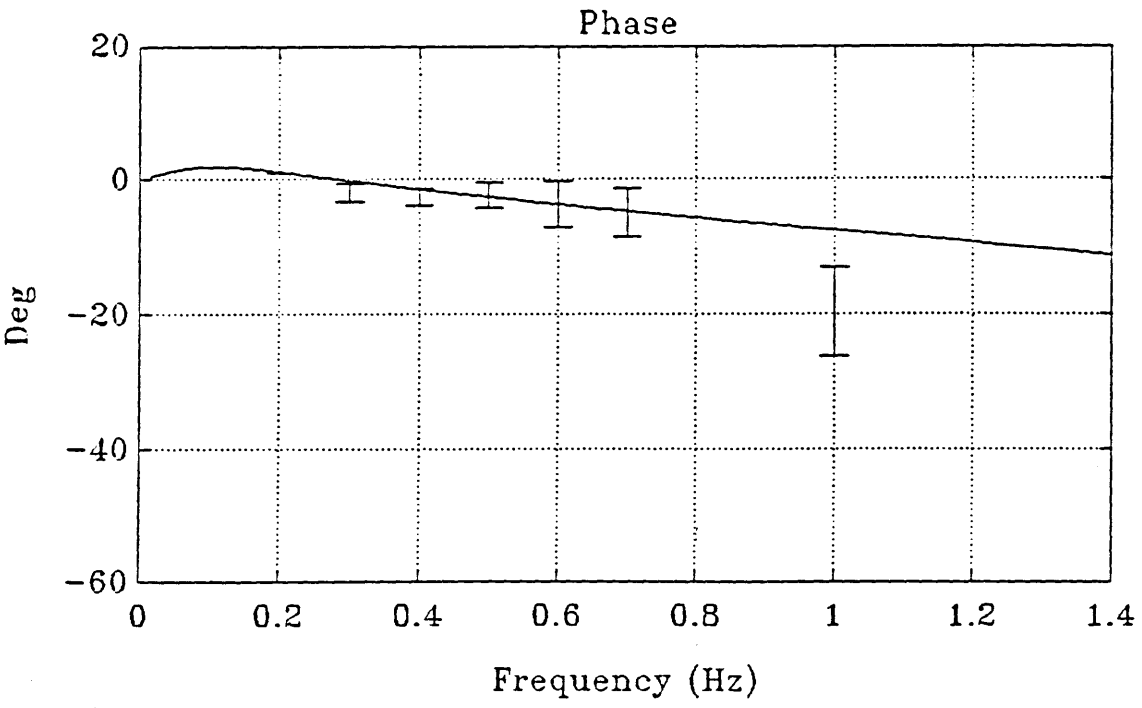
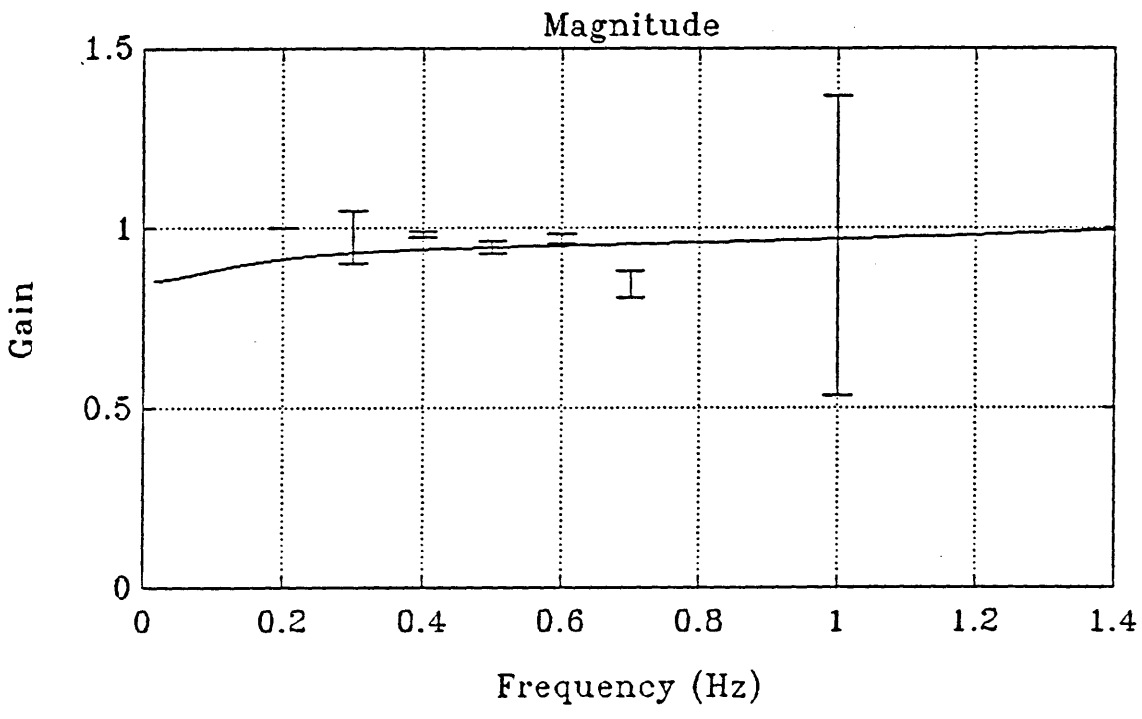


Figure 5.12 Model transfer function and experiment results for subject J VV/sine. (Solid lines are model transfer function; bars are experiment data, ± 1 s.d. centered at mean.)

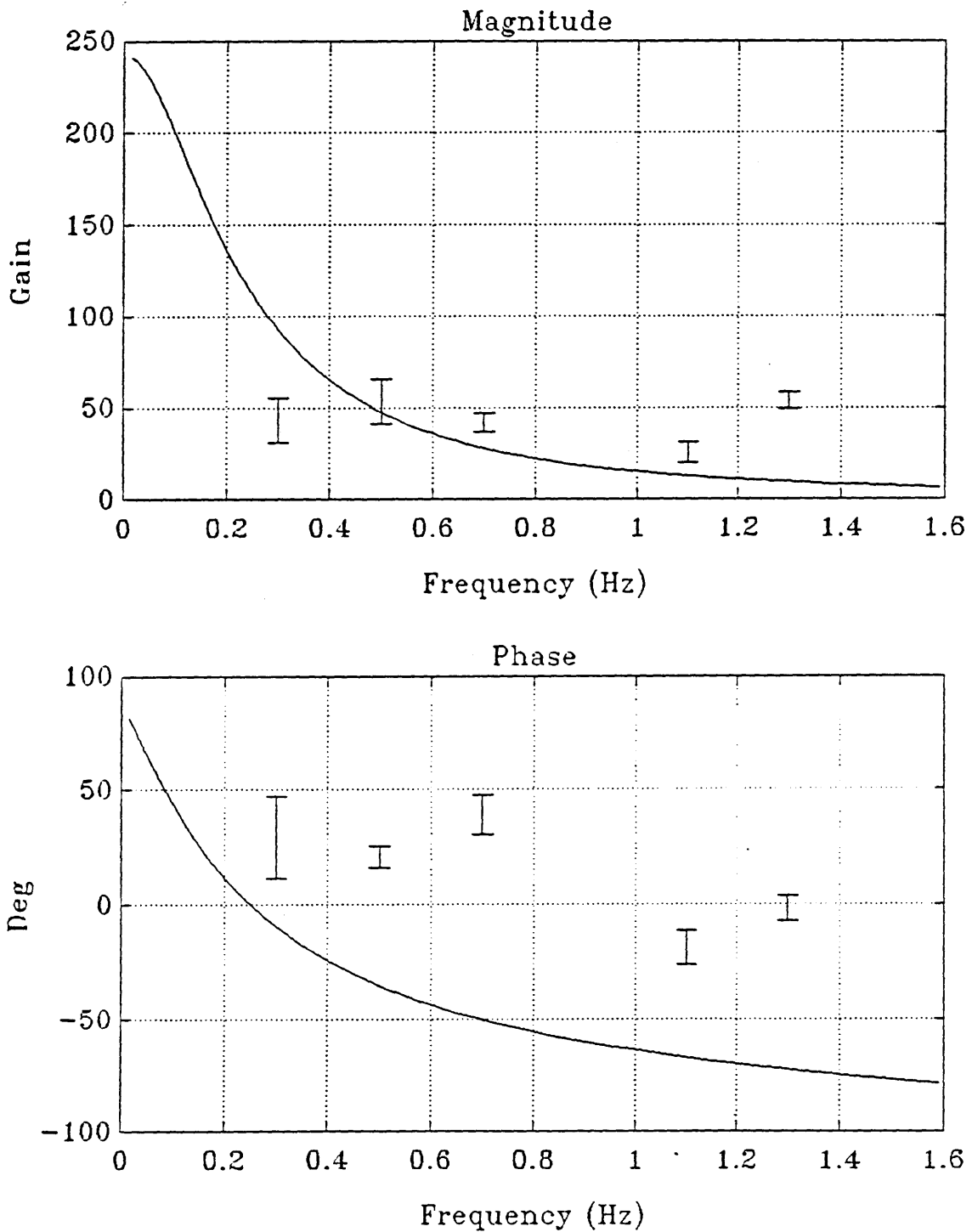


Figure 5.13 Model transfer function and experiment results for subject J AI/SOS. (Solid lines are model transfer function; bars are experiment data, ± 1 s.d. centered at mean.)

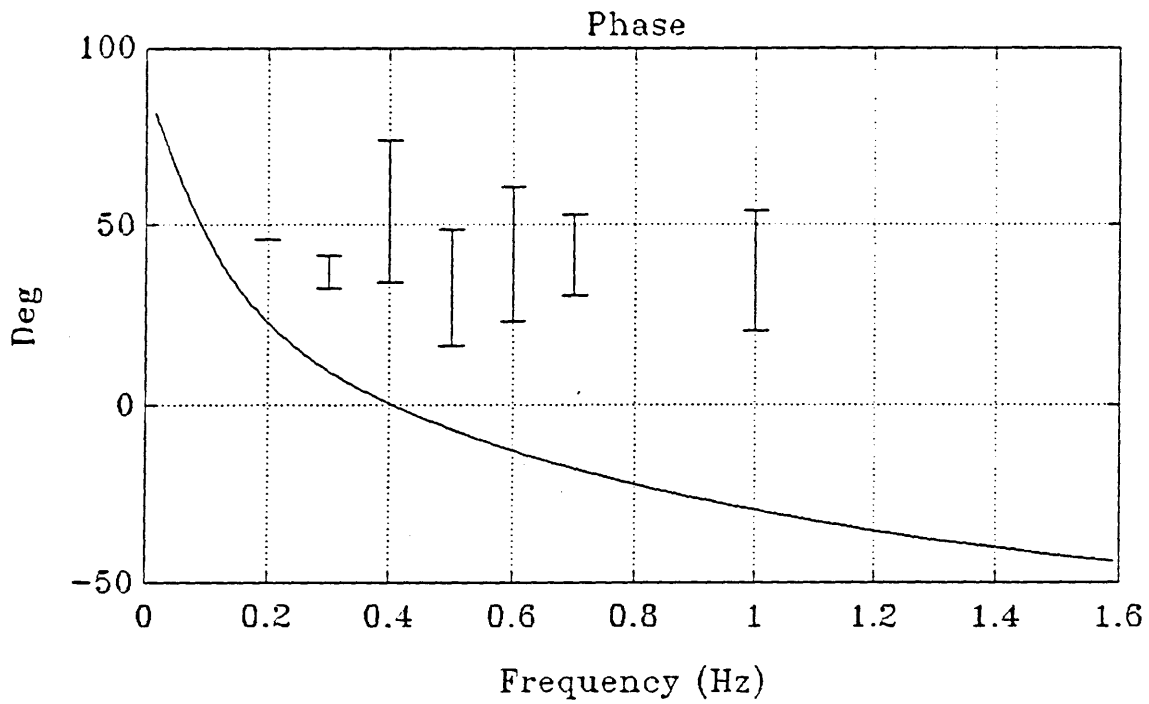
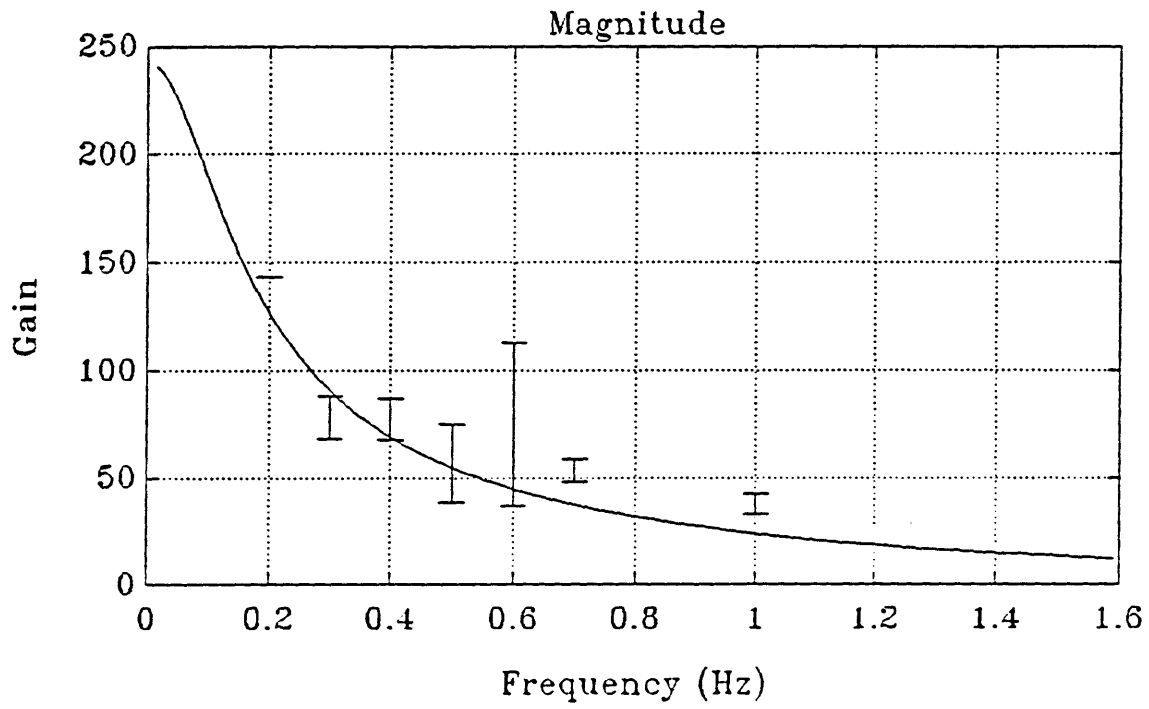


Figure 5.14 Model transfer function and experiment results for subject J AI/sine. (Solid lines are model transfer function; bars are experiment data, ± 1 s.d. centered at mean.)

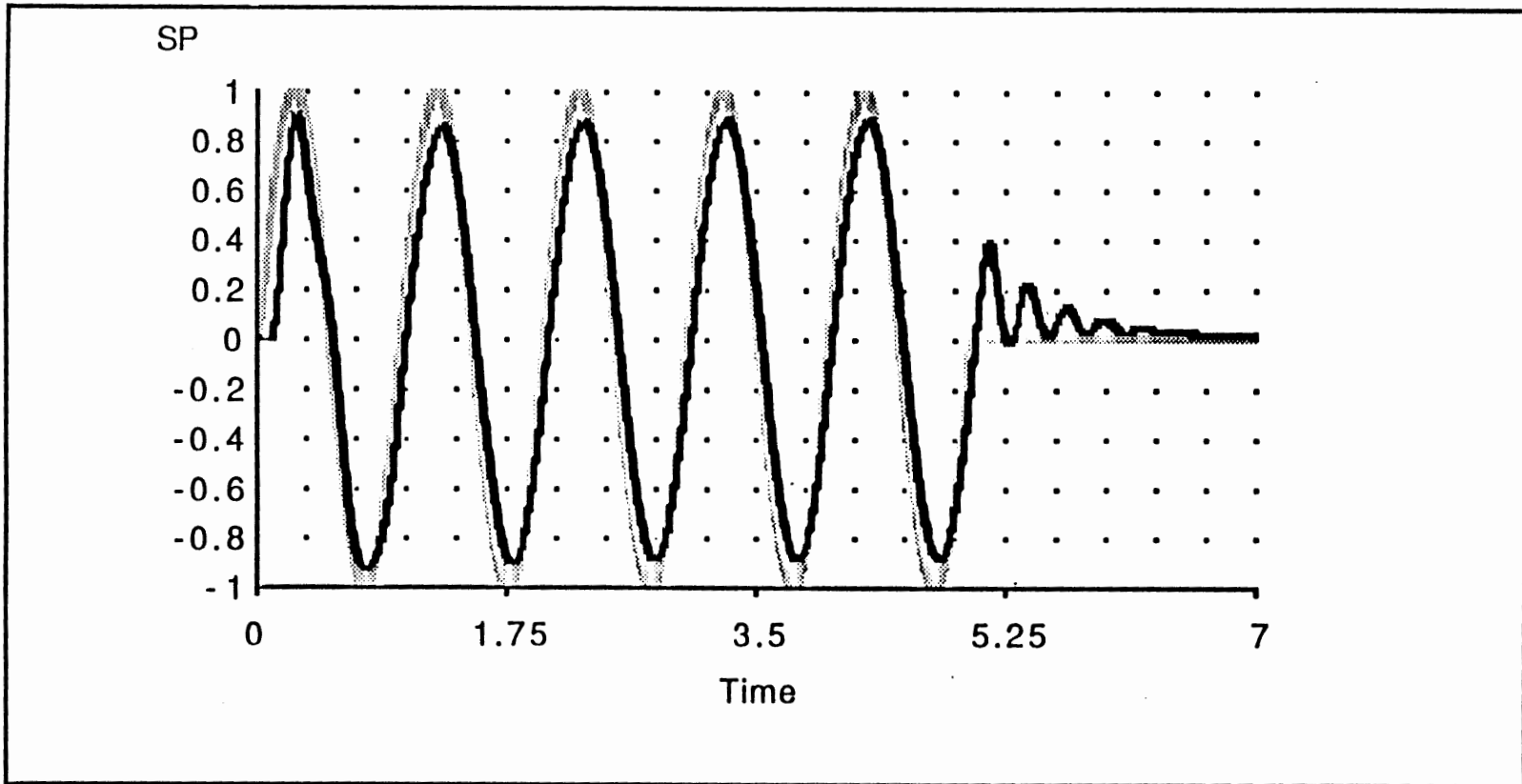


Figure 5.15 Result of SP/SOS model simulation, using parameter values for subject J. Frequency=1.0 Hz. (Light line is input stimulus, dark line is model output.)

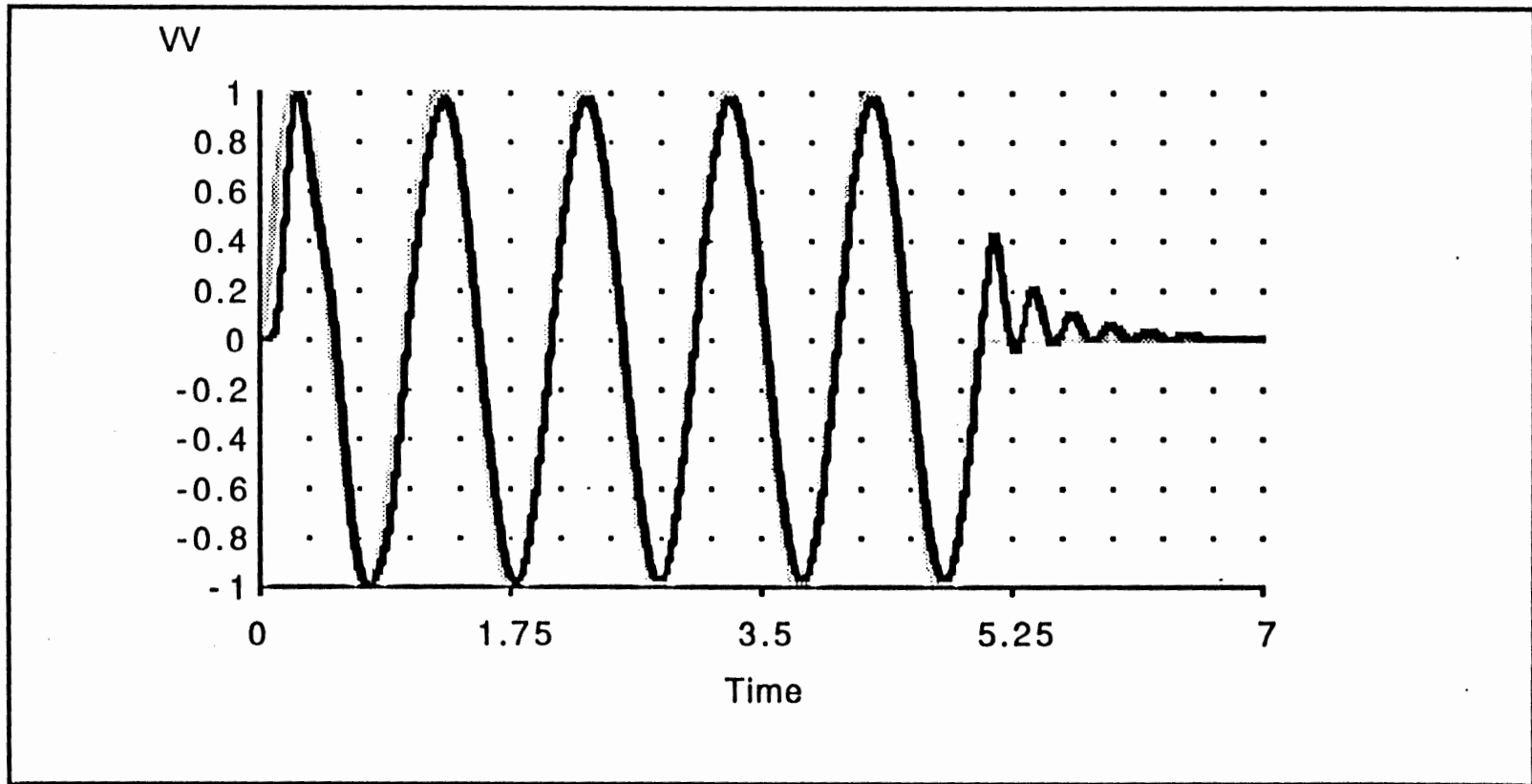


Figure 5.16 Result of VV/SOS model simulation, using parameter values for subject J. Frequency=1.0 Hz. (Light line is input stimulus, dark line is model output.)

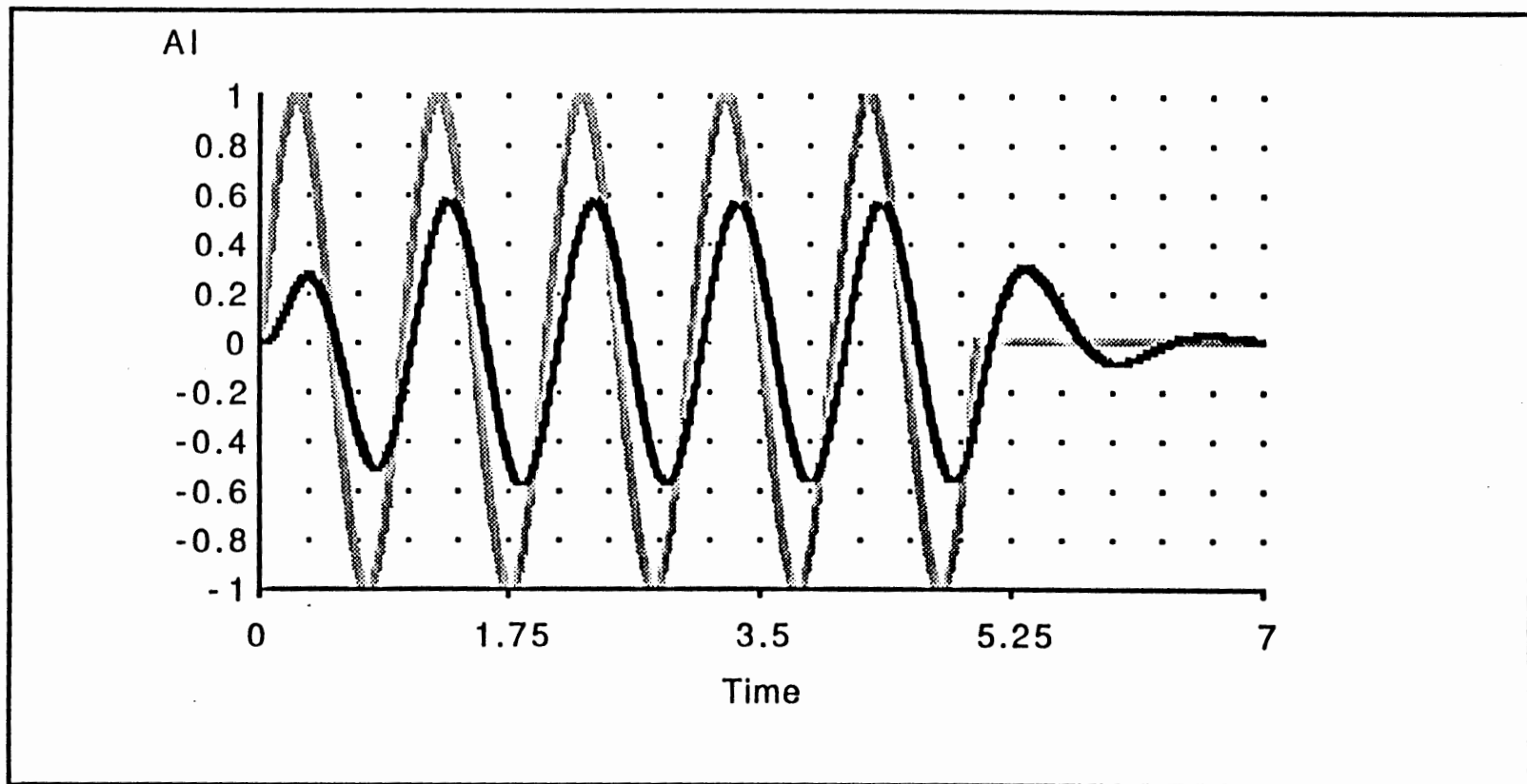


Figure 5.17 Result of AI/SOS model simulation, using parameter values for subject J. Frequency=1.0 Hz. (Light line is input stimulus, dark line is model output.)

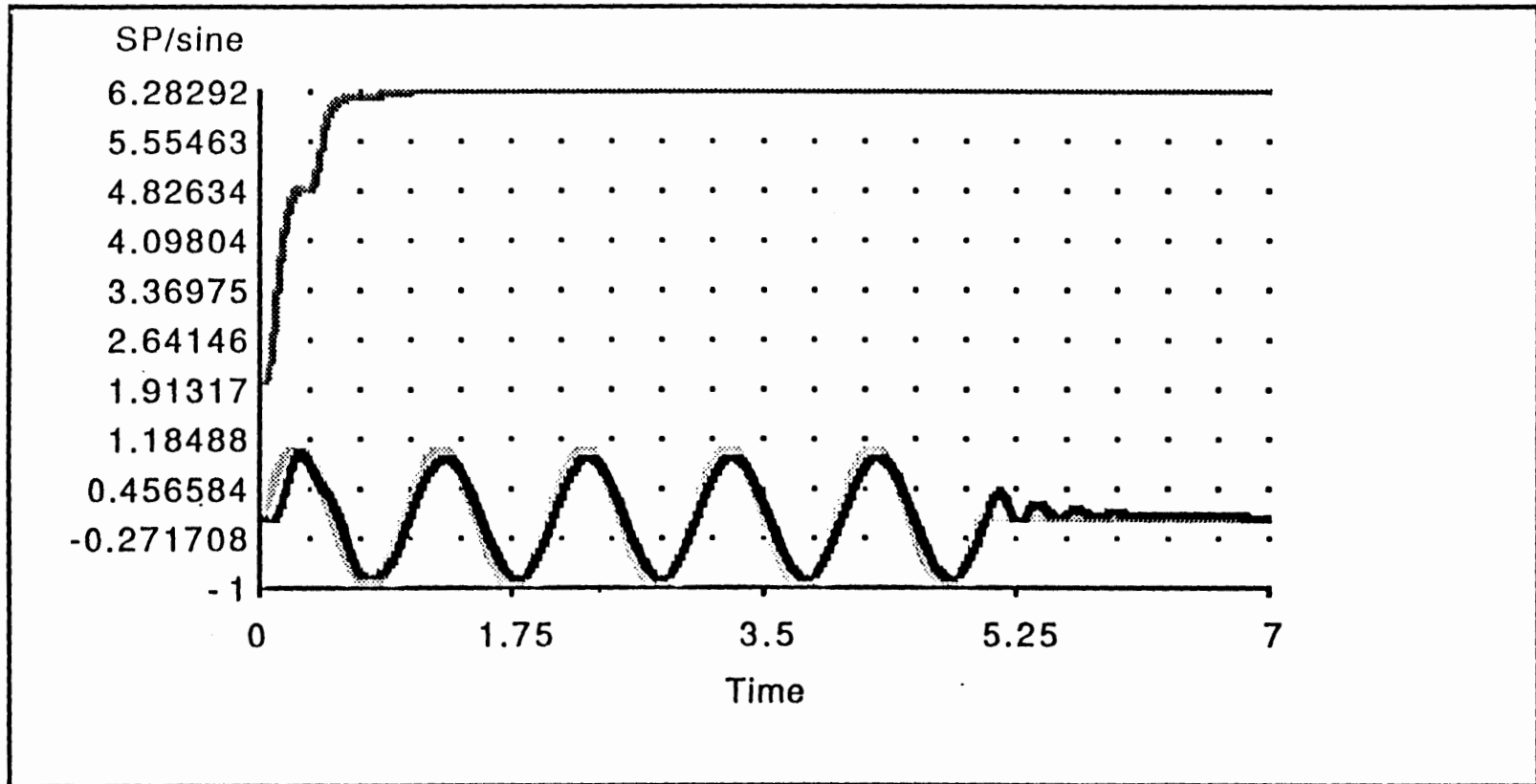


Figure 5.18 Result of SP/sine model simulation, using parameter values for subject J. Frequency=1.0 Hz. (Light line is input stimulus, dark line is model output, top line is output of frequency estimator subsystem ω .)

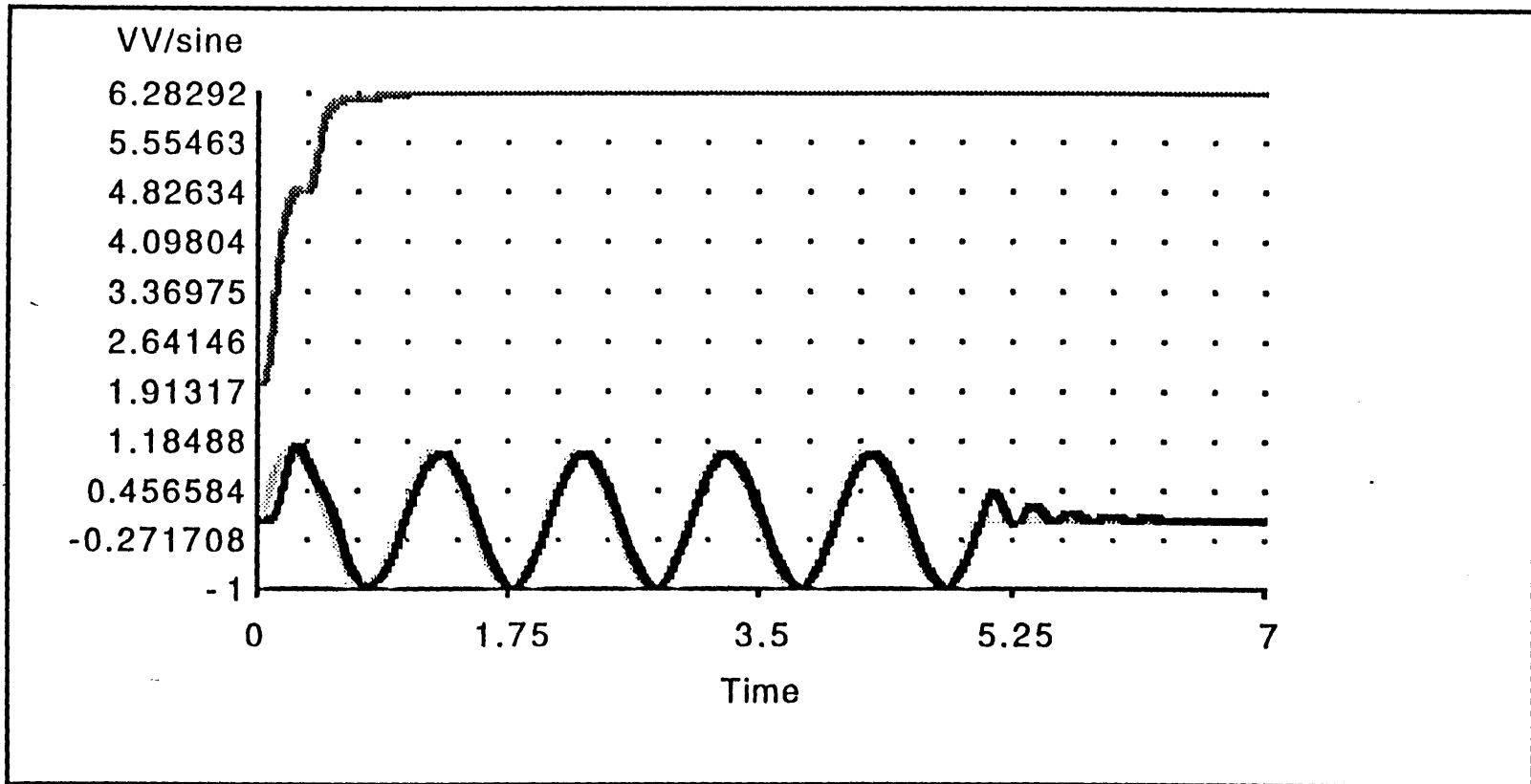


Figure 5.19 Result of VV/sine model simulation, using parameter values for subject J. Frequency=1.0 Hz. (Light line is input stimulus, dark line is model output, top line is output of frequency estimator subsystem ω .)

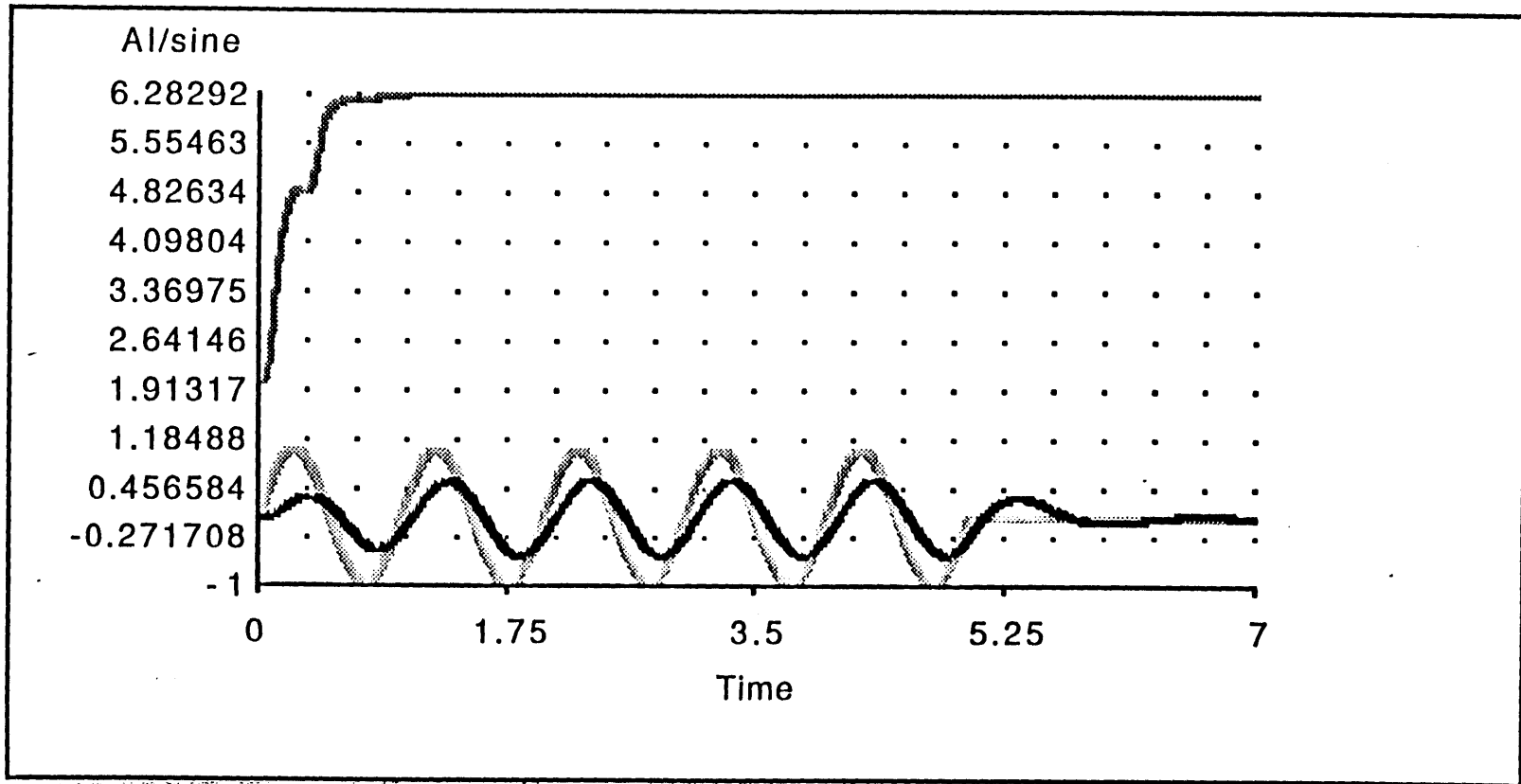


Figure 5.20 Result of AI/sine model simulation, using parameter values for subject J. Frequency=1.0 Hz. (Light line is input stimulus, dark line is model output, top line is output of frequency estimator subsystem ω .)

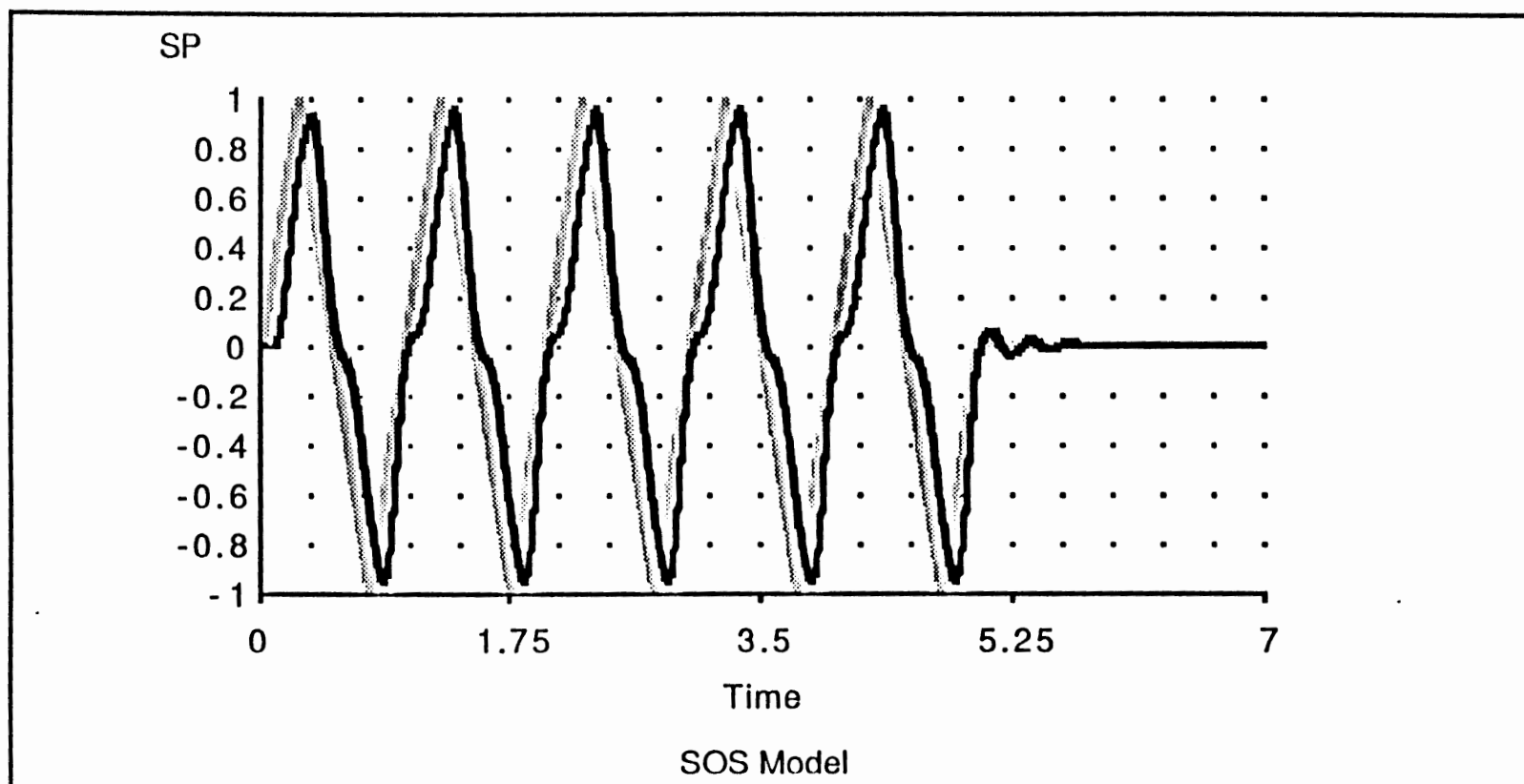


Figure 5.21 Result of SP/SOS model simulation, using parameter values for subject J. Velocity triangle stimulus test. (Light line is input stimulus, dark line is model output.)

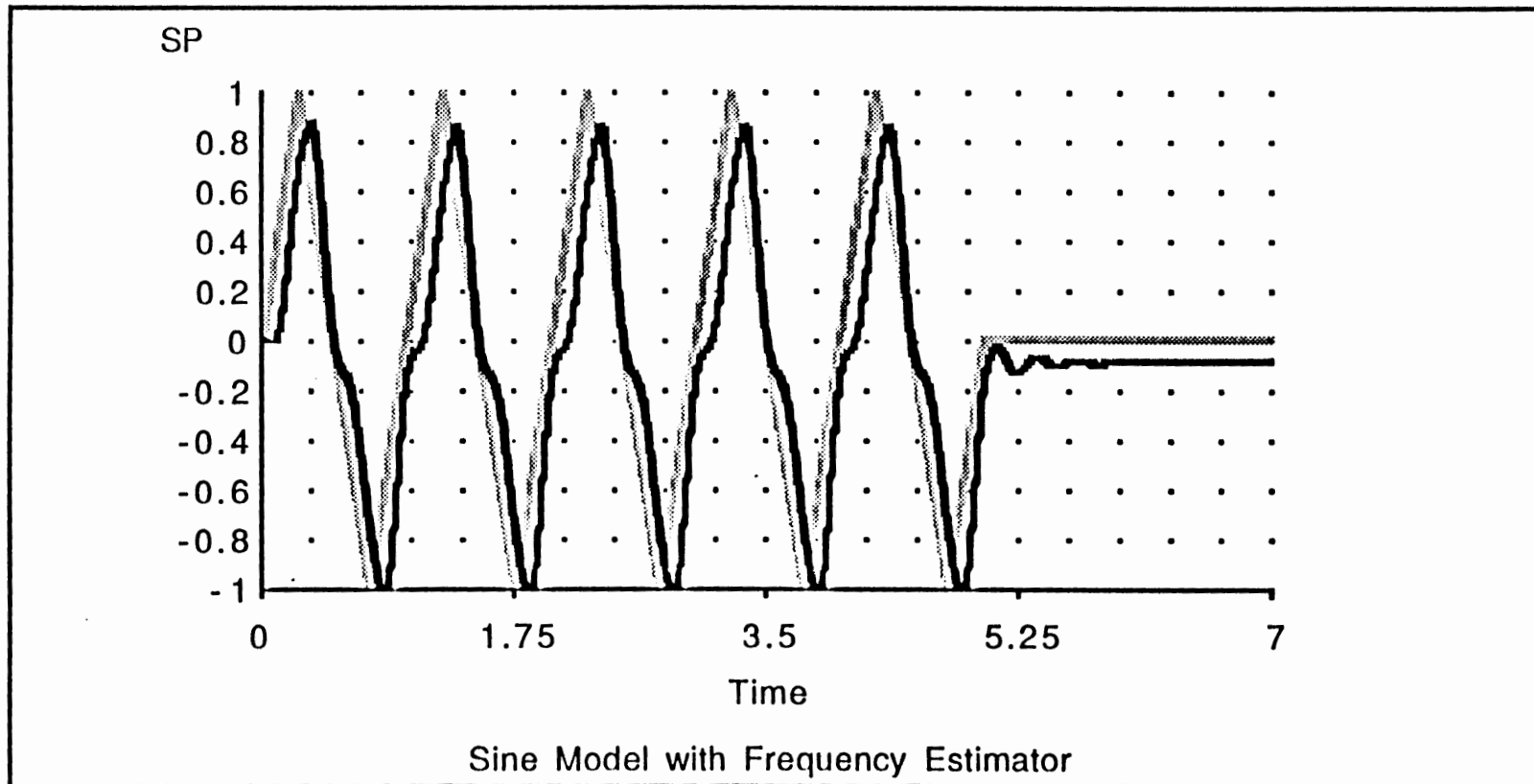


Figure 5.22 Result of SP/sine model simulation, using parameter values for subject J. Velocity triangle stimulus test. (Light line is input stimulus, dark line is model output.)

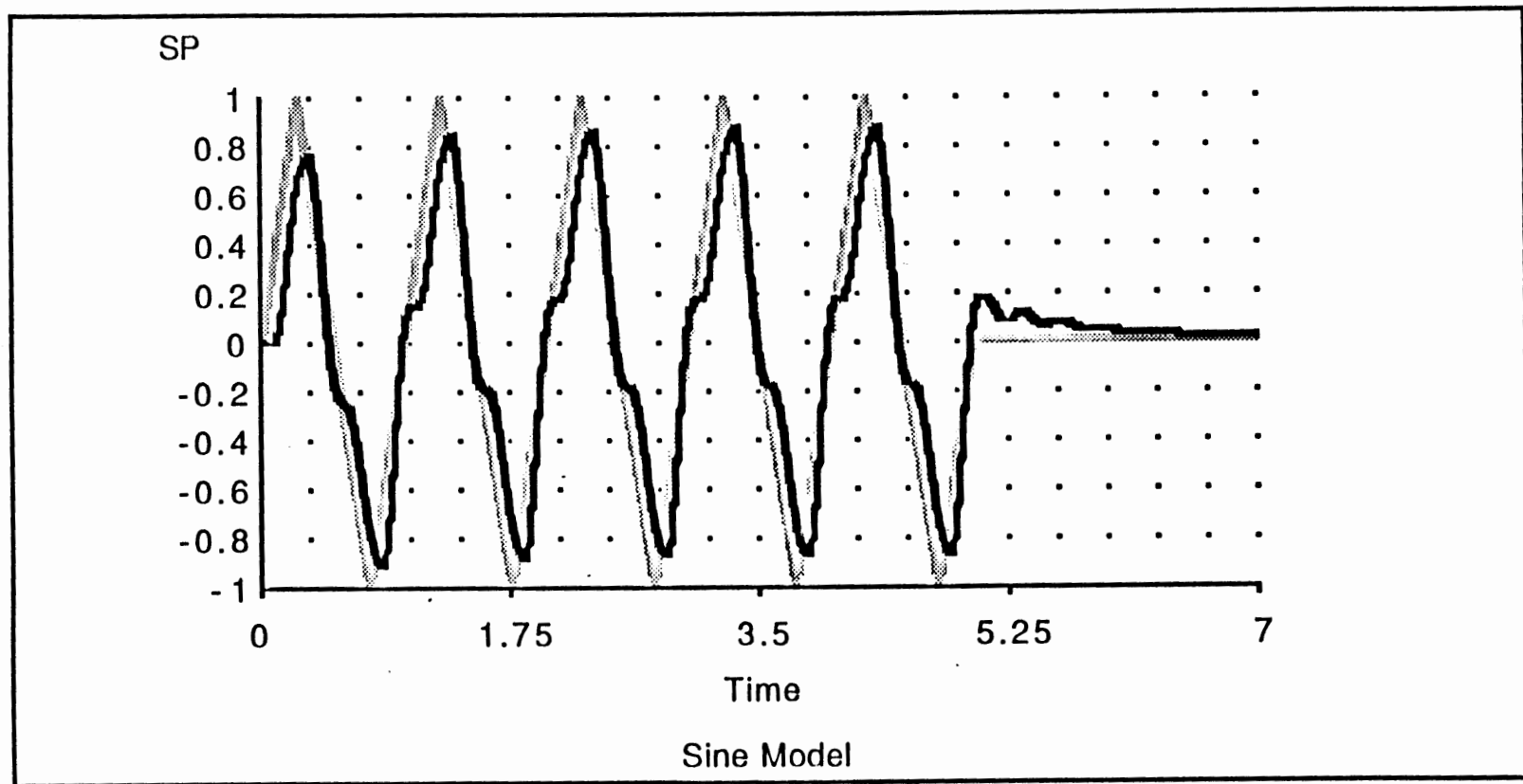


Figure 5.23 Result of SP/sine model simulation, using parameter values for subject J. Velocity triangle stimulus test. Frequency estimate is set to correct value a priori. (Light line is input stimulus, dark line is model output.)

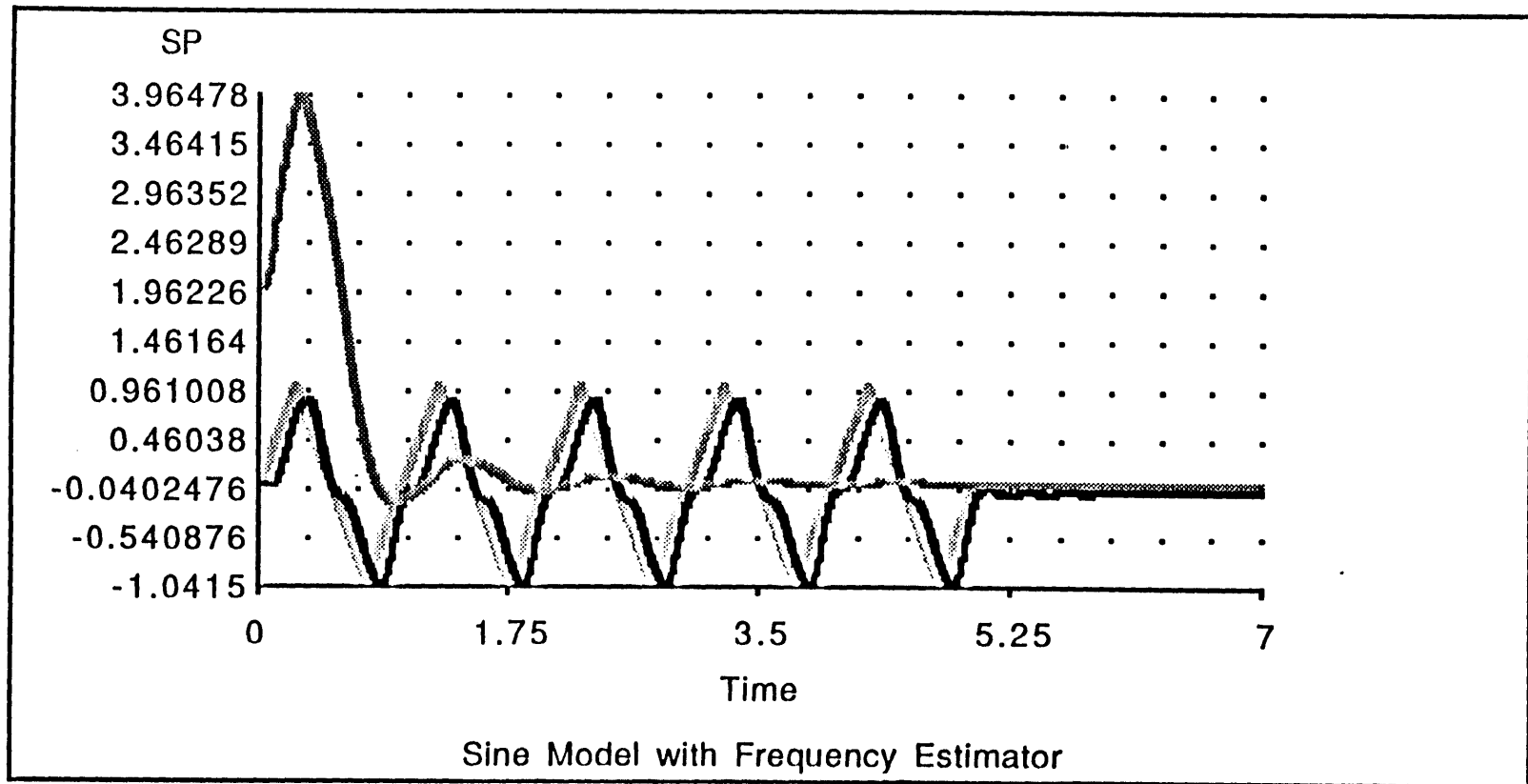
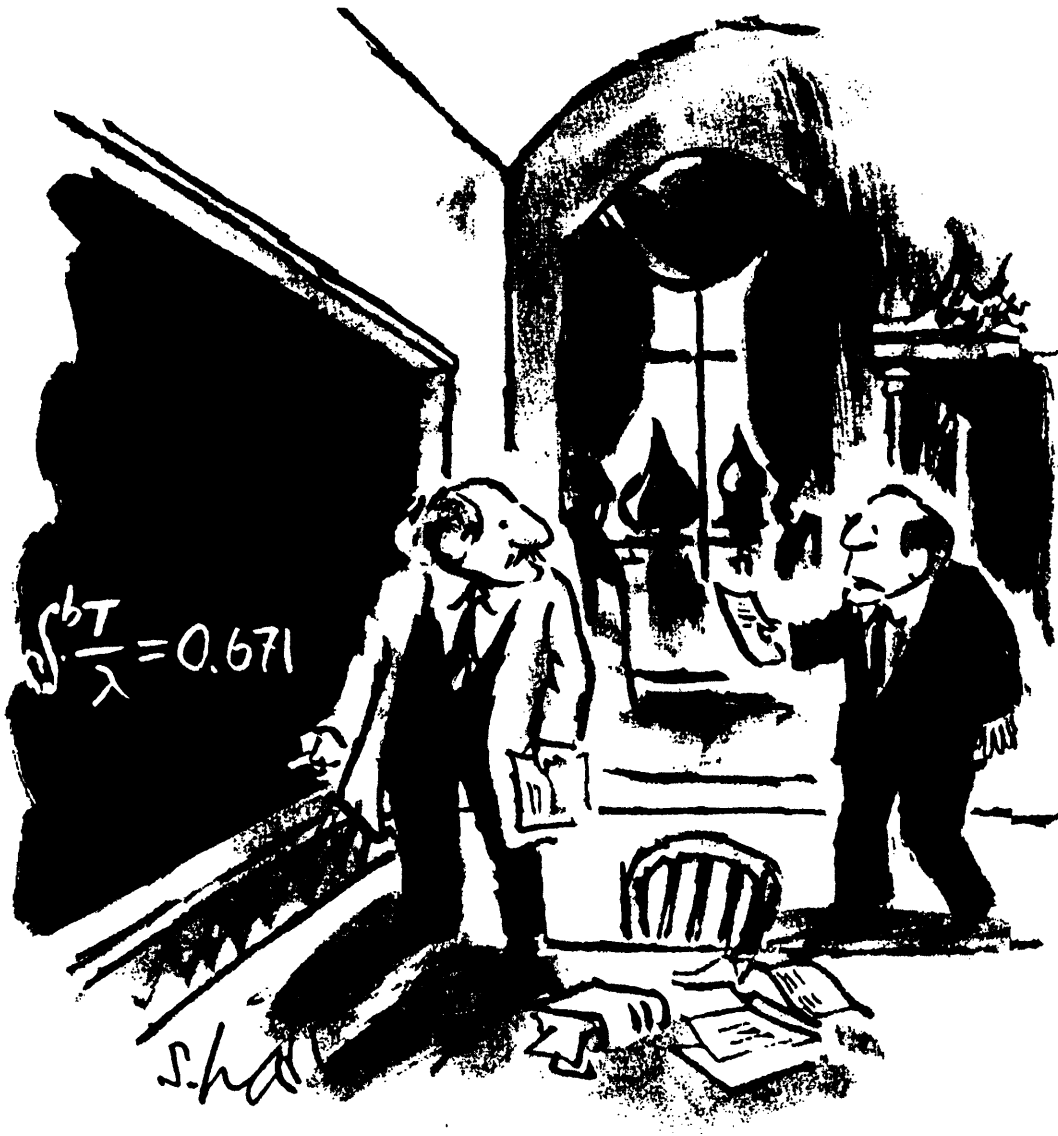


Figure 5.24 Result of SP/sine model simulation, using parameter values for subject J. Velocity triangle stimulus test. (Light line is input stimulus, dark line is model output, medium line is output of frequency estimator subsystem ω .)

VI Conclusions



"Comrade—the Commissar of Mathematics wants it to equal 29.86."

Horizontal eye movements in humans were studied under several stimulus conditions. The linear vestibulo-ocular reflex (LVOR), tested with lateral accelerations in the dark, was highly variable, with an acceleration threshold of about 0.3g for sinusoidal stimulation. Gain was about fifteen degrees per second of eye movement per g of acceleration, relatively constant across the frequency range 0.2 to 1.3 Hz. This confirmed earlier reports, and stimulated the subsequent experiments on various facets of otolith-stimulated compensatory horizontal eye movements.

Experiments showed that tracking of a fixed retinal after-image (AI) during linear accelerations AI improved the gain of the LVOR by a factor of two to ten, and significantly increased its phase lead. This provides support for a theory in which oculomotor efferent copy information is used to reconstruct an internal representation of target velocity, which is then tracked by the oculomotor system. The AI results are rather dramatic, and may be useful in future research in which a reliable and consistent way to stimulate LVOR is required.

In several of the experimental conditions, but most notably in the AI case, eye movement responses continued for a short time after the stimulus ended, when using pure sine stimulation. This indicates the possible presence of an internal pattern generator which predicts the stimulus motion (with predictable stimuli), a concept which was investigated in the modelling portion of the research.

A narrow homogeneous horizontal luminous line was tested for its ability to affect LVOR gain by controlling ocular vergence, but results were not encouraging. LVOR acceleration step responses seemed to be velocity-dependent rather than acceleration-dependent. Fixation suppression (FS) of LVOR by fixating on a subject-stationary target light during linear acceleration significantly reduced the gain of the oculomotor response.

Smooth pursuit (SP) in response to a moving visual target confirmed earlier results of reduced-phase tracking with predictable (sinusoidal) stimuli, compared to unpredictable (sum-of-sines: SOS) stimuli. Addition of vestibular information by tracking a stationary target while undergoing linear accelerations improved the smooth pursuit response gain slightly but consistently. Acceleration step responses showed a velocity saturation with visual stimulation only (SP), which was overcome with the added vestibular stimulation (VV). The VV condition also reduced the SP latency somewhat. The VV steps often produced an initial anti-compensatory eye movement, which may be smooth pursuit in the compensatory direction upon which is superimposed a saccade in the opposite direction.

A Kalman filter-based model of the combination of visual and vestibular information for oculomotor tracking was developed. This model treats the eye movements as the output of an estimator which combines sensory information to produce an internal estimate of head and body motion. The model concentrates on predictable (sinusoidal) target motion, and contains a central pattern generator (CPG) which predicts target motion and hence enhances the response. The CPG is a natural formulation of the Kalman filter when the input is known to be sinusoidal. The CPG requires an instantaneous estimate of the input frequency, provided by a frequency estimator subsystem derived from a Kalman filter. The model encompasses the SP/SOS, SP/sine, VV/SOS, VV/sine, AI/SOS, and AI/sine conditions with a small number of parameters.

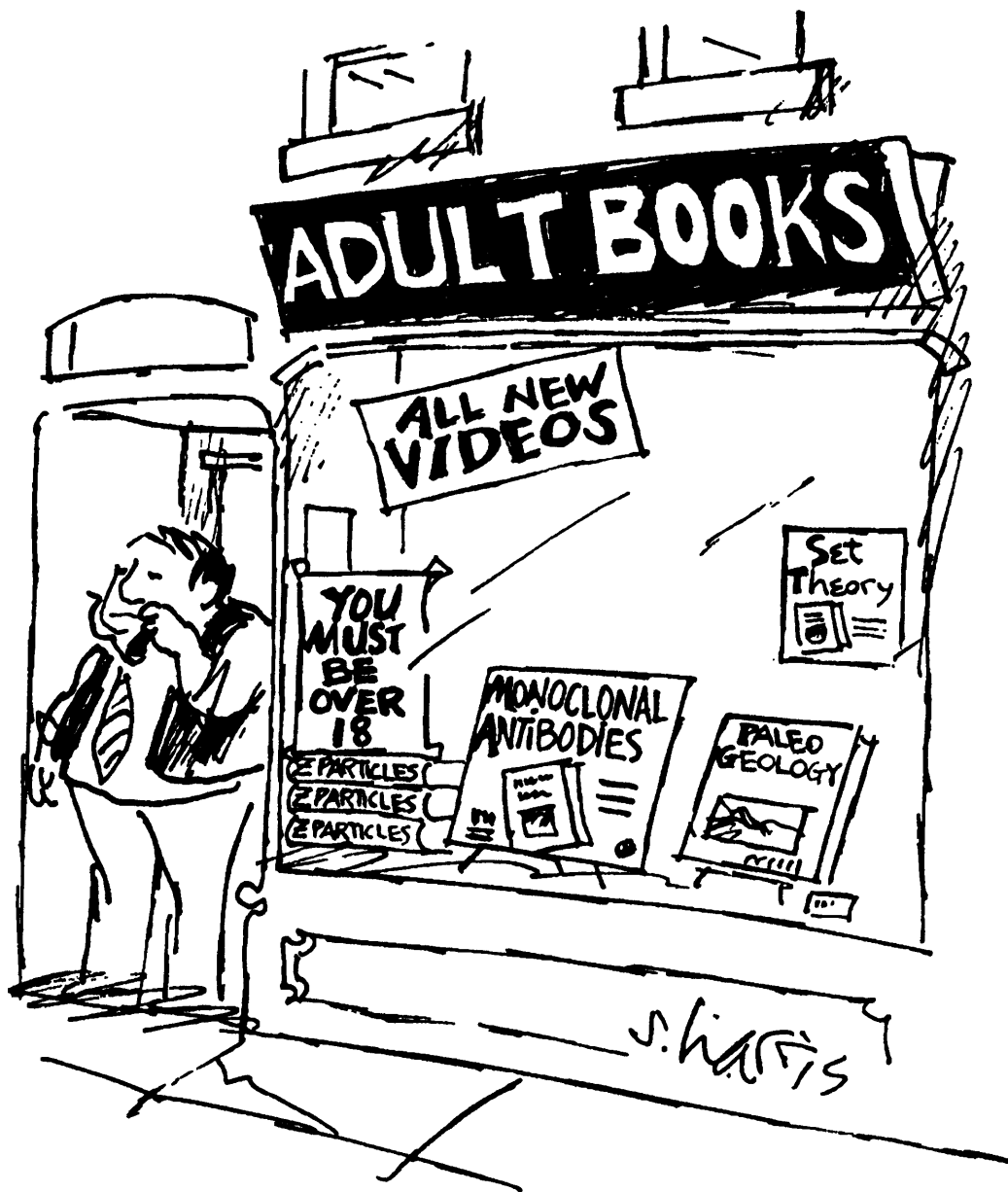
The model presented appears to be one of only a few presented in the literature which is specifically aimed at the predictable stimulus case. It performs well for the sinusoidal stimuli considered, although it is not clear if a natural extension can be made for other types of predictable stimuli. Some time domain aspects of predictable tracking, such as responses which continue somewhat after the stimulus ends and responses which will

persist during a short drop-out in the stimulus, are natural consequences of the internal model structure used. A speculative argument was made for explaining response variability in terms of Kalman filter error covariance, which might lead to some interesting work in studying and quantifying normal variability of physiological responses.

RECOMMENDATIONS FOR FURTHER WORK

The Kalman filter model, already applied to some problems in spatial orientation and vection, might find useful application in other areas of oculomotor control. The combination of otolith and semicircular canal inputs might provide insight into the bias component of OVAR. Further addition of wide-field visual cues could lead to higher-order models of multi-sensory integration. Beyond that, proprioceptive and kinesthetic information could be added to the model with slight modifications. The Kalman filter structure allows inputs to be added in a straightforward manner, and may lend itself to many areas of multi-sensory integration.

References



- E A Baarsma, H Collewijn 1975
Eye Movements Due to Linear Accelerations in the Rabbit
Journal of Physiology. 245:227-247.
- A T Bahill, J D McDonald 1983a
Model Emulates Human Smooth Pursuit System Producing Zero-Latency Target Tracking
Biological Cybernetics. 48:212-222.
- A T Bahill, J D McDonald 1983b
Smooth Pursuit Eye Movements in Response to Predictable Target Motions
Vision Research. 23(12):1573-1583.
- G R Barnes, A J Benson, A R J Prior 1978
Visual-Vestibular Interaction in the Control of Eye Movement
Aviation, Space, and Environmental Medicine. 49:557-564.
- C C Barr, L W Schultheis, D A Robinson 1976
Voluntary, Non-visual Control of the Human Vestibulo-Ocular Reflex
Acta Otolaryngologica. 81:365-375.
- A J Benson, M A Bodin 1966
Interaction of Linear and Angular Acceleration on vestibular Receptors in Man
Aerospace Medicine. 36:144-158.
- A Berthoz, I Israel, T Vieville, D Zee 1987
Linear Head Displacement Measured by the Otoliths can be Reproduced Through the Saccadic System
Neuroscience Letters. 82:285-290.
- W Bles 1979
Sensory Interactions and Human Posture.
Amsterdam: Academische Pers
- W Bles, T S Kapteyn 1973
Separate Recording of the Movements of the Human Eyes During Parallel Swing Tests
Acta Otolaryngologica. 75:6-9.
- W Bles, T Kloren, W Buchele, T Brandt 1983
Somatosensory Nystagmus: Physiological and Clinical Aspects
In: C R Pfaltz (ed), *Advances in Oto-Rhino-Laryngology, Vol. 30*,
Basel: Karger.
- T Brandt, W Buchele, F Arnold 1977
Arthrokinetic Nystagmus and Ego-motion Sensation
Experimental Brain Research. 30:331-338.
- J L Brown 1965
Afterimages
In: C H Graham (ed), *Vision and Visual Perception*,
New York: John Wiley and Sons.
- A Buizza, A Leger, A Berthoz, R Schmid 1979
Otolithic-Acoustic Interaction in the Control of Eye Movement
Experimental Brain Research. 46:509-522.

- A Buizza, A Leger, J Droulez, A Berthoz, R Schmid 1980
Influence of Otolithic Stimulation by Horizontal Acceleration on Optokinetic Nystagmus and Visual Motion Perception
Experimental Brain Research. 39:165-176.
- A Buizza, R Schmid, J Droulez 1981
Influence of Linear Acceleration on Oculomotor Control
In: A F Fuchs, W Becker (eds), *Progress in Oculomotor Research*. New York: Elsevier/North-Holland Biomedical Press.
- A Buizza, R Schmid 1986
Velocity Characteristics of Smooth Pursuit Eye Movements to Different Patterns of Target Motion
Experimental Brain Research. 63:395-401.
- B Cohen, J-I Suzuki, T Raphan 1983
Role of the Otolith Organs in Generation of Horizontal Nystagmus: Effects of Selective Labyrinthine Lesions
Brain Research. 276:159-164.
- H Collewijn 1979
The Modifiability of the Adult Vestibulo-Ocular Reflex
Trends in Neuroscience. 2(4):98-102.
- H Collewijn, A F Grootendorst 1979
Adaptation of Optokinetic and Vestibulo-Ocular Reflexes to Modified Visual Input in the Rabbit
In: R Granit & O Pompeiano (eds), *Reflex Control of Posture and Movement (Progress in Brain Research, Vol 50)*. New York: Elsevier/North-Holland Biomedical Press.
- H Collewijn, E P Tamminga 1984
Human Smooth and Saccadic Eye Movements During Voluntary Pursuit of Different Target Motions on Different Backgrounds
Journal of Physiology. 351:217-250.
- M J Correia, F E Guedry, Jr. 1966
Modification of Vestibular Responses as a Function of Rate of Rotation About an Earth-Horizontal Axis
Acta Oto-laryngologica. 62:297-308.
- M J Correia, K E Money 1970
The Effect of Blockage of All Six Semicircular Canal Ducts on Nystagmus Produced by Dynamic Linear Acceleration in Cat
Acta Otolaryngologica. 69:7-16.
- P J Dallos, R W Jones 1963
Learning Behavior of the Eye Fixation Control System
IEEE Transactions on Automatic Control. AC-8:218-227.

N G Daunton, C A Christensen, D D Thomsen 1981
Visual Modulation of Otolith Responses: A Paradigm for the Study of Self-Motion Perception and Its Neural Substrates
In: T Gualtierotti (ed.), *The Vestibular System: Function and Morphology (Ch. 27)*. New York: Springer-Verlag.

W D T Davies 1970
System Identification for Self-Adaptive Control
New York: Wiley-Interscience.

R Eckmiller, M Mackeben 1978
Pursuit Eye Movements and their Neural Control in the Monkey
Pflügers Archive. 377:15-23.

C Fernandez, J M Goldberg 1976
Physiology of Peripheral Neurons Innervating Otolith Organs of the Squirrel Monkey. III. Response Dynamics
Journal of Neurophysiology. 39(5):996-1008.

A Gelb (ed.) 1974
Applied Optimal Estimation
Cambridge, MA: M.I.T. Press.

J Goldberg, E Icaza 1985
Effects of Imagined Target Distance on Vestibuloocular Responses
Presented at the *15th meeting of the Society for Neuroscience*, Dallas, TX.

J M Goldberg, C Fernandez 1982
Eye Movements and Vestibular Nerve Responses Produced in the Squirrel Monkey by Rotations About an Earth-Horizontal Axis
Experimental Brain Research. 46:393-402.

G M Goodwin, D I McCloskey, P B C Matthews 1972
The Contribution of Muscle Afferents to Kinesthesia Shown by Vibration Induced Illusions of Movement and the Effects of Paralyzing Joint Afferents
Brain. 95:705-748.

A Graybiel, C W Stockwell, F E Guedry 1972
Evidence for a Test of Dynamic Otolith Function Considered in Relation to Responses from a Patient with Idiopathic Progressive Vestibular Degeneration
Acta Otolaryngologica. 73:1-3.

J J Groen 1957
Adaptation
Pract. Oto-rhino-laryngology. 19:524-530.

J J Groen 1960
Problems of the Semicircular Canal from a Mechanico-Physiological Point of View
Acta Oto-laryngologica. Suppl. 163.

O-J Grüsser, U Grüsser-Cornehls 1973
Neuronal Elements of Visual Movement Perception and Some Psychophysical and Behavioral Correlations
In: R Jung (ed), *Handbook of Sensory Physiology, Vol. VII, Part 3. Central Processing of Visual Information. A: Integrative Functions and Comparative Data*. New York: Springer-Verlag.

F E Guedry 1974
Psychophysics of Vestibular Sensation
In: H H Kornhuber (ed), *Handbook of Sensory Physiology, Vol. VII/2. Vestibular System. Part 2. Psychophysics, Applied Aspects and General Interpretations*. New York: Springer-Verlag.

F E Guedry, C S Harris 1963
Labyrinthine Function Related to Experiments on the Parallel Swing
Bureau of Medicine and Surgery Project MR005.13-6001, Subtask 1, Report No. 86 and NASA Order No. R-93. Pensacola, FL: Naval School of Aviation Medicine.

T C Hain 1986
A Model of the Nystagmus Induced by Off Vertical Axis Rotation
Biological Cybernetics. 54:337-350.

R W Hamming 1973
Numerical Methods for Scientists and Engineers
New York: McGraw-Hill.

V Henn, B Cohen, L R Young 1982
Visual-Vestibular Interaction in Motion Perception and the Generation of Nystagmus
Neurosciences Research Program Bulletin. Volume 18, Number 4.

D W Hiltner 1983
A Closed-Loop Otolith System Assessment Procedure
SM Thesis, Department of Aeronautics and Astronautics, MIT.

D Hydén, Y E Istl, D W F Schwarz 1982
Human Visuo-Vestibular Interaction as a Basis for Quantitative Clinical Diagnostics
Acta Otolaryngologica. 94:53-60.

J B Janeke, L B Jongkees, W J Oosterveld 1970
Relationships Between Otoliths and Nystagmus
Acta Otolaryngologica. 69:1-6.

L B W Jongkees 1961
The Influence of Some Drugs Upon the Function of the Labyrinth
Acta Otolaryngologica. 52:281-285.

B J Kitchen 1983
Horizontal and vertical Eye Deviations in Response to Linear Accelerations
SB Thesis, Department of Electrical Engineering and Computer Science, MIT.

E Kowler, B J Murphy, R M Steinman 1978
Velocity Matching During Smooth Pursuit of Different Targets on Different Backgrounds
Vision Research. 18:603-605.

- J Lackner 1975
Pursuit Eye Movements Elicited by Muscle Afferent Information
Neuroscience Letters. 1:25-28.
- J Lackner 1977
Induction of Illusory Self-Rotation and Nystagmus by a Rotating Sound Field
Aviation, Space, and Environmental Medicine. 48:129-131.
- J R Lackner, J E Evanoff 1977
Smooth Pursuit Eye Movements Elicited by Somatosensory Stimulation
Neuroscience Letters. 4:43-48.
- H W Leibowitz 1955
Effect of Reference Lines on the Discrimination of Movement
Journal of the Optical Society of America. 45:829-830.
- M S Levine, J R Lackner 1979
Some Sensory and Motor Factors Influencing the Control and Appreciation of Eye and Limb Position
Experimental Brain Research. 36:275-283.
- B K Lichtenberg 1979
Ocular Counterrolling Induced in Humans by Horizontal Accelerations
ScD Thesis, M.I.T. Interdepartmental Program in Biomedical Engineering.
- S G Lisberger, C Evinger, G W Johanson, A F Fuchs 1981
Relationship Between Eye Acceleration and Retinal Image Velocity During Foveal Smooth Pursuit in Man and Monkey
Journal of Neurophysiology. 46(2):229-249.
- A Mack, R Fendrich, J Pleune 1979
Smooth Pursuit Eye Movements: Is Perceived Motion Necessary?
Science. 203:1361-1363.
- D M MacKay 1973
Visual Stability and Voluntary Eye Movements
In: R Jung (ed), *Handbook of Sensory Physiology, Vol VII, Part 3. Central Processing of Visual Information. A: Integrative Functions and Comparative Data*. New York: Springer-Verlag.
- A Mack, R Fendrich, E Wong 1982
Is Perceived Motion A Stimulus for Smooth Pursuit
Vision Research. 22:77-88.
- J A Mather, J R Lackner 1980
Multiple Sensory and Motor Cues Enhance the Accuracy of Smooth Pursuit Eye Movements
Aviation, Space, and Environmental Medicine. 51:586-589.
- B F McCabe 1964
Nystagmus Response of the Otolith Organs
Laryngoscope. 74:372-381.

- G Melvill Jones 1964
Predominance of Anti-compensatory Oculomotor Response During Rapid Head Rotation
Aerospace Medicine. 35(10):965-968.
- G Melvill Jones, J H Milsum 1969
Neural Response of the Vestibular System to Translational Acceleration
Proceedings of the Symposium on Systems Analysis Approach to Neurophysiological Problems, pp 105-117, Brainherd.
- D M Merfeld 1990
Spatial Orientation in the Squirrel Monkey: An Experimental and Theoretical Investigation
Ph.D. Thesis, M.I.T. Interdepartmental Program in Biomedical Engineering.
- C H Meyer, A G Lasker, D A Robinson 1985
The Upper Limit of Human Smooth Pursuit Velocity
Vision Research. 25(4):561-563.
- J A Michael, G Melvill Jones 1966
Dependence of Visual Tracking Capability upon Stimulus Predictability
Vision Research. 6: 707-716.
- R Muratore, D S Zee 1979
Pursuit After-Nystagmus
Vision Research. 19:1057-1059.
- J L Niven, W C Hixson, M J Correia 1966
Elicitation of Horizontal Nystagmus by Periodic Linear Acceleration
Acta Oto-laryngologica. 62:429-441.
- G D Paige, D L Tomko 1988
Linear Vestibulo-Ocular Reflex (LVOR) of Squirrel Monkey: I. Visual-Vestibular Interactions
Abstract 138.2, presented at the *18th meeting of the Society for Neuroscience*, Toronto, Canada.
- A A Perachio 1981
Responses of Neurons in the Vestibular Nuclei of Awake Squirrel Monkeys During Linear Acceleration
In: T Gualtierotti (ed.), *The Vestibular System: Function and Morphology (Ch. 26)*. New York: Springer-Verlag.
- R B Post, H W Leibowitz 1982
The Effect of Convergence on the Vestibulo-Ocular Reflex and Implications for Perceived Movement
Vision Research. 22:461-465.
- P D Pulaski, D S Zee, D A Robinson 1981
The Behavior of the Vestibulo-Ocular Reflex at High Velocities of Head Rotation
Brain Research. 222:159-165.
- T Raphan, B Cohen 1985
Velocity Storage and the Ocular Response to Multidimensional Vestibular Stimuli
Chapter 8 In: A Berthoz, G Melvill Jones (eds.) *Adaptive Mechanisms in Gaze Control*. New York: Elsevier/North-Holland Biomedical Press.

- T Raphan, V Matsuo, B Cohen 1979
Velocity Storage in the Vestibulo-Ocular Reflex Arc (VOR)
Experimental Brain Research. 35:229-248.
- J T Reason 1978
Motion Sickness Adaptation: A Neural Mismatch Model
Journal of the Royal Society of Medicine. 71:819-829.
- D A Robinson 1975
Oculomotor Control Signals
In: G Lennerstrand, P Bach-y-Rita (eds), *Basic Mechanisms of Ocular Motility and Their Clinical Implications*. New York: Pergamon.
- D A Robinson 1981
Control of Eye Movements
In: V B Brooks (ed), *The Nervous System, Handbook of Physiology, Vol II, Part 2*. Baltimore: Williams & Wilkins. pp. 1275-1320.
- D A Robinson 1982
A Model of Cancellation of the Vestibulo-Ocular Reflex
In: G Lennerstrand, D S Zee & E L Keller (eds), *Functional Basis of Ocular Motility Disorders*. New York: Pergamon.
- D A Robinson, J L Gordon, S E Gordon 1986
A Model of the Smooth Pursuit Eye Movement System
Biological Cybernetics. 55: 43-57.
- H A Sedgwick, L Festinger 1976
Eye Movements, Efference, and Visual Perception
In: R A Monty & J W Senders (eds), *Eye Movements and Psychological Processes*. Hillsdale. NJ: Lawrence Earlbaum.
- J A Sharpe, T O Sylvester 1978
Effect of Aging on Horizontal Smooth Pursuit
Investigative Ophthalmology and Visual Sciences. 17(5):465-468.
- A A Sjoberg 1931
Experimentelle Studien uber den Auslosungsmechanismus der Seekrankheit
Acta Otolaryngologica. Suppl. 14.
- J W Spooner, S M Sakala, R W Baloh 1980
Effect of Aging on Eye Tracking
Archives of Neurology. 37:575-576.
- L Stark, G Vossius, L R Young 1962
Predictive Control of Eye Tracking Movements
IRE Transactions on Human Factors in Electronics. HFE-3:52-56.
- M J Steinbach 1969
Eye Tracking of Self-Moved Targets: The Role of Efference
Journal of Experimental Psychology. 82(2):366-376.

- M J Steinbach 1976
Pursuing the Perceptual Rather than the Retinal Stimulus
Vision Research. 16:1371-1376.
- M J Steinbach, R Held 1968
Eye Tracking of Observer-Generated Target Movements
Science. 161:187-188.
- R M Steinman, A A Skavenski, R V Sansbury 1969
Voluntary Control of Smooth Pursuit Velocity
Vision Research. 9:1167-1171.
- G J St-Cyr, D H Fender 1969
Nonlinearities of the Human Oculomotor System: Time Delays
Vision Research. 9:1491-1503.
- O Tokunaga 1977
The Influence of Linear Acceleration on Optokinetic Nystagmus in Human Subjects
Acta Otolaryngologica. 84:338-343.
- D L Tomko, G D Paige 1988
Linear Vestibulo-Ocular Reflex (LVOR) of Squirrel Monkey: I. Basic Characteristics
Abstract 138.1, presented at the *18th meeting of the Society for Neuroscience*, Toronto, Canada.
- W A van de Grind, O-J Grüsser, H-U Lunkenheimer 1973
Temporal Transfer Properties of the Afferent Visual System
In: R Jung (ed), *Handbook of Sensory Physiology, Vol VII, Part 3. Central Processing of Visual Information. A: Integrative Functions and Comparative Data*. New York: Springer-Verlag.
- V B Veenhof 1965
On the Influence of Linear Acceleration on Optokinetic Nystagmus
Acta Oto-laryngologica. 60:339-346.
- E Virre, D Tweed, K Milner, T Vilis 1986
A Reexamination of the Gain of the Vestibuloocular Reflex
Journal of Neurophysiology. 56(2):439-450.
- E von Holst, H Mittelstaedt 1950
Das Reafferenzprinzip (Wechselwirkungen zwischen Zentralnervensystem und Peripherie)
Naturwissenschaften. 10:464-476.
- G K von Noorden, G Mackensen 1962
Pursuit Movements of Normal and Amblyopic Eyes. 1. Physiology of Pursuit Movements
American Journal of Ophthalmology. 53(2):325-336.
- S G Whittaker, G Eaholtz 1982
Learning Patterns of Eye Motion for Foveal Pursuit
Investigative Ophthalmology and Visual Sciences. 23(3):393-397.

S Yasui 1973

Nystagmus Generation, Oculomotor Tracking and Visual Motion Perception
Ph.D. Thesis, Department of Aeronautics and Astronautics, MIT.

S Yasui, L R Young 1975a

Eye Movements During After-Image Tracking Under Sinusoidal and Random Vestibular Stimulation

In: G Lennerstrand, P Bach-y-Rita (eds), *Basic Mechanisms of Ocular Motility and Their Clinical Implications*. New York: Pergamon.

S Yasui, L R Young 1975b

Perceived Visual Motion as Effective Stimulus to Pursuit Eye Movement System
Science. 190:906-908.

S Yasui, L R Young 1984

On the Predictive Control of Foveal Eye Tracking and Slow Phases of Optokinetic and Vestibular Nystagmus

Journal of Physiology. 347:17-33.

L R Young 1977

Pursuit Eye Movement - What Is Being Pursued?

In: Baker, A Berthoz (eds), *Control of Gaze by Brain Stem Neurons*. Elsevier/North-Holland Biomedical Press.

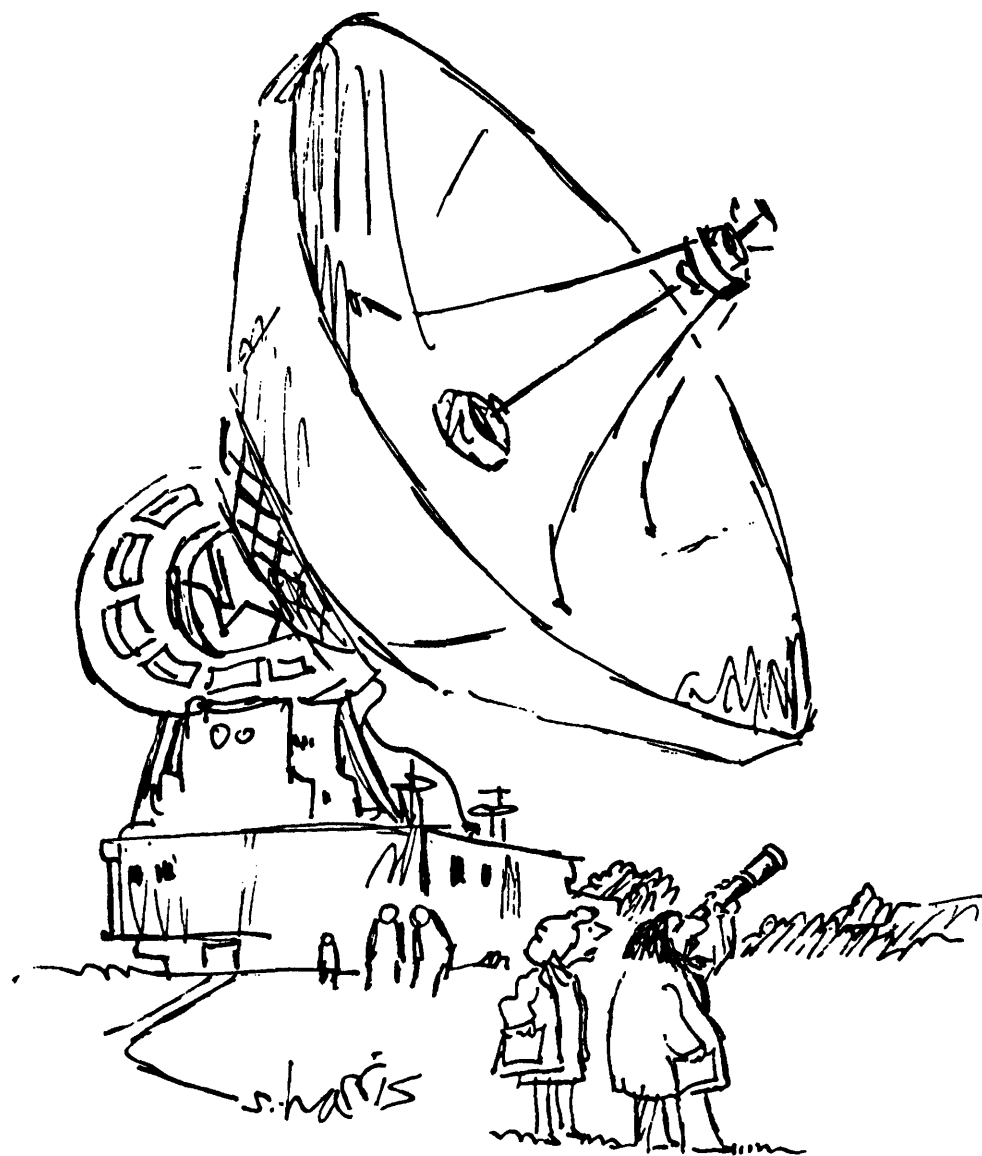
D Zambarbieri, R Schmid, C Prablanc, G Mages 1981

Characteristics of Eye Movements Evoked by the Presentation of Acoustic Targets

In: A F Fuchs, W Becker (eds), *Progress in Oculomotor Research*. New York: Elsevier/North-Holland Biomedical Press.

Appendix A

Clinical Test Data



"JUST CHECKING."

SUMMARY OF CLINICAL TESTING OF EXPERIMENTAL SUBJECTS

Tests were performed in the Vestibular Laboratory of the Massachusetts Eye and Ear Infirmary (MEEI), November 29 and December 1, 7, and 8, 1989.

1. Horizontal smooth pursuit of sinusoidal targets (PUR). Stimuli were 0.2 Hz / 22.6 deg/sec and 0.3 Hz / 33.9 deg/sec. Response gain and phase were measured.
2. Horizontal saccades to random targets (RANSAC). Stimuli were randomly-placed points targets, requiring saccades of up to 40 deg to the right or to the left. Response latency, accuracy, and peak velocity were measured.
3. Vestibulo-ocular reflex (VOR). Sinusoidal rotations in the dark, with an alerting task, were performed. Frequencies were 0.01, 0.02, 0.05, 0.10, 0.20, 0.5, and 1.00 Hz. Peak velocity was 50 deg/sec for all frequencies. Measurements were response gain, phase, and asymmetry.
4. Fixation suppression (FIX). At 0.05 Hz sinusoidal rotation, a fixation point was provided for visual suppression of the VOR. Measurements were the same as for VOR (above).
5. Optokinetic reflex (OKN). An OKN drum surrounding the rotating chair provided an optokinetic stimulus at 0.05 Hz. Measurements were taken as for VOR (above).
6. Visual vestibulo-ocular reflex (VVOR). The subject maintained gaze on a point fixed in the laboratory during rotation at 0.05 Hz. Measurements same as for VOR (above).

7. Posturography. Translation and tilt disturbances were applied at the feet of the standing subject, along with a stable visual field, one that tilted along with the applied disturbance, or with eyes closed. Stress distribution patterns on the foot platform provided a measure of the ability to maintain steady upright posture.

8. Z-axis recumbent ("BBQ spit") rotation (ZAR). The subject, in an earth-horizontal orientation, was rotated in the dark with a velocity trapezoid of 61.2 seconds duration, peak velocity of 60 deg/s, and 100 deg/s² acceleration and deceleration segments. Ten complete revolutions were performed at the peak velocity. Slow phase eye velocity (SPV) was processed to yield values for amplitude (AMP) and decay time constant (TAU) of an exponential component, amplitude of a sinusoidal component at the stimulus frequency (0.167 Hz) (MOD, the "modulation component"), and a constant bias (BIAS). The response model is:

$$SPV = BIAS + AMP \exp(-t/TAU) + MOD \sin(\omega t + \phi).$$

Data were compared with a normative database maintained at the laboratory.

The PUR and RANSAC data are summarized in Table A.1; the ZAR data in Table A.2, and the VOR, FIX, OKN, and VVOR results in Figures A.1-A.9.

Smooth Pursuit 0.2 Hz 22.6 deg/sec

Subject	J	S	T
Gain	0.92	0.95	0.97
Phase (deg)	0	-4	0

Smooth Pursuit 0.3 Hz 33.9 deg/sec

Subject	J	S	T
Gain	1.01	0.92	0.94
Phase (deg)	1	-3	0

Random Saccades

Subject	J	S	T
L/L delay	0.186 msec	0.211 msec	0.173 msec
L/L accuracy	98%	72%	88%
R/L delay	0.185	0.207	0.168
R/L accuracy	91	66	81
R/R delay	0.157	0.211	0.159
R/R accuracy	99	94	100
L/R delay		0.212	0.172
L/R accuracy		92	81

R/L means Right eye moving to the Left, etc.

Table A.1

Z-Axis Rotation

Value	Rotation	J	S	T
TAU	R	16.9	5.5	29.3
	L	18.2	6.2	18.8
MOD	R	0.26	1.58	3.7
	L	0.41	5.0	6.6
BIAS	R	0.006	0.009	0.64
	L	0.057	2.6	0.86
AMP	R	19.0	21.5	37.0
	L	21.7	16.4	16.4

See text for explanation of value names

Table A.2

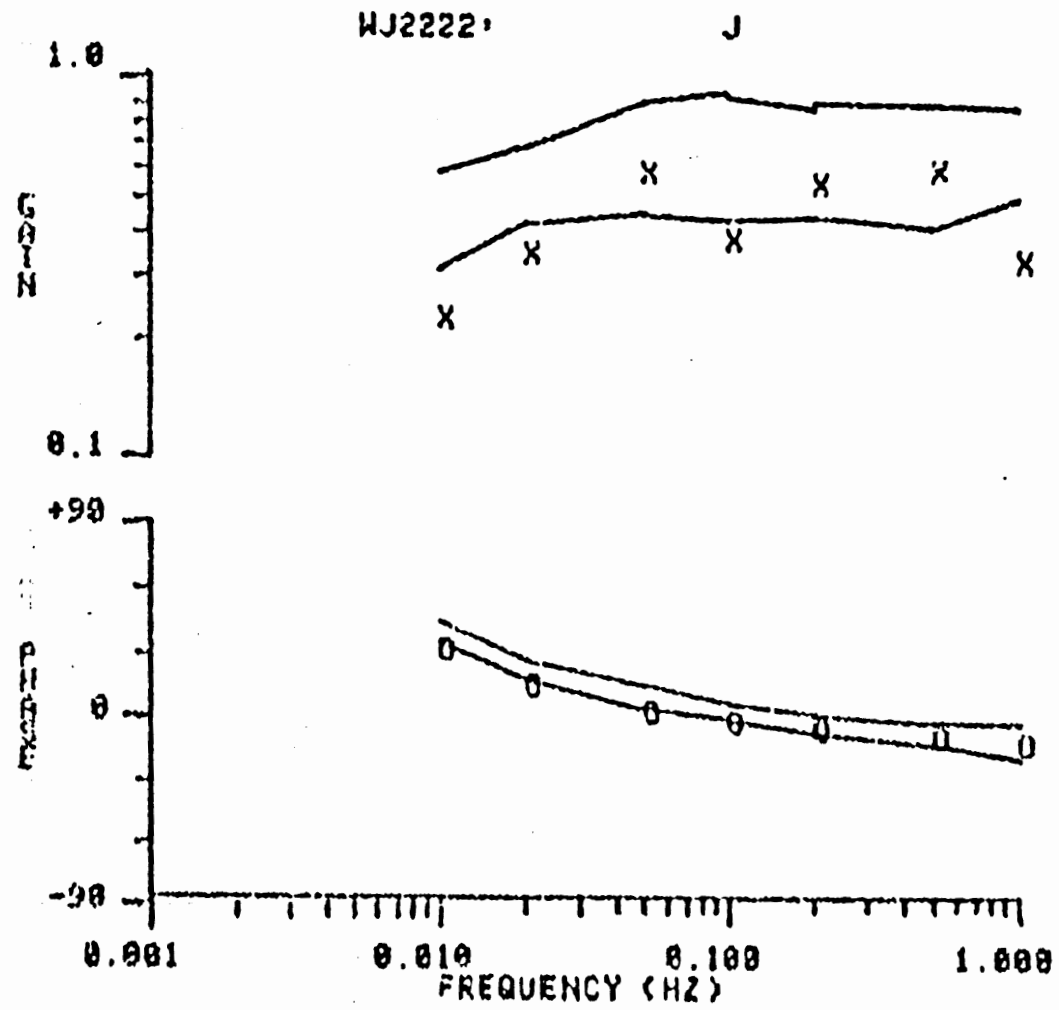


Figure A.1 Clinical VOR gain (top) and phase (bottom) for subject J.

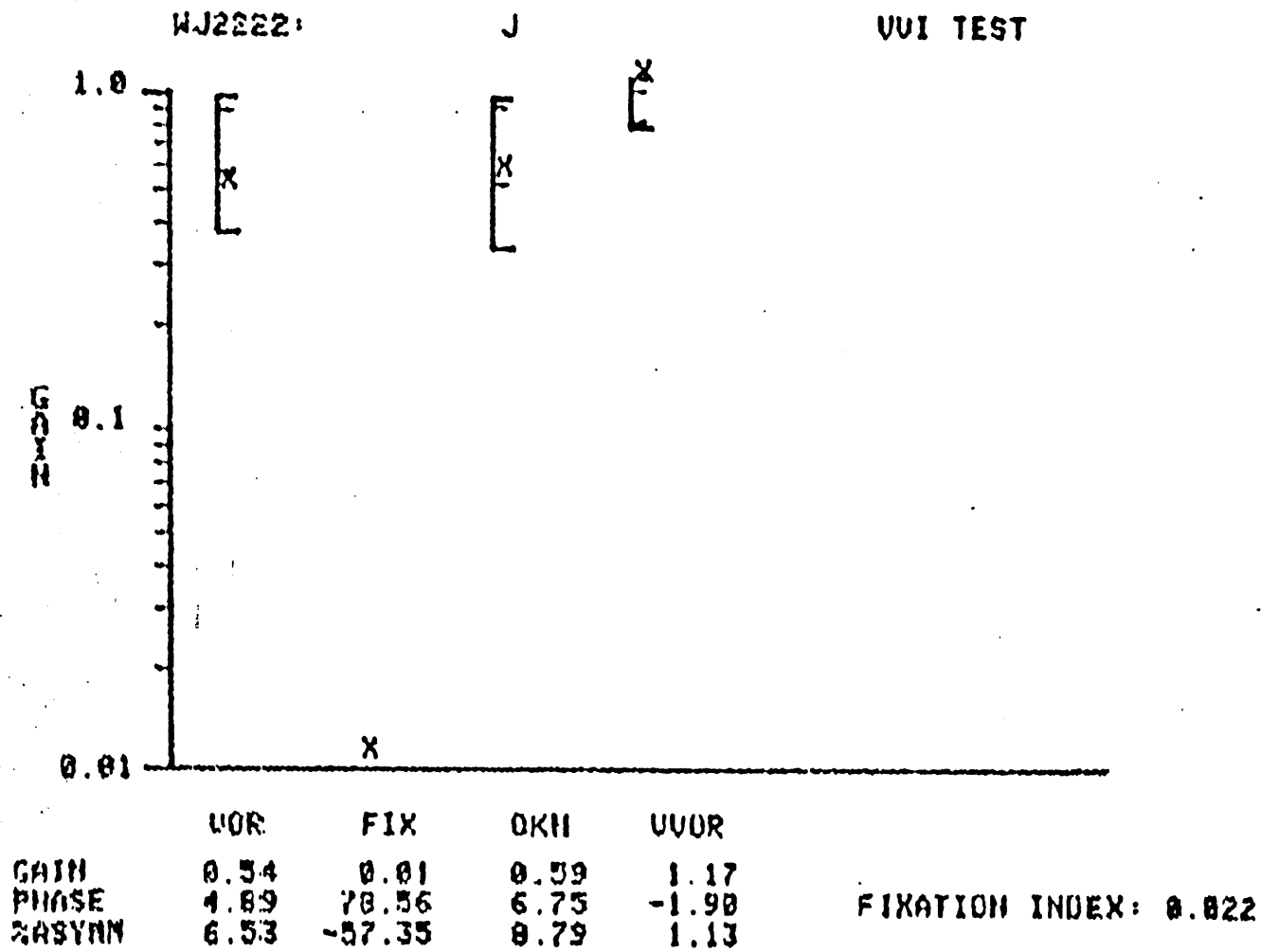


Figure A.2 Clinical VOR, FIX, OKN, and VVOR gains for subject J.

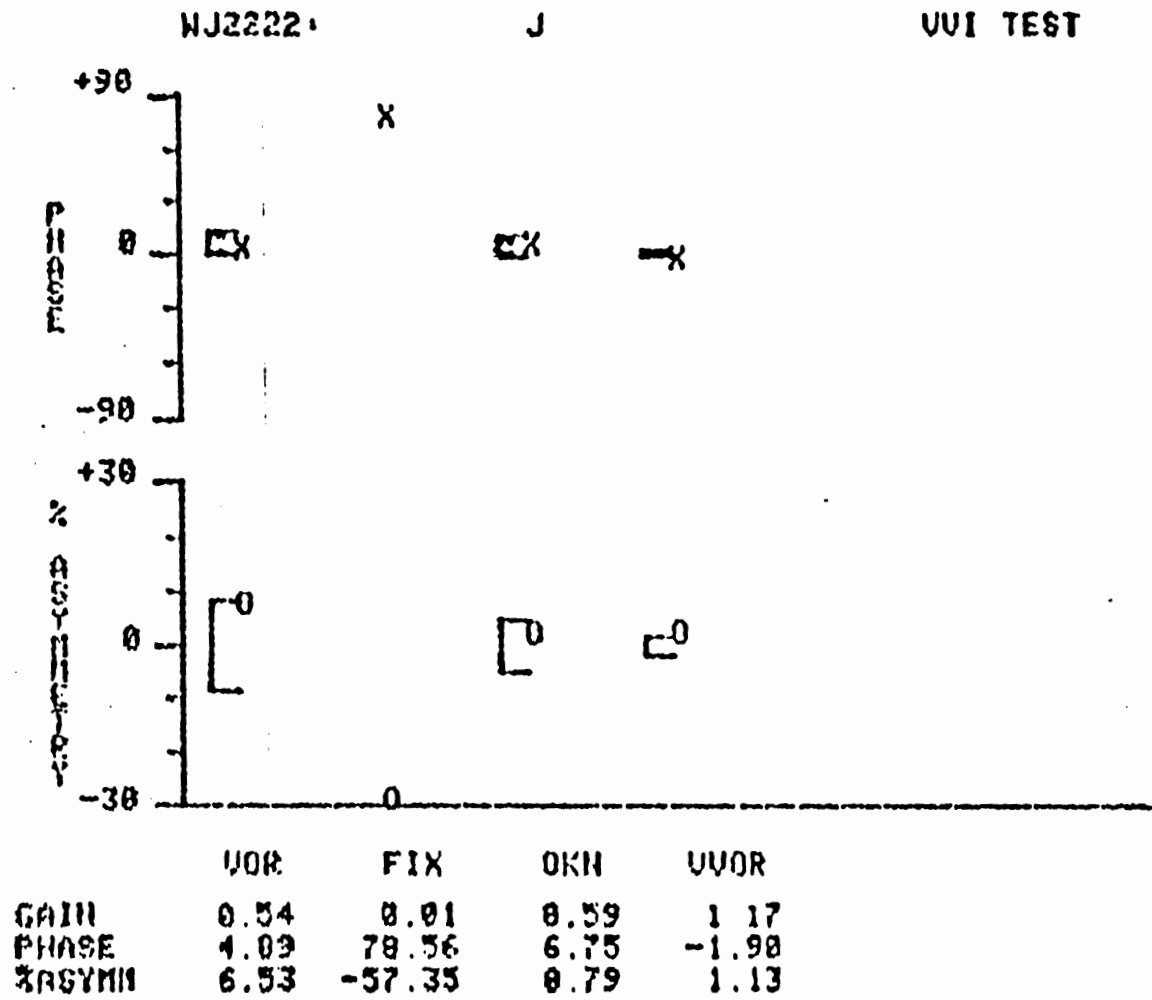


Figure A.3 Clinical VOR, FIX, OKN, and VVOR phases and asymmetries for subject J.

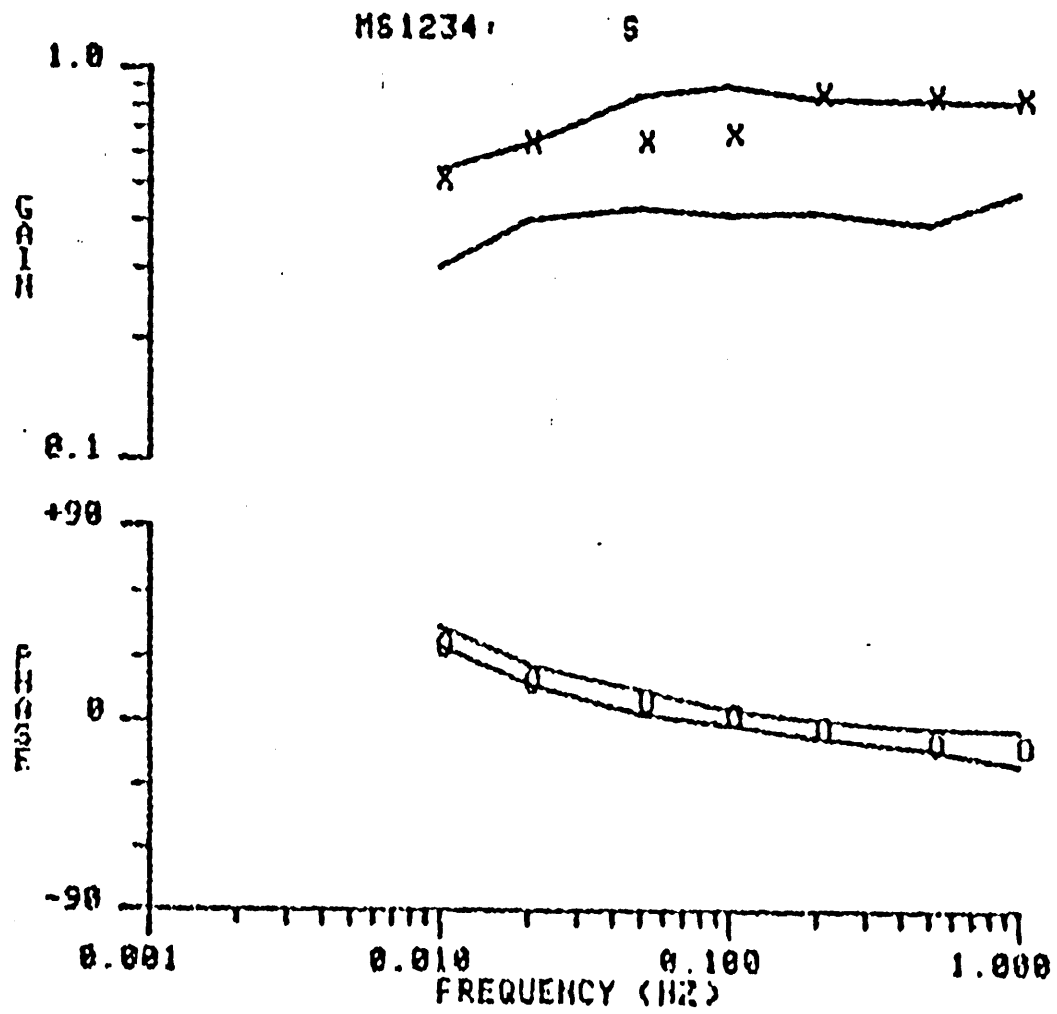


Figure A.4 Clinical VOR gain (top) and phase (bottom) for subject S.

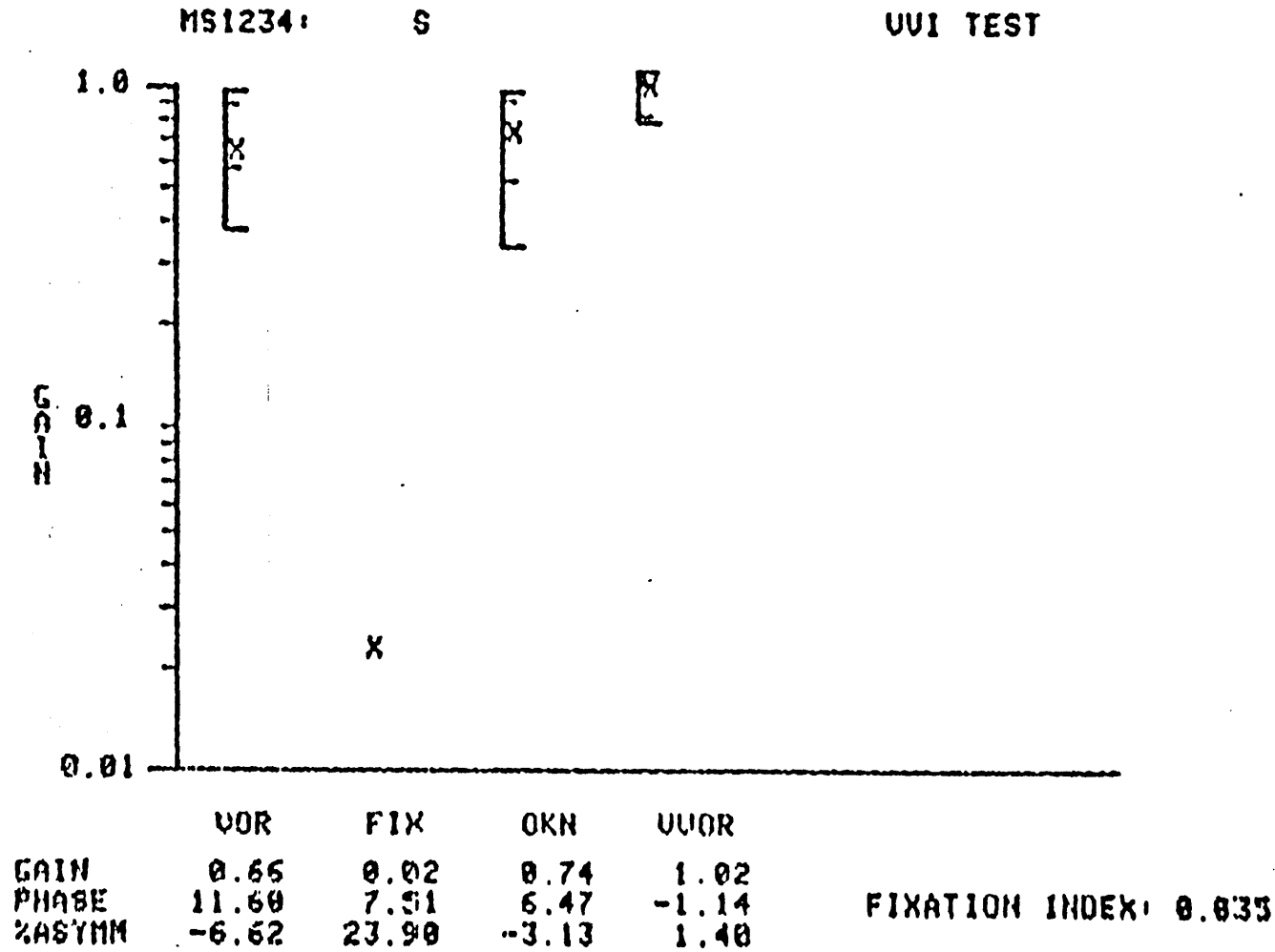


Figure A.5 Clinical VOR, FIX, OKN, and VVOR gains for subject S.

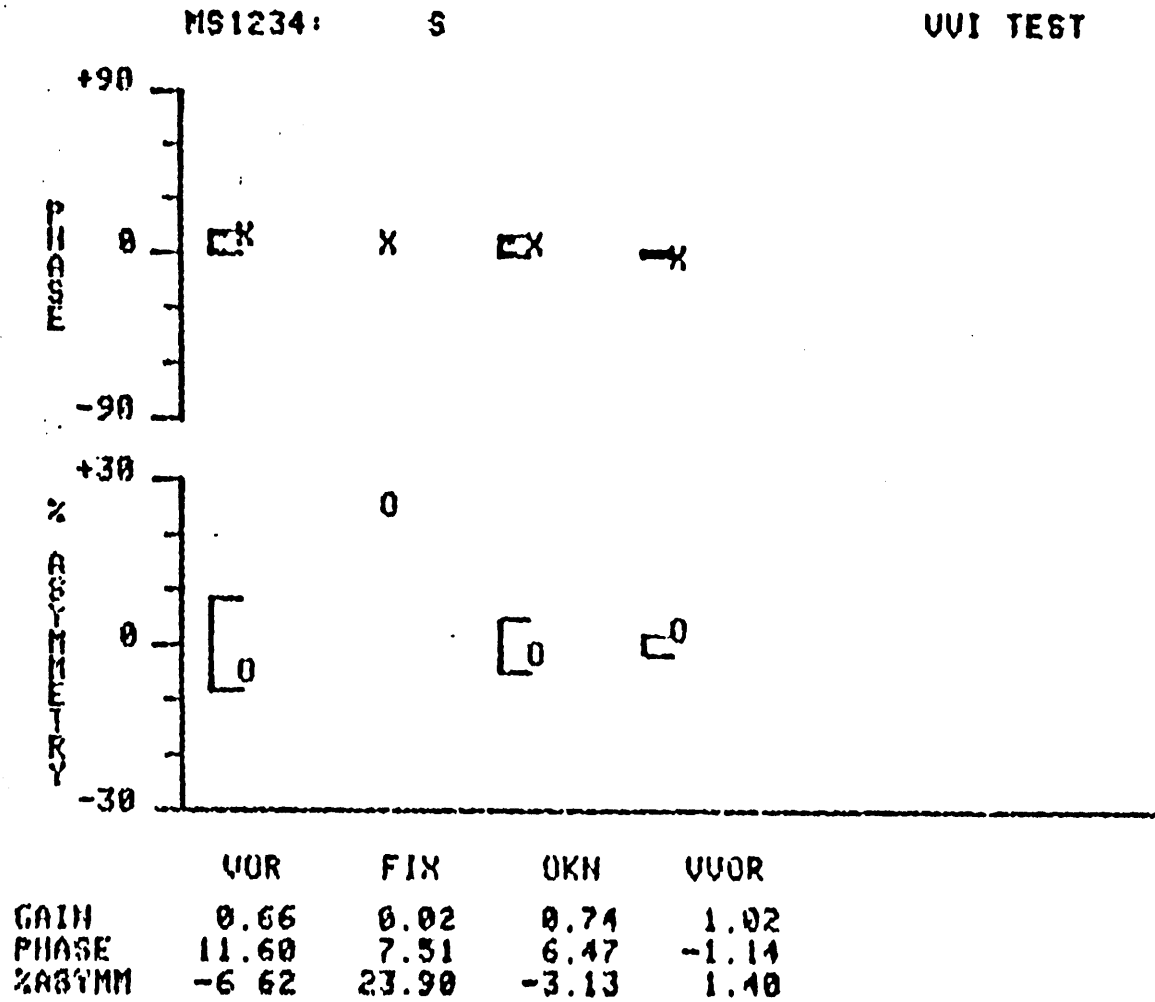


Figure A.6 Clinical VOR, FIX, OKN, and VVOR phases and asymmetries for subject S.

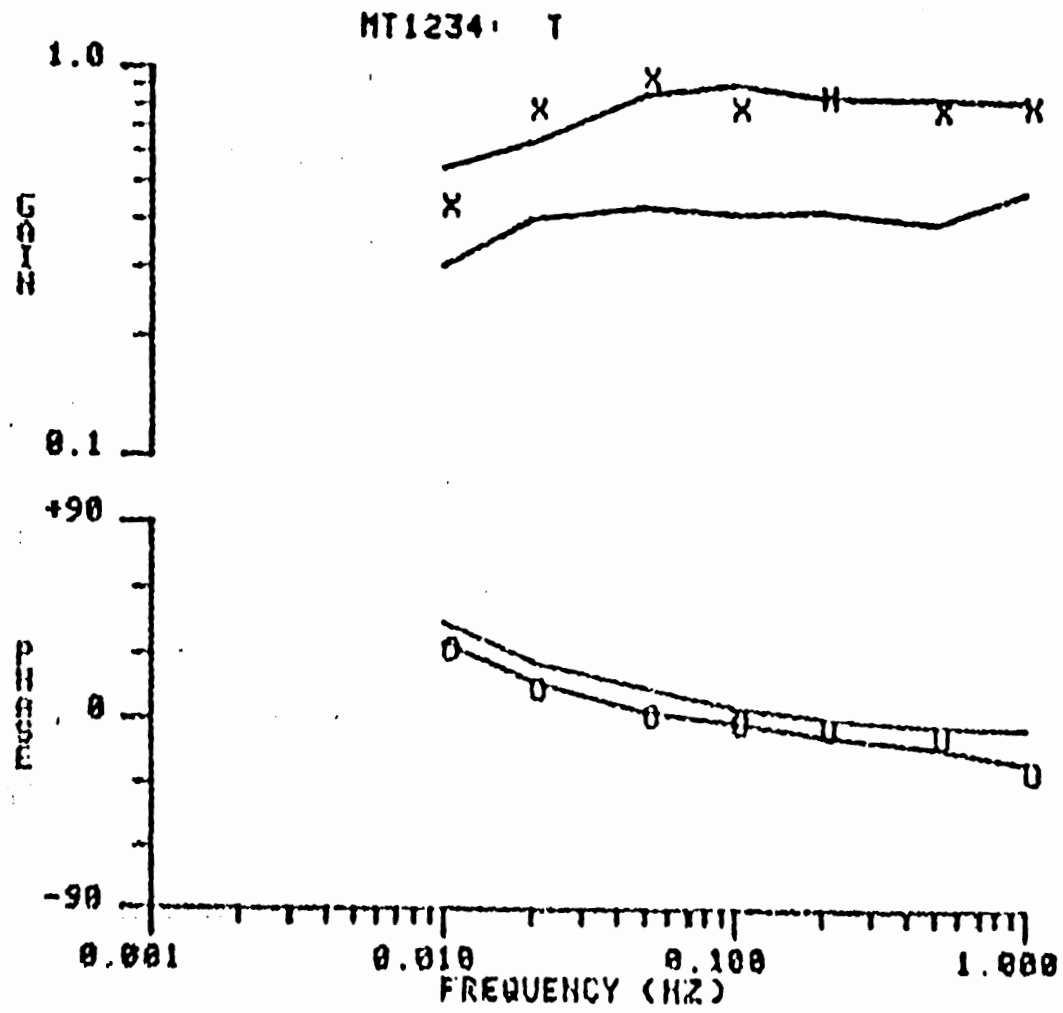


Figure A.7 Clinical VOR gain (top) and phase (bottom) for subject T.

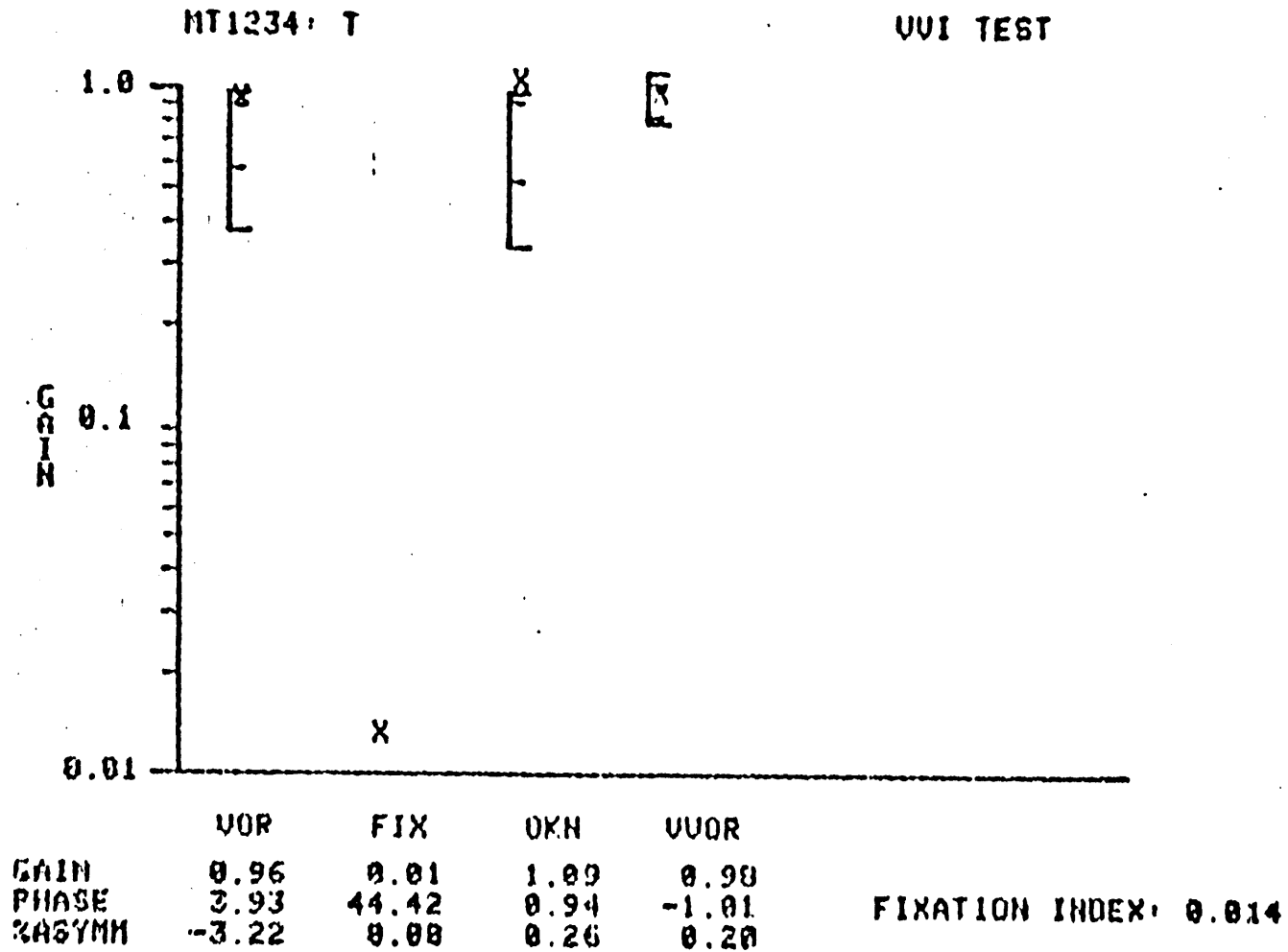


Figure A.8 Clinical VOR, FIX, OKN, and VVOR gains for subject T.

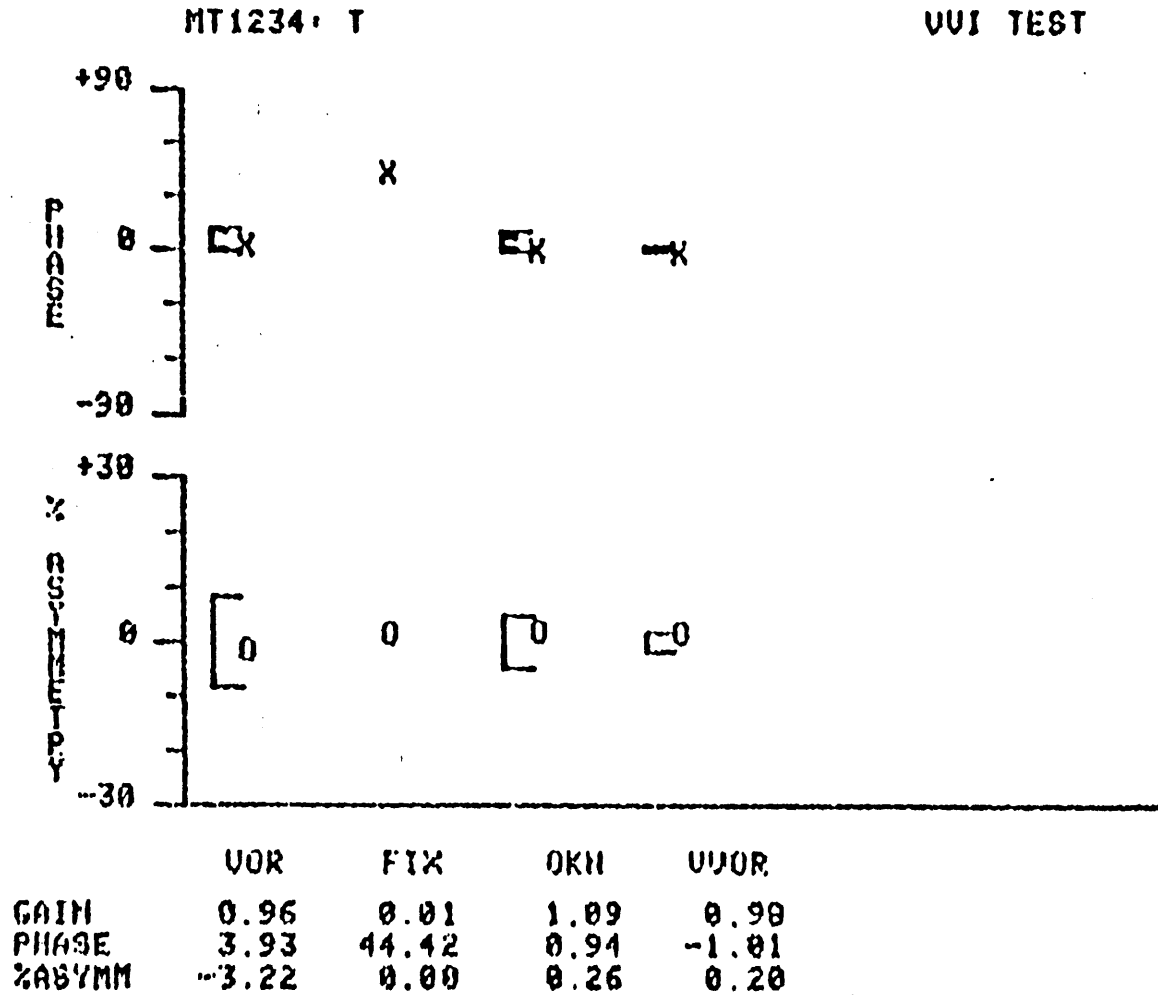
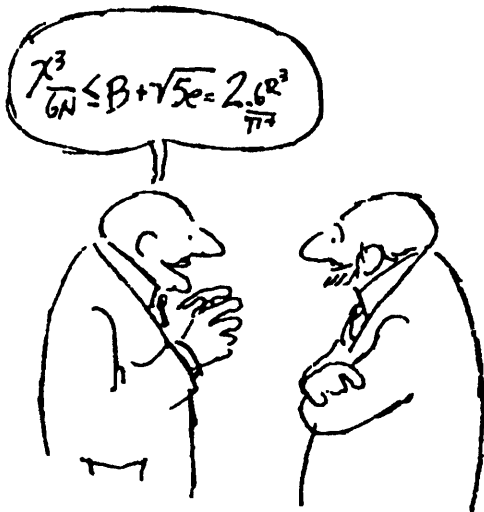
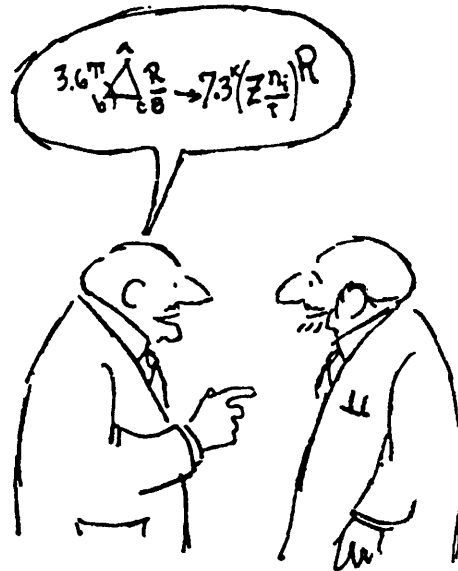
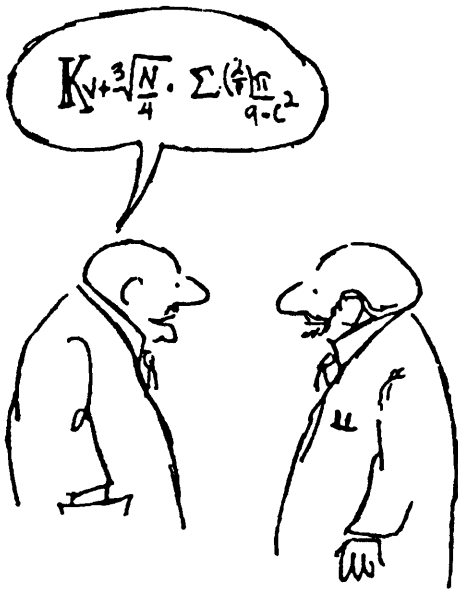


Figure A.9 Clinical VOR, FIX, OKN, and VVOR phases and asymmetries for subject T.

Appendix B

Models and Transfer Functions



General form of parameters and system equations for all models. See Figure B.1.

All cross-terms equal zero: $K_{12}=K_{21}=C_{12}=C_{21}=0$

Input matrix (note that K_{eye} is incorporated in the C matrix): $B = \begin{bmatrix} 1 & 0 \\ 0 & K_{oto} \end{bmatrix}$

Kalman feedback matrix (three feedback loops incorporated into element 1,1):

$$C = \begin{bmatrix} C_{11}-K_{eye}K_eD_e+K_{eye}D_1D_2 & 0 \\ 0 & C_{22} \end{bmatrix}$$

Kalman gain matrix: $K = \begin{bmatrix} K_{11} & 0 \\ 0 & K_{22} \end{bmatrix}$

Slow phase eye velocity output: $SPV = D_1 [1 \ 0] [sI-A+KC]^{-1} K \begin{bmatrix} v \\ \alpha_{sv} \end{bmatrix}$

The D_1 term represents the fact that the velocity state variable $x_1(t)$ is delayed before becoming the SPV output. The next row vector selects $x_1(t)$ as the output state variable. The final column matrix contains the input quantities, velocity and acceleration (see below). The remaining portion is the equation for the Kalman filter transfer function.

For the after-image (AI) transfer functions, results are expressed in terms of SPV per

acceleration (in g-units), which is obtained from: $\frac{SPV}{\text{accel [g]}} = \begin{bmatrix} SPV \\ v \end{bmatrix} \frac{1}{\alpha s}$

The term α represents the transformation from deg/sec (for the visual velocity input) to m/sec (for the acceleration input, which is m/s²). For a target distance of two meters, $\alpha=1/27$ (exactly valid only for the center of the stimulus excursion).

Smooth Pursuit/unpredictable stimuli (SP/SOS). Figure B.2

$$A = \begin{bmatrix} 0 & 1 \\ 0 & 0 \end{bmatrix}$$

$$K_{oto} = K_{22} = C_{22} = 0$$

$$\frac{SPV}{v} = \frac{K_{eye}K_{11}D_1D_2}{s + K_{11}(K_{eye}(D_1D_2 - K_eD_e) + C_{11})}$$

Visual+Vestibular/unpredictable stimuli (VV/SOS). Figure B.3

$$A = \begin{bmatrix} 0 & 1 \\ 0 & 0 \end{bmatrix}$$

$$\frac{SPV}{v} = \frac{(\alpha K_{oto}K_{22} + K_{eye}K_{11}D_1)s + K_{eye}K_{11}K_{22}C_{22}D_1}{s^2 + (K_{eye}K_{11}(D_1D_2 - K_eD_e) + K_{11}C_{11} + K_{22}C_{22})s + K_{eye}K_{11}K_{22}C_{22}(D_1D_2 - K_eD_e) + K_{11}K_{22}C_{11}C_{22}}$$

After-Image/unpredictable stimuli (AI/SOS). Figure B.4

Retinal slip velocity = 0 [mathematically, set $D_1=0$]

$$A = \begin{bmatrix} 0 & 1 \\ 0 & 0 \end{bmatrix}$$

$$\frac{SPV}{v} = \frac{\alpha K_{oto}K_{22}D_2s}{(K_{eye}K_{11}(-K_eD_e) + K_{11}C_{11} + K_{22}C_{22})s + K_{eye}K_{11}K_{22}C_{22}(-K_eD_e) + K_{11}K_{22}C_{11}C_{22}}$$

Smooth Pursuit/predictable stimuli (SP/sine). Figure B.5

$$K_{oto}=K_{22}=C_{22}=0$$

$$A = \begin{bmatrix} 0 & 1 \\ -\omega_0^2 & 0 \end{bmatrix} = \begin{bmatrix} 0 & 1 \\ s^2 & 0 \end{bmatrix}$$

$$\frac{SPV}{v} = \frac{K_{eye}D_1D_2}{K_{eye}(D_1D_2 - K_eD_e) + C_{11}}$$

Note that, compared to the SP/SOS transfer function, the s term in the denominator is removed by virtue of the fact that $-\omega_0^2=s^2$ causes a cancellation of terms in the derivation.

Visual+Vestibular/predictable stimuli (VV/sine). Figure B.6

$$A = \begin{bmatrix} 0 & 1 \\ -\omega_0^2 & 0 \end{bmatrix} = \begin{bmatrix} 0 & 1 \\ s^2 & 0 \end{bmatrix}$$

Note that $-\omega_0^2 = s^2$ only when ω_0 is the correct value (i.e. when the frequency estimator has converged).

$$\frac{SPV}{v} = \frac{(\alpha K_{oto} K_{22} + K_{eye} K_{11} D_1) s + K_{eye} K_{11} K_{22} C_{22} D_1}{(K_{eye} K_{11} (D_1 D_2 - K_e D_e) + K_{11} C_{11} + K_{22} C_{22}) s + K_{eye} K_{11} K_{22} C_{22} (D_1 D_2 - K_e D_e) + K_{11} K_{22} C_{11} C_{22}}$$

As for the case with SP/SOS and SP/sine, note that this transfer function is the VV/SOS transfer function with the denominator s^2 term eliminated by virtue of $-\omega_0^2 = s^2$. This has the effect of improving the overall system response.

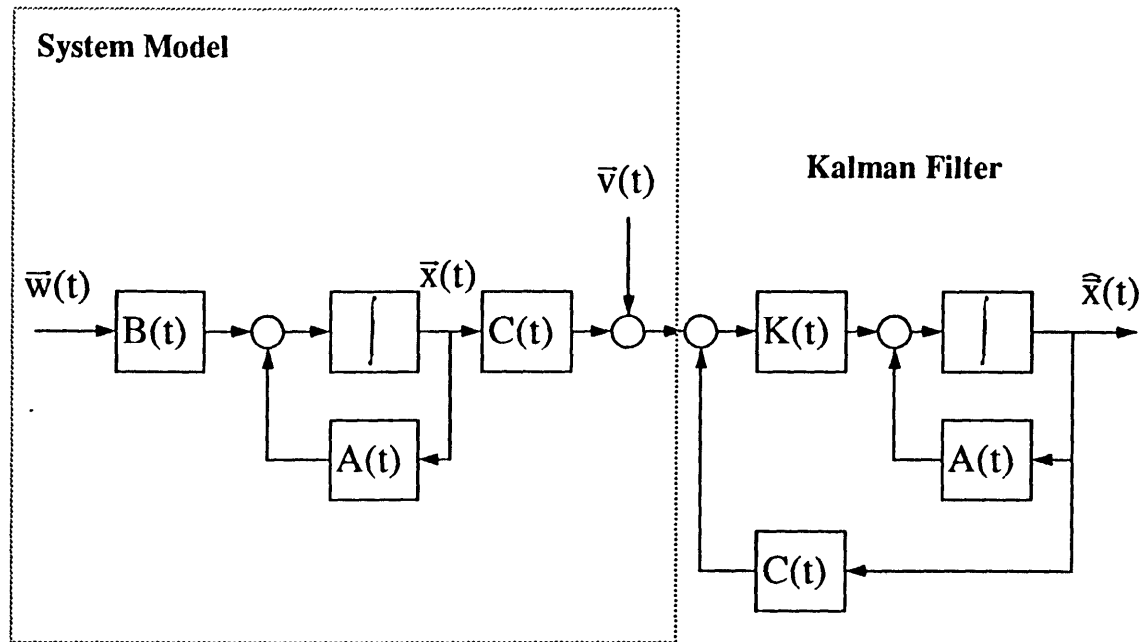
After-Image/predictable stimuli (AI/sine). Figure B.7

Retinal slip velocity = 0 [mathematically, set $D_1=0$]

$$A = \begin{bmatrix} 0 & 1 \\ -\omega_0^2 & 0 \end{bmatrix} = \begin{bmatrix} 0 & 1 \\ s^2 & 0 \end{bmatrix}$$

$$\frac{SPV}{v} = \frac{\alpha K_{oto} K_{22} D_2 s}{s^2 + (K_{eye} K_{11} (-K_e D_e) + K_{11} C_{11} + K_{22} C_{22}) s + K_{eye} K_{11} K_{22} C_{22} (-K_e D_e) + K_{11} K_{22} C_{11} C_{22}}$$

Compare this to the AI/SOS transfer function, and see the comments on the SP/sine and VV/sine equations.



System
 $\dot{\bar{x}}(t) = A\bar{x}(t) + B\bar{w}(t)$
 $\bar{w}(t) \sim N(0, Q(t))$

Measurement
 $\bar{y}(t) = C\bar{x}(t) + \bar{v}(t)$
 $\bar{v}(t) \sim N(0, R(t))$

State Estimate $\hat{\bar{x}}(t) = A\hat{\bar{x}}(t) + K(t)[\bar{y}(t) - C\hat{\bar{x}}(t)]$

Error Covariance $\dot{P}(t) = AP(t) + P(t)A^T + BQ(t)B^T - P(t)C^TR^{-1}(t)CP(t)$

Kalman Gain $K(t) = P(t)C^TR^{-1}(t)$

Figure B.1 Conceptual model of Kalman filter (from Gelb, 1974).

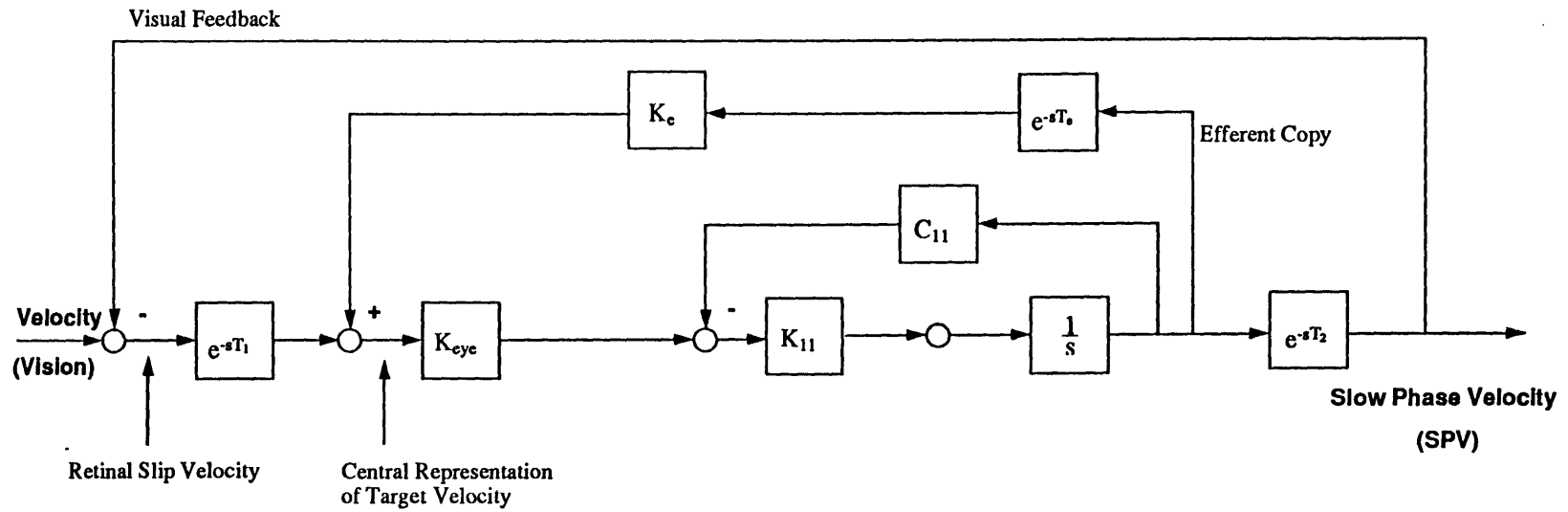


Figure B.2 Smooth pursuit / unpredictable stimuli model (SP/SOS).

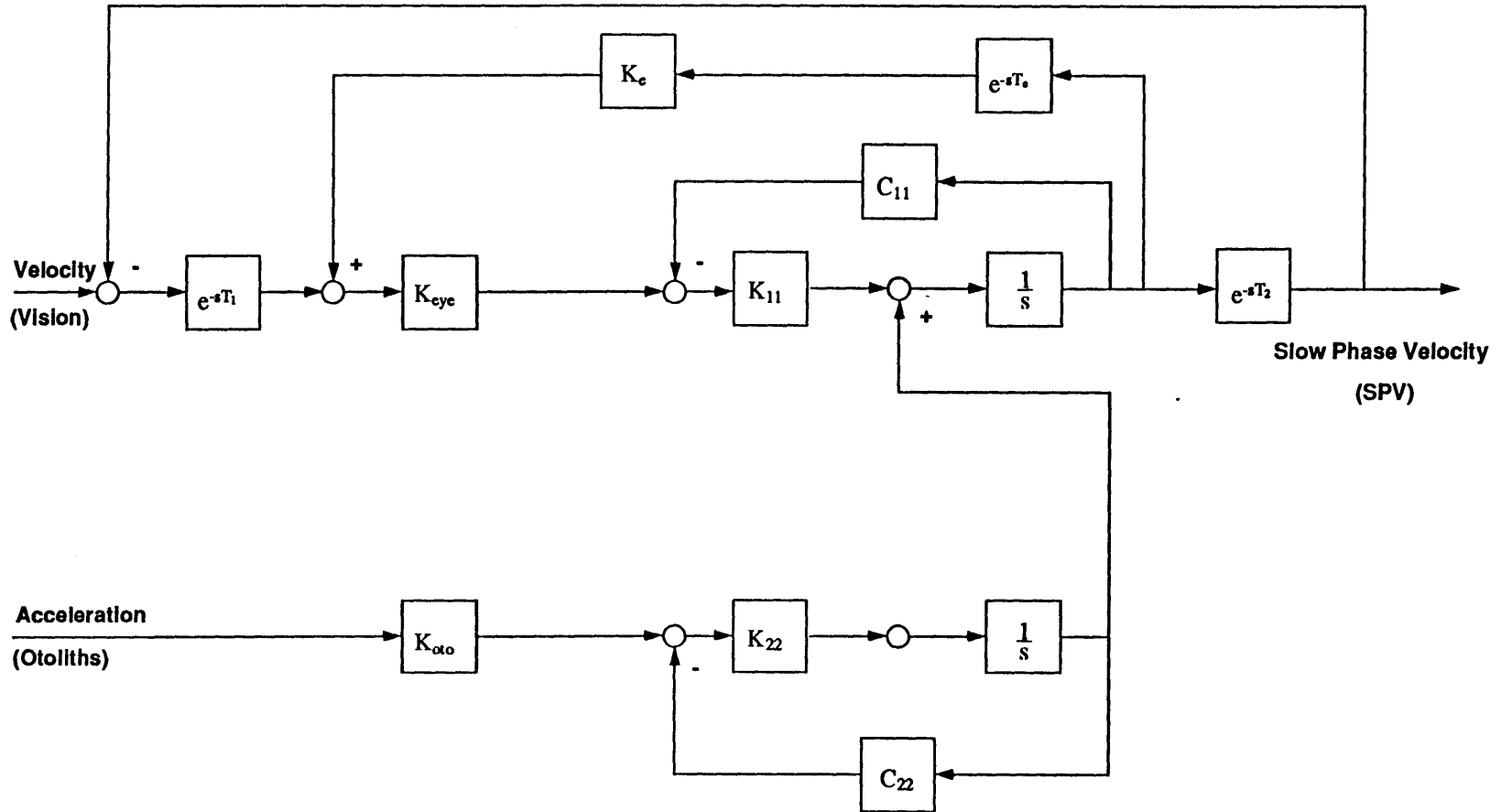


Figure B.3 Visual+vestibular / unpredictable stimuli model (VV/SOS).

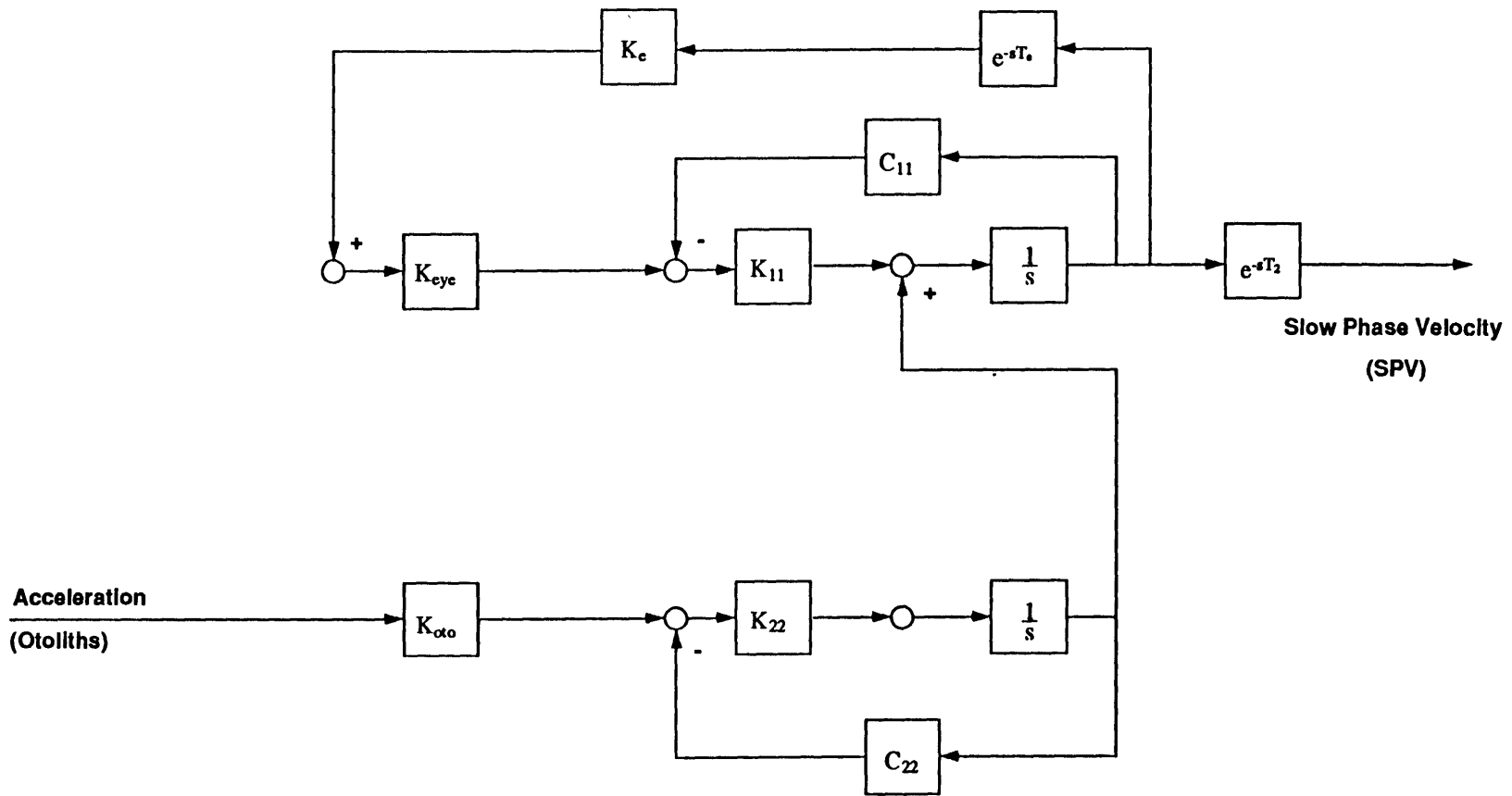


Figure B.4 After-image / unpredictable stimuli model (AI/SOS).

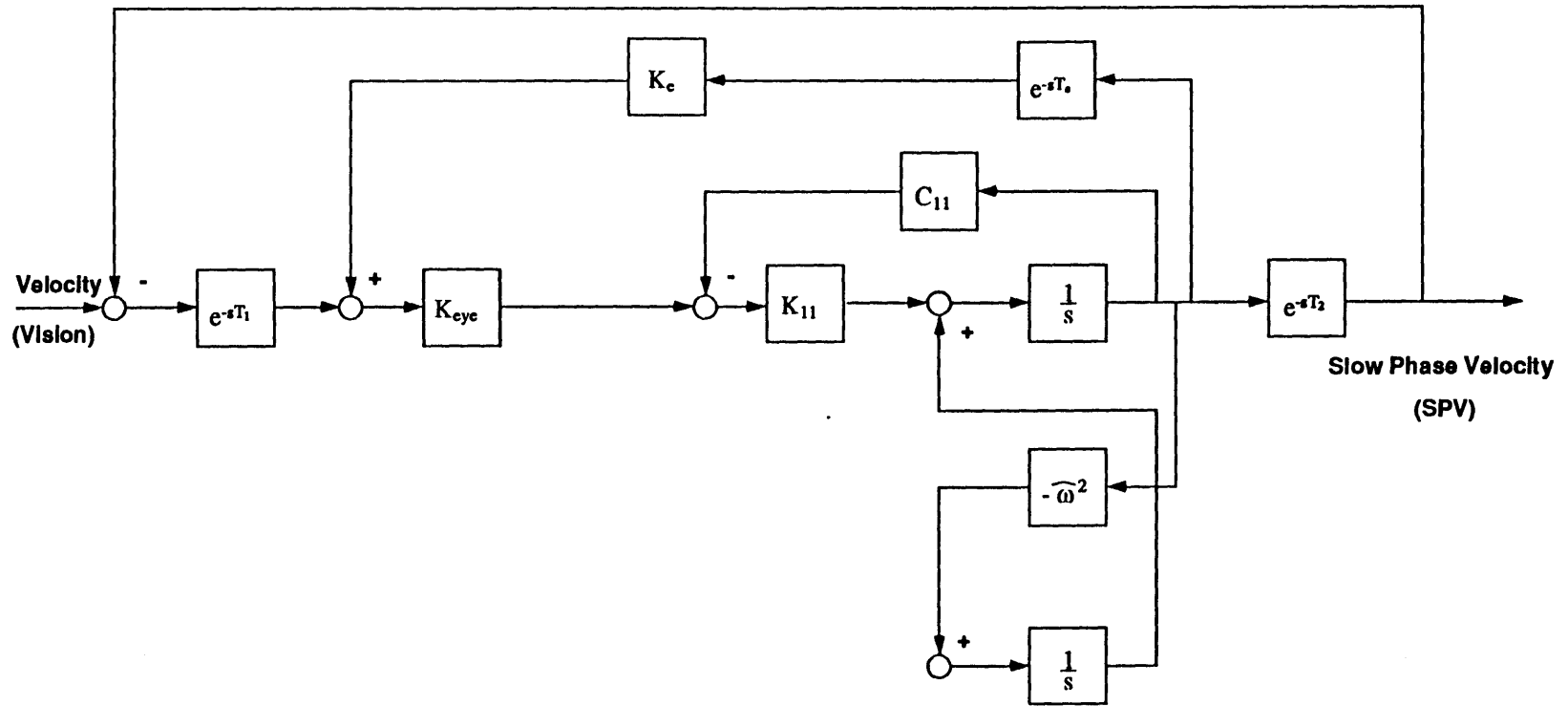


Figure B.5 Smooth pursuit / predictable stimuli model (SP/sine).

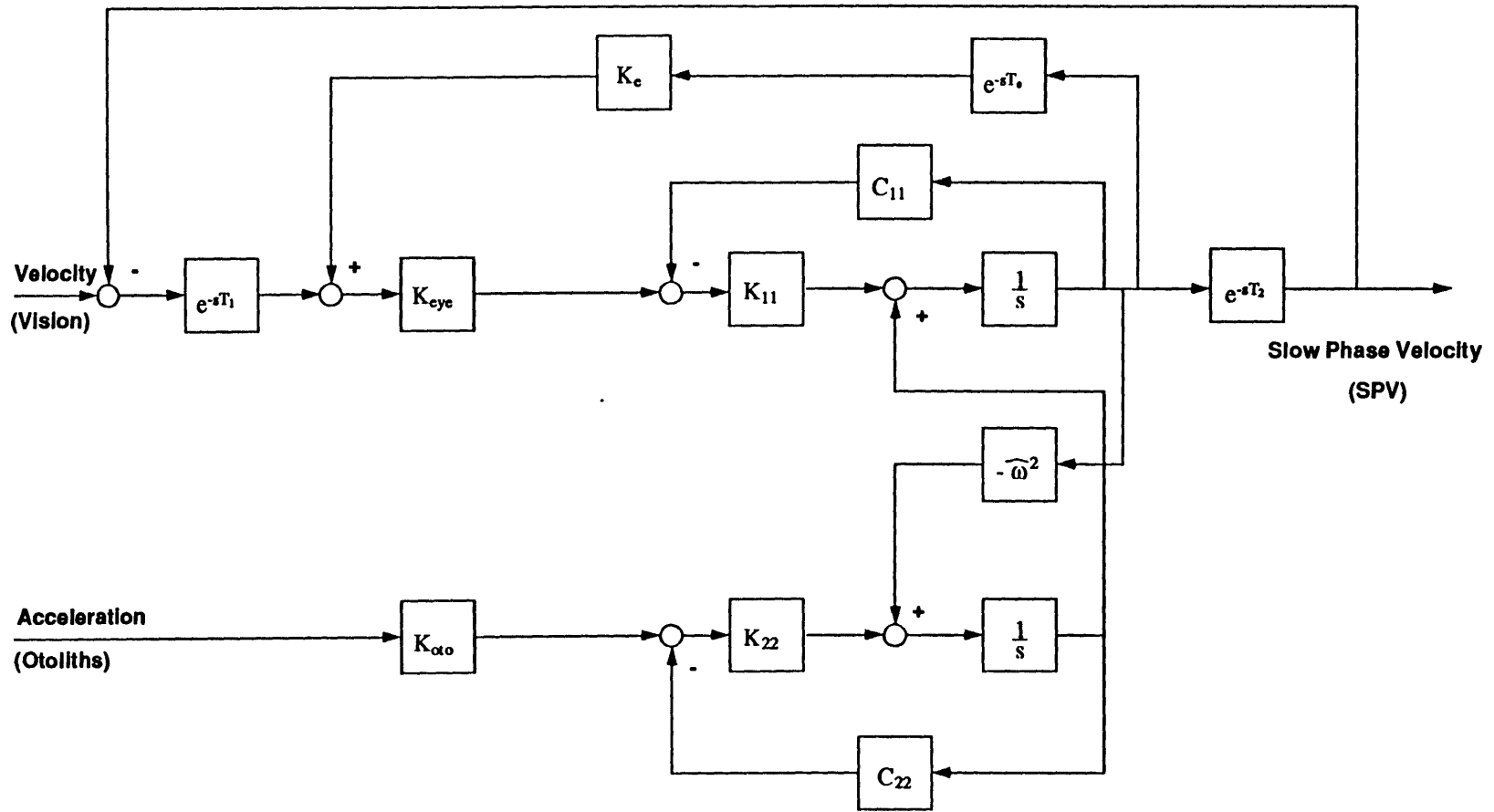


Figure B.6 Visual+vestibular / predictable stimuli model (VV/sine).

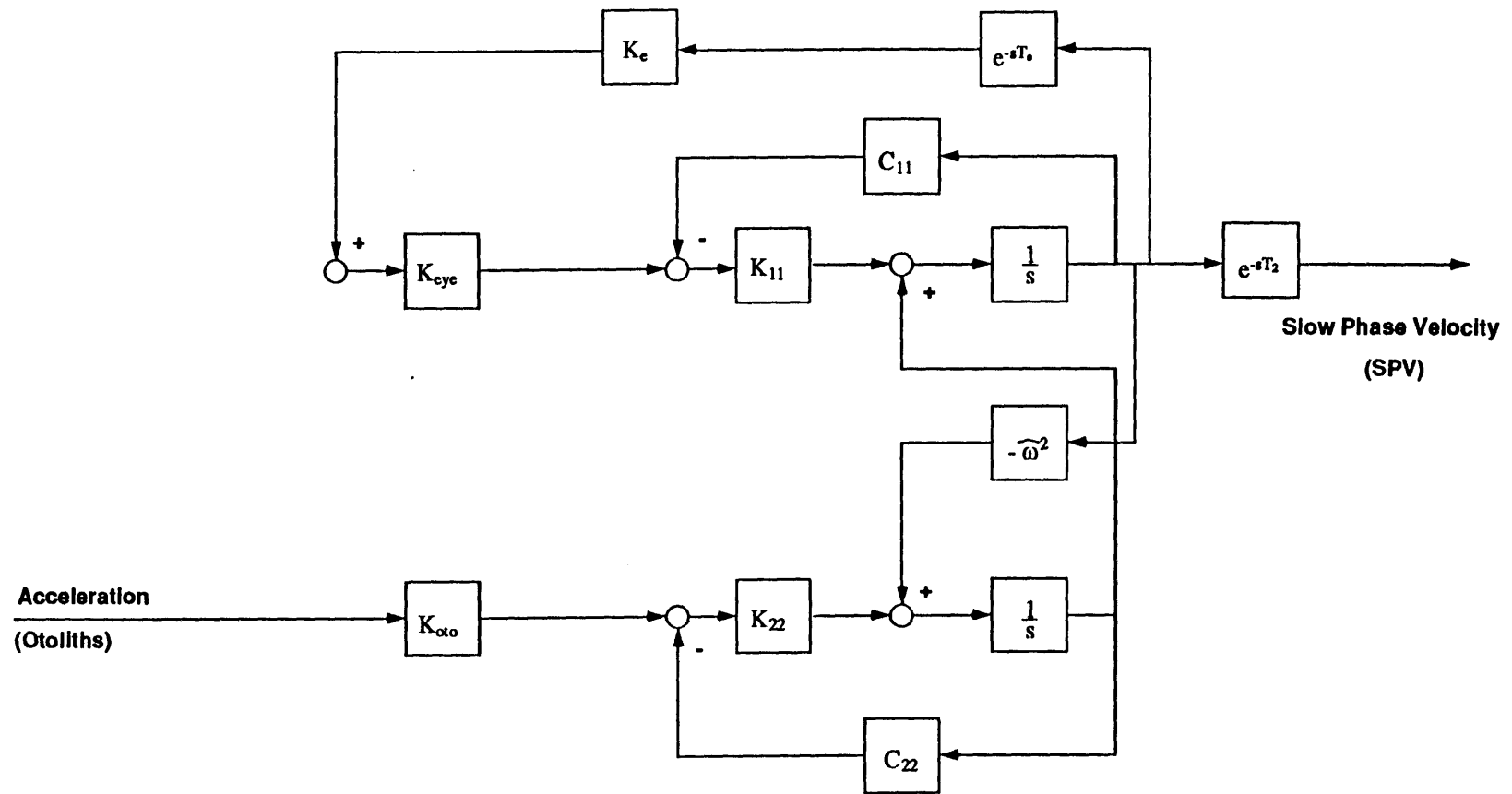


Figure B.7 After-image / predictable stimuli model (AI/sine).

**PC-MATLAB
Transfer Function
Programs**


```

% mfit130.m
% SP/VV sine
%
% Enter t1, t2, te, k11, k22, Ke, alpha, Koto, Keye
%          k12, k21, c1, c2

n=128;
w=logspace(-1,1,n);
j=sqrt(-1);
s=j*w;

D1=exp(-t1*s);
D2=exp(-t2*s);
De=exp(-te*s);

cc=c11-Keye*De*Ke+Keye*D1.*D2;
K=[k11 k12; k21 k22];

for i=1:n

ss=s(i);
A=[0 1; ss^2 0];
C=[cc(i) c12; c21 c22];
H=inv(ss*eye(2)-A+K*C);
Hv(i)=[1 0]*H*K*[Keye*D1(i); Koto*alpha*ss];
end;

Hv=D2.*Hv;

mag=abs(Hv);
p=57*atan(imag(Hv)./real(Hv));

f=w/2/pi;

subplot(211),plot(f,mag),grid;

subplot(212),plot(f,p),grid;

return;

```

PC-MATLAB SP/sine and VV/sine model transfer function program.

```

% mfitl31.m
% SP/SOS
%
% Enter t1, t2, te, k11, k22, Ke, alpha, Koto, Keye
%       k12, k21, c1, c2

n=128;
w=logspace(-1,1,n);
j=sqrt(-1);
s=j*w;

D1=exp(-t1*s);
D2=exp(-t2*s);
De=exp(-te*s);

cc=c11-Keye*De*Ke+Keye*D1.*D2;
K=[k11 0; 0 0];

for i=1:n

ss=s(i);
A=[0 0; 0 0];
C=[cc(i) 0; 0 0];
H=inv(ss*eye(2)-A+K*C);
Hv(i)=[1 0]*H*K*[Keye*D1(i); 0];
end;

Hv=D2.*Hv;

mag=abs(Hv);
p=57*atan(imag(Hv)./real(Hv));

f=w/2/pi;

subplot(211),plot(f,mag),grid;

subplot(212),plot(f,p),grid;

return;

```

PC-MATLAB SP/SOS model transfer function program.

```

% mfit132.m
% VV/SOS
%
% Enter t1, t2, te, k11, k22, Ke, alpha, Koto, Keye
%      k12, k21, c1, c2

n=128;
w=logspace(-1,1,n);
j=sqrt(-1);
s=j*w;

D1=exp(-t1*s);
D2=exp(-t2*s);
De=exp(-te*s);

cc=c11-Keye*De*Ke+Keye*D1.*D2;
K=[k11 k12; k21 k22];

for i=1:n

ss=s(i);
A=[0 1; 0 0];
C=[cc(i) c12; c21 c22];
H=inv(ss*eye(2)-A+K*C);
Hv(i)=[1 0]*H*K*[Keye*D1(i); Koto*alpha*ss];
end;

Hv=D2.*Hv;

mag=abs(Hv);
p=57*atan(imag(Hv)./real(Hv));

f=w/2/pi;

subplot(211),plot(f,mag),grid;

subplot(212),plot(f,p),grid;

return;

```

PC-MATLAB VV/SOS model transfer function program.

```

% mfit133.m
% AI/SOS
% Gain in deg/s / g
% Phase is vel w.r.t. vel
%
% Enter t1, t2, te, k11, k22, Ke, alpha, Koto, Keye
%          k12, k21, c1, c2

n=128;
w=logspace(-1,1,n);
j=sqrt(-1);
s=j*w;

D1=exp(-t1*s);
D2=exp(-t2*s);
De=exp(-te*s);

cc=c11-Keye*De*Ke;
K=[k11 k12; k21 k22];

for i=1:n

ss=s(i);
A=[0 1; 0 0];
C=[cc(i) c12; c21 c22];
H=inv(ss*eye(2)-A+K*C);
Hv(i)=[1 0]*H*K*[0; Koto*alpha*ss];
end;

Hv=D2.*Hv;
p=57*atan(imag(Hv)./real(Hv));
Hv=Hv*(9.81)./(alpha*s);
mag=abs(Hv);

f=w/2/pi;
subplot(211),plot(f,mag),grid;
subplot(212),plot(f,p),grid;

return;

```

PC-MATLAB AI/SOS model transfer function program.

```

% mfit134.m
% AI/sine
% Gain in deg/s / g
% Phase is vel w.r.t. vel
%
% Enter t1, t2, te, k11, k22, Ke, alpha, Koto, Keye
%           k12, k21, c1, c2

n=128;
w=logspace(-1,1,n);
j=sqrt(-1);
s=j*w;

D1=exp(-t1*s);
D2=exp(-t2*s);
De=exp(-te*s);

cc=c11-Keye*De*Ke;
K=[k11 k12; k21 k22];

for i=1:n

ss=s(i);
A=[0 1; ss^2 0];
C=[cc(i) c12; c21 c22];
H=inv(ss*eye(2)-A+K*C);
Hv(i)=[1 0]*H*K*[0; Koto*alpha*ss];
end;

Hv=D2.*Hv;
p=57*atan(imag(Hv)./real(Hv));
Hv=Hv*(9.81)./(alpha*s);
mag=abs(Hv);

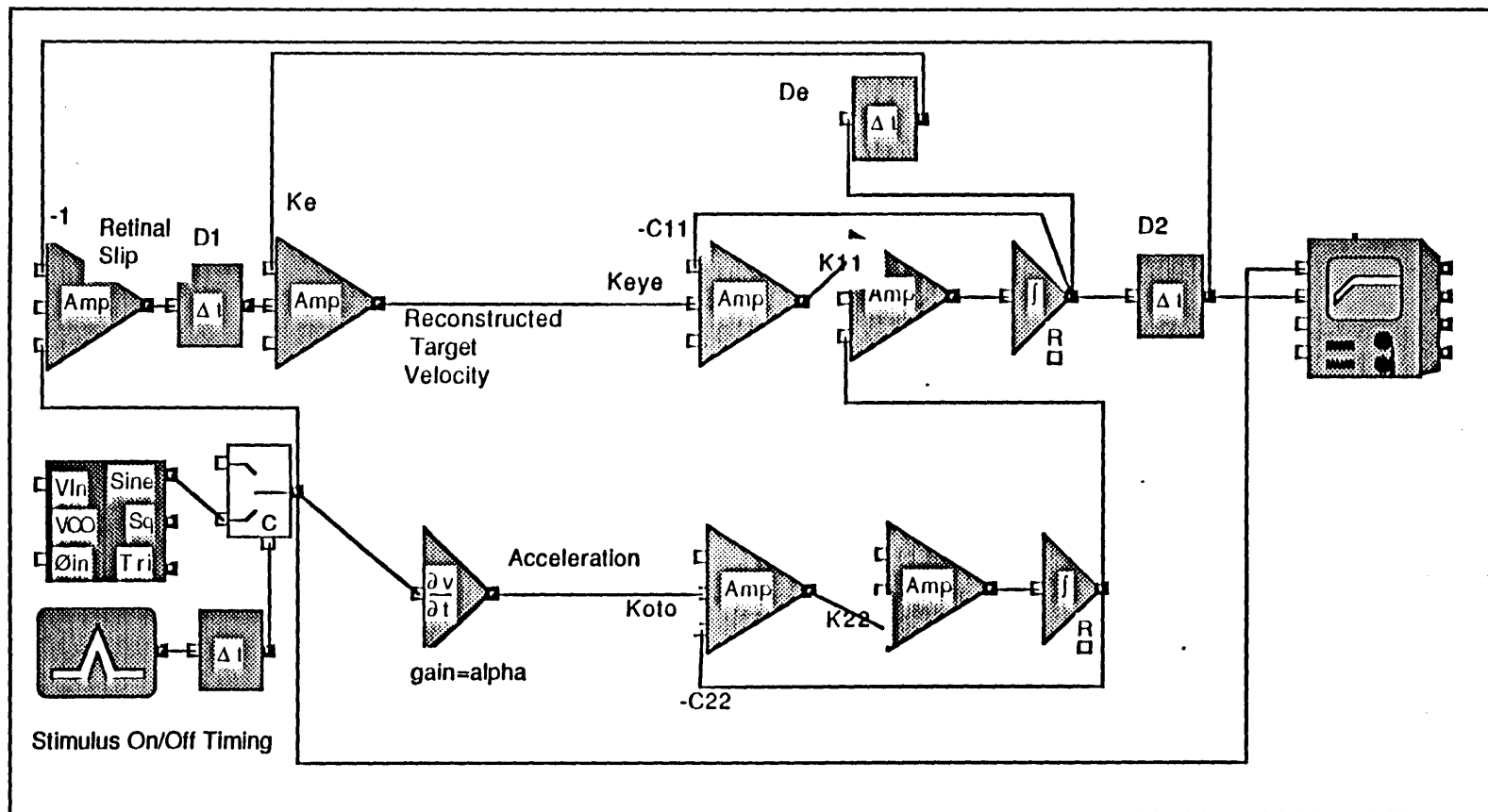
f=w/2/pi;
subplot(211),plot(f,mag),grid;
subplot(212),plot(f,p),grid;

return;

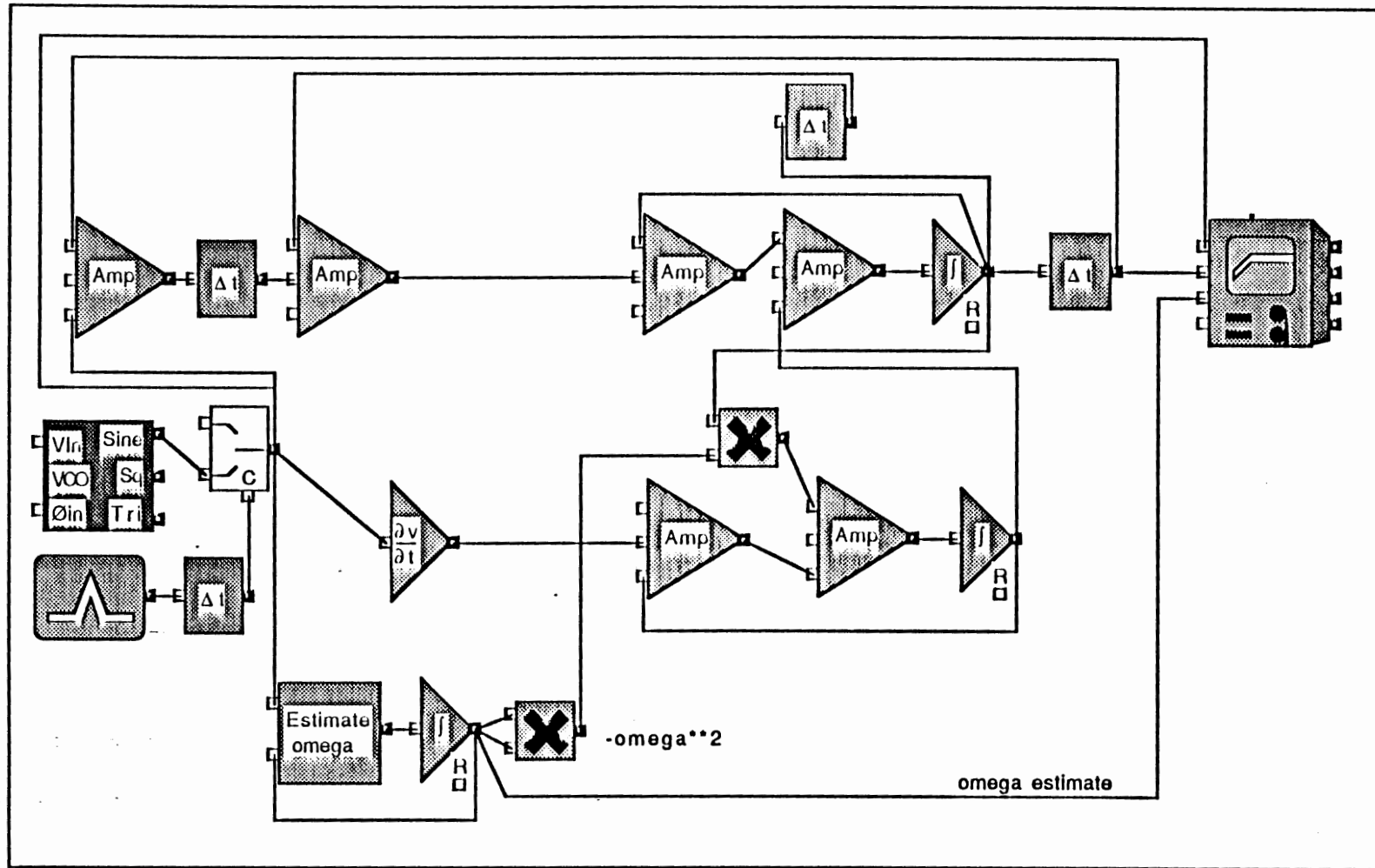
```

PC-MATLAB AI/sine model transfer function program.

EXTEND Models



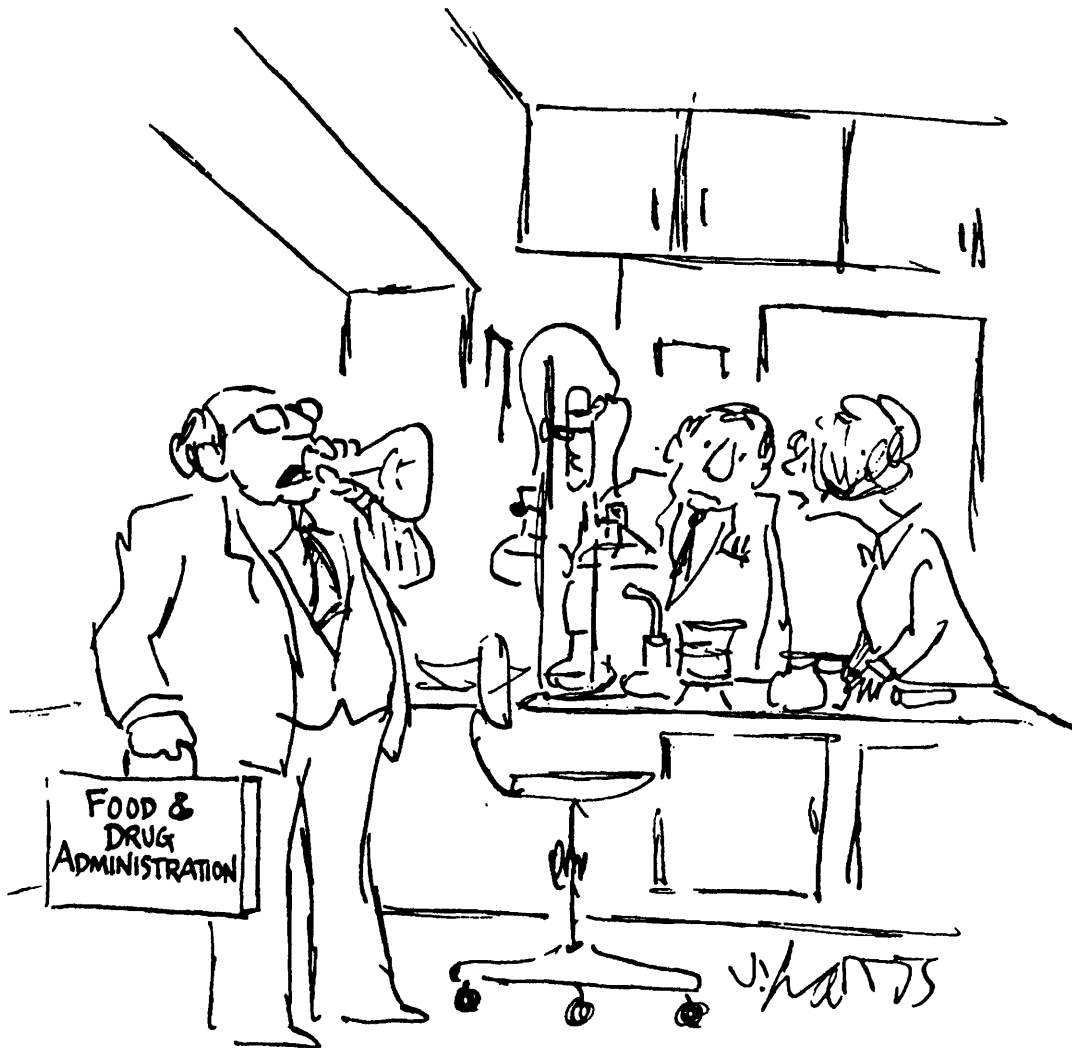
EXTEND implementation of SOS model.



EXTEND implementation of sine model, with frequency estimator.

Appendix C

Frequency Estimator



"I THOUGHT HE WOULD RUN ALL SORTS OF SCIENTIFIC TESTS."

Following Gelb (1974), this appendix derives a linearized Kalman filter to estimate the frequency of a sinusoidal stimulus.

The standard Kalman filter system and measurement models (see Figure 5.1):

$$\dot{x} = Ax + Bw$$

$$y = Cx + v$$

are replaced by more general non-linear versions:

$$\dot{x} = f(x) + w$$

$$y = h(x) + v$$

(It is understood that all quantities throughout may be time-dependent.)

Likewise, the state estimate, error covariance propagation, and Kalman gain equations:

$$\hat{x} = A\hat{x} + K[y - C\hat{x}]$$

$$\dot{P} = AP + PA^T + BQB^T - PC^TR^{-1}CP$$

$$K = PC^TR^{-1}$$

are replaced by:

$$\hat{x} = f(\hat{x}) + K[y - h(\hat{x})]$$

$$\dot{P} = F(\hat{x})P + PF^T(\hat{x}) + BQB^T - PH^T(\hat{x})R^{-1}H(\hat{x})P$$

$$K = PH^T(\hat{x})R^{-1}$$

where:

$$F(\hat{x}) = \left[\frac{\partial f(x)}{\partial x} \right]_{x=\hat{x}}$$

$$H(\hat{x}) = \left[\frac{\partial h(x)}{\partial x} \right]_{x=\hat{x}}$$

These last two quantities perform the linearization about the current estimate \hat{x} .

For the present application, the system model is:

$$\dot{x} \equiv \dot{\omega} = f(\omega) = 0$$

The state variable to be estimated is ω , which is assumed to be a constant (corresponding to a single fixed-frequency stimulus). No process noise is assumed (i.e. $B=Q=0$).

The measurement equation is:

$$y = h(\omega) + v = \sin(\omega t) + v(t)$$

This represents the fact that the only access that the Kalman estimator has to the state ω is from observing a sine wave with that frequency. To conform to the Kalman structure, the stimulus $\sin(\omega t)$ is treated as the state variable ω subjected to a sinusoidally-varying measurement process.

Carrying out the calculations:

$$F(\hat{\omega}) = \left[\frac{\partial f(\omega)}{\partial \omega} \right]_{\omega=\hat{\omega}} = 0$$

$$H(\hat{\omega}) = \left[\frac{\partial h(\omega)}{\partial \omega} \right]_{\omega=\hat{\omega}} = t \cos(\hat{\omega}t)$$

$$\hat{\omega} = 0 + K[y - \sin(\hat{\omega}t)]$$

$$\dot{P} = \frac{-P^2 t^2 \cos^2(\hat{\omega}t)}{R}$$

$$K = \frac{P H}{R} = \frac{P t \cos(\hat{\omega}t)}{R}$$

Solving the above Riccati equation for P:

$$P = \frac{24 R \hat{\omega}^3}{(6t^2\hat{\omega}^2 - 3)\sin(2\hat{\omega}t) + 6\hat{\omega}t\cos(2\hat{\omega}t) + (4t^3 + 24c')\hat{\omega}^3}$$

where c' is a constant which defines the initial value of the error covariance P:

$$P(0) = \frac{R}{c'}$$

The filter is implemented using:

$$\hat{\omega} = K[y - \sin(\hat{\omega}t)]$$

where y is the measurement (the stimulus) and $K=PH/R$, and $P(t)$ is computed from the above Riccati equation solution. Note that the parameters R (measurement noise) and $P(0)$ are free. Varying these parameters effects the convergence of the filter (see below). In particular, large values of $P(0)$ indicate to the estimator that the initial estimate $\hat{\omega}$ is very poor (i.e. has a low confidence associated with it) and so new information (the stimulus input) is to be weighted very heavily in updating the estimate. This yields a rapid convergence.

The performance of the estimator was characterized with computer simulation trials with input frequencies $f=0.2, 0.5, 1.0,$ and 1.5 Hz; initial frequency estimates $\hat{f}_0=0.1, 1.0,$ and 2.0 Hz; measurement noises $R=1, 1000$; and initial error covariances $P_0=1, 1000$. (These values were chosen somewhat arbitrarily, based on experience with the estimator. The input frequency range spans the frequencies used in the human experiments in this thesis.) Results are consistent in at least one respect: for any tested combination of R and P_0 , only $R=1/P_0=1000$ produced significant rapid convergence of \hat{f} to the true value f within one input stimulus cycle. In the other cases, often no change from f_0 took place at all.

With $R=1$ and $P_0=1000$, on the other hand, convergence was completed within one half cycle of the input stimulus sinusoid, and often much sooner. A typical example of a series of trials for $\hat{f}_0=0.1$ and $f=0.5$ is in Figure C.1, where the $R=1/P_0=1000$ case produces the only useful performance. Convergence occurs in about one quarter cycle. The one set of values for which R and P_0 which did not work was $\hat{f}_0=0.1$ and $f=1.5$, for which \hat{f} eventually settled to zero. It seems that a good set of parameter values for this estimator subsystem is $R=1$, $P_0=1000$, and $\hat{f}_0=1.0$, which gives good performance for sinusoidal inputs at least from 0.2 to 1.5 Hz, for which convergence occurs within one half cycle.

Performance with non-sinusoidal stimuli was uniformly disappointing. As example is in Figure C.2, where the input signal is a sum of sinusoids at 0.3, 0.5, 0.7, 1.1, and 1.3 Hz (see Methods chapter). Frequency estimates tend to remain at their initial values, or else converge rapidly to zero. This behavior is typical for a variety of non-sinusoidal input signals. (See also discussion of triangular waveform tracking in Model chapter.)

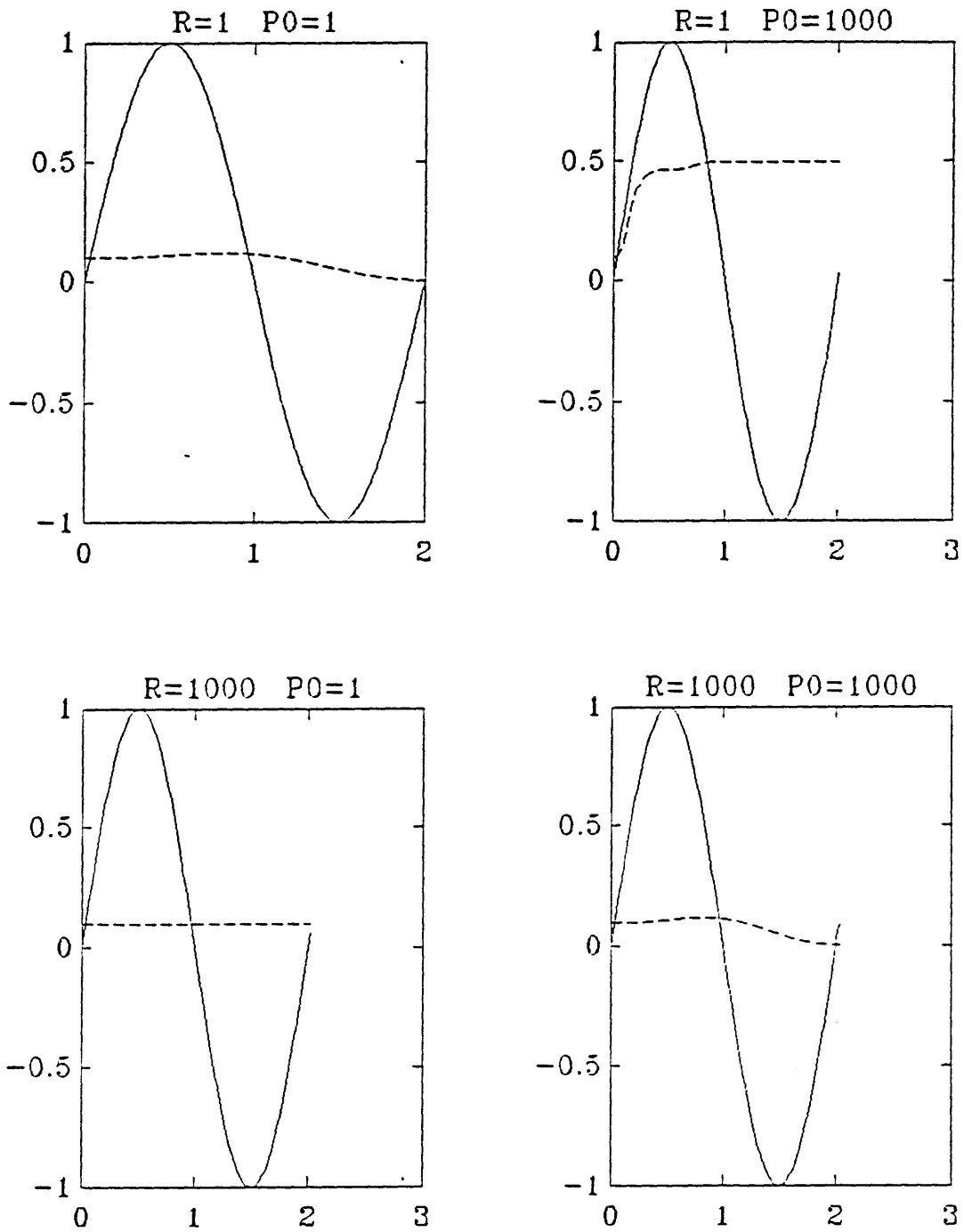


Figure C.1 Examples of frequency estimator performance with a 0.5 Hz sinusoid and an initial estimate of 0.1 Hz. (Solid line is stimulus input, dashed line is frequency estimate in Hz.)

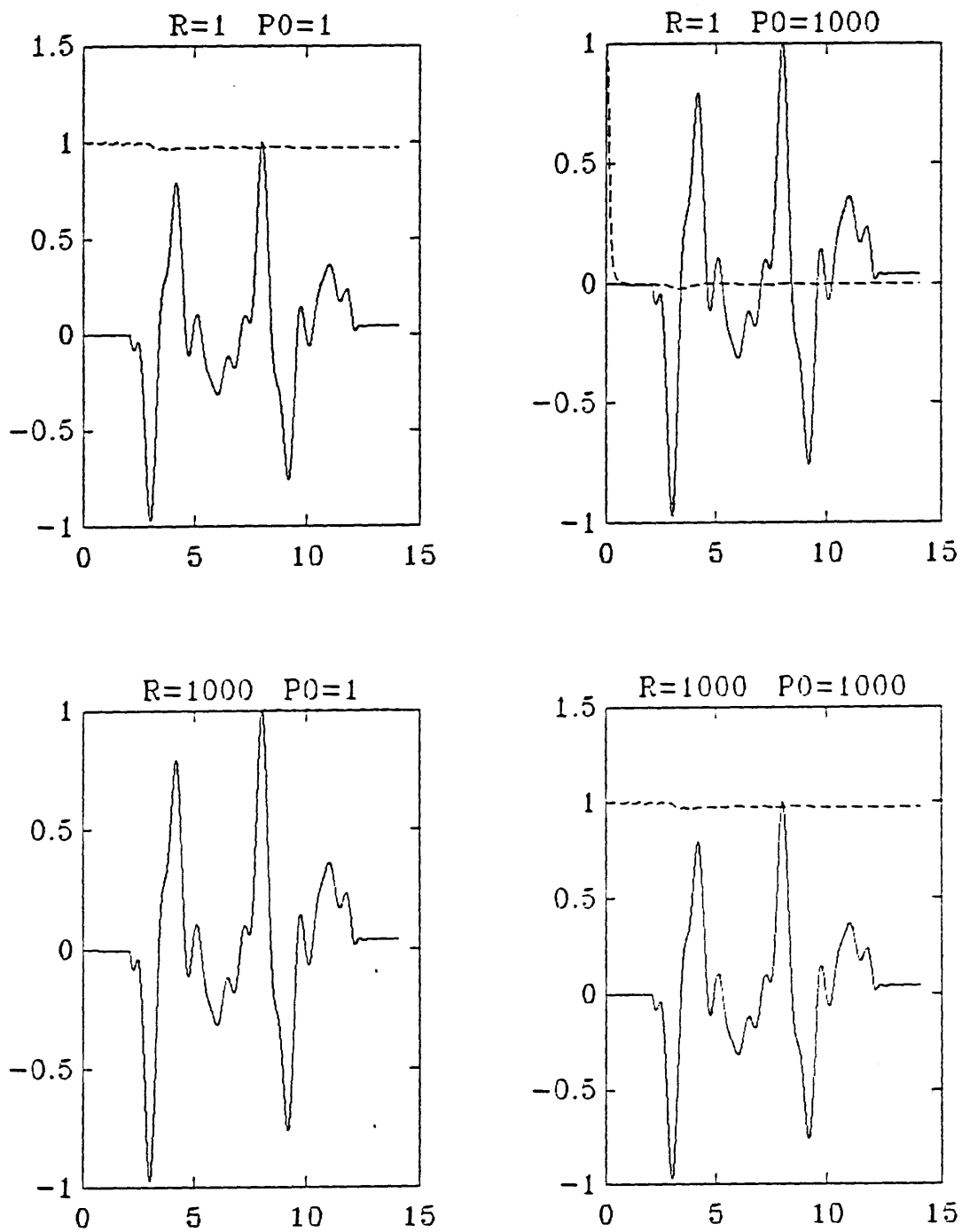
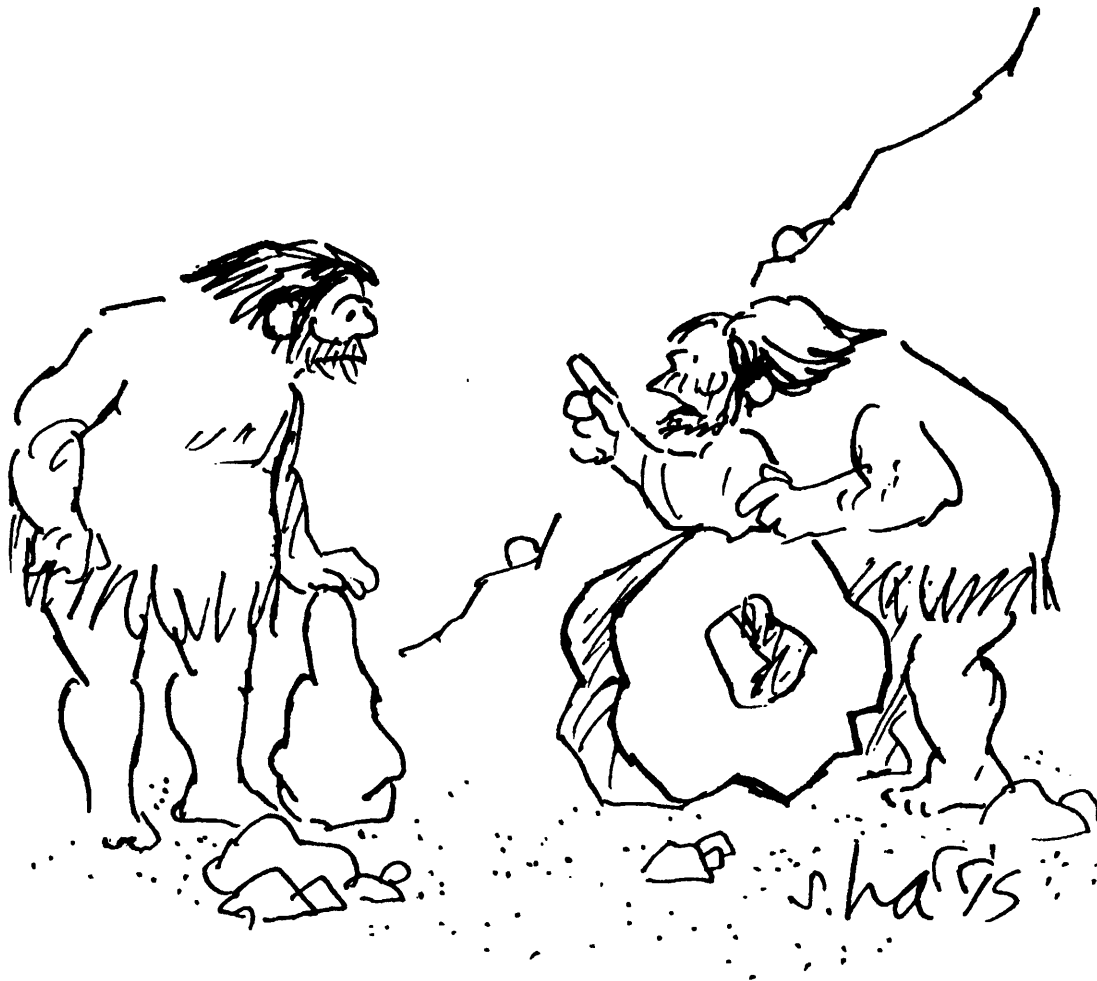


Figure C.2 Examples of frequency estimator performance with a sum-of-sines input and an initial estimate of 1.0 Hz. (Solid line is stimulus input, dashed line is frequency estimate in Hz.)

Appendix D

Parameters and Model Fitting



"IT MAY NOT BE A PERFECT WHEEL, BUT IT'S
A STATE-OF-THE-ART WHEEL."

As described in the text, model parameters were determined on a somewhat ad hoc basis, through extensive interactive computer sessions. A brief outline of the approach will now be presented. First, the input and output processing delays T_1 and T_2 were set to assumed values (see below). Then, the efferent copy delay T_e was set to the sum of these. The SP/sine model was approached first, requiring the additional parameters K_e , K_{eye} , and C_{11} . K_e was set sequentially to several values from zero to one, and the K_{eye}/C_{11} ratio was determined for each setting by visually matching the transfer function to the overlaid experimental data (at this point only the ratio could be determined). The SP/SOS model depended further on K_{11} and the values of K_{eye} and C_{11} (not just their ratio), and it was utilized next. Simultaneously varying K_{eye} and C_{11} (but maintaining their ratio) and also K_{11} , this transfer function was fit to the data. Moving on to the VV models, α was determined by the target distance (see Appendix B), leaving K_{oto} , K_{22} , and C_{22} to determine. K_{22} and C_{22} had a relatively small effect, and a large K_{oto} was necessary to produce the necessary gain increase from the SP models. K_{22} and C_{22} mostly fine-tuned the phase response. The AI models were not separately determined, but just used the parameters already determined. In this sense, the AI gain transfer functions are surprisingly good; this also explains why the phases are rather poor. It was decided that these poor phase responses were worth the simplicity of the modelling approach.

Using the nominal input and output delay values given by Robinson, Gordon, and Gordon (1986) produced good results for subjects J and T (who also had similar saccadic latencies; see Appendix A). Subject S, however, had significantly higher saccadic latencies (0.210 versus about 0.170 sec). So, for S's model, the nominal delay values were increased by the ratio 0.210/0.170.

In table D.1 is a listing of the final parameter values selected. The following sets of figures show the model transfer functions and overlaid experimental data for each subject.

Note that, although the parameters selected for J work quite well for T, there is some discrepancy in the VV and SP SOS phase responses. An argument can be made that the missing high-frequency SOS components (T was not tested with the wide-bandwidth SOS) would significantly affect the phase lag at the higher frequencies (as for the other subjects), requiring that a compromise in the lower-frequency phase values be made. This is only speculative, but in view of the adequate performance in the other cases it was decided to retain the J values.

Parameter	Subjects J&T	Subject S
K_e	0.25	0.75
K_{eye}	1.19	1
K_{11}	20	100
C_{11}	0.5	1.18
\tilde{C}_{11}	1.39	1.43
K_{oto}	100	500
K_{22}	1	2
C_{22}	1	1

Table D.1 Model parameter values for all subjects.

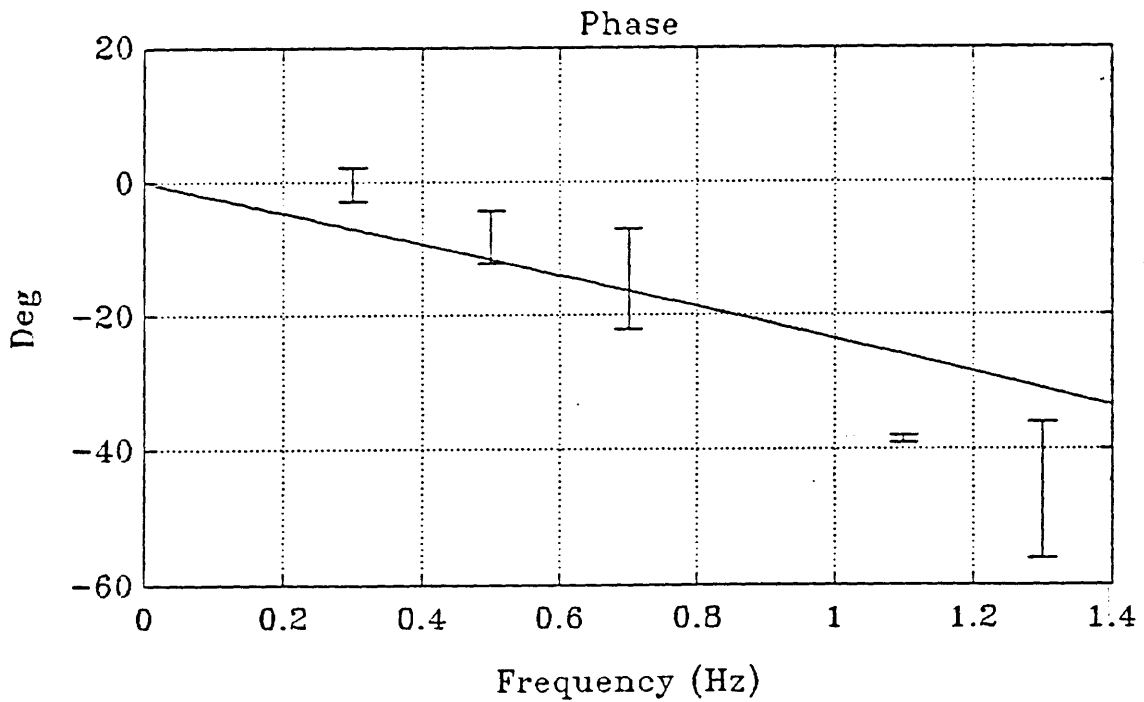
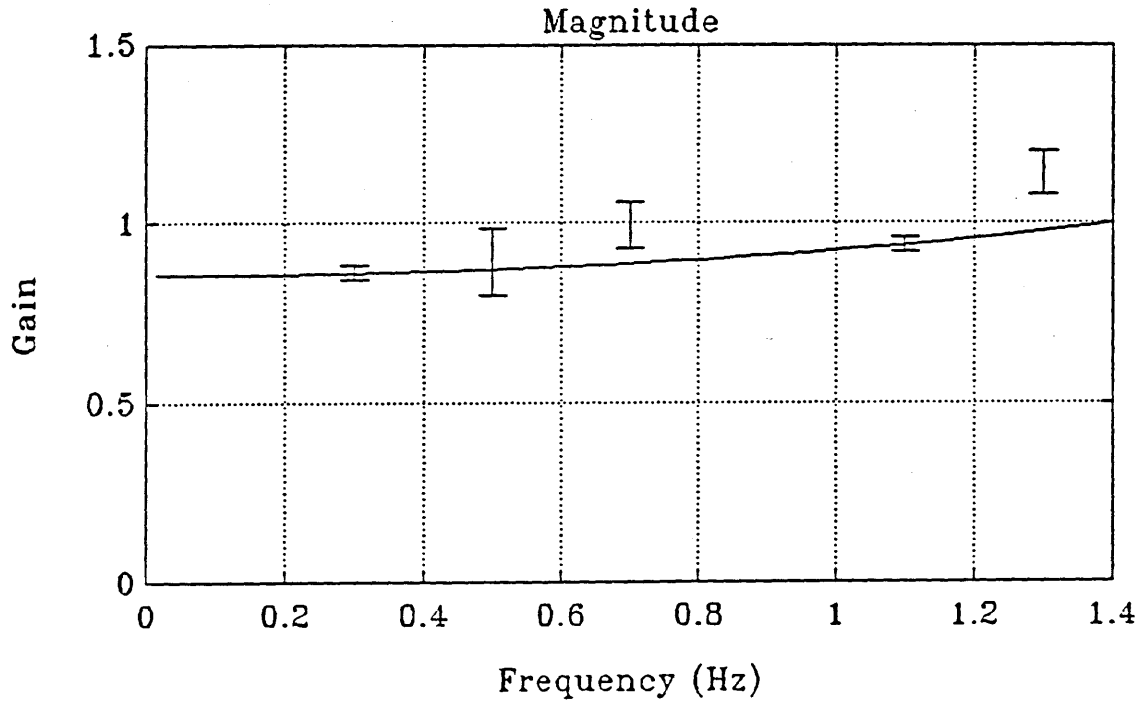


Figure D.1 Model transfer function and experiment results for subject J SP/SOS. (Solid lines are model transfer function; bars are experiment data, ± 1 s.d. centered at mean.)

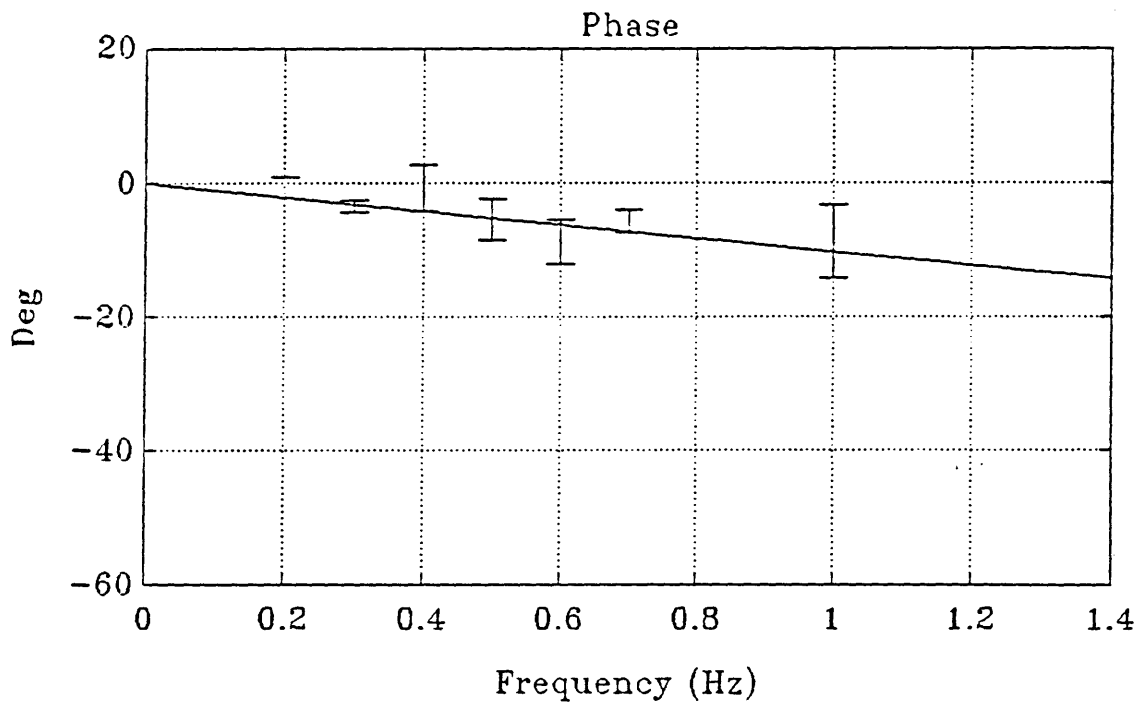
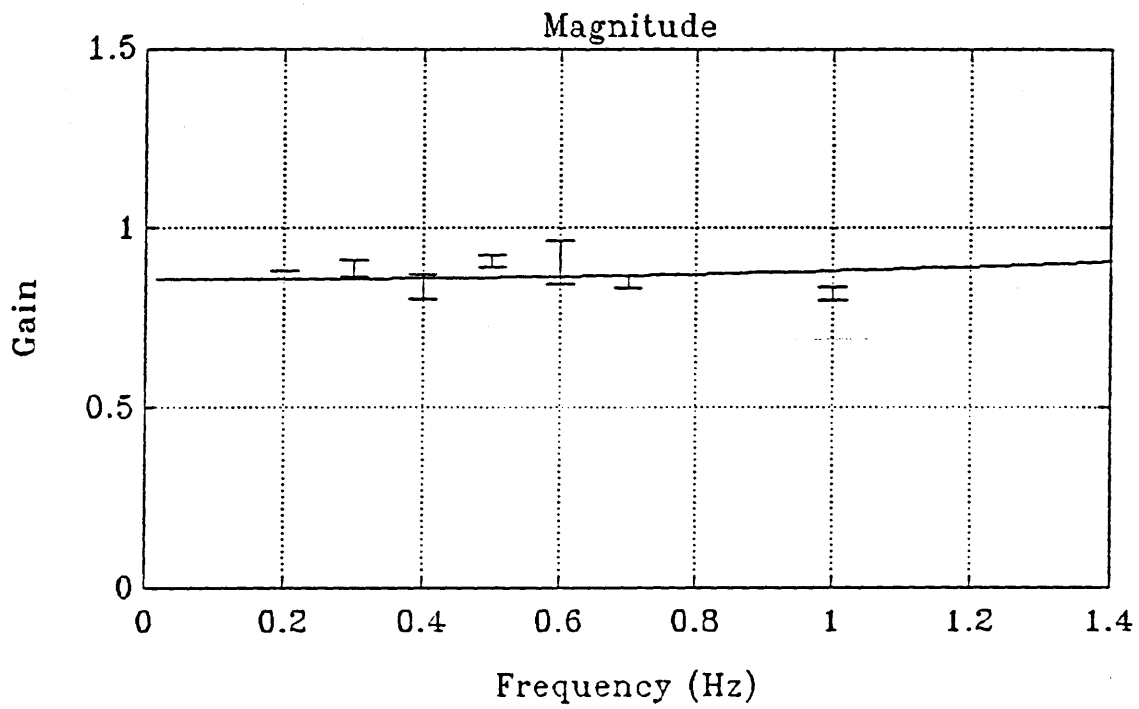


Figure D.2 Model transfer function and experiment results for subject J SP/sine. (Solid lines are model transfer function; bars are experiment data, ± 1 s.d. centered at mean.)

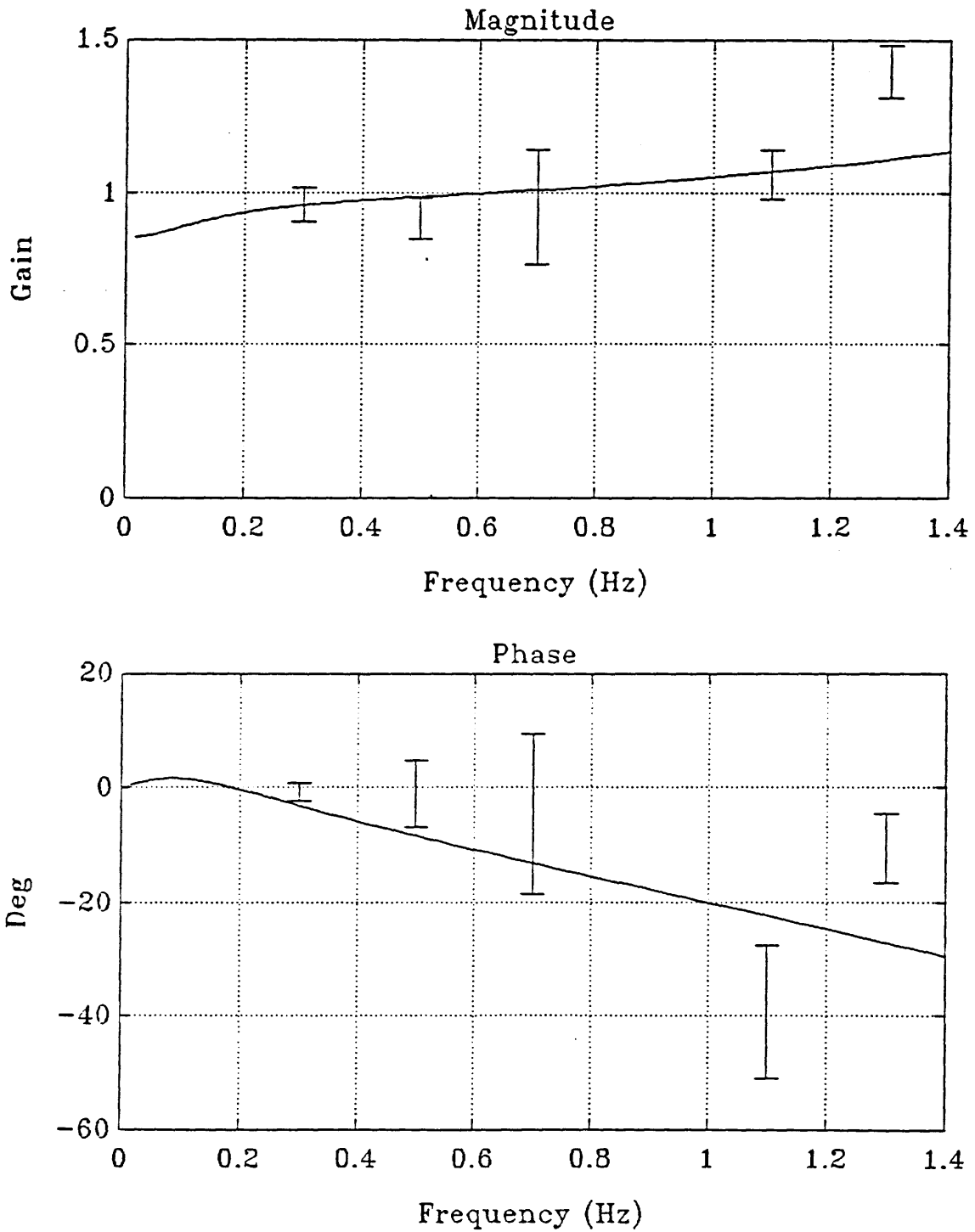


Figure D.3 Model transfer function and experiment results for subject J VV/SOS. (Solid lines are model transfer function; bars are experiment data, ± 1 s.d. centered at mean.)

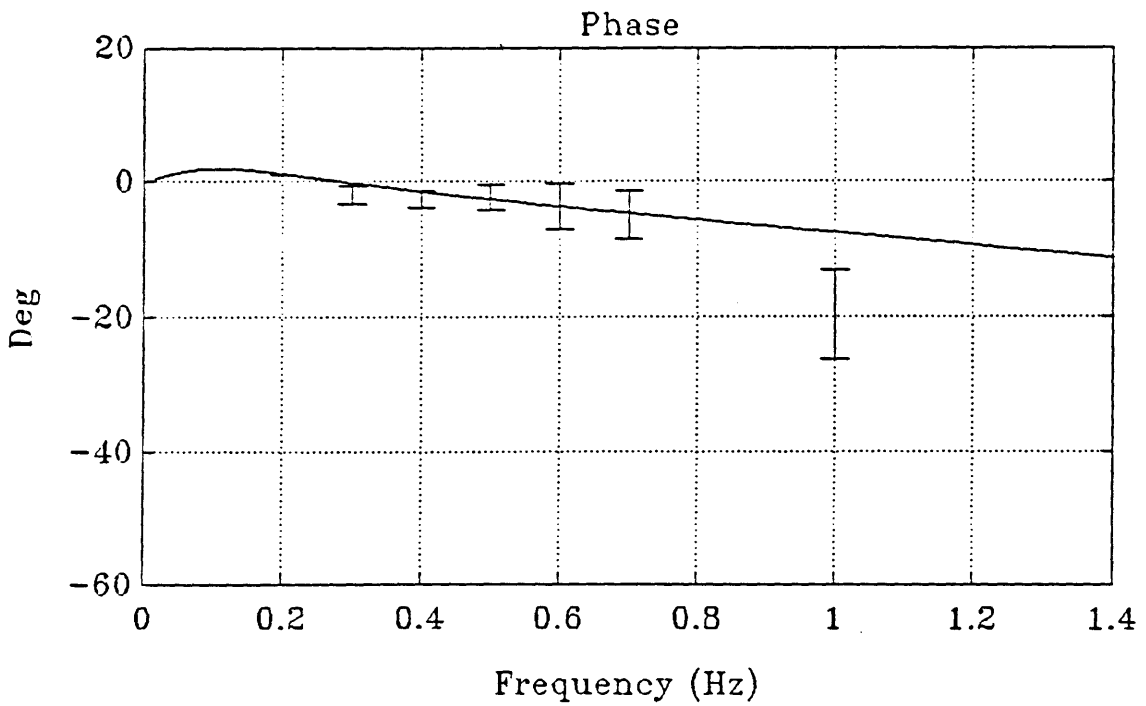
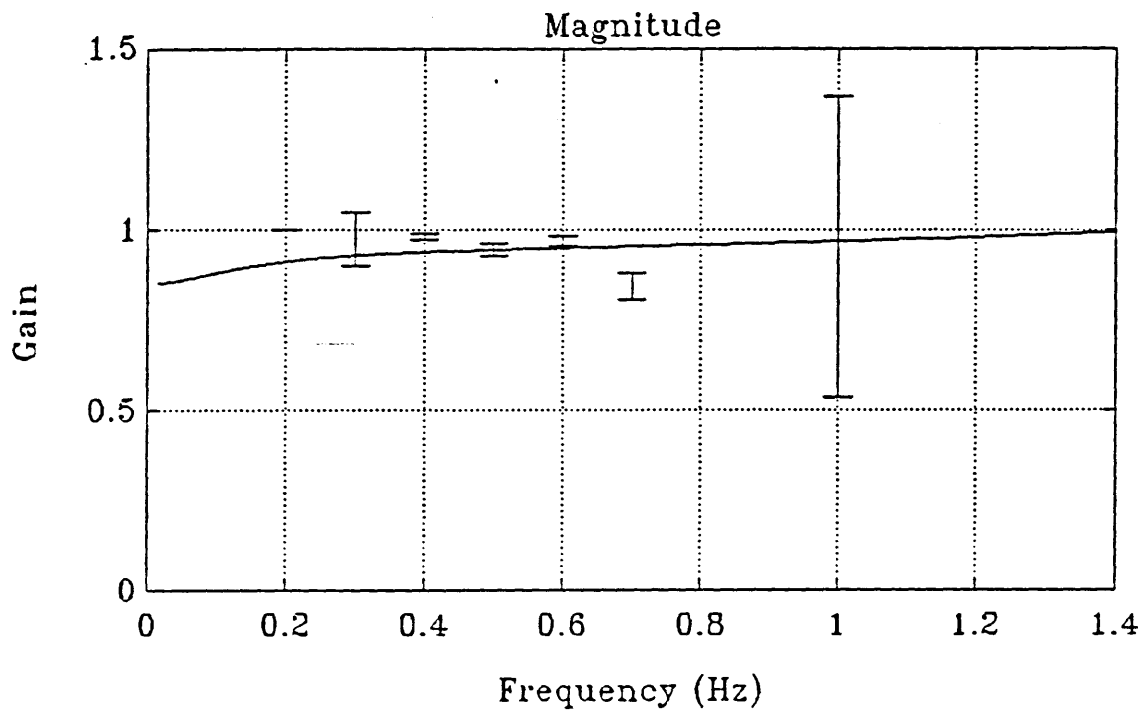


Figure D.4 Model transfer function and experiment results for subject J VV/sine. (Solid lines are model transfer function; bars are experiment data, ± 1 s.d. centered at mean.)

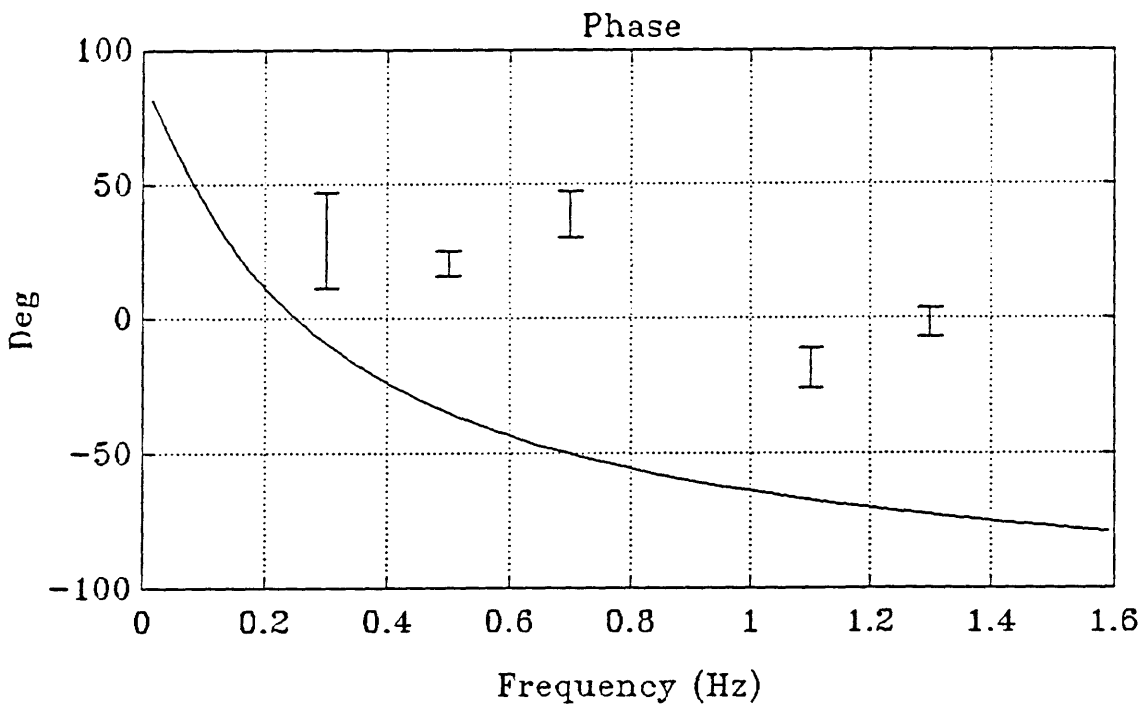
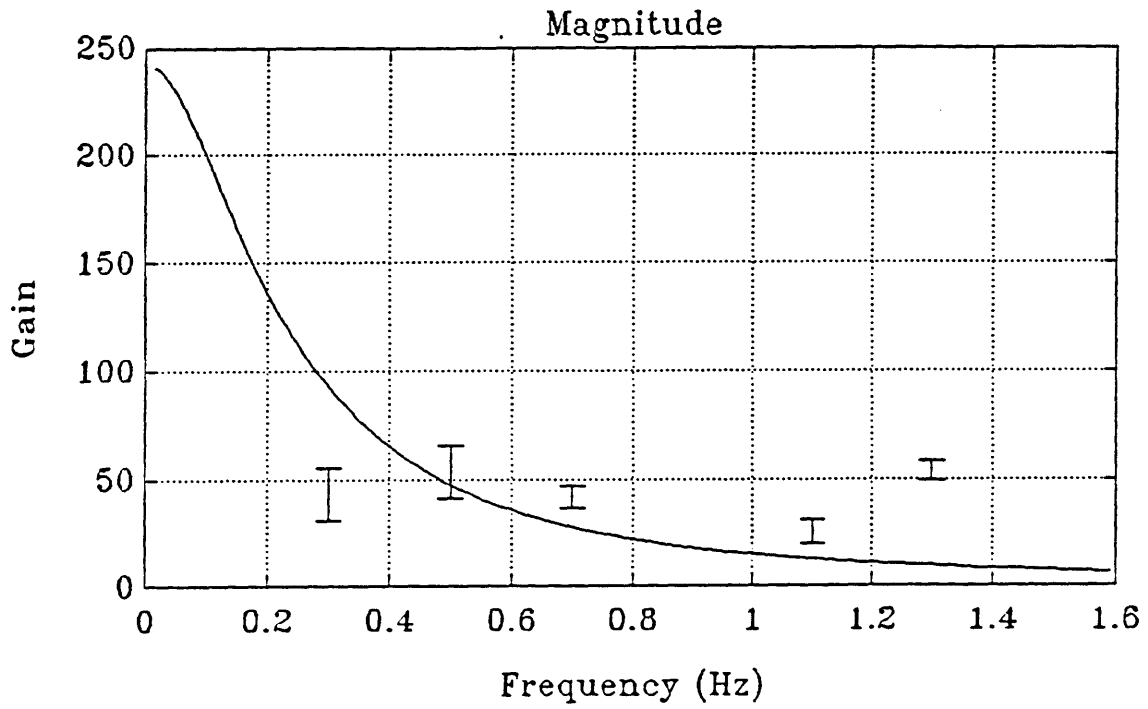


Figure D.5 Model transfer function and experiment results for subject J AI/SOS. (Solid lines are model transfer function; bars are experiment data, ± 1 s.d. centered at mean.)

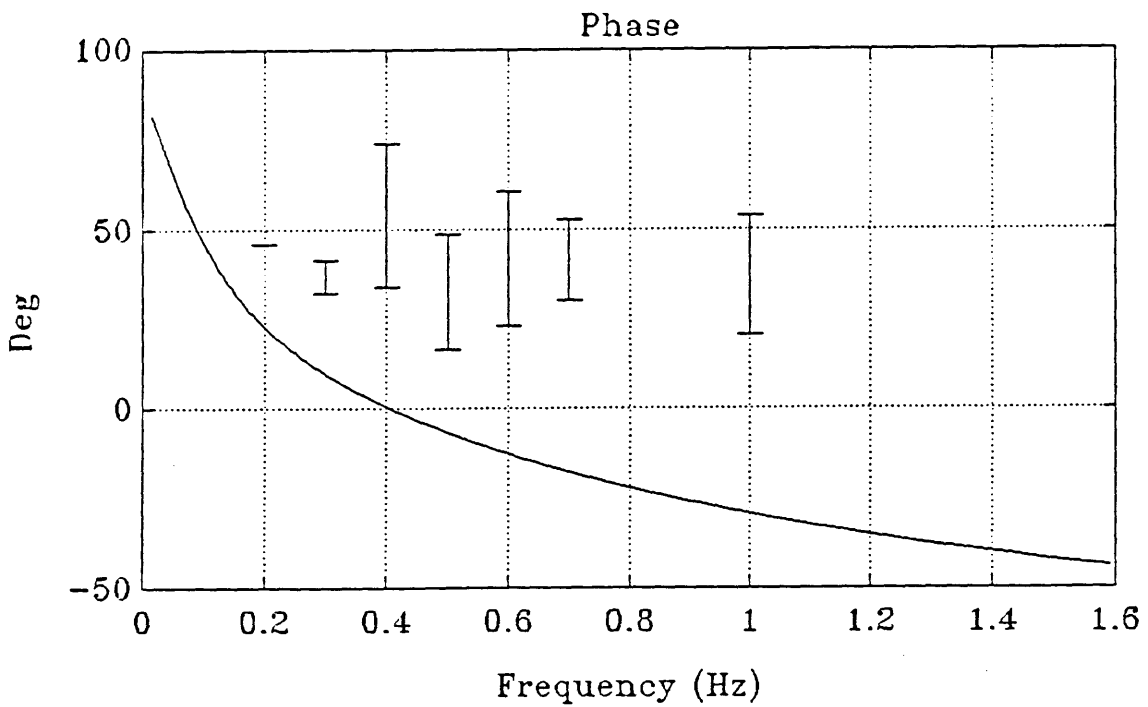
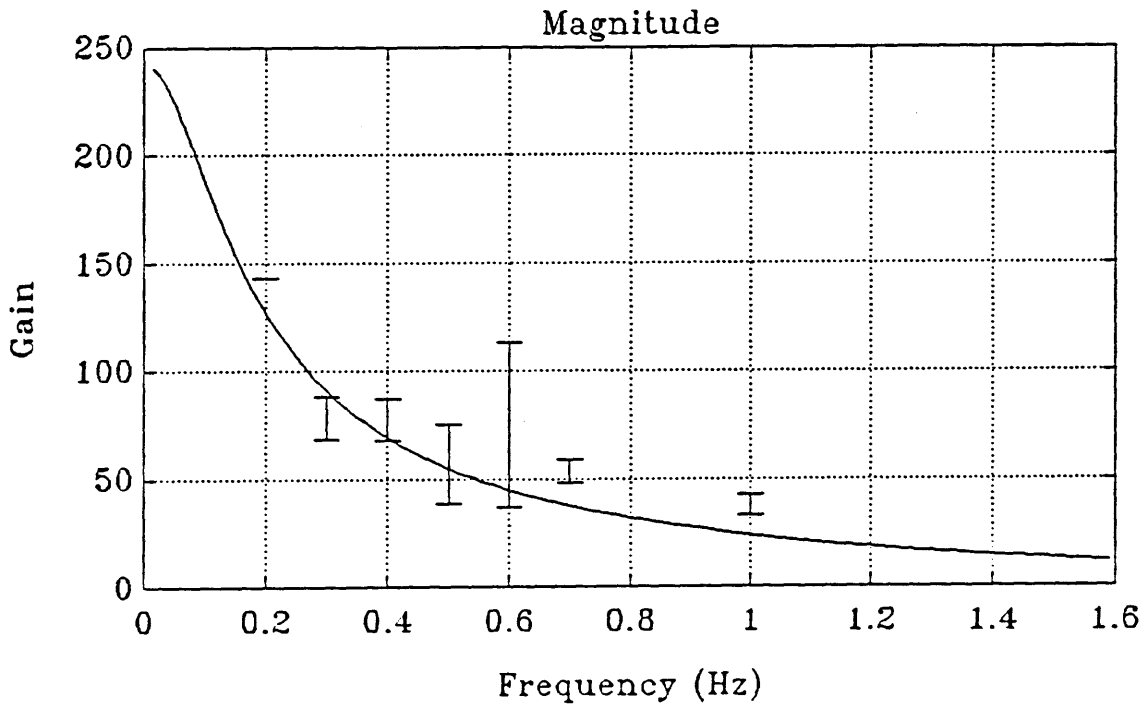


Figure D.6 Model transfer function and experiment results for subject J AI/sine. (Solid lines are model transfer function; bars are experiment data, ± 1 s.d. centered at mean.)

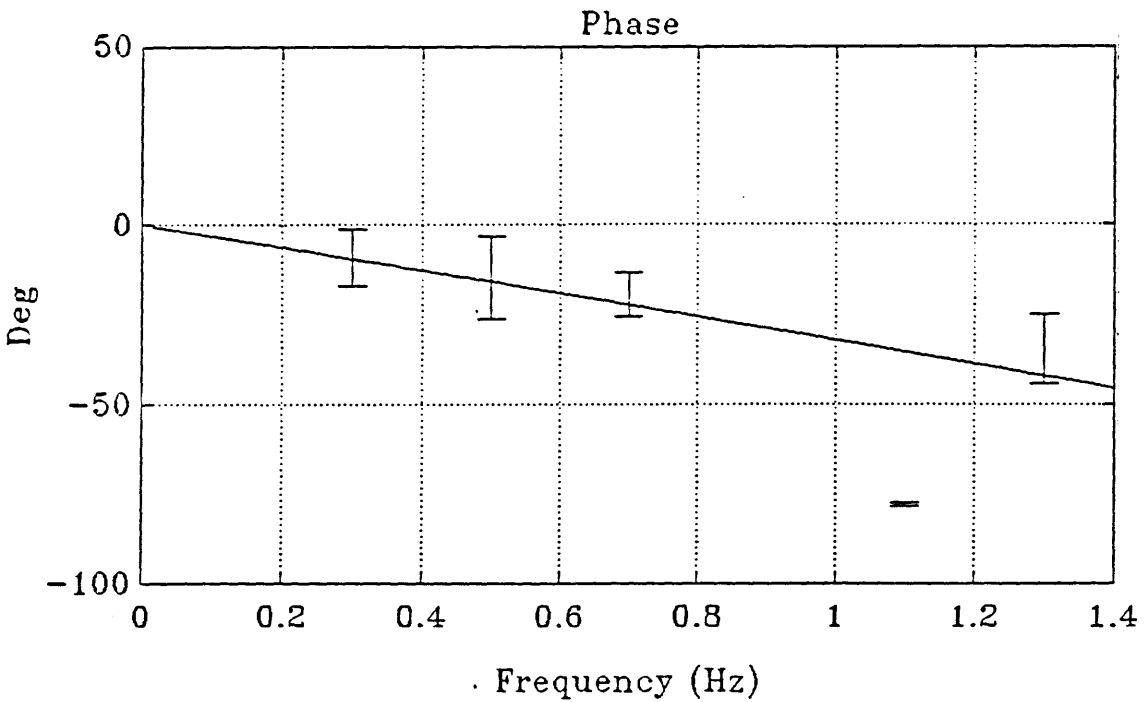
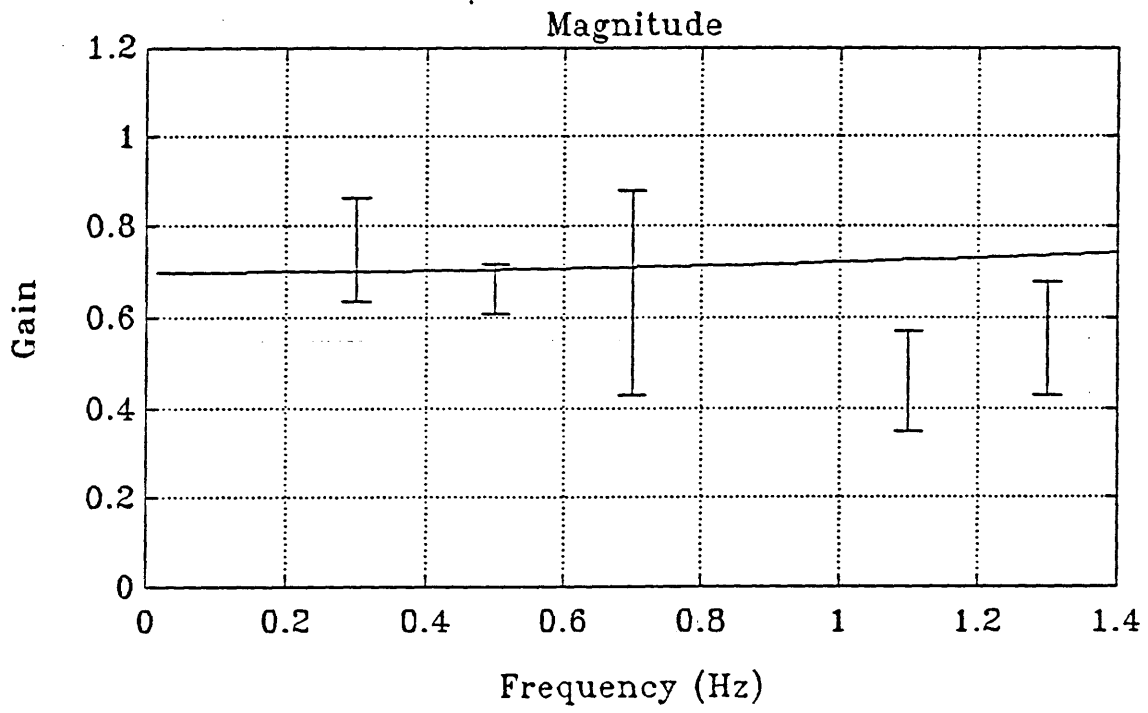


Figure D.7 Model transfer function and experiment results for subject S SP/SOS. (Solid lines are model transfer function; bars are experiment data, ± 1 s.d. centered at mean.)

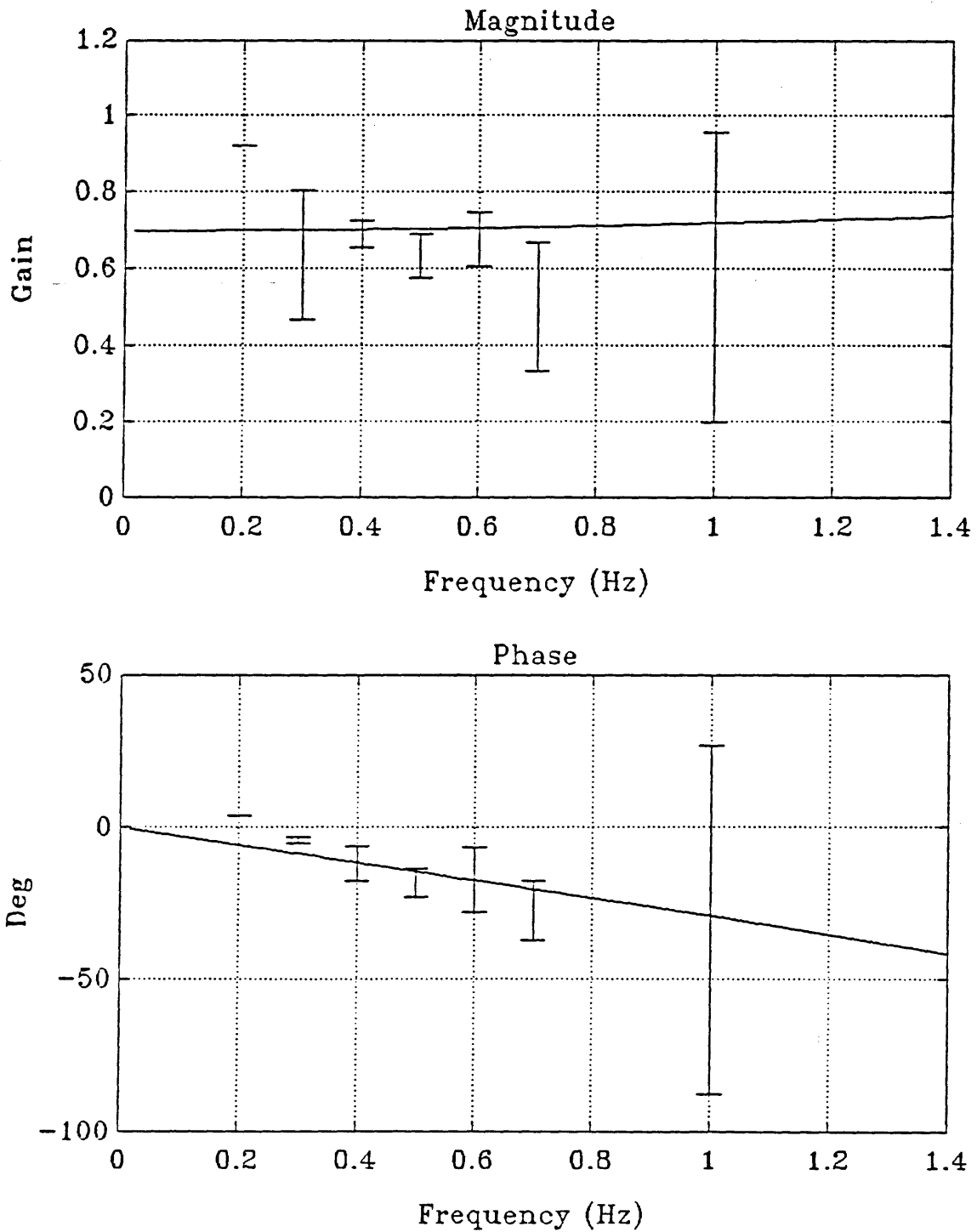


Figure D.8 Model transfer function and experiment results for subject S SP/sine. (Solid lines are model transfer function; bars are experiment data, ± 1 s.d. centered at mean.)

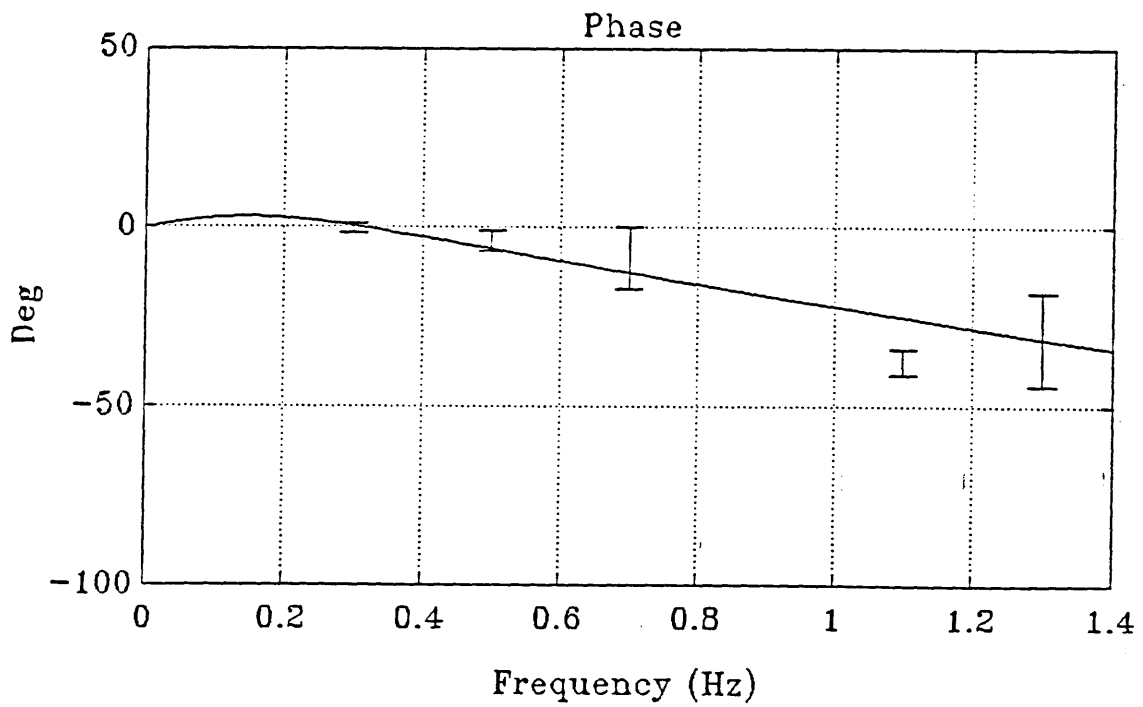
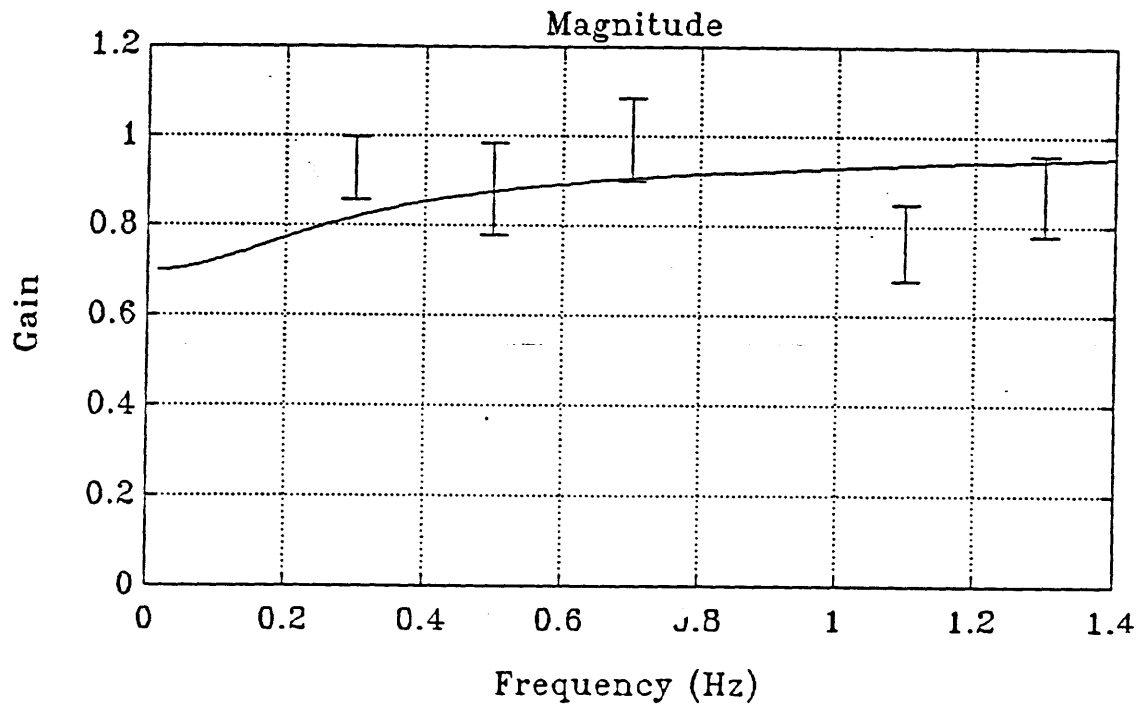


Figure D.9 Model transfer function and experiment results for subject S VV/SOS. (Solid lines are model transfer function; bars are experiment data, ± 1 s.d. centered at mean.)

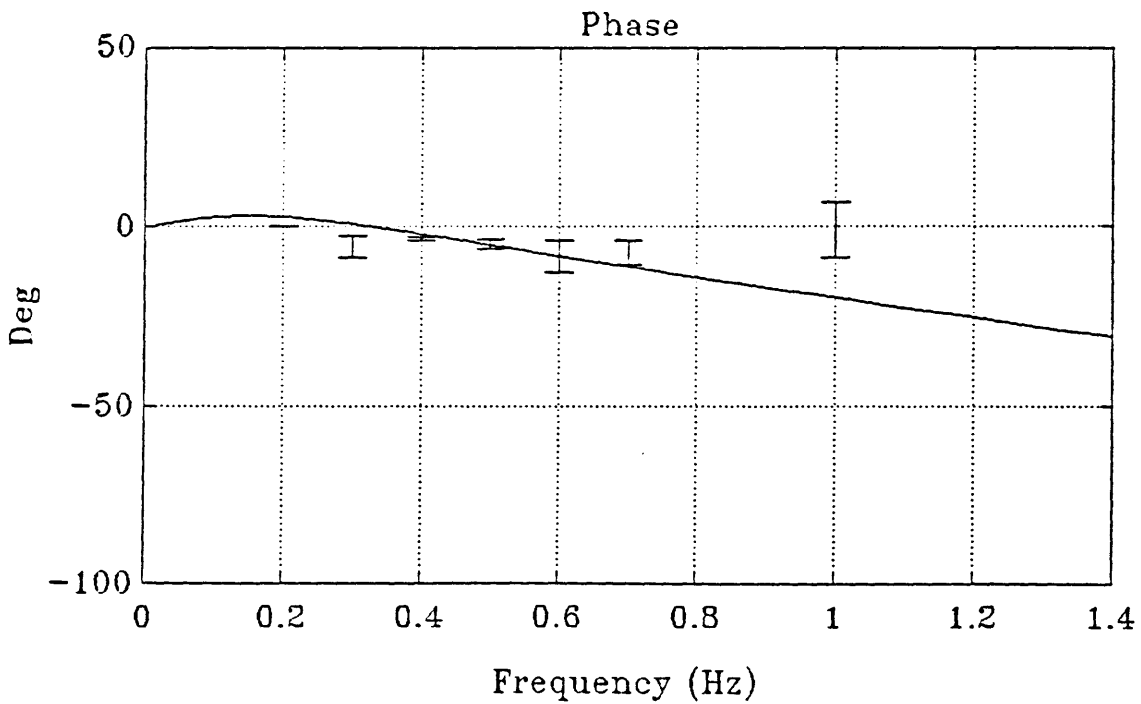
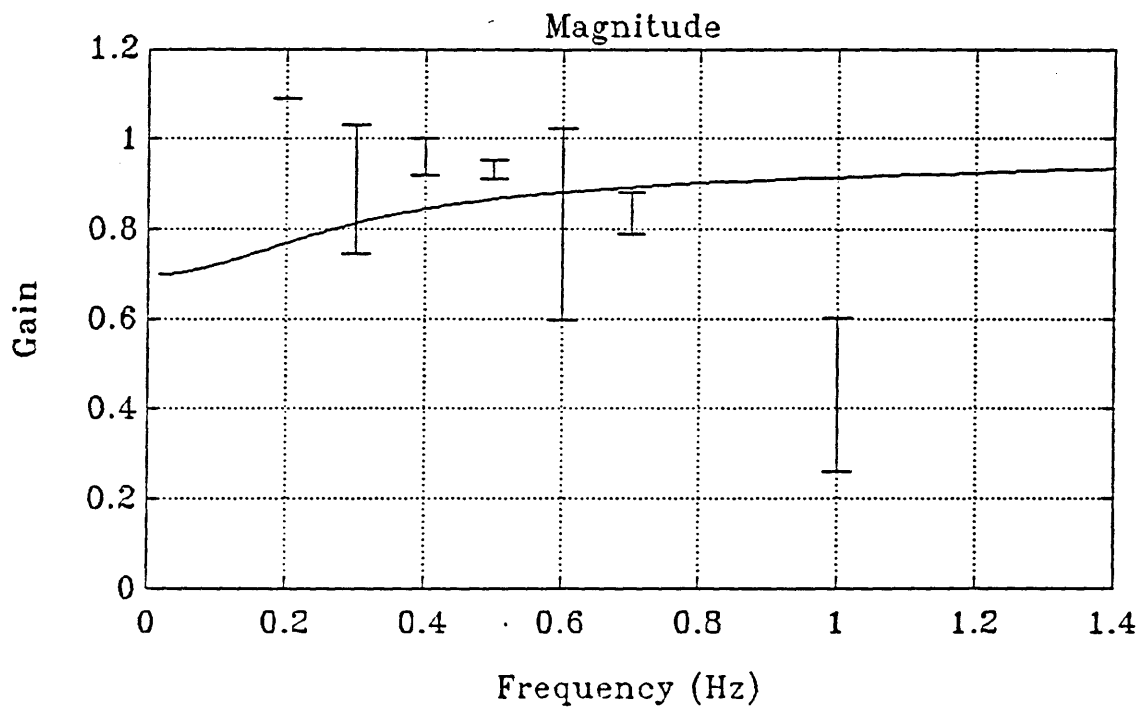


Figure D.10 Model transfer function and experiment results for subject S VV/sine. (Solid lines are model transfer function; bars are experiment data, ± 1 s.d. centered at mean.)

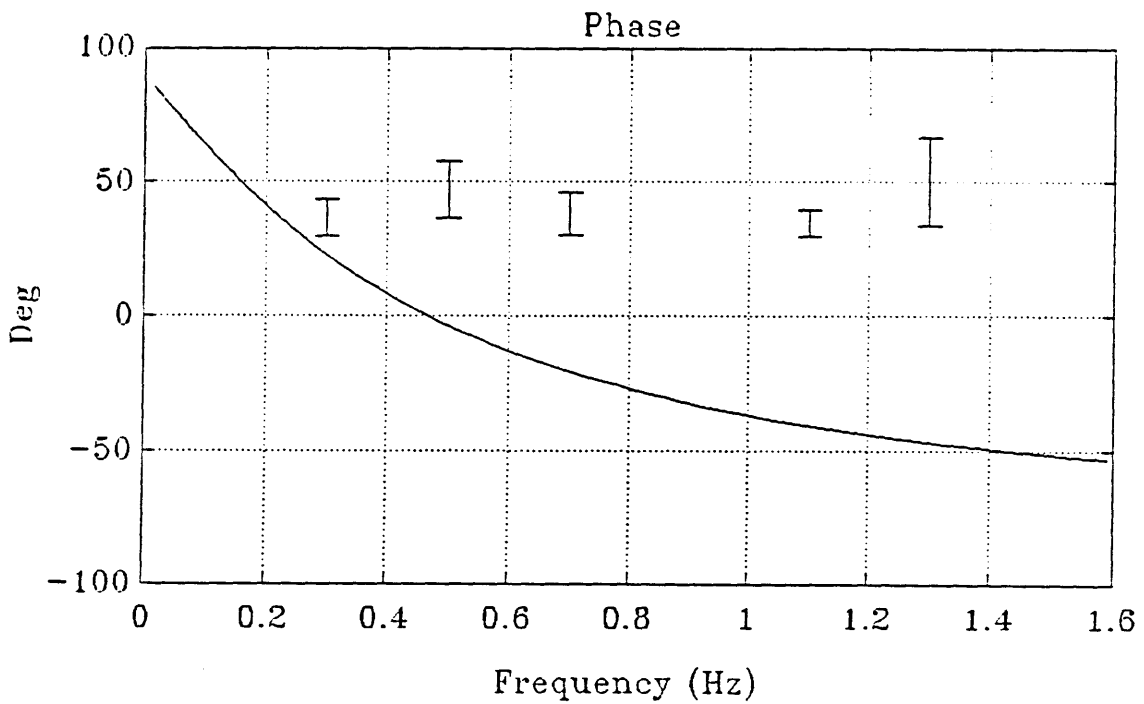
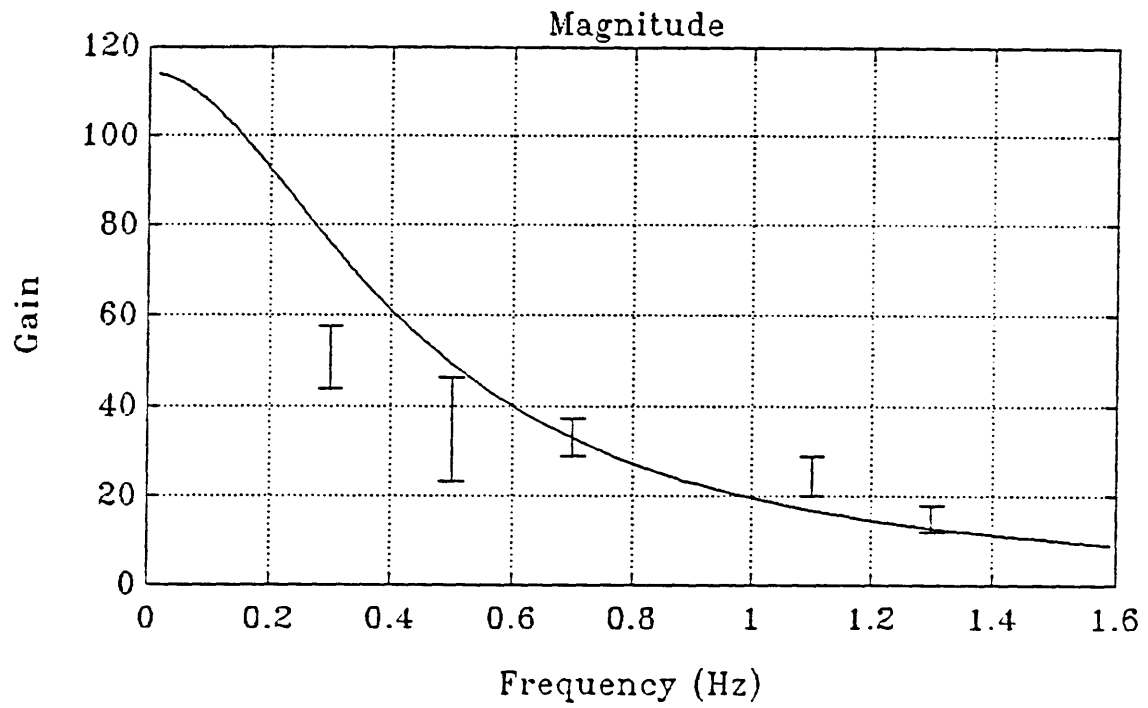


Figure D.11 Model transfer function and experiment results for subject S AI/SOS. (Solid lines are model transfer function; bars are experiment data, ± 1 s.d. centered at mean.)

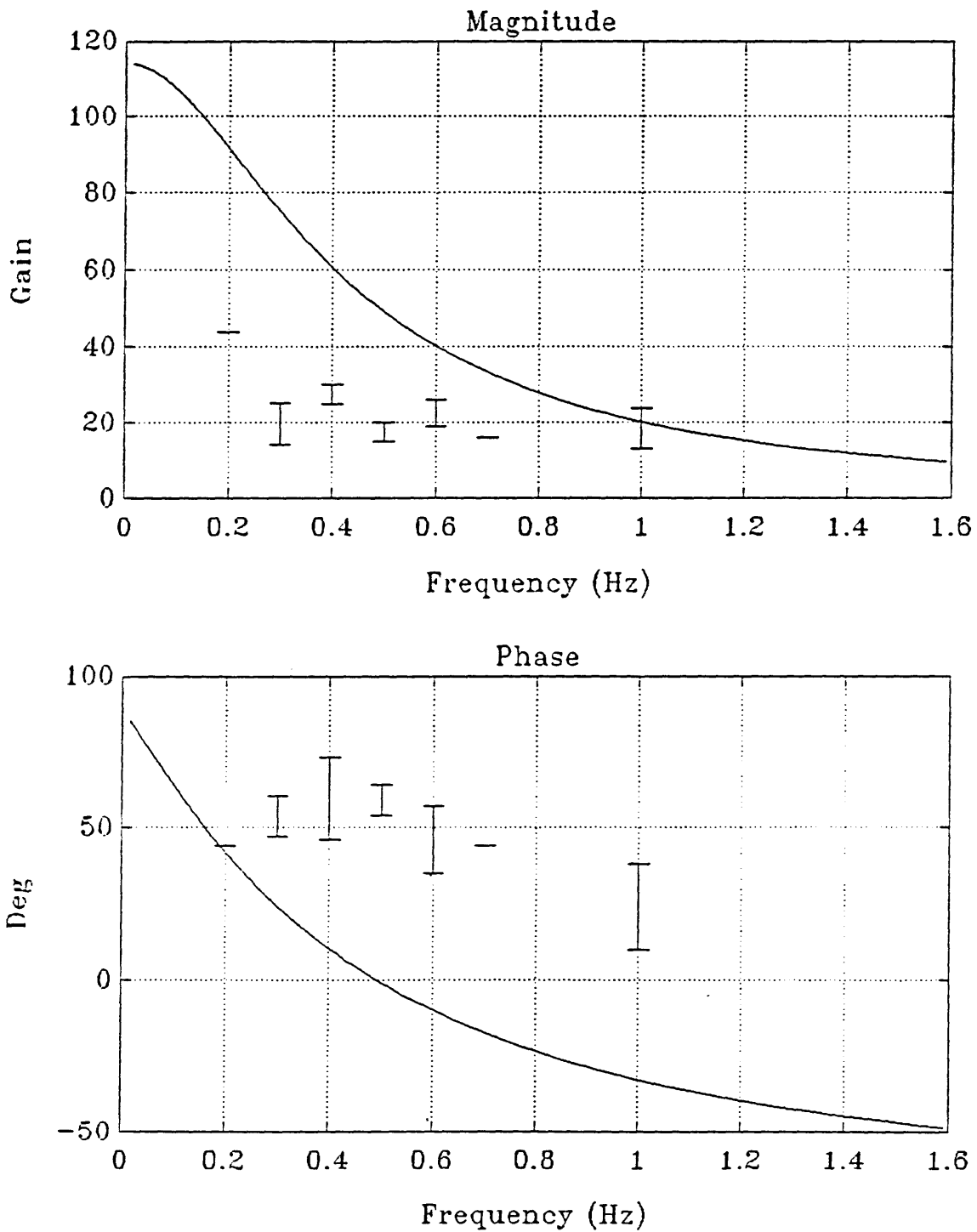


Figure D.12 Model transfer function and experiment results for subject S AI/sine. (Solid lines are model transfer function; bars are experiment data, ± 1 s.d. centered at mean.)

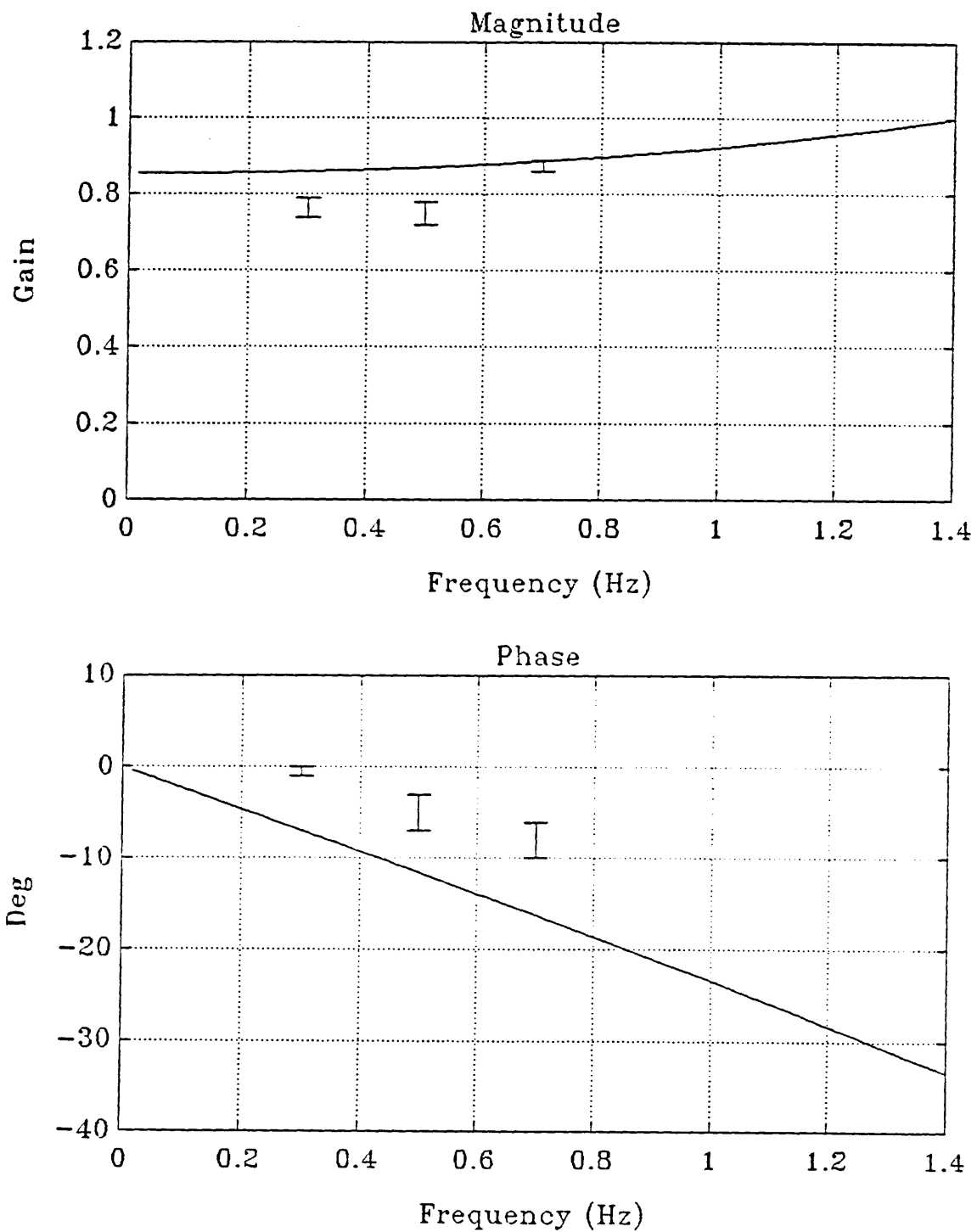


Figure D.13 Model transfer function and experiment results for subject T SP/SOS. (Solid lines are model transfer function; bars are experiment data, ± 1 s.d. centered at mean.)

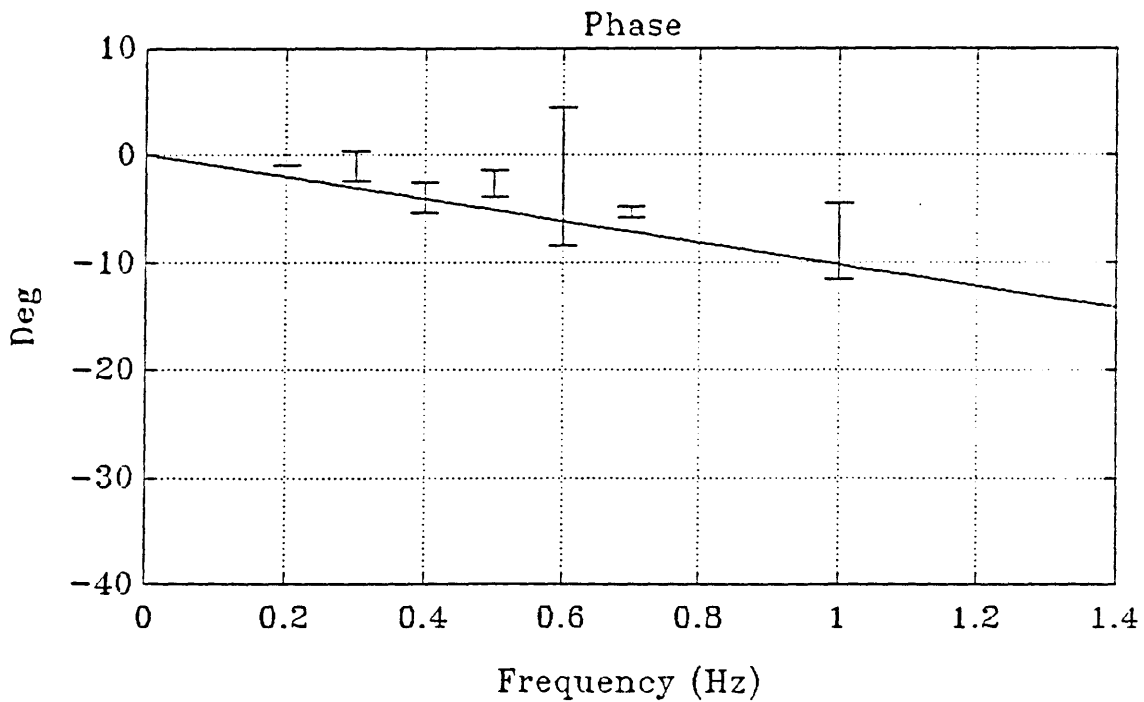
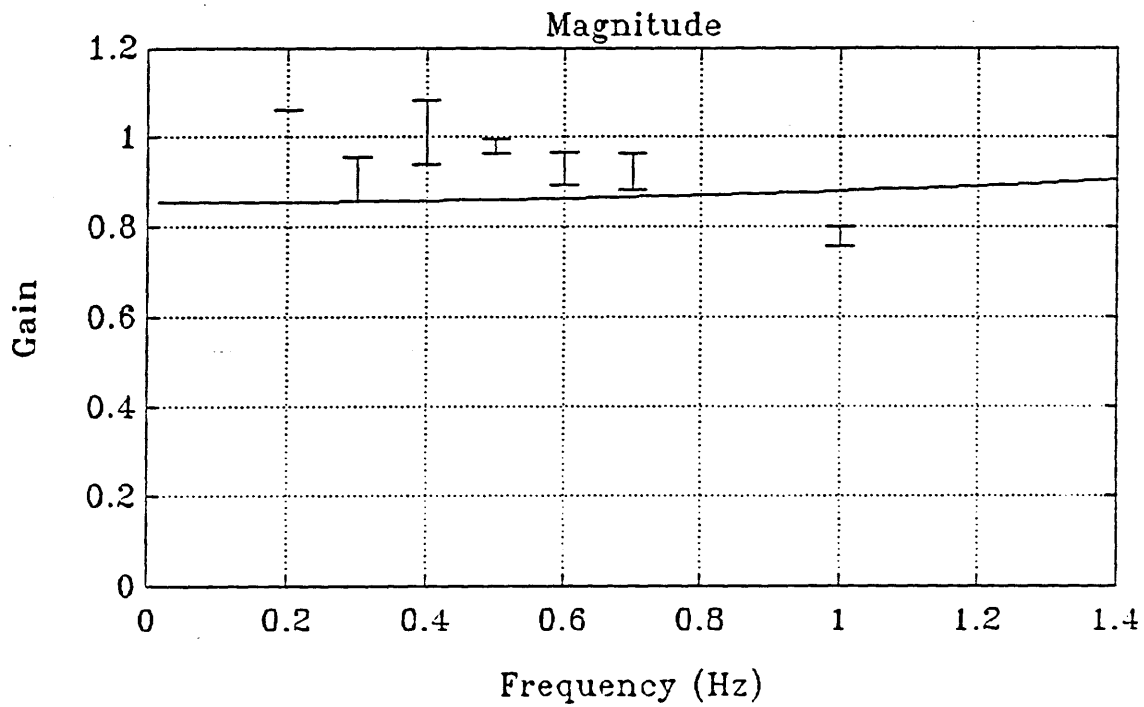


Figure D.14 Model transfer function and experiment results for subject T SP/sine. (Solid lines are model transfer function; bars are experiment data, ± 1 s.d. centered at mean.)

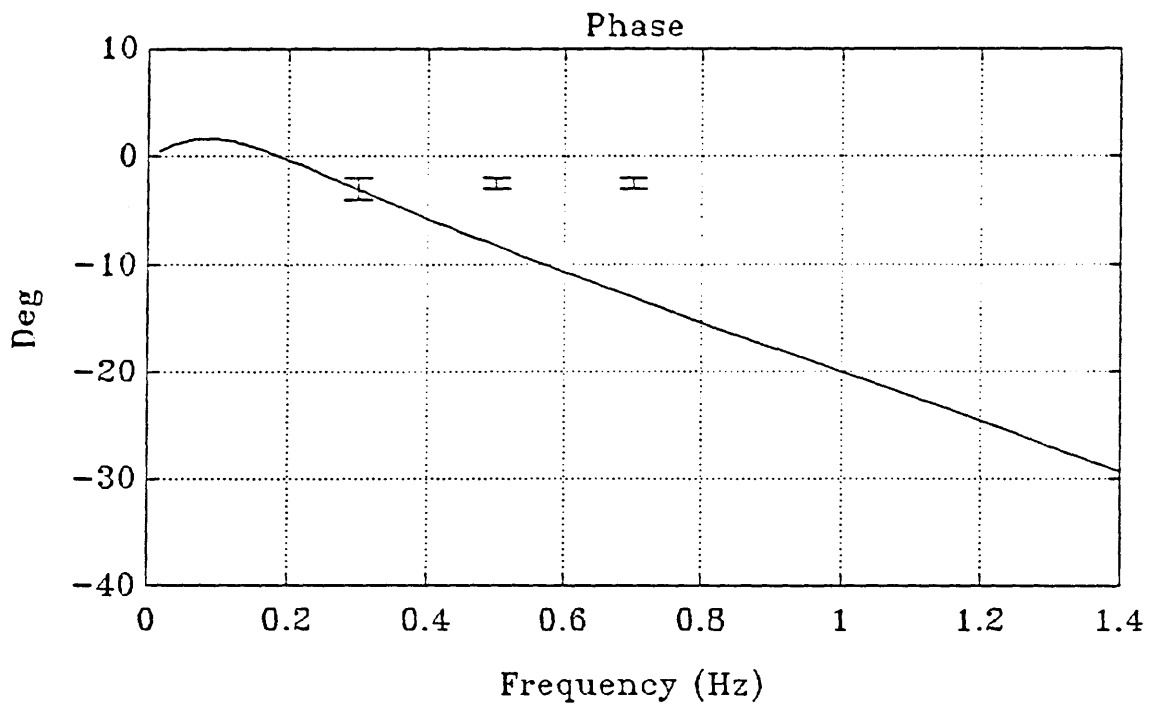
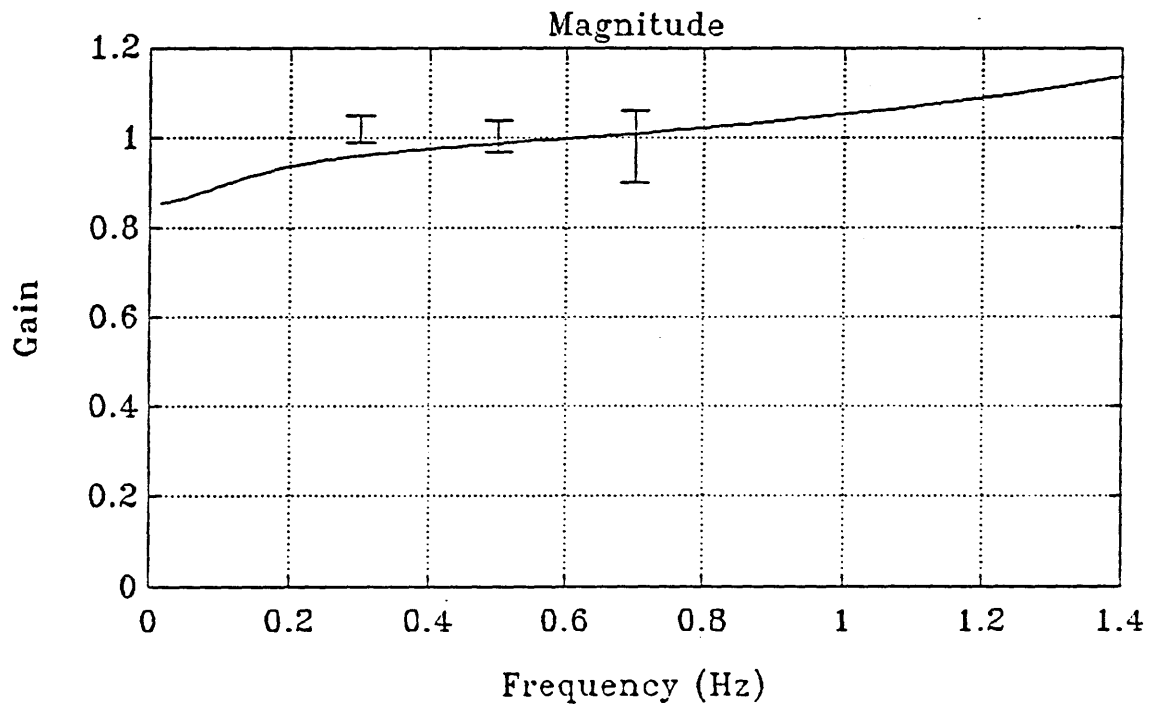


Figure D.15 Model transfer function and experiment results for subject T VV/SOS. (Solid lines are model transfer function; bars are experiment data, ± 1 s.d. centered at mean.)

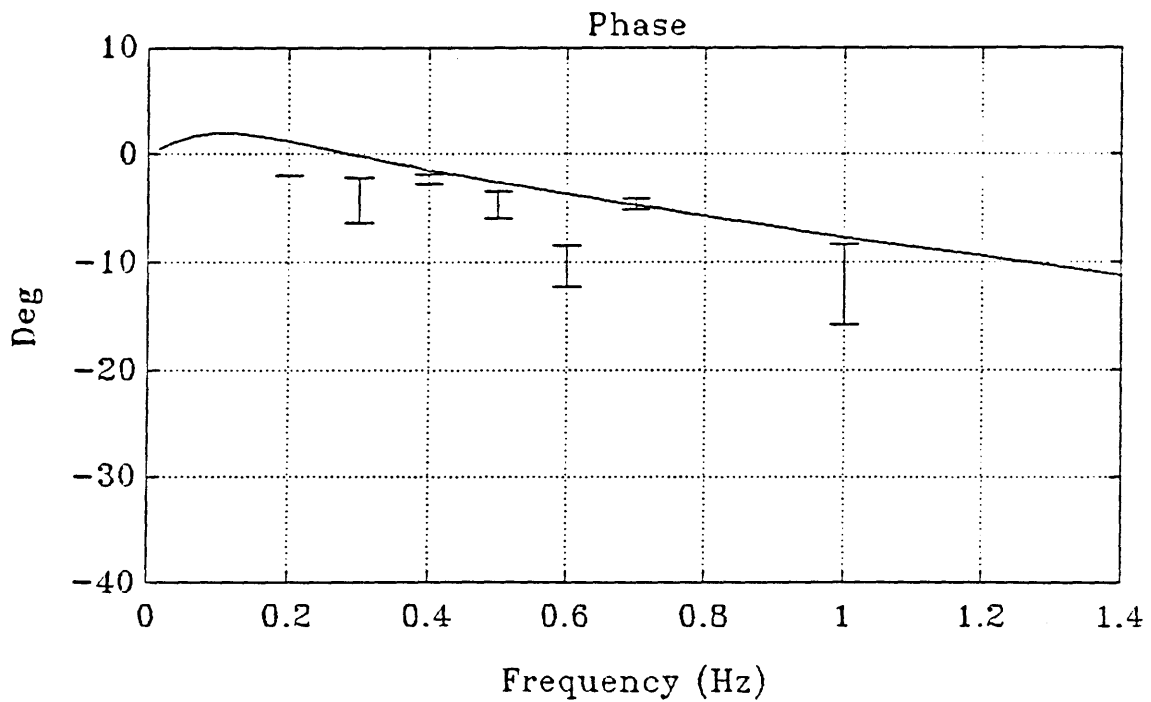
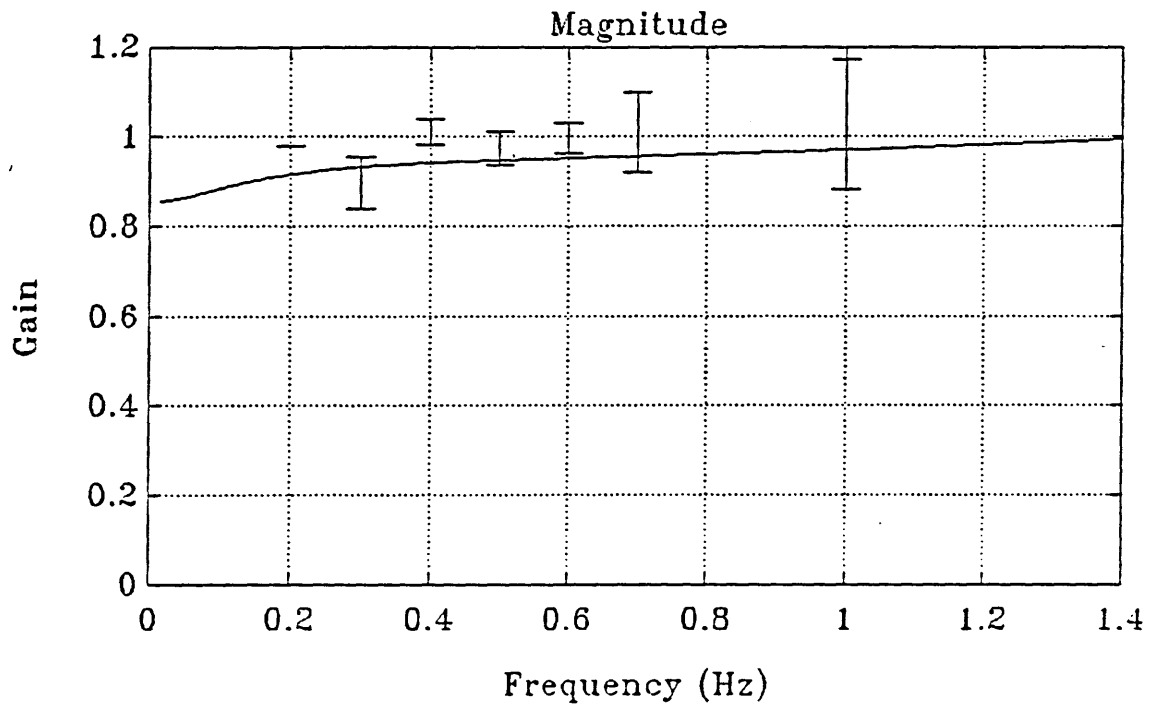


Figure D.16 Model transfer function and experiment results for subject T VV/sine. (Solid lines are model transfer function; bars are experiment data, ± 1 s.d. centered at mean.)

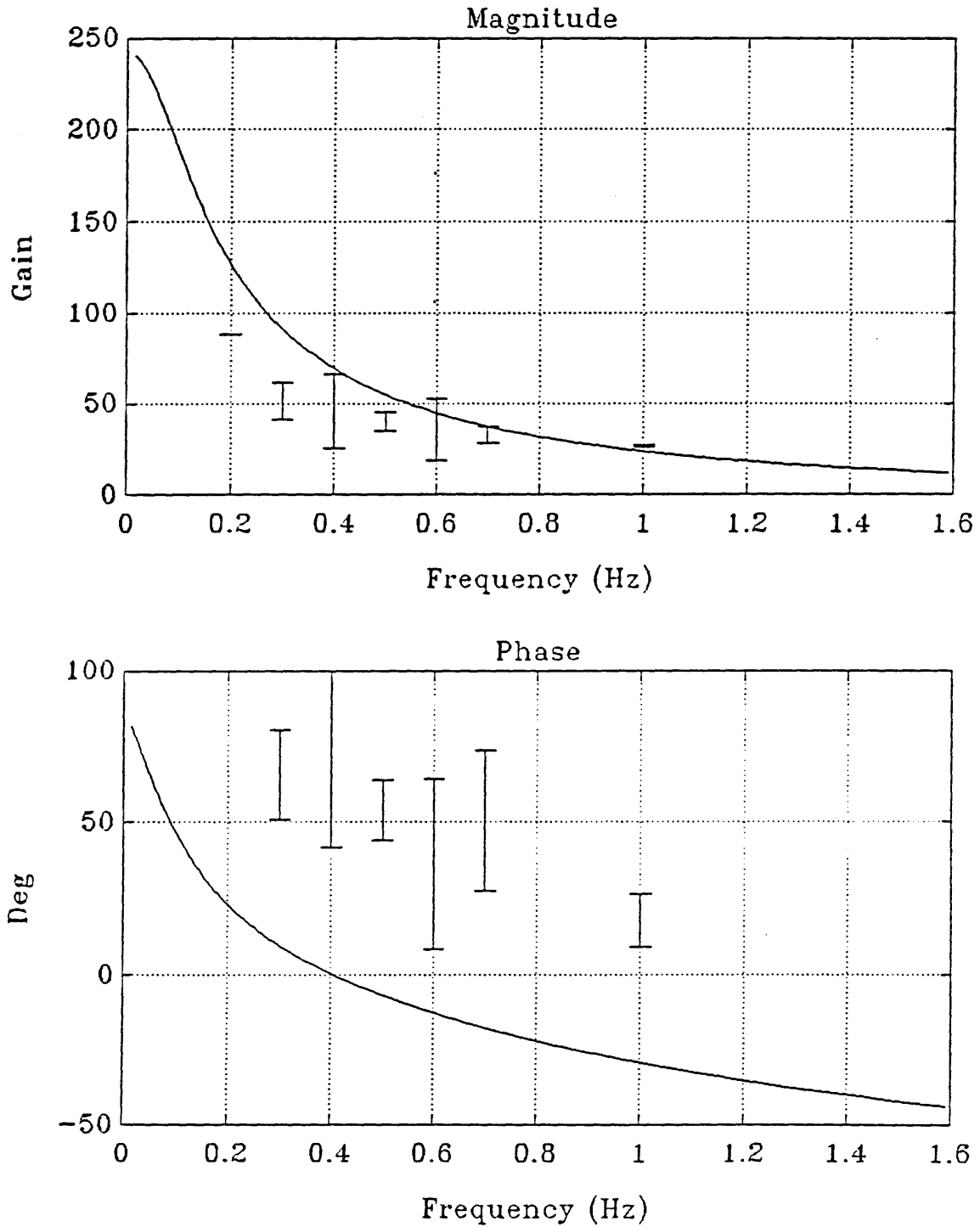
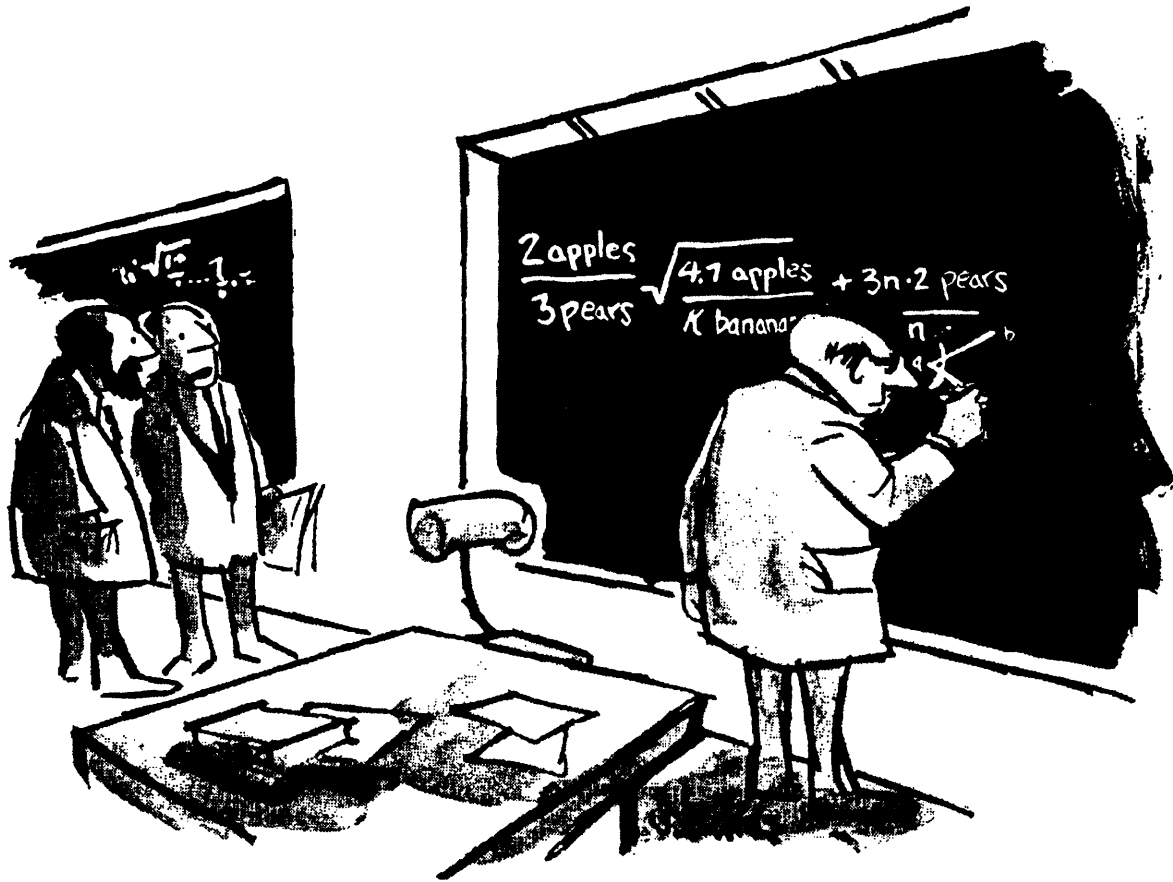


Figure D.17 Model transfer function and experiment results for subject T AI/sine. (Solid lines are model transfer function; bars are experiment data, ± 1 s.d. centered at mean.)

Appendix E

Process and Measurement Noises



"If only he could think in abstract terms."

Begin by assuming values for the measurement noise process covariance matrix R . For this somewhat speculative analysis we use the argument that the resolution of a given sensory system can be modelled by its corresponding measurement noise process. Thus this noise determines the stimulus threshold.

For linear acceleration and the otolith system, we adopt a threshold value of 0.01 g for lateral motions, which seems to be a reasonable choice based on the compiled data (Guedry, 1974). This gives $R_{22} = (0.1 \text{ m/s}^2)^2 = 0.01 \text{ (m/s}^2)^2$.

Visual velocity threshold values, for a photopic target in the dark, range from about 1 to 8 arc-min/sec (Leibowitz, 1955). Choosing a value of 3 min/sec gives 0.05 deg/sec or $R_{11} = 0.0025 \text{ (deg/sec)}^2$. Cross-terms R_{12} and R_{21} are assumed to be zero; it seems reasonable that there is no interaction between the sensory systems. This assumption could be changed in later work, based on considerations such as a change in visual discrimination during head motion (linear acceleration).

We can find P easily, since $K=PC^TR^{-1}$ (see later for explanation of \tilde{C}_{11}):

$$P = KRC^{-T} = \begin{bmatrix} K_{11} & 0 \\ 0 & K_{22} \end{bmatrix} \begin{bmatrix} R_{11} & 0 \\ 0 & R_{22} \end{bmatrix} \begin{bmatrix} \tilde{C}_{11} & 0 \\ 0 & C_{22} \end{bmatrix}^{-T}$$

$$= \begin{bmatrix} \frac{K_{11}R_{11}}{\tilde{C}_{11}} & 0 \\ 0 & \frac{K_{22}R_{22}}{C_{22}} \end{bmatrix}$$

The three feedback loops in the visual velocity path of the model (see Figure 5.3) complicate the analysis. These can be conceptually collapsed into a single equivalent feedback loop with gain \tilde{C}_{11} :

$$\tilde{C}_{11} = C_{11} - K_{eye}K_eD_e + K_{eye}D_1D_2$$

Ignoring for this simplified analysis the effects of the delay terms D_i , and using the model parameters from Appendix D, the values for each subject are found:

$$\tilde{C}_{11}(JT) = 1.39 \qquad \tilde{C}_{11}(S) = 1.43$$

Now we find P directly:

$$P(JT) = \begin{bmatrix} 0.036 & 0 \\ 0 & 0.01 \end{bmatrix} \qquad P(S) = \begin{bmatrix} 0.17 & 0 \\ 0 & 0.02 \end{bmatrix}$$

To find Q, we use the Ricatti equation in the steady state:

$$\dot{P} = 0 = AP + PA^T + BQB^T - KRK^T$$

The solution is straightforward with the aid of the MACSYMA symbolic mathematics computer package. For the SOS condition, using the matrix definitions in Appendix B:

$$Q(JT) = \begin{bmatrix} 1.0 & -10^{-5} \\ -10^{-5} & 10^{-6} \end{bmatrix} \qquad Q(S) = \begin{bmatrix} 25 & -4 \times 10^{-5} \\ -4 \times 10^{-5} & 1.6 \times 10^{-7} \end{bmatrix}$$

$$\text{units} \equiv \begin{bmatrix} \left(\frac{\text{deg}}{\text{sec}}\right)^2 & \left(\frac{\text{deg}}{\text{sec}}\right) \times \left(\frac{\text{m}}{\text{sec}^2}\right) \\ \left(\frac{\text{deg}}{\text{sec}}\right) \times \left(\frac{\text{m}}{\text{sec}^2}\right) & \left(\frac{\text{m}}{\text{sec}^2}\right)^2 \end{bmatrix}$$

BIOGRAPHICAL SKETCH

Mark Shelhamer was born in 1959 in Trenton, New Jersey, and raised in Fairless Hills, Pennsylvania. He graduated from Pennsbury High School, where he participated in a variety of music programs, and then attended Drexel University in Philadelphia from 1977 to 1982. He received the Master's and Bachelor's degrees in Electrical Engineering with highest honors. His Master's thesis research on signal processing and auditory evoked potentials was performed at the Temple University Medical School in Philadelphia.

Upon entering MIT with an NSF fellowship, Dr. Shelhamer participated in visual-vestibular interaction experiments on the Spacelab-1 and D-1 flights of the Space Shuttle. His doctoral thesis research grew out of an interest in multi-sensory integration and spatial orientation. After leaving MIT, he undertook post-doctoral research on modelling of oculomotor and vestibular adaptation at the Johns Hopkins Medical School in Baltimore, Maryland.

Dr. Shelhamer's research interests include sensory systems, spatial orientation, and signal processing. He is an avid amateur radio and short-wave radio enthusiast, and counts among his other hobbies electronics, writing, hiking, camping, skiing, and SCUBA diving.